Durham E-Theses

Development of a simplified test method for compliant layered bearings

Marsden, Hollie Rebecca

How to cite:

Marsden, Hollie Rebecca (1998) *Development of a simplified test method for compliant layered bearings*, Durham theses, Durham University. Available at Durham E-Theses Online: http://etheses.dur.ac.uk/4913/

Use policy

The full-text may be used and/or reproduced, and given to third parties in any format or medium, without prior permission or charge, for personal research or study, educational, or not-for-profit purposes provided that:

- a full bibliographic reference is made to the original source
- a link is made to the metadata record in Durham E-Theses
- the full-text is not changed in any way

The full-text must not be sold in any format or medium without the formal permission of the copyright holders.

Please consult the full Durham E-Theses policy for further details.

Academic Support Office, The Palatine Centre, Durham University, Stockton Road, Durham, DH1 3LE
e-mail: e-theses.admin@durham.ac.uk Tel: +44 0191 334 6107
http://etheses.dur.ac.uk

Development of a Simplified Test Method for Compliant Layered Bearings

Hollie Rebecca Marsden, M.Eng.

A thesis submitted for the degree of Doctor of Philosophy at the University of Durham

April 1998

The copyright of this thesis rests
with the author. No quotation
from it should be published
without the written consent of the
author and information derived
from it should be acknowledged.

Centre for Biomedical Engineering, School of Engineering, University of Durham

12 AUG 1998

Abstract

Compliant layered bearings could improve the useful life of replacement load-bearing joints. By incorporating an elastic bearing material, fluid film separation of the articulating surfaces can be maintained and so low friction and negligible wear should occur. Compliant bearings are still under development and so require extensive testing before they can be implanted. To give a realistic evaluation of their performance, the test conditions must be representative of the in vivo situation. To date this has meant using joint simulators.

A simplified test method has been developed to measure the friction of compliant layered bearings. It uses a reciprocating materials-screening apparatus adapted to include a dynamic load, very low friction bearings, and a curved counterface. It has been validated by comparison with simulator tests and predictions made from Hertzian contact and elastohydrodynamic theories. An alternative to the Sommerfeld parameter has been defined to allow comparison of the different test methods. Tests have shown that of the parameters which affect friction, the predicted Hertzian contact area was the most important. Similar predicted areas gave rise to similar coefficients of friction in both mixed and fluid film lubrication regimes. The simplified method showed improved repeatability and lower systematic errors than the simulator.

The method has been used to examine the effect of design factors on the friction generated in compliant layered bearings, comparing the results obtained with those of the simulator. Increased load, decreased counterface roughness, increased entraining velocity and the use of a compliant layer over UHMWPE all reduced the coefficient of friction. Bearing conformity had a mixed effect on friction. Point contacts and line contacts showed similar trends. The mechanical properties of the compliant materials have also been considered including hardness, hysteresis in compression, and creep.

Acknowledgements

This thesis would never have been possible without the help of many - both in the School of Engineering at the University of Durham and elsewhere. Many thanks to all the following:

Prof. Tony Unsworth for his three years of supervision, for helping me to find the right track when I'd lost it, for learning to live with my stubbornness, and for the late nights, early mornings, and weekend meetings in proof-reading this thesis which have enabled me to submit in time.

Nigel Smith, Eric Jones, Christina Doyle and to all the staff at Howmedica Limerick for making me welcome during my visit. Particular thanks to Nigel, for all his interest, advice and constructive comments over the last three years, not to mention the free lunches. Thanks must also go to Dudley Finch at Brunel University for all his instruction in investigating the chemistry of polyurethanes as well as his more general help and advice on my research.

Susan Carter for her moral support, and help in numerous ways including keeping me out of trouble on occasions, and for many a good natter. "Never say never".

George Turnbull, Colin Wintrip, Brian Blackburn, Roger Little, Ian Hutchinson, Milos Kolar and everyone else in the mechanical, electrical, and microprocessing workshops who diligently carried out my designs, got me out of spots of bother, or generally put machines back together after I had used them. In particular, thanks to George and Colin who have not only done a brilliant job with all my half-baked ideas but have also furnished me with many ideas of their own.

Susan, Hayley, Simon, Alistair, Petra, Dr. Martin, and the much-missed Dr. Steve, and anyone else who has ever frequented the engineering coffee bar. Without you my time in Durham would have been much less fun and my research much more difficult if I hadn't had you all as sounding boards. Particular thanks to Susan for putting up with a noisy Southerner in her office for almost three years and to Hayley for answering all my stupid questions on thesis writing, plus thanks to you both for some good Tetris games. Special thanks to Sue for the great photography.

The long-departed Dr. Ian Burgess and Dr. Richard Hall for all their patience and help in my first two years, as well as a now-infamous episode involving nine pints of Guinness and a barmaid's hairstyle.

I am forever indebted to Dr. Bob Allen at the University of Southampton for being a constant source of inspiration over the last seven years of studying and for coercing me into bio-medical engineering in the first place (you all have him to blame).

My research at Durham has been funded by Howmedica International and the Engineering and Physical Sciences Research Council for which I am very grateful.

On an extra-curricular front, the following people have made a non-academic contribution to my enjoyment of Durham and have helped to keep me sane.

Louisa, Caroline, Abi, bow-turned-great-cox-Narch (take me to the stupid cow), and new-girl-at-bow-Sarah, for providing such complete relief from the stress of work, so much fun messing about in boats, so much bad singing, a lot of riotous behaviour and such a great collection of silverware (I use the term silver very loosely). Thanks also to Dyfrig and the Women in Black for more of the same this year. Lou-Lou you've been the best that bow-side could ever be and a great (if often very damp) friend besides. I'll see you all and that Redgrave bloke in June.

Everyone else I've met at Durham for your significant contributions to a great 3 years. You include: Eli, 2 Gills, Lorraine, Charlie, Duncan (for the Gary Barlow impressions), Dionne, Dawn, Dr. Freeman, Chuundeeer, Dr. H. H. Wilson, Councillor Pinner, Jan, Frank and Dick for homes in the North, and anyone I haven't mentioned.

And in the tradition of leaving the most important to last,

Mum and Peter for always believing I could do it even when I didn't, for letting me find my own way, and for bringing me up to have the determination to stick at this.

And finally, Richard, who doesn't believe me but really has been my reason to get up in the mornings on my worst days, and my reason to come home on all of them. For all your limitless love and support and words of wisdom, for putting up with tears, tantrums, tiredness and a real shortage of my time, and for making my life easier and better in so many ways.

Contents

Page

Abstract
Acknowledgements i
Contents iii
List of Figures vii
List of Tables x
Nomenclature xi
Abbreviations xiv

Chapter 1. Introduction 1

Chapter 2. Review of Published Work 4

2.0 Tribology theory - friction and wear 4
2.1 Lubrication of natural joints 7
2.2 Lubrication of conventional prosthetic joints 16
  2.2.1 Factors affecting friction 17
  2.2.2 Factors affecting wear 20
2.3 Compliant layered joints 23
  2.3.0 Lubrication 23
  2.3.1 Contact mechanics of compliant layers 28
    2.3.1.1 Numerical solutions 29
    2.3.1.2 Experimental measurement 38
  2.3.2 Medical grade polyurethane and other possible materials 40
    2.3.3.1 Polyurethane elastomer chemistry 41
    2.3.3.2 Adhesion of compliant layer to substrate 45
2.4 Machines for measurement of friction and wear 46
  2.4.1 Description of test machines 47
  2.4.2 Methods of measurement of friction and wear 48
  2.4.3 Comparison of different machines 49

Chapter 3. Apparatus 55

3.0 Introduction 55
3.1 Durham Hip Function Friction Simulator 56
  3.1.1 Application and measurement of load 59
  3.1.2 Application and measurement of motion 60
  3.1.3 Measurement of frictional torque 62
  3.1.4 Instrumentation and control 63
3.2 Pin-on-plate Friction Measurement Machine 64

3.2.1 The original Durham pin-on-plate friction measuring machine 64
3.2.2 Modified design 66
3.2.2.1 Dynamic loading 68
3.2.2.2 Air Bearings 72
3.2.2.3 Instrumentation and control 78

Chapter 4 Materials and Methods **80**

4.0 Introduction 80
4.1 Materials 80
4.2 Friction measurement on the simulator 84
4.2.1 Mounting and elimination of misalignment errors 84
4.2.2 Calibration and analysis of errors 87
4.2.3 Standard experimental protocol 88
4.2.4 Analysis of results 90
4.3 Friction measurement on the pin-on-plate apparatus 92
4.3.1 Calibration and analysis of errors 93
4.3.2 Standard experimental protocol 98
4.3.3 Analysis of results 100
4.4 Lubricants 103
4.5 Measurement of surface topography of samples 103

Chapter 5. Results and Discussion - Validation of Pin-on-plate Test Method **105**

5.0 Introduction 105
5.0.1 Elastohydrodynamic and micro-elastohydrodynamic theory 105
5.1 Repeatability of new pin-on-plate test method 107
5.1.1 Steady-state friction of UHMWPE-metal bearings 107
5.1.2 Compliant layers 109
5.1.2.1 Steady-state friction with distilled water 110
5.1.2.2 Stribeck Analyses 111
5.2 Use of different lubricants 118
5.2.1 Comparison of lubricants on pin-on-plate machine 119
5.2.2 Comparison of lubricants on the simulator 120
5.2.3 Comparison of experimental results with EHL theory 121
5.2.4 Summary 123
5.3 Effect of contact geometry 124
5.4 Effect of applied load 127
5.4.1 Observations - effect of applied load 130
5.4.2 Comparison with elastohydrodynamic theory 131
5.4.3 Comparison of pin-on-plate and simulator results 132
5.4.4 Discussion 134
5.5 Effect of bearing conformity 136
5.5.1 Comparison of POP and Sim results for 0.2 m equivalent radius 138
5.5.2 Comparison of results for 0.1 and 0.2 m equivalent radius 141
5.5.2.1 Observations 146
5.5.2.2 Discussion 147

5.5.3 Comparison of bearing conformities on simulator 150
5.5.4 Summary 152

Chapter 6. Results and Discussion - Verification of Published Results **154**

6.1 Effect of hard counterface roughness 154
6.1.1 Observations 156
6.1.2 Discussion 159
6.1.3 Summary 160
6.2 Comparison of compliant layers with conventional joint materials 161
6.2.1 Comparison of UHMWPE and compliant layered bearings 163
6.2.1.1 Observations 167
6.2.1.2 Discussion 168
6.2.1.3 Summary 171
6.2.2 Comparison of UHMWPE friction on two apparatus 172
6.2.2.1 Observations 173
6.2.2.2 Discussion 174
6.2.2.3 Summary 175

Chapter 7. Results and Discussion - Cylinder Experiment **176**

7.0 Introduction 176
7.1 Effect of entraining velocity 179
7.2 Effect of compliant layer roughness 182
7.2.1 Pin-on-plate apparatus 182
7.2.2 Simulator 186
7.2.3 Summary 187
7.3 Comparison of experimental and theoretical results 187
7.4 Effect of hard counterface roughness 189
7.5 Comparison of pin-on-plate and simulator results 191
7.6 Summary 194

Chapter 8. Summary of Results and Discussion **195**

8.0 Introduction 195
8.1 Validation of pin-on-plate method 195
8.1.1 Repeatability 195
8.1.2 Comparison with the simulator 196
8.1.3 Comparison with theory 201
8.1.3.1 Hertzian contact theory 201
8.1.3.2 EHL and micro-EHL theories 204
8.2 Effect of design parameters 207
8.2.1 Bearing conformity 208
8.2.2 Hard counterface roughness 208
8.2.3 Compliant layer roughness 209
8.2.4 Comparison of compliant layers and conventional materials 209

8.3 Use of a new Sommerfeld parameter 210

Chapter 9. Investigation of the Mechanical Properties of Polyurethane 212

9.0 Introduction 212
9.1 Hardness testing 212
    9.1.1 Positional repeatability 213
    9.1.2 Effect of conditioning treatments 215
9.2 Hysteresis measurement 217
9.3 Creep measurement 223
    9.3.1 Friction results 224
    9.3.2 Replica measurements 230
    9.3.3 Discussion 232

Chapter 10. Conclusions 234

10.0 Introduction 234
10.1 Development of a simplified test method 235
10.2 Validation of the simplified test method 236
10.3 Effect of design parameters 237
10.4 Recommendations for future work 239

References 241

Appendices

A - Repeatability of load application on simulator 271
B - Losses in roller bearings 275
C - Air bearing design calculations 277
D - Losses in air bearings 280
E - Calibration of pin-on-plate apparatus load cell 284
F - Surface roughness measurements 287
G - Simulator friction factor traces 289

List of Figures

Page

2.1 Typical Stribeck curve 6
2.2 The synovial joint 8
2.3 Anatomic planes of motion of the hip 9
2.4 Schematic diagram of polyurethane reactions 42
2.5 Chemical structure of polyurethane monomers 43

3.1 Hip function friction simulator 57
3.2 Hip joint in simulator 57
3.3 Knee joint in simulator 58
3.4 Comparison of simulator load cycle and Paul cycle 59
3.5 Comparison of simulator motion cycle and Johnson Smidt cycle 61
3.6 Schematic representation of the simulator control 63
3.7 Original Durham pin-on-plate friction apparatus 65
3.8 Plane inclined slider bearing 66
3.9 Dynamic loading arrangement 69
3.10 Schematic of dynamic loading arrangement 70
3.11 Air bearings 73
3.12 Schematic representation of air bearing assembly 74
3.13 Schematic of modified transducer connection 77
3.14 Instrumentation and control of pin-on-plate apparatus 79

4.1 Examples of UHMWPE and polyurethane components 82
4.2 Examples of femoral heads and spherical pins 83
4.3 Examples of cylinders for simulator and pin-on-plate apparatus 84
4.4 Forward and reverse loading cycles on simulator 85
4.5 Simulator load and motion cycles 91
4.6 Typical friction and load trace from XYT plotter 101

5.1 Repeatability: UHMWPE with distilled water 108
5.2 Repeatability: compliant layers with distilled water 110
5.3 Repeatability of Stribeck analyses on pin-on-plate apparatus 112
5.4 Typical simulator result (BB98 against 32 mm head) 113
5.5 Comparison of CMC and silicone fluids on pin-on-plate apparatus 119
5.6 Comparison of CMC and silicone fluids on simulator 121
5.7 Effect of equivalent contact geometry 126
5.8 Effect of applied load measured on pin-on-plate apparatus (0.1 m) 129
5.9 Effect of applied load measured on simulator (0.1 m) 129
5.10 EHL theory prediction of effect of applied load 131
5.11 Comparison of POP and Sim results for 0.1 m equivalent radius 133
5.12 Effect of applied load on measured pin-on-plate apparatus (0.2 m) 139
5.13 Effect of applied load measured on simulator (0.2 m) 139
5.14 Comparison of POP and Sim results for 0.2 m equivalent radius 140
5.15 Effect of bearing conformity measured on POP apparatus under 40 N load 142

5.15 Effect of bearing conformity measured on POP apparatus under 40 N load 142
5.16 Effect of bearing conformity measured on POP apparatus under 70 N load 142
5.17 Effect of bearing conformity measured on POP apparatus under 100 N load 143
5.18 Effect of bearing conformity measured on POP apparatus under 150 N load 143
5.19 Effect of bearing conformity measured on simulator under 250 N load 144
5.20 Effect of bearing conformity measured on simulator under 500 N load 144
5.21 Effect of bearing conformity measured on simulator under 1000 N load 145
5.22 Effect of bearing conformity measured on simulator under 2000 N load 145
5.23 Effect of bearing conformity on simulator (BB98 vs 28, 30 & 32 mm heads) 150

6.1 Effect of hard counterface roughness measured on POP under 40 N load 157
6.2 Effect of hard counterface roughness measured on POP under 70 N load 157
6.3 Effect of hard counterface roughness measured on POP under 100 N load 158
6.4 Effect of hard counterface roughness measured on POP under 150 N load 158
6.5 Comparison of UHMWPE and PU measured on POP under 40 N load 164
6.6 Comparison of UHMWPE and PU measured on POP under 100 N load 164
6.7 Comparison of UHMWPE and PU measured on POP under 150 N load 165
6.8 Comparison of UHMWPE and PU measured on simulator under 500 load 165
6.9 Comparison of UHMWPE and PU measured on simulator under 1000 load 166
6.10 Comparison of UHMWPE and PU measured on simulator under 2000 load 166
6.11 Comparison of UHMWPE experimental results for POP apparatus and Sim 172
6.12 Comparison of UHMWPE theoretical results for POP apparatus and Sim 173

7.1 Effect of entraining velocity (super finished cylinder against C1) 179
7.2 Effect of entraining velocity (super finished cylinder against C3) 179
7.3 Effect of entraining velocity (super finished cylinder against C4) 180
7.4 Effect of compliant layer roughness (normal cylinder at 9 mm/sec on POP) 182
7.5 Effect of compliant layer roughness (normal cylinder at 50 mm/sec on POP) 183
7.6 Effect of compliant layer roughness (SF cylinder at 9 mm/sec on POP) 183
7.7 Effect of compliant layer roughness (SF cylinder at 50 mm/sec on POP) 184
7.8 Effect of compliant layer roughness (normal cylinder on simulator) 186
7.9 Effect of hard counterface roughness (C1 at 9 mm/sec on POP) 189
7.10 Effect of hard counterface roughness (C1 at 50 mm/sec on POP) 190
7.11 Effect of hard counterface roughness (M3/M4 on simulator) 190
7.12 Comparison of line contact results for pin-on-plate apparatus and simulator 192

8.1 Typical simulator trace of frictional torque (0.000818 Pa s) 197
8.2 Typical simulator trace of frictional torque (0.00934 Pa s) 198
8.3 Typical simulator trace of frictional torque (29.25 Pa s) 198
8.4 Typical pin-on-plate traces of frictional torque 199
8.5 Relationship between friction-load power factor B and lubricant viscosity 203
8.6 Predicted EHL film thickness vs. measured coefficient of friction 206
8.7 Predicted micro-EHL film thickness vs. measured coefficient of friction 206
8.8 POP and simulator friction results plotted against $\eta ua/L$ 211
8.9 POP and simulator friction results plotted against $\eta uh_{cen}/L$ 211

9.1 Positional reproducibility of hardness on a new unbonded sample 213
9.2 Positional reproducibility of hardness on an aged bonded sample 214
9.3 Preparation of samples for conditioning 216

9.4 Deformation of plate during testing 217
9.5 A typical hysteresis measurement 218
9.6 Effect of hysteresis on measured friction for PU (CC21A 200 mm B 150N) 220
9.7 Comparison of POP and Sim results after adjustment for hysteresis of layer 221
9.8 Effect of hysteresis on measured friction for PE (PE4 200 mm B 150N) 221
9.9 Average measured friction for C1 cups in creep test 225
9.10 Average measured friction for C2 cups in creep test 225
9.11 Average measured friction for C3 cups in creep test 226
9.12 Deformation of creep cups over 7 days loading 226
9.13 Friction results for creep and re-creep of cup BB 78 (C1) 228
9.14 Friction results for creep and re-creep of cup BB 100 (C2) 228
9.15 Friction results for creep and re-creep of cup BB 76 (C3) 229
9.16 Deformation of cups BB78, BB100, BB76 during creep and re-creep 229
9.17 Microscope photograph of tears on surface of C3 cup 233

A.1 Block diagram of load control system of simulator 271
A.2 ADC calibration curves for six different temperatures 273
A.3 DAC calibration curves for six different temperatures 273
A.4 Relationship between intercept of DAC calibration and temperature 274
A.5 Relationship between intercept of ADC calibration and temperature 274
B.1 Calibration of friction transducer through roller bearings 275
B.2 Direct calibration of friction transducer 276
C.1 A single jet hydrostatic bearing 277
D.1 Comparison of friction calibrations at x 2 mV 280
D.2 Comparison of friction calibrations at x 5 mV 281
D.3 Comparison of friction calibrations at x 10 mV 281
D.4 Comparison of friction calibrations at x 20 mV 282
D.5 Comparison of friction calibrations at x 50 mV 282
D.6 Comparison of friction calibrations at x 100 mV 283
E.1 Calibration of load cell against load at x 0.5 mV 285
E.2 Calibration of load cell against load at x 1.0 mV 285
E.3 Calibration of load cell against pressure for 10 mm cylinder 286
E.4 Calibration of load cell against pressure for 25 mm cylinder 286
G.1 Typical simulator friction factor trace (0.000818 Pa s) 289
G.2 Typical simulator friction factor trace (0.00934 Pa s) 289
G.3 Typical simulator friction factor trace (29.25 Pa s) 290

List of Tables

Page

2.1 Summary of advantages of different test methods 49
2.2 Summary of simple materials-screening machines 50
2.3 Summary of joint simulator machines 52

4.1 Simulator testing protocol 89
4.2 Specifications of components of POP measurement systems 95
4.3 Calculated systematic errors 97
4.4 Pin-on-plate experimental protocol 99

5.1 Experimental conditions and contact parameters for 0.1 m equivalent radius 125
5.2 Theoretical contact parameters for 100 mm pin under various loads 128
5.3 Theoretical contact parameters for 28 mm head under various loads 128
5.4 Experimental conditions for 0.2 m equivalent radius bearings 136
5.5 Theoretical contact parameters for 200 mm pin B under various loads 137
5.6 Theoretical contact parameters for 30 mm head under various loads 137
5.7 Rank of measured friction curves compared with contact half-width 140

6.1 Theoretical contact parameters for 200 mm pins A and B 155
6.2 Experimental conditions for comparison of UHMWPE and compliant layers 162

7.1 Experimental parameters for cylinder tests 178

8.1 Theoretical values of friction-load power factor, B 202
8.2 Average experimental friction-load power factors, B 202

9.1 Positional reproducibility of hardness on a new unbonded sample 213
9.2 Positional reproducibility of hardness on an aged bonded sample 214
9.3 Hardness of a conditioned and aged bonded sample 214
9.4 Effect of conditioning on hardness of polyurethanes 216
9.5 Hysteresis measurements 220
9.6 CMM measurements of replicas in creep and re-creep experiments 231

C.1 Air bearing calculations 279
D.1 Calculated calibration coefficients and losses in the air bearings 280
F.1 Surface roughness measurements of soft counterfaces 287
F.2 Surface roughness measurements of hard counterfaces 288

Nomenclature

a	major elliptical Hertzian contact radius, half-width (for spheres) (m) half-length (for cylinders) (m)
A_i	angle of flexion-extension at point i (°)
A_f , A_{fi}	angle of flexion-extension from a forward loading cycle at point i (°)
A_r , A_{ri}	angle of flexion-extension from a reverse loading cycle at point i (°)
b	minor elliptical Hertzian contact radius, half-width (for cylinders) (m)
B	factor relating applied load to coefficient of friction such that $\mu = A.L^B$
C_L	optimum load coefficient of hydrostatic bearing
E^*	adjusted modulus $E^* = \dfrac{2}{\left(\dfrac{1-\nu_1^{\ 2}}{E_1} + \dfrac{1-\nu_2^{\ 2}}{E_2}\right)}$ (Pa)
E_{adj}	adjusted modulus $E_{adj} = \dfrac{4LRh_T}{\pi a^4}\left\{\dfrac{(1+\nu_2)(1-2\nu_2)}{(1-\nu_2)}\right\}$ (Pa)
E'	elastic modulus of material $\dfrac{1}{E'} = \dfrac{1-\nu_2^{\ 2}}{E_{adj}}$ (Pa)
E''	elastic modulus of material $\dfrac{1}{E''} = \dfrac{(1+\nu_2)(1-2\nu_2)}{(1-\nu_2)E_{adj}}$ where $\upsilon_2 = 0.4$ (Pa)
E_1	elastic modulus of material of hard counterface (head or pin) (Pa)
E_2	elastic modulus of material of soft counterface (cup or plate) (Pa)
f	friction factor
	frequency of simulator flexion-extension motion (Hz)
F	frictional force (N)
	force supported by contact in Dumbleton's definition of wear (N) [1978]
G	hydrostatic bearing slot factor
h_{cen}	central elastohydrodynamic film thickness (m)
h_i	inlet film thickness (m)
h_{min}	minimum elastohydrodynamic film thickness (m)
$h_{\mu,min}$	minimum micro-elastohydrodynamic film thickness (m)
h_T	compliant layer thickness (m)
h_o	outlet film thickness (m)
	hydrostatic bearing clearance (m)
i	point in simulator cycle (i = 0 to 128)
k	wear factor (mm^3/Nm)
	ellipticity ratio a/b
	hydrostatic bearing pressure factor
k*	ellipticity parameter $k^* = 1.03\left(\dfrac{a}{b}\right)^{0.64}$
k_1	ellipticity constant such that $k_1 = \dfrac{1-\nu_1^{\ 2}}{\pi E_1}$

k_2	ellipticity constant such that $k_2 = \frac{1-\nu_2^2}{\pi E_2}$
L	mean applied load (N)
	length of plane inclined slider bearing
L_i	applied load at point i (N)
L_f , L_{fi}	applied load from a forward loading cycle at point i (N)
L_r , L_{ri}	applied load from a reverse loading cycle at point i (N)
n	factor relating contact area to load such that $a \propto L^n$
P	load per unit length (N/m)
	maximum contact pressure (Pa)
P_a	atmospheric pressure (absolute) to hydrostatic bearing (Pa)
P_{ent}	load per unit length supported by entraining action(N/m)
P_i	pressure at orifice (absolute) of hydrostatic bearing (Pa)
P_s	supply pressure (absolute) to hydrostatic bearing (Pa)
P_{sq}	load per unit length supported by squeeze film action (N/m)
PV	surface roughness peak-valley height (distance from highest peak to lowest valley) (m)
Q	volume flow rate of hydrostatic bearing (m^3/sec)
r_i	inner radius of hydrostatic bearing (m)
r_o	outer radius of hydrostatic bearing (m)
R	equivalent radius of bearing (m)
	correlation coefficient
R_1	radius of femoral head or hard counterface (m)
R_2	radius of acetabular cup or soft counterface (m)
R_a	surface roughness (arithmetic deviation from mean plane) (m)
R_{cyl}	radius of curvature of simple cylinder (m)
RMS	root mean square surface roughness (m)
R_{sk}	skew roughness (symmetry of deviations from mean plane) (m)
S	Sommerfeld parameter $S = \frac{\eta\omega}{P}$
S_T	stroke ratio, contact radius / stroke length
u	entraining velocity
u_i	entraining velocity on simulator at point i
v	velocity of approach of surfaces in squeeze film action
V	volumetric wear (m^3)
w	width of bearing (m)
W	applied load (N)
	load capacity of hydrostatic bearing (N)
x	total sliding distance (m)
Z	pin-on-plate Sommerfeld parameter $Z = \frac{\eta u R}{L}$
Z_i	pin-on-plate Sommerfeld parameter at point i

α	amplitude of flexion-extension motion on simulator (°)
Δ	deviation in CMM measurements from mean diameter (m)
ϕ	diameter (m)
η	viscosity (Pa s)
λ	surface separation ratio
	hydrostatic bearing stiffness (N/m)
λ_c	roughness correlation length (m)
μ	coefficient of friction
σ	combined RMS roughness of two bearing surfaces (m)
σ_1	RMS roughness of hard counterface (pin or femoral head) (m)
σ_2	RMS roughness of soft counterface (plate or cups) (m)
T	true frictional torque (Nm)
T_e	misalignment torque (Nm)
T_F	frictional torque from a forward loading cycle (Nm)
T_{fi}	frictional torque from a forward loading cycle at point i (Nm)
T_i	true frictional torque at point i (Nm)
T_R	frictional torque from a reverse loading cycle (Nm)
T_{ri}	frictional torque from a reverse loading cycle at point i (Nm)
υ_1	Poisson's ratio of hard counterface (pin or femoral head)
υ_2	Poisson's ratio soft counterface (plate or acetabular cups)
ω	angular velocity of articulation of joint (rads/sec)

Abbreviations

AA	abduction - adduction (motion of hip in frontal plane)
ADC	analogue to digital converter
BDO	1,4-butanediol
BW	body weight
75D	Corethane 75D
C80A	Corethane 80A
CA	charge amplifier
CMC	carboxymethyl cellulose
CMM	co-ordinate measuring machine
CoCrMo	cobalt chrome molybdenum
DAC	digital to analogue converter
EDA	ethylene diamine
EHL	elastohydrodynamic lubrication
ESC	environmental stress cracking
FE	flexion - extension (motion of hip in sagittal plane)
FS	full scale
HMDI	4,4-methylene bicyclohexane diisocyanate or hydrogenated methylene diisocyanate
IE	internal - external rotation (motion of hip in transverse plane)
micro-EHL	micro-elastohydrodynamic lubrication
MDI	4,4-methylene bisphenyl diisocyanate or methylene diisocyanate
MIO	metal ion oxidation
PHECD	poly[1,6-hexyl 1,2 ethyl carbonate] diol
POP	modified pin-on-plate friction measurement apparatus
PTMEG	polytetramethylene ether glycol
PU	polyurethane
SGA	strain gauge amplifier
Si	silicone fluid
SIM	hip function friction simulator
TDI	toluene diisocyanate
UHMWPE	ultra-high molecular weight polyethylene

I confirm that no part of the material offered has previously been submitted for a degree in this or any other University. The work of others has been acknowledged and quotations and paraphrases suitably indicated.

The copyright of this thesis rests with the author. No quotation from it should be published without her prior written consent and information derived from it should be acknowledged.

1 Introduction

Total replacement joints are today commonplace with almost 40,000 total hip operations and 18,000 total knee operations being performed by orthopaedic surgeons every year in the UK [Bonfield 1996]. With 50 years of design and development behind them, these joints now have a 90% survival rate at 10 years and can provide as many as 20 additional years of pain-free active life for their recipients [Murray *et al* 1995]. However, 18% of all replacement joint procedures are revision operations [Bonfield 1996], and the main cause of these revisions is widely recognised as being long-term aseptic loosening [Morscher 1992, Poss *et al* 1988].

Long-term aseptic loosening describes the body's response to debris generated through the wear of the replacement joint components. At present, the majority of total hip replacements have a metallic femoral head articulating against an acetabular component of ultra high molecular weight polyethylene (UHMWPE) and as in any bearing system, wear of the softer component (UHMWPE) occurs as the joint articulates. The joints function well for long periods of time which implies the body is able to tolerate this debris. However, over longer periods, or in cases of excessive wear, the body's response seems to be to resorption of the bone around the implant. This resorption leads to loosening of the implant and its eventual failure [Willert and Semlitsch 1975, 1977, Howie *et al* 1988, Shanbhag *et al* 1994].

In order to improve the life of total replacement joints, it is obviously necessary to limit the amount of wear debris occurring. Approaches to the problem have been to consider other materials to replace the 'harmful' UHMWPE component, or to improve the design of the present joints to try and limit their wear. Hard bearing surfaces, such as all metal or ceramic joints as used in the earliest designs, are being reconsidered [Semlitsch 1993]. One particular new area of research is compliant layered joints, where the UHMWPE is replaced by a much softer polymer layer on a rigid backing, more closely simulating the natural joint. They have shown to operate with much lower friction and wear than currently used materials [Unsworth *et al* 1987, Auger *et al* 1993].

To understand the potential benefits of compliant layered joints, the fundamentals of tribology should be considered. How are friction and wear caused and what factors have the greatest influence on them? Having identified the most important factors, the materials and geometry of the compliant layered bearing can then be optimised to achieve the best possible tribological performance when implanted. The design must then be rigorously tested under realistic conditions before it can be tested clinically.

The development of compliant layered bearings at Durham is fairly advanced, with suitable materials and geometries identified. To date, the usual method of predicting the performance of replacement joints when implanted has been through testing the joint on a joint simulator. Such machines are designed to imitate the motion and loading characteristics which occur in normal walking and are a useful tool in predicting the life of artificial joints. Their disadvantage is that they are very expensive machines which use actual components in testing, meaning testing iterative changes in designs could be very costly.

The aim of this research was to develop a simplified test method for compliant layered bearings. It had to include all the characteristics of loading and motion which were important to the tribological performance of the bearing so that it results could be used to predict results after implantation. It should also be simple, cheap to construct, easy to use, and use basic component geometries so that different design features and conditions could be examined.

The research began by considering the work of others in this field. Fundamental tribology has been considered and the lubrication mechanisms which occur in natural synovial joints have been discussed along with the experimental studies undertaken to investigate these lubrication mechanisms. The lubrication of conventional replacement joints has then been considered together with the factors affecting their friction and wear. This leads on to the compliant layer concept where its improved tribological performance has been discussed. The development of a numerical solution to model the behaviour of such layers has been presented as well as experimental work carried out to verify the models. A discussion of possible candidate materials for compliant layer bearings then follows. Finally the currently used test methods for assessing materials and designs have been reviewed with a view to developing a simplified test method for compliant layered joints.

Having reviewed the work in the field, a simplified test method has been developed to measure the friction of compliant layered bearings. In order to validate the method, experiments have been undertaken under various conditions and the results obtained compared to those of a hip function friction simulator. The apparatus and test methods used are described in detail in Chapters 3 and 4 respectively. The systematic errors in measuring friction on the two machines has been compared also. A new dimensionless parameter has been defined by which the friction measured on two different machines can be compared.

Contact theory and tribology has been used to predict the factors which influence the friction generated in the compliant layered bearings. With this in mind, the test conditions used (including load, motion, and contact geometry) have been varied to give comparable results on the two machines. In doing this, the most important parameters in achieving equivalence between the two systems have been identified. Having achieved comparable results, the new test method could then be used to assess the effects of various design parameters and test conditions on the friction generated in compliant bearings. The trends found have been again compared to those found on the simulator. Comparisons have also been made with the published results of other authors, and theoretical predictions.

The mechanical properties of the compliant materials have also been briefly considered. In particular, the changes in properties which occur when under physiological conditions have been investigated, and the way in which these changes can affect the tribological performance of the bearing.

In conclusion, the effectiveness of the simplified test method has been discussed. Recommendations have been made as to how the method could be improved and where further work could be undertaken.

2. Review of published work

2.0 Tribology Theory - Friction and Wear

The definition of friction as we know it today goes back to the work of Leonardo de Vinci (circa 1400) and Amontons (1699), and more recently Coulomb (1785). These early researchers considered friction to be mainly due to the interaction of surface asperities on the sliding surfaces. Tabor [1981], however, reported that there are three factors which influence the friction of unlubricated contacts: the true area of contact of the bearing surfaces, the strength of the bond which is formed at the interface, and the shearing of the material around the contacting region. In lubricated contacts, such as natural synovial joints and their replacements, the load is supported by a combination of both the contact between surface asperities and the fluid trapped between the two surfaces, and so the friction is influenced by a fourth factor, the shearing of the lubricant.

The proportion of the load carried by the fluid and by asperity contact defines the lubrication regime in operation. Where all the load is carried by the contact between surface asperities, the mechanism is known as boundary lubrication, as first described by Professor Boys in 1908 and reinforced by the findings of Hardy and Doubleday in 1922. It is so called because the articulating surfaces are lubricated not by free-flowing fluid between them, but by extremely thin boundary layers of lubricant which are formed on the counterfaces and assist their relative sliding. Where no asperity contact occurs and all the load is carried by the lubricating fluid, hydrodynamic or fluid film lubrication is described. In this situation, friction is entirely dependent on the properties of the lubricant, and notably on its dynamic viscosity. This mechanism was first identified by Tower in 1885 and Petrov in 1883, and closely followed by the now classical analytical paper of Reynolds in 1886, in which he produced a simultaneous solution of a reduced form of the Navier-Stokes equation combined with the continuity equation to generate a second order differential equation for the pressure in a fluid in a narrow converging gap between two surfaces [Hamrock 1994]. Johnson and Greenwood [1973] defined the surface separation ratio, λ, such that

$$\lambda = \frac{h_{cen}}{\sigma} \qquad \text{Eqn. 2.1}$$

where h_{cen} was the central thickness of the generated fluid film and σ, the combined roughness of the two surfaces. λ greater than 3 implies fluid film lubrication would occur although other mechanisms have subsequently been proven to allow fluid film lubrication to occur at much lower values of λ [Auger *et al* 1993].

Over the last 40 years, much of the research into tribology has been into defining more precisely the behaviour which occurs between these extremes. One particular advance has been in the discovery that when the pressure in the fluid film is sufficiently high, it can lead to elastic deformation of the bearing surfaces causing an increase in the viscosity of the lubricant and further encouraging the formation of the fluid film. This mechanism is known as elastohydrodynamic lubrication. During the last 20 years, a further development has been in the understanding that between the regimes of boundary and fluid film lubrication, a combination of the two actions, known as partial or mixed lubrication, occurs where the load is partly carried by both the fluid film and the contact between asperities.

The transition from fluid film to boundary via mixed lubrication is most commonly represented by means of a Stribeck curve (Figure 2.1) first presented by Gumbel in 1914 [Dowson 1993]. The Stribeck curve plots the coefficient of friction, μ, (Eqn. 2.2) as a function of a dimensionless group known as the Sommerfeld number, S, defined by equation 2.3

$$\mu = \frac{frictional.\ force}{normal.\ load} \qquad \text{Eqn. 2.2}$$

$$S = \frac{\eta\omega}{P} \qquad \text{Eqn. 2.3}$$

where η, is the lubricant viscosity, ω, the angular velocity of articulation, and P, the load per unit area.

Unsworth *et al* [1974a, b] extended its use to synovial joints by defining a similar dimensionless measure of friction, friction factor, which took into account the variation in frictional torque throughout the joint (Eqn. 2.4)

$$f = \frac{T}{R.L} \qquad \text{Eqn. 2.4}$$

where T is the frictional torque, L the mean load, and R the radius of the joint.

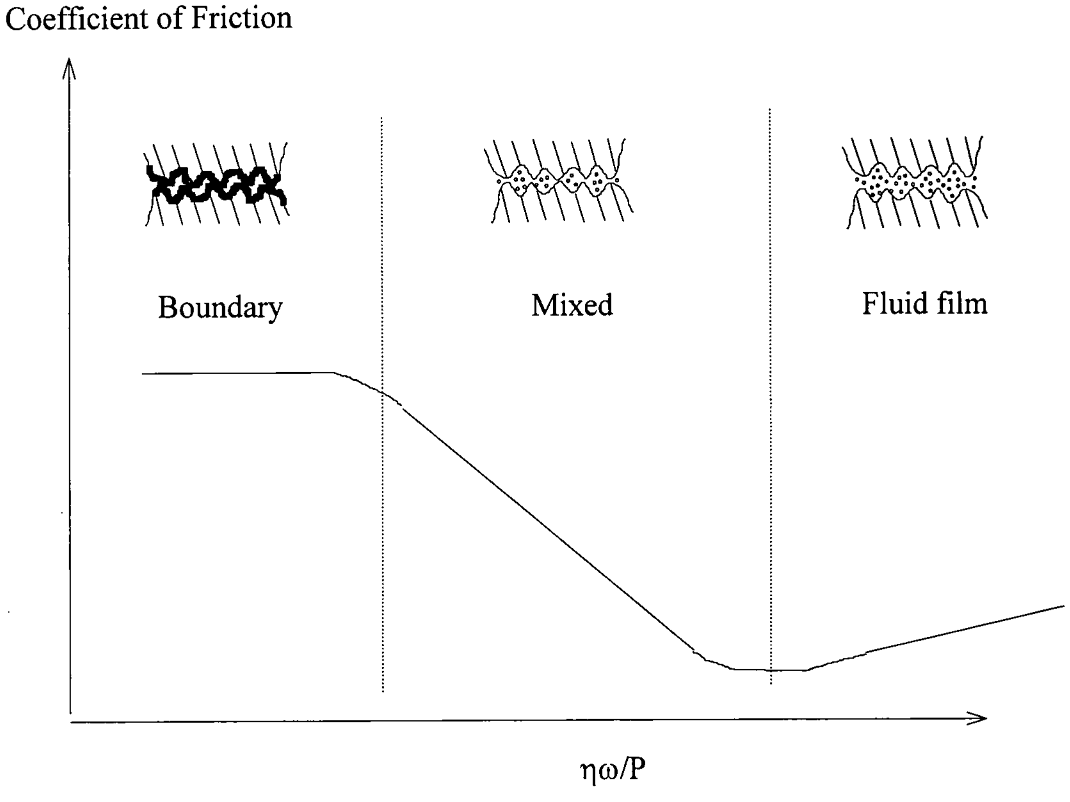

Figure 2.1 Typical Stribeck Curve

Figure 2.1 shows a typical Stribeck curve, distinguishing clearly between the three lubrication regimes. The minimum coefficient of friction, for fluid film lubrication, is 0.001, with boundary lubrication typically giving a value of between 0.1 and 1 depending on the bearing materials. Between these two regimes is the steep curve representing mixed lubrication, showing the significant reduction in friction that can be achieved by promotion of hydrodynamic action, and the substantial increase that can be caused by asperity contact.

Just as the amount of asperity contact determines the friction generated, it is the interaction of the surface asperities which causes wear, as first proposed by Archard in 1953. As one asperity passes over another there is a possibility that it will produce a wear particle, and the probability that this will occur is described by a material's wear factor k (mm^3/Nm) [Dumbleton 1978]. The total volumetric wear , V, has been shown to be

$$V = k.F.x \qquad \text{Eqn. 2.5.}$$

where F is the force supported by the contacts and x the total sliding distance.

This result has been confirmed since in similar derivations by other research groups and by experimental results. These relationships and the other factors which affect the friction and wear will be discussed in more detail with reference to the specific bearing examples of natural and artificial joints.

2.1 Lubrication of natural joints

The human synovial joint represents a unique form of self contained bearing as shown in Figure 2.2. It consists of a layer of elastic, porous cartilage covering each of the bone surfaces surrounded by a protein-rich lubricant, synovial fluid, all contained within a low friction capsule, the synovial membrane.

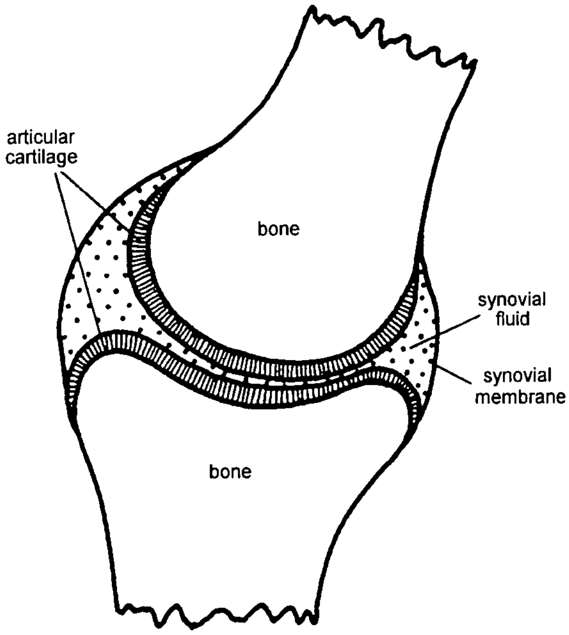
articular
cartilage
bone
synovial
fluid
synovial
membrane
bone

Figure 2.2 The synovial joint

As well as their amazing low friction properties, many of these joints also have a geometry which allows movement in three separate planes: frontal, sagittal and transverse. Considering the human hip joint, it is capable of 74° of abduction-adduction (AA) in the frontal plane, 120° of flexion-extension (FE) in the sagittal plane and 90° of internal-external rotation (IE) in the transverse plane. These motions and their relevant planes are shown in Figure 2.3.

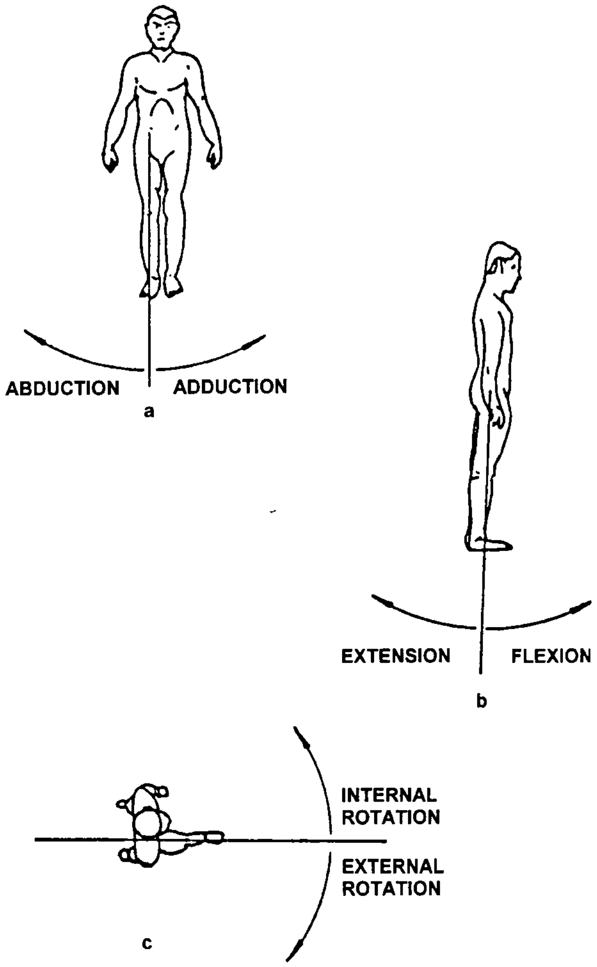

a: frontal plane, b: sagittal plane, c: transverse plane

Figure 2.3 Anatomic planes of motion of the hip [Duff-Barclay and Spillman 1967]

When describing the theory of fluid film lubrication in 1886, Reynolds' remarked on its biological importance, attributing the remarkable tribological characteristics of human and animal joints to this mechanism. MacConnaill [1932] suggested that the anatomy of the joints could give rise to the wedge shaped film required for a successful hydrodynamic regime. These hypotheses were confirmed by the experiments of Jones [1934], in which he showed that a human interphalangeal finger joint in a pendulum machine gave an exponential decay in amplitude with time, concluding there was viscous damping in the joint and hence fluid film lubrication. Charnley [1959, 1960] reached a different conclusion from his similar experiments on cadaveric ankle joints, showing a linear decay in amplitude with time, a result more indicative of solid-solid action and therefore boundary lubrication. He argued that the disparity arose because

Jones had used an intact joint (for improved stability) rather than severing the ligaments as he had, although his results did however yield extremely low coefficients of friction (0.005-0.024) for the suggested boundary lubrication regime. The disparity could equally well have come from the systematic errors incorporated in estimating friction by means of a decay in amplitude of oscillation as later proved by Barnett and Cobold [1962]. They showed Charnley's objection to be correct in testing ankle joints intact and dissected, demonstrating rates of decay characteristic of hydrodynamic and boundary lubrication respectively. When testing a hydrostatic brass bearing though they also showed boundary lubrication to be occurring.

Several workers revived the case for fluid film lubrication in synovial joints, whilst proposing that various mechanisms were responsible for generating and maintaining the fluid film throughout the two phases of a normal walking cycle: the high load, low velocity stance phase and the low load, high velocity swing phase.

The very low coefficients of friction recorded by Charnley led McCutchen [1959] to suggest the concept of 'weeping lubrication', a form of self-pressurising hydrostatic action, relying on the porosity and elasticity of the cartilage to trap pockets of fluid. He argued that pressure on the joint pressurised the pockets of fluid which would then carry at least part of the load. The name 'weeping lubrication' arose from the replenishing of these pockets from the fluid in the bulk of the cartilage. He went on to demonstrate this effect as well as the effect of sustained loading. 'Wringing out' the fluid resulted in an increase in friction [McCutchen 1966], and he subsequently coupled this weeping action with a unique form of boundary lubrication [McCutchen 1967]. Drawing from the work of Ogston and Stanier [1950] on the constituents of synovial fluid, McCutchen suggested whilst the sponge-like nature of the cartilage would explain its very low friction, this would not explain that he had noticed synovial fluid to give much lower friction than other lubricants. He explained this as the action of long chain molecules of hyaluronic acid-protein complexes (mucin) from the synovial fluid attaching themselves to the cartilage surface in loops which could then trap fluid within themselves at an osmotic pressure. McCutchen defined this as osmotic lubrication. This meant that when contact did occur it would be at very low friction unless the surfaces were subjected to heavy constant loading when the pressurised fluid would be squeezed out of the loops. He did not however explain why other long chain molecules could not produce the same effect.

By this time advances in the understanding of the lubrication of heavily-loaded contacts in other engineering applications had generated the theory of elastohydrodynamic lubrication (EHL). Dintenfass [1963] applied this theory to the human joint, and his findings were reinforced by the work of Tanner [1966] and Dowson [1967]. They suggested that whilst it seemed unlikely that the lack of congruity and the reciprocating motion in a human synovial joint would give rise to conditions favourable for hydrodynamic lubrication, it was possible that the deformation of the soft cartilage surfaces could produce the desired 'wedge' effect. Tanner estimated a fluid film thickness in the hip of 10 μm under the entraining action of elastohydrodynamic lubrication, giving rise to a coefficient of friction of 0.003. The fact that this value was lower than seen experimentally of around 0.02 [Charnley 1959] Tanner put down to the fact that he did not include any allowance for the boundary lubrication which may have taken place during the walking cycle. Whilst elastohydrodynamic action could explain the very low friction of synovial joints whilst reasonable entraining velocities were occurring (swing phase), it did not explain the ability of the joint to carry a load under heavy loading and very slow velocities (stance phase) so clearly fluid film lubrication in synovial joints could not be due to elastohydrodynamic action alone.

Mow [1969] suggested that a better term for the lubrication of the synovial joints would be 'elastorheodynamic' as the rheological properties of the cartilage and synovial fluid were also contributory to the joint's lubrication regime. This was echoed by Dintenfass [1963] who indicated that the thixotropic nature of the synovial fluid (its viscosity increased as the shear rate decreased) as well as its affinity with cartilage and its viscoelastic resistance to squeeze were all likely to play an important role in the lubrication of joints, along with the elastic property of cartilage. Linn and Radin [1968] demonstrated the importance of the hyaluronic acid-protein complexes (mucin) by attempting to alter the properties of synovial fluid by various means. They showed that reducing the viscosity of the fluid had no effect on the lubricant but by digesting its constituent proteins, the measured friction was increased markedly. Roberts *et al* [1980] later contradicted this finding showing viscosity to have a greater effect although the disparity may well be due to the unknown nature of the lubricant or the exact effects of the digestion agents. Tests by Walker [1968a] showed that the concentration of hyaluronic acid alone was not important. It would seem that it was the formation of acid-protein complexes which was most important to the lubricating properties of synovial fluid, whether in its effect on the viscosity or the chemical composition.

Maroudas [1967,1969] demonstrated the formation of gels on the cartilage surfaces when subjected to pressure. She suggested that rather than fluid flowing into the joint through the porous cartilage when loaded (weeping lubrication), it flowed out of the cartilage leaving a high viscosity filtrate of hyaluronic acid-protein complexes, too large to fit through the minute cartilage pores. The high viscosity of these gels was then capable of producing the load carrying capacity of the synovial joint in the stance phase. Meanwhile Dowson [1967] and Fein [1967] pointed out the importance of a 'squeeze film' mechanism under dynamic loads, demonstrating that the fluid pressure between the cartilage surfaces allowed a film of fluid to be trapped. Fein measured these films using an interferometric method and showed considerable fluid entrapment and that the squeeze films could be maintained for long periods of time. Dowson [1967] reinforced these findings calculating the elastohydrodynamic action could generate a film of 2μm (as opposed to 1×10^{-4} μm for hydrodynamic action alone) and that it would take 360 seconds of constant loading to decrease this film to the height of the average roughness of cartilage surface, measured by Jones and Walker [1968] to be approx. 1μm. They concluded, as did Fein [1967], that a squeeze film mechanism carried the load when the velocity was low and the load high (stance phase of walking cycle) and this was replenished by hydrodynamic action when the loads were low and the velocity high (swing phase). When squeeze films did collapse the long chain complexes in synovial fluid provided low friction boundary lubrication.

Dowson *et al* [1968] undertook experimental measurement of the friction of cartilage and rubber on glass plates in a reciprocating machine and concluded that the elasticity of cartilage and the squeeze film generated were not responsible alone for the low friction produced in joints, suggesting that the porous nature of the cartilage was also important. Walker *et al* [1968a] suggested that the squeeze film action in joints could be enhanced by an increase in viscosity of the lubricant in keeping with Maroudas's gel lubrication theory for cartilage. Walker and colleagues called this 'boosted lubrication' and reinforced their theories with results from experiments where cartilage was articulated on glass in a reciprocating machine [Walker and Gold 1973]. In another experiment, they 'froze' the generated films using liquid nitrogen [Walker *et al* 1970] to demonstrate film thicknesses of between 0.25 and 10 μm, although they suggested films could be even thicker in parts due to trapped pools of fluid. A mathematical analysis of this 'boosted squeeze film' lubrication by Dowson *et al* [1970] verified its effectiveness in maintaining squeeze films and showed a good correlation with film thicknesses calculated from experimental measurements [Walker *et al* 1970]. They did however, as McCutchen had for his weeping lubrication theory, fail to explain why this boosted squeeze film effect could not be reproduced for other lubricants with large molecule solutes.

The effect of squeeze film in reducing friction was reinforced by the experimental work of Unsworth *et al* [1974a, b] in which they showed suddenly applied loads to produce much lower coefficients of friction in cadaveric joints than constant loads of equivalent magnitudes. Higginson and Norman [1974b], and Higginson [1977, 1978b] all provided further experimental verification of the benefits of squeeze film lubrication. Moreover, they agreed with Walker *et al* [1970] in finding that their experimentally measured film thicknesses often exceeded their theoretical predictions due to the pools of trapped fluid between the cartilage surface asperities.

These early experiments highlighted two interesting observations of the early studies of synovial joints. Firstly, although Walker *et al* [1968a] and McCutchen [1959] relied on the same experimental results, they proposed different theories for the lubrication mechanisms occurring. Secondly, these two studies, undertaken on reciprocating machines, had produced results indicative of fluid film lubrication, whilst experimental work on pendulum machines had suggested either boundary or fluid film lubrication to be the dominant regime in human synovial joints.

Further work in this area provided a solution to both these disparities. Radin and Paul [1972] took a step back and reviewed the theories proposed to date. They found that whilst Fein [1967] and Dowson [1967] had probably been right in suggesting a combination of elastohydrodynamic, squeeze film and boundary lubrication from the hyaluronic acid complexes, the cases for weeping and boundary lubrication were less solid. The cartilage might indeed weep fluid into the gap between the surfaces but this would only be immediately in front of the zone of contact where substantial amounts of fluid had already been entrained. Similarly, under squeeze film action, the concentration of molecules in the fluid could be raised as in 'boosted lubrication' but there was no real evidence for this either. Ling [1974] developed a model of two porous elastic cylindrical discs which demonstrated the co-existence of both weeping and boosted lubrication. However, Higginson and Norman [1974a] stated that the permeability of the cartilage layer was much too low for either weeping or boosted lubrication to be important. Jin and Dowson [1992] subsequently showed porosity to have little effect on film thickness until it becomes very small, and that if anything, porosity depleted the film thickness rather than increasing it, discrediting McCutchen's 'weeping lubrication' theory.

Unsworth *et al* [1975] and Dowson *et al* [1975] pointed out the difficulties in inferring information on lubrication regimes from the results of pendulum machines. They showed that the same joint was capable of achieving fluid film and boundary conditions under different conditions and concluded that the viscous friction term giving rise to an exponential decay (indicative of fluid film) was so small that it could not be accurately measured. They concluded that the errors involved could explain the conflicting results which had been previously obtained, and instead instigated design and development of test methods where the frictional torque could be measured directly. The development of more representative friction measurement techniques, including the first simulators [Unsworth 1974a, b, 1975], using a reciprocating motion, dynamic loading, and direct measurement of frictional torque, have proven irrefutably that natural synovial joints operate with fluid film lubrication, the film being maintained by a combination of squeeze film and hydrodynamic actions [Unsworth 1975, O'Kelly 1978, Roberts 1982].

Numerical modelling of the mechanisms occurring has also added to our understanding of natural joint lubrication. Higginson's analysis of squeeze film [Higginson and Norman 1974b, Higginson and Unsworth 1981] have shown theoretically the possibility of the mechanism. Medley at al [1984a] considered a combination of transient elastohydrodynamic, squeeze film and fluid entraining actions to develop a theoretical model of the human ankle joint and estimate the cyclic variation in film thickness over a typical walking/loading cycle. They calculated that a film thickness of 0.7 μm could be sustained for cartilage with little cyclic variation, but concluded that the possibility of fluid film lubrication could only be supported by very high viscosity lubricants (such as produced through boosted lubrication).

The modelling work of Dowson and Jin [1986, 1987, 1992a, b] and Yao and Unsworth [1993] highlighted an additional lubrication mechanism. Dowson and Jin extended analysis of the elastohydrodynamic action of joints to include micro-elastohydrodynamic effects (micro-EHL), considering a quasi-static model in their first study and a more representative case of physiological loading and walking cycle in the second. For a human ankle model, they found that locally generated high pressures in the fluid film could cause substantial flattening of the surface asperities, allowing fluid film to be generated on surfaces usually assumed to be too rough, i.e. showing inadequate separation. This represented the first theoretical analysis to suggest that fluid film lubrication in a synovial joint was possible although they estimated the wavelength of the cartilage roughness to be of the order of milimetres and so grossly over-estimated the film thicknesses achieved. Yao and Unsworth [1993] extended this analysis to include the effects of both secondary and tertiary roughnesses, in transverse, longitudinal and isotropic directions, showing asperity flattening at all levels and again suggesting, for a more realistic wavelength, that fluid film lubrication was operative with lubricants of physiological viscosity under a dynamic load.

The developments in the understanding of the lubrication of natural joints over the last 50 years have been summarised on numerous occasions in comprehensive review papers, notably Higginson 1978a, Medley at al 1984a, Dowson 1990, Unsworth 1991, and Unsworth 1993. From the extensive published literature we can conclude that the friction of natural joints is influenced by:

- the elasticity, and to a lesser extent the porosity of articular cartilage
- the unique properties of synovial fluid
- the geometry of the joint
- the loading and motion cycles which occur physiologically

Operating in a fluid film lubrication regime, the articular cartilage surfaces theoretically experience zero wear, as minimal contact occurs, although degradation of cartilage through disease is common, roughening its surface finish and reducing its elasticity, as well as affecting the properties of the synovial fluid. In such cases, the load and motion of the joint will influence the wear that occurs as predicted by theory.

2.2 Lubrication of conventional prosthetic joints

In designing the first total replacements for the human synovial joint, early bio-engineers saw two factors to be important: that the material was strong enough to support the load applied, and that it had sufficient resistance to the harsh biological environment to sustain a long working life. With this in mind, the early joints were most commonly sliding pairs of similar metals, usually cobalt molybdenum or medical grade stainless steel, their hardness giving them a good resistance to wear. Over the years use of metal-metal pairings has become more limited due to concerns about the high levels of friction generated because of the ionic attraction between metallic surfaces. In more recent times, wear of the UHMWPE counterface has become the greatest concern and so such hard pairings are gaining favour once more [Semlitsch 1993].

In 1946, Jean and Robert Judet [1950, 1952] introduced an acrylic femoral head for hip hemiarthroplasty, maintaining the natural acetabulum. The squeaking of such joints prompted Charnley to consider the important role of friction and lubrication in replacement joints and to develop his own design [Charnley 1959]. His combination of polytetrafluoroethylene (PTFE) acetabular cup and 22 mm diameter stainless steel femoral head was introduced in 1959 with an aim of reducing the frictional torque by using a reduced head radius and an 'intrinsically slippy' material such as PTFE [Charnley 1961]. Unfortunately, he had not planned for the dramatic wear which PTFE sustained under physiological conditions and after 3 years and 300 operations, use of PTFE was suspended.

Charnley introduced his hugely successful UHMWPE acetabular cup in 1962, replacing the PTFE component of his earlier joint [Charnley 1966, Charnley *et al* 1969]. Although UHMWPE has a higher coefficient of friction than PTFE, it has a much greater wear resistance, and today more than 90% of all prosthetic joints consist of UHMWPE acetabular cups in articulation with hard ceramic or metallic femoral components [Fisher and Dowson 1991]. The UHMWPE-metal joint, as designed by Charnley and Muller, is still the most widely used worldwide today [Murray *et al* 1995].

Since the importance of both the friction and wear of replacement joints were first highlighted, there has been extensive testing of the various joint designs and their constituent materials in simulator and reciprocating materials-testing machines.

2.2.1 Factors affecting friction

Probably the single most important observation made during the extensive studies of the lubrication of synovial joints and their replacements is that, while natural synovial joints enjoy fluid film lubrication, lubrication of artificial joints is primarily through boundary layers, or at best through a combination of both mechanisms in a mixed regime. Unsworth and colleagues noted the importance of the lubricant viscosity [1978] and the loading mechanics in their tests on various joint designs [1974b, 1978], concluding that mixed lubrication occurred under physiological conditions and static loading, but that dynamic loading increased the squeeze film and so encouraged fluid film action. They found that for all joints, the coefficient of friction decreased if the applied load was increased suggesting contact of surfaces and a mixed lubrication regime. O'Kelly *et al* [1977] used the same machine and by using high viscosity silicone fluids, produced a classic Stribeck curve for a Charnley joint, demonstrating the rising trend of full fluid film lubrication for viscosities greater than 0.5 Pa s.

Unsworth *et al*'s tests [1974b, 1978] also showed the significant improvements in coefficient of friction for metal-plastic prostheses such as Charnley's, compared with metal-metal prostheses such as the McKee-Farrar, measuring 0.05 and 0.25 respectively. This reinforced the findings of both Duff Barclay and Spillman [1967] and Scales *et al* [1969] who had noted the coefficient of friction in metal-on-plastic joints to be between 25 to 50% of that of metal-on-metal. Weightman *et al* [1973] conducted a similar comparison of Charnley, Muller (UHMWPE - vitallium) and McKee-Farrar prostheses and showed a less marked result, the material combinations showing similar values of friction for low loads but at higher loads, the coefficient of friction of metal-plastic becoming increasingly lower than the metal-metal. They proposed that this was due to the combination of elastic and plastic deformation of asperities for the polymer, whilst the metal only deformed plastically. They also noted the effect of lubricant, synovial fluid reducing the coefficient of friction of metal-metal joints from 0.55 to 0.12, citing the presence of proteins as an explanation. They concluded that boundary lubrication was predominant. Simon *et al* [1975] demonstrated the beneficial effect of squeeze film in Charnley prostheses. They measured much higher friction under a constant static load than under a dynamic load, and also showed lower friction with synovial fluid than water. They suggested this was either due to the slower squeeze out of the synovial fluid because of its higher viscosity, or a demonstration of its boundary lubricating effect. Contradictorily, Cipera and Medley [1996] showed serum to give higher friction than water for cobalt based alloys against themselves when using a cylinder on flat arrangement in a reciprocating machine.

More recent studies have served to reinforce these early results as well as to introduce the importance of other parameters.

Saikko [1992b] tested 14 metal-UHMWPE and ceramic-UHMWPE combinations of various designs and diameters on a joint simulator and also measured the friction of the pairing on a pin-on-plate materials testing machine. He found that a 22 mm joint gave the lowest friction but that the friction factor was dependent on a combination of many parameters: head diameter, surface finish of counterfaces, material combination, clearance ratio of joint (ratio of radius of head to cup), the thickness of the acetabular cup, and the stiffness of any backing material. He then extended his study of material combinations on a reciprocating machine for Co-Cr-Mo, alumina and other ceramic materials demonstrating mixed lubrication for all. [Saikko 1993b, d].

Other authors have considered various other factors affecting friction. Ceramic femoral heads have since been shown to give a reduction in friction compared to metallic femoral heads [Kumar *et al* 1991, McKellop 1983, Saikko 1993c], which has been suggested because of their superior wettability and resistance to abrasion, although there continue to be concerns over the use of ceramic heads due to the brittle nature of the material. Unsworth *et al* [1994] and Scholes *et al* [1997] have both contradicted these previous findings and shown no benefit of a ceramic head over a metallic head when coupled with UHMWPE. In addition, Unsworth *et al* [1995] showed that in spite of their ability to attract lubricant, ceramic-UHMWPE pairings still showed mixed lubrication. McKellop [1983] showed the roughness of the ceramic counterface to be an important factor, and considered the difference in friction for irradiated and non-irradiated UHMWPE. Whilst he found no significant difference between the values of coefficient of friction measured, Shen and Dumbleton [1974] showed unirradiated polyethylene samples to give the lowest friction due to the transfer of a film of polyethylene onto the metallic surface, not occurring for irradiated samples. McKellop *et al* [1977] compared the friction of various metals, stainless steel, titanium and Co-Cr-Mo, against UHMWPE and showed the titanium and cobalt alloys to give rise to lower coefficients of friction, 0.04 to 0.07 compared to 0.06 to 0.11 for stainless steel.

The work of Hall *et al* [1994] again showed metal-on-plastic joints to articulate with mixed lubrication, showing a decrease in friction factor on the Stribeck curve as the lubricant viscosity was increased. Their subsequent analysis of the new and explanted

Charnley prostheses [Hall *et al* 1994, 1997b, Unsworth *et al* 1995], showed a large proportion (30%) of the explanted joints to have an increased friction factor (greater than 0.16). Cement particles found in the acetabular surfaces were held responsible. However, from clinical records, they found no correlation between increased friction factors and loosening of the joint.

2.2.2 Factors affecting wear

Although UHMWPE has been used extensively now for 30 years and shown to give both low friction and good wear resistance in the laboratory and *in vivo*, there has become increasing concern about the volume of wear debris generated and in particular, the body's response to this debris. Over the last decade, the mechanism of polyethylene wear has been widely investigated, considering the wear rate of UHMWPE under various operating conditions [McKellop 1981, Weightman 1972], in order to pinpoint the important governing factors.

In laboratory tests, the surface roughness of the opposing counterface has been shown to be one of the most important factors in the wear rate of UHMWPE. An increase in roughness from R_a of 0.01 to 0.1 μm gave a 13 fold increase in wear rate [Dowson *et al* 1984], and a single imperfection had a dramatic effect [Dowson *et al* 1987]. These results were achieved however for water lubrication and so have questionable clinical relevance. Subsequently, Weightman and Light [1986] showed that an increase in surface roughness of either alumina or stainless steel counterfaces gave rise to increased friction even when lubricated with bovine serum. Caravia *et al* [1990] demonstrated the damage caused by bone and bone cement particles on stainless steel surfaces and suggested that the increase in counterface roughness caused would give rise to increased polyethylene wear. Hall *et al* [1997b] have subsequently shown that clinical wear factors are affected much less by surface roughness than laboratory wear factors.

Wear rate has been shown to be directly related to contact stress [Rose *et al* 1983, Jin *et al* 1994]. Much higher wear rates were shown when the contact stress was near

UHMWPE's compressive limit [Rostoker and Galante 1979]. Treharne *et al* [1981] showed a similar result for UHMWPE knees, where the measured wear rate increased as the contact area decreased. Barbour *et al* [1995] subsequently confirmed this using a finite element analysis. This has implications on the design of prostheses [Bartel *et al* 1985, 1986]. Head diameters of 22 mm were previously favoured as they produced lower wear volumes but more recently, medium sized heads (28 mm diameter), have been shown to give the same wear volume but lower penetration depth [Livermore *et al* 1990]. Hall *et al* [1997b] raised questions over this result finding that whilst wear rate was directly related to head diameter the penetration depth showed less of a dependence, suggesting that smaller diameter heads (22 mm) would be optimal.

Studies have shown that the dominant mechanisms in the wear of UHMWPE against a smooth counterface were abrasion and fatigue [Nusbaum *et al* 1979, Lancaster 1991] after wear was initiated by adhesion between the surfaces. Many experimental studies have demonstrated a two stage wear process [Brown *et al* 1976]. Abrasion occurred due to the interaction of asperities, but there were many more asperities than the wear particles produced implying that the majority of asperity interactions led to elastic deformation. Over a period of cyclic loading, these deformations induced residual fatigue stress in the polymer surface [Tabor 1987, Lancaster 1990]. Thus, as well as the molecular scale wear particles produced by abrasion, larger scale wear debris was produced from the propagation of surface and sub-surface fatigue cracks [Nusbaum *et al* 1979]. Where the UHMWPE was in sliding contact with a very rough surface, the rate of abrasion meant that the surface was abraded before residual stresses could develop. These mechanisms of abrasion and fatigue have been subsequently described as microscopic and macroscopic wear [Cooper *et al* 1992, 1993b] and Wang *et al* [1995] stated the obvious in suggesting that the transition between these two mechanisms was governed by the mechanical properties of the polyethylene. This would explain to some extent the difference in reported wear rates as even for a particular prosthesis, the mechanical properties of the polyethylene could vary. It has recently been discussed that the relative size of the wear particles may be important to the body's reaction to them, smaller wear particles perhaps being critical in causing bone resorption and so aseptic joint loosening.

The materials of both counterfaces have been shown to have an effect on the UHMWPE wear. The properties of the UHMWPE can have a substantial effect on its wear rate. Increasing the stiffness of polyethylene (and so improving its fatigue properties) was found by Davidson *et al* [1992] to increase the contact stress and so the wear rate of the polyethylene. The moulding conditions of the polyethylene were seen to affect its wear rate by Seedhom *et al* [1973], graphite filling was seen to have a detrimental effect short-term but no long-term effect on polyethylene wear by Rostoker and Galante [1976]. Shen and Dumbleton [1974] demonstrated the detrimental effect of irradiating polyethylene but other authors have subsequently shown the opposite effect as irradiation encourages cross-linking of the polymer and so surface hardening [Jones *et al* 1981, Roe *et al* 1981, Bruck and Mueller 1988]. Various studies have also considered the wear of polyethylene in various modified forms on itself for use in applications under lower loads e.g. finger joint [Atkinson 1976, Stokoe 1990, Sibly and Unsworth 1991, Joyce *et al* 1996].

The material of the hard counterface was also viewed to be important and many studies have demonstrated the improved wear rate of UHMWPE when in sliding contact with a ceramic rather than a metallic counterface [Kumar *et al* 1991, Ben Abdallah and Treheux 1991, Saikko *et al* 1992b, Cooper *et al* 1993, Saikko *et al* 1993c, Saikko 1995]. This was widely recognised to be due to the transfer film of polyethylene which formed on the metallic counterface when water-lubricated, but was not normally encountered on ceramic counterfaces. Once formed, the transfer film roughened the surface of the head creating more abrasive action, and when removed in subsequent motion formed loose particles which then acted as further abrasives within the joint. In a similar way, the lubricant has also been shown to be an important factor in experimental wear rates. Wear surfaces of samples tested in serum have been shown to resemble more closely those found in explanted prostheses [Rose and Radin 1982, McKellop *et al* 1977]. Whilst a transfer film of polyethylene was formed on the hard counterface when lubricated with water this was not found for serum or *in vivo*.

2.3 Compliant Layered Joints

Because of the well-documented problems of UHMWPE wear, the emphasis in recent years has been in the research of alternative materials to replace the UHMWPE counterface. This has led to re-investigation of the properties of both metal and ceramic joints because of their excellent wear resistance. A new approach, however, has been to consider the use of layers of compliant polymers, creating an elastic surface more representative of the natural cartilage and hopefully bringing with it some of its benefits in terms of elastohydrodynamic lubrication [Unsworth *et al* 1981].

2.3.0 Lubrication

Cudworth and Higginson in 1976 first demonstrated the ability of soft elastic layers to extend the fluid film lubrication region of engineering bearings to lower values of $\eta\omega/p$ through micro-elastohydrodynamic action. Medley *et al* [1980b] and Gladstone [1988] suggested the use of an elastomeric layer on a metallic femoral head for hemiarthroplasty but it was Unsworth *et al* [1987] who then took the logical step of incorporating compliant layers into acetabular cups to examine their possible use in replacement hip joints. The study tested prototype acetabular components made from stainless steel lined with different thicknesses of polyurethane 0.5, 1, 2, and 3 mm layers, but all with the same internal diameter. Varying compositions of polyurethane were also examined to consider the effect of hardness of the layer. The friction of these new joints was measured in the Durham hip function simulator under dynamic loading while articulating with a standard 32.25 mm diameter stainless steel ball (radial clearance of all joints 0.25 mm). This was compared with a standard Muller UHMWPE on cobalt chrome molybdenum joint tested in the same way. They concluded that while the Muller prosthesis showed a falling Stribeck curve for increasing lubricant viscosity, for polyurethanes of certain hardness, the coefficient of friction increased with increasing viscosity and so suggested fluid film lubrication was occurring even with low viscosities. Their results pointed to an elastic hardness of 4 N/mm^2 and a 2 mm layer being the optimal configuration.

Unsworth *et al* then extended their work to compare a wider range of conventional and compliant-layered hip prostheses [1988]. They again demonstrated friction results indicative of fluid film lubrication for the compliant-layered joints, and of mixed lubrication for the conventional joints. In addition, they showed that for compliant layer hardness between 4 and 8 N/mm^2 fluid film lubrication could be achieved even at very low viscosities. A coefficient of friction as low as 0.005 was measured, an order of magnitude less than the best conventional prosthesis and two orders of magnitude lower than metal-on-metal.

In Gladstone and Medley's paper of 1990, they used a modified wear-screening apparatus (pin-on-disc configuration) to measure the friction developed between a glass plate and cylindrical pins with compliant silicone rubber layers under constant loading. They showed good agreement between the experimental results and those predicted by a theoretical plane inclined model [Medley and Dowson 1984, Smith and Medley 1986] as well as an increase in coefficient of friction with increasing viscosity suggesting fluid film lubrication was occurring in spite of the non-conforming geometry and constant loading.

Jin and Dowson undertook similar experiments on a similar apparatus using polyurethane pins of different cone angles sliding on a smooth metal plate of different surface finishes to investigate the effect of the geometry of the test specimen, and surface roughness of the counterface on their wear and friction [1993a]. They showed that fluid film lubrication was achieved for the smaller angles (30°), whilst mixed lubrication occurred for the larger angles (55°). The geometry at the edge of the contact restricted the entry of the fluid film. These results were translated to the wear factors obtained, and the pins with smaller cone angles showed less wear than those with larger angles The surface roughness of the counterface was also found to be important in that the smoother metal plates gave lower wear volumes and lower friction than the rougher ones.

Caravia *et al* considered the friction of hard spherical indentors on compliant layers in situations of low velocity or constant loading where mixed or boundary lubrication would prevail. Their first published experiments [1993a, b] considered start-up (after various periods of pre-loading) and steady state friction (during entraining motion) for compliant layers of different elastic moduli and indentors of different surface finish. They showed that the start-up friction was dependent on the pre-loading time up to around 80 seconds when the friction reached a maximum which approached the dry contact value. This implied the majority of fluid had been squeezed from the coupling and a high level of contact was occurring. A lower modulus compliant layer significantly reduced start-up friction. This was explained by an increase in micro-deformation and therefore the amount of trapped fluid. Similarly, the rougher indentor gave the lowest start-up friction again due to more trapped fluid, and in addition less real contact between surfaces. This was in contrast to the steady-state results which showed lowest friction was measured for the smoothest contact, and the lowest modulus material. They concluded that the lower values of coefficient of friction achieved of less than 0.01 suggested a high degree of fluid film lubrication. As theory predicted a film thickness of 0.05 μm under test conditions compared to polyurethane roughness of 0.08, micro-elastohydrodynamic lubrication must have been important.

Following the low friction results achieved for low modulus polyurethane, Caravia *et al* then extended their tests to include low elastic modulus hydrogel materials [1993c]. They showed that under pre-loading, when the fluid film broke down, the coefficient of friction of high modulus polyurethane increased ten-fold, but that lower modulus polyurethane gave lower start-up and steady state friction (μ = 0.04). Decreasing the roughness of the indentor again gave rise to lower friction, although the lowest values of friction were consistently recorded for the hydrogel materials (μ = 0.01). Bovine serum was seen to produce higher friction than deionised water. A fourth study by Caravia *et al* [1995] considered like pairings of hydrogel-hydrogel and polyurethane-polyurethane and showed that while the hydrogel pairing still gave extremely low friction, the polyurethane showed significantly higher friction against itself than against metal or glass.

From these studies, Caravia *et al* concluded that whilst polyurethanes showed excellent lubrication characteristics under entraining motion or light loads, under heavy loads and low sliding velocities compliant layers showed unacceptably high friction (1.0 compared with 0.1 for UHMWPE). Hydrogels however showed much lower friction.

There are two important observations to make concerning these conclusions.

Firstly, although the low friction produced by hydrogels makes them attractive for use as bearing counterfaces, Unsworth *et al* [1987] had an extremely good reason for considering polyurethanes of a certain minimum modulus. Whilst decreasing the modulus of the compliant layer further may have encouraged further elastohydrodynamic and micro-elastohydrodynamic action, the elastic modulus influenced the long-term mechanical strength of the material, and under the harsh cyclic loading environment of the body, it is highly unlikely that a hydrogel material could be developed to withstand a few, let alone over 20 years. Unsworth *et al* [1987] showed that moduli below 4 N/mm^2 actually showed higher coefficients of friction so it could be concluded that it was the porous properties of hydrogels which gave them their excellent lubricating abilities, but this does not detract from the fact that hydrogels have inherently very low elastic moduli, E = 0.5 MPa as compared with 20 MPa for a typical medical grade polyurethane.

Secondly, whilst Caravia *et al* have concluded that polyurethane layers showed unacceptably high friction under certain conditions, in all cases these conditions included a static load. Early studies of the lubrication of synovial joints have already pointed out the enormous importance of the squeeze film mechanism in maintaining fluid film lubrication [Unsworth 1974a, O'Kelly 1978, Roberts 1982] and so it is not unexpected that other compliant materials such as polyurethane would show very high friction if the load were applied statically and the squeeze film action removed. It is almost surprising to see how low the friction measured under such conditions was (μ = 0.04) under the purely hydrodynamic action of the entraining motion. In addition, in all tests, Caravia *et al* [1993a, b, c, 1995] use a non-reciprocating motion in one direction only, considering only one cycle even in their 'steady-state' measurements and so the application of any of their results to the *in vivo* situation is questionable. It would seem sensible to this author that if compliant layers were to be considered for use in arthroplasty, an attempt should be made to test them under conditions approximating those *in vivo*.

More representative tests of compliant layers in hip and knee prostheses have been described by several workers. Auger *et al* [1993, 1995a] considered two elastohydrodynamically equivalent (same theoretical contact areas and fluid film thicknesses) hip joints: one including an UHMWPE component, and the other, a 'cushion cup' including a low modulus layer. They were both tested in a simulator apparatus in articulation with the same ball component (radius 15.86 mm) under approximated physiological loading and motion cycles. They found that whilst a minimum friction factor of 0.017 was recorded for the UHMWPE cup, a minimum of 0.003 was recorded for the 'cushion cup'. The friction factor was consistently less than 0.01 throughout the cycle. They concluded that such low values of friction were consistent with fluid film lubrication, the film being preserved by micro-elastohydrodynamic action. They compared their results to the theoretical predictions of Dowson *et al* [1991] and Jin *et al* [1993b] to show that micro-elastohydrodynamic lubrication must be responsible for the reduced friction in the polyurethane cup. They predicted that the polyurethane roughness would be smoothed by 1 MPa of fluid pressure, whereas 8 MPa would be expected in the cushion cup under simulator conditions. The higher elastic modulus of the polyethylene cup would require 100 MPa to smooth its asperities, and only 10 MPa was generated in normal use. Ikeuchi *et al* [1993a, b] also investigated the effect of varying the elastic modulus of the compliant layer and again demonstrated the benefits of compliant polyurethane layers over UHMWPE. Burgess *et al* [1997] considered compliant polyurethane layered components in a similar experiment examining the effects of different elastic modulus of the layer as well as varying the clearance of the cup. They found that a 38 MPa layer showed the lowest friction ($\mu = 0.008$) and that a optimum clearance could be seen, depending on the modulus, to minimise grabbing between the bearing surfaces and yet maximise the elastohydrodynamic effectiveness. They also suggested that creep of the compliant layers could be important as the cups appeared to have different internal diameters before and after testing. Stewart and Fisher [1996] have considered similar compliant layered bearings for knees and again showed them to operate with fluid film lubrication and extremely low coefficients of friction, finding a 4 mm layer of 20 MPa elastic modulus to give optimal performance.

Dowson *et al* [1991] outlined 4 main advantages in the lubrication of the cushion form joint:

- its elasticity - encouraging elastohydrodynamic and micro-elastohydrodynamic lubrication,
- its ability to trap pockets of fluid and so improve squeeze film lubrication,
- its ability to deform to accommodate any out-of-roundness,
- the different contact stress distribution - cushion form bearings showing lower stress near the surface and so being less prone to fatigue damage than UHMWPE.

2.3.1 Contact Mechanics of Compliant Layers

In addition to the work highlighted above where the friction of compliant layered bearings has been measured experimentally, numerous studies have predicted the thickness of the fluid film and the area of contact which occurs between the surfaces and from this indirectly calculated the friction occurring and so the lubrication mechanism in operation. Theoretical models have been derived from Reynolds' original solution of Navier-Stokes and continuity equations, adding the effects of the elasticity and thickness of the layer, and have been used to predict the contact area, film thickness, and friction, as well as contact stresses generated in the layer. Experimental methods have also been developed, using optical interferometry and electrical resistance methods, in which the film thickness was measured, and by comparison, used to verify the theoretical models.

2.3.1.1 Numerical solutions

The work of Hooke and O'Donoghue [1972] is a widely referred to numerical analysis of the elastohydrodynamic lubrication of soft, deformed contacts. They considered the compliant material to be a semi-infinite solid and a line contact to occur. By analysing the inlet and outlet conditions of the bearing separately, the theoretical minimum film thickness was calculated. Their solution was validated for Hertzian contact conditions by comparison with other models, and then applied to specific bearings including a cylinder sliding on an elastomeric surface. They estimated the minimum film thickness to be given by

$$h_{\min} = 2.12R\left\{\frac{\eta u}{ER}\right\}^{0.6}\left\{\frac{W}{ER}\right\}^{-0.2} \qquad \text{Eqn. 2.6.}$$

where h was the viscosity of the lubricant, u the entraining velocity of the fluid, W the applied load on the joint. R_1 is the equivalent radius of the joint calculated from the R1, the radius of the femoral component and R_2 the radius of the acetabular component as shown in equation 2.7. E^* is the combined elastic modulus allowing for the elastic modulus, E_1, E_2, and the Poisson's ratios, ν_1, ν_2, of the femoral and acetabular components as given by equation 2.8.

$$R = \frac{R_1 R_2}{R_1 + R_2} \qquad \text{Eqn. 2.7.}$$

$$E^* = \frac{2}{\left(\dfrac{1-\nu_1^2}{E_1} + \dfrac{1-\nu_2^2}{E_2}\right)} \qquad \text{Eqn. 2.8.}$$

Hamrock and Dowson [1976a] derived a simultaneous solution of Reynolds' equation and the elasticity equations to evaluate numerically an isothermal elastohydrodynamic point contact, by dividing the contact zone into rectangular areas assuming a uniform pressure over each area. (The point contact was more applicable to hip joints than the previously considered line contact.) They then extended their model to other values of the ellipticity parameter [Hamrock and Dowson 1976b], before applying it to fully-flooded and starved lubrication scenarios [Hamrock and Dowson 1976c, 1977]. For the fully-flooded scenario, they investigated the influence of the ellipticity parameter, k^*, the dimensionless speed, load and material parameters on the minimum film thickness and by studying 34 cases, fitting a least squares fit to the data they achieved the following empirical relationship,

$$h_{\min} = 3.63R\left\{\frac{\eta u}{E^*R}\right\}^{0.68}\left\{\frac{E^*}{p}\right\}^{0.49}\left\{\frac{W}{E^*R}\right\}^{-0.073}(1-e^{-0.68k^*}) \qquad \text{Eqn. 2.9.}$$

$$\text{where } k^* = 1.03\left(\frac{a}{b}\right)^{0.64} \qquad \text{Eqn. 2.10.}$$

This implied the speed to be the most important parameter in determining film thickness.

Hamrock and Dowson continued this work to produce the first complete numerical solution of elastohydrodynamic lubrication of elliptical contacts for materials of a low modulus in 1978. They then used this solution to calculate $h_{\min}$ in 17 cases and by curve fitting, obtained empirical formulae for central and minimum film thickness.

$$h_{\min} = 7.43R\left\{\frac{\eta u}{E^*R}\right\}^{0.65}\left\{\frac{W}{E^*R^2}\right\}^{-0.21}(1-0.85e^{-0.31k}) \qquad \text{Eqn. 2.11.}$$

$$h_{cen} = 7.32R\left\{\frac{\eta u}{E^*R}\right\}^{0.64}\left\{\frac{W}{E^*R^2}\right\}^{-0.22}(1-0.72e^{-0.28k}) \qquad \text{Eqn. 2.12.}$$

It is interesting to note that in this set of formulae the material parameter is no longer included as pressure was shown to have a negligible effect on viscosity and the material's elasticity is automatically included through calculating the contact area.

Medley *et al* [1984b] performed a similar solution of Reynolds' equation, using a plane strain column model, this time allowing for transient variation in film pressure and therefore elastic deformation, in order to develop a model of the cyclic variation in film thickness in the human ankle joint. They then simplified his solution for a model with a plane inclined surface. A remarkable agreement was shown between the results achieved for the cylindrical model of the ankle joint and the plane inclined model which was judged to give a very reasonable approximation of an otherwise very complex lubrication situation. Although the film thicknesses calculated were less than the roughnesses of the surfaces, Stribeck style plots of the predicted friction showed a rising trend characteristic of fluid film lubrication. By considering 8 specific cases they developed an empirical formula for aspect ratios of $a/h_T>2$

$$h_{\min} = 1.76R\left\{\frac{\eta u}{E^*R}\right\}^{0.6}\left\{\frac{W}{E^*R}\right\}^{-0.2}\left\{\frac{h_T}{a}\right\}^{0.4875} \qquad \text{Eqn. 2.13.}$$

Up to this stage, the analyses had been limited to studying semi-infinite solids, but Dowson and Yao's work [1990] took the numerical modelling a step further by considering finite thickness compliant layers mounted on rigid backings, again using a plane strain column model. Their solution was valid for $a/h_T >10$. In addition to the complete numerical solutions generated, they also indicated correction factors which could be incorporated to allow for side leakage effects. For the same operating conditions, this model gave a minimum film thickness of 3.02 μm compared to 9.57 for the Hamrock and Dowson model, representing the effect of a finite layer thickness as opposed to a semi-infinite solid. A minimum film thickness of around 1 μm was predicted for the hip joint.

Dowson *et al* [1991] applied the plane strain column model used by Medley *et al* to an elliptical contact to gain the expression,

$$h_{\min} = 1.37R\left\{\frac{\eta u}{E^*R}\right\}^{0.56}\left\{\frac{W}{E^*R^2}\right\}^{-0.19}\left\{\frac{h_T}{R}\right\}^{0.37} \qquad \text{Eqn. 2.14.}$$

This model, as with all previous models, was restricted to compliant materials with a Poisson's ratio less than 0.4, while articular cartilage and suitable polyurethanes have Poisson's ratios closer to 0.5 than 0.4. In order to produce a more accurate approximation, an adjusted value of the effective elastic modulus (E_{adj}) was calculated to give a dry contact area from the column model with Poisson's ratio of 0.4, identical to that for the full elasticity solution with Poisson's ratio of 0.5 allowing incompressible layers to be considered.

$$E_{adj} = \frac{4LRh_T}{\pi a^4}\left\{\frac{(1 + \nu_2)(1 - 2\nu_2)}{1 - \nu_2}\right\} \qquad \text{Eqn. 2.15.}$$

where a is the contact half-radius given by

$$a = 0.94h_T^{0.38}\left(\frac{LR}{E_2}\right)^{0.21} \qquad \text{Eqn. 2.16.}$$

The modulus terms are then given by Hertzian contact theory:

$$\frac{1}{E'} = \frac{1-\nu_2^2}{E_{adj}} \qquad \text{Eqn. 2.17.}$$

$$\frac{1}{E''} = \frac{(1+\nu_2)(1-2\nu_2)}{(1-\nu_2)E_{adj}} \qquad \text{where } \nu_2 = 0.4 \text{ throughout} \qquad \text{Eqn. 2.18.}$$

The model was used to evaluate the effects of the different design parameters on the minimum elastohydrodynamic film thickness, squeeze film thickness, contact area and elastic deformation and an optimal design specification for a 'cushion' form joint suggested. For a 1 MPa contact pressure, it was calculated that the cushion-form bearing would have a minimum film thickness of 0.25 μm compared with 0.034 μm for a UHMWPE joint.

Dowson and Jin [1992a] then extended their earlier work to include the effects of micro-elastohydrodynamic lubrication to produce firstly a simplified two-dimensional solution for a compliant wavy layered surface bonded to a rigid backing, followed by a complete numerical solution incorporating the full elasticity model [Dowson and Jin 1992b]. Good agreement between the two models was obtained and so the authors suggested that the simpler model was the more suitable in view of the computing time of the more complete solution.

Simplified equations for line contact of incompressible and compressible elastic layers bonded to a rigid cylindrical substrate under entraining motion was provided by Jin *et al* [1993], using Eqn 2.17, the minimum film thickness for incompressible layers being given by:

$$h_{\min} = 1.85R\left\{\frac{\eta u}{E'R}\right\}^{0.5}\left\{\frac{W}{E'R^2}\right\}^{-0.3}\left\{\frac{h_T}{R}\right\}^{0.6} \qquad \text{Eqn. 2.19.}$$

They found excellent agreement between their simplified solution and more complex full numerical solutions except where elastic deformation was very small i.e. the load was low and the elastic modulus high. Furthermore they showed little difference between the compressible and incompressible layer solutions provided the corresponding dry contact half-width was used (as in Dowson's adjusted modulus calculation).

Jin *et al* [1993b, c] provided an alternative method to the full numerical solution of Dowson and Yao [1990] using the principle of superposition to combine the film thickness equations for entraining motion and squeeze film to give the transient film thickness in a point contact under dynamic conditions. A solution of the now-familiar form was again produced

$$h_{\min} = 1.25R\left\{\frac{\eta u}{E'R}\right\}^{0.52}\left\{\frac{W}{E'R^2}\right\}^{-0.15}\left\{\frac{h_T}{R}\right\}^{0.37} \qquad \text{Eqn. 2.20.}$$

which showed excellent agreement with the full numerical solution [Dowson and Yao 1990]. Their results also confirmed those of Medley *et al* [1984a] in that squeeze film was important in the first half-cycle when loads were high and velocity low, and entraining action important in the second half-cycle when loads were low and velocities high, over the whole cycle an almost constant, continuous film thickness of 0.7 μm was maintained.

Formulae used in this research

The two part study by Dowson and Yao [1994 a, b] considered rigidly-backed soft layers at elliptical contacts, considering first an elasticity analysis and then a film thickness analysis. In the elasticity analysis they produced a generalised solution before considering the effect of imposing certain limitations. They concluded that for Poisson's ratio greater than 0.4 a rigorous solution must be used if high accuracy is required, but for ν less than 0.4, the column model could be used where the aspect ratio was large and that for small aspect ratios a semi-infinite solution became applicable. In the film thickness analysis, they use a constrained column model of elasticity along with the Reynolds's equation for an elliptical contact to evaluate 21 specific cases and so develop the usual empirical equation for the minimum and central film thickness, this time including a new 'layer' parameter.

$$h_{\min} = 1.59R\left\{\frac{\eta u}{E'R}\right\}^{0.56}\left\{\frac{W}{E'R^2}\right\}^{-0.20}\left\{\frac{h_T E'}{E''R}\right\}^{0.36} \qquad \text{Eqn. 2.21.}$$

$$h_{cen} = 1.68R\left\{\frac{\eta u}{E'R}\right\}^{0.54}\left\{\frac{W}{E'R^2}\right\}^{-0.18}\left\{\frac{h_T E'}{E''R}\right\}^{0.37} \qquad \text{Eqn. 2.22}$$

By using Dowson's adjusted moduli [Dowson *et al* 1991], equations 2.17 and 2.18, these equations apply to incompressible (ν = 0.5) soft layers of finite thickness bonded to rigid backing at point contacts, and so can be applied to hip joints or pin-on-plate situations provided the aspect ratio is greater than 5 and so provide arguably the most valid simple model. The study also produced more general solutions for ellipticity parameters between 1 and 24 and showed that the film thickness increased as the ellipticity increased. Minimal and central film thicknesses of 0.59 and 0.84 μm respectively were calculated for a hip joint under normal conditions and values of 0.43 and 0.63 μm respectively for a knee joint.

The above equations, 2.21 and 2.22, have been used to predict theoretically the elastohydrodynamic film thicknesses generated for compliant layers under spherical indentors under all the test conditions considered in the course of this research. In the experiments described in Chapter 8, a simple cylinder was used in tests to investigate the tribology of compliant layered bearings in a line contact, which would be more representative of a knee joint. Dowson and Yao [1994a, b] also provided expressions for the film thickness in the more complicated case of an elliptical contact. The entraining action is along the minor axis and in the case of knee joints, the load would be distributed over two condyles. The same adjusted modulus scheme was used as for hips as given in equations 2.15, 2.17 and 2.18.

$$h_{\min} = 3.54R\left\{\frac{\eta u}{E'R}\right\}^{0.56}\left\{\frac{h_T E'}{E''R}\right\}^{0.36}\left\{\frac{W}{E'R^2}\right\}^{-0.20}(1-0.64e^{-0.15k}) \qquad \text{Eqn. 2.23.}$$

$$h_{cen} = 3.66R\left\{\frac{\eta u}{E'R}\right\}^{0.54}\left\{\frac{h_T E'}{E''R}\right\}^{0.37}\left\{\frac{W}{E'R^2}\right\}^{-0.18}(1-0.61e^{-0.12k}) \qquad \text{Eqn. 2.24.}$$

where k is the ellipticity ratio a/b where a and b are the contact half-length and half-width of the contact in the major and minor axes. In the case of a simple cylinder the contact area is rectangular and so a is simply the half the length of the cylinder or elastic counterface (whichever is smaller). The half-width of the area, b, (in the axis of entraining motion) is given by

$$b = \sqrt{\frac{4P}{R_{cyl}}} \qquad \text{Eqn. 2.25.}$$

where P is the applied load per unit length R_{cyl} is the radius of the cylinder and k_1 and k_2 are given by

$$k_1 = \frac{1 - \nu_1^2}{\pi E_1},\ k_2 = \frac{1 - \nu_2^2}{\pi E_2} \quad \text{[Timoshenko and Goodier 1970]} \qquad \text{Eqn. 2.26..}$$

The other condition considered during this research was the use of a harder bearing surface such as UHMWPE. The generated film thicknesses for a material such as UHMWPE requires less extensive analysis as the problems of elastomeric layers and high Poisson's ratios are not involved and so can be found from the formulae of Hamrock and Dowson [1978] as given in equation 2.27 and 2.28.

$$h_{\min} = 2.798R\left\{\frac{\eta u}{E^*R}\right\}^{0.65}\left\{\frac{W}{E^*R^2}\right\}^{-0.21} \qquad \text{Eqn. 2.27}$$

$$h_{cen} = 3.337R\left\{\frac{\eta u}{E^*R}\right\}^{0.64}\left\{\frac{W}{E^*R^2}\right\}^{-0.22} \qquad \text{Eqn. 2.28}$$

Having estimated the central film thickness for a particular condition from the appropriate equation, the theoretical coefficient of friction can then be calculated from equation 2.29 using the shear stress relationship for a Newtonian fluid [Auger et al 1993]. The relation assumes that the film of lubricant is the same shape as the dry contact area given by the relative Hertzian contact area equation above (2.16 for spheres, 2.25 for simple cylinder).

$$\mu = \frac{\pi a^2 \eta \frac{u}{h_{cen}}}{W} \qquad \text{Eqn. 2.29}$$

This relationship has been used to estimate the theroretical coefficient of friction under all conditions tested in order to compare theoretical predictions with experimental results.

In addition to elastohydrodynamic film thickness predictions, the work of Yao and Unsworth [1993] allows a theoretical prediction of the minimum micro-elastohydrodynamic film thickness generated. Their work considered various types of waviness, of which isotropic is the most relevant to the bearings used in this research and equation 2.30 gives an expression for the minimum film thickness generated $h_{\mu,min}$ where λ_c is the correlation length of the surface roughness (typ. 100 μm for PU). The theoretical maximum coefficient of friction according to micro-elastohydrodynamic theory can be estimated by substituting $h_{\mu,min}$ for h_{cen} in equation 2.29.

$$h_{\mu,\min} = 1.94\left\{\frac{\eta u\left(1-v_2^2\right)}{E_2}\right\}^{0.65}\left\{\frac{\lambda^2}{4\pi^2\sigma_2}\right\}^{0.77}\left(\lambda_c\left(\sigma_2 - h_{\min} + h_{\mu,\min}\right)\right)^{-0.21} \qquad \text{Eqn. 2.30.}$$

It should be noted that this expression derives from the asperity lubrication model of Yao and Unsworth [1993] and so becomes more accurate as the wavelength shortens and the roughness increases. Examining the expression suggest that it has no real roots when the predicted elastohydrodynamic film thickness, h_{min}, exceeds the amplitude of the compliant surface roughness σ_2. Since the surface asperities will be smoothed by EHL and micro-EHL effects, the theory is only valid therefore for low viscosity lubricants, typically 0.1 Pa s or less.

Finite Element Analyses

Although the solutions described above have a wider application to different cases, it should be noted that a number of workers have used finite element methods to consider the contact mechanics, in particular contact stress, of compliant layers in specific situations. Although only applicable to individual cases, these methods do allow the true geometry of the contact to be considered and so present some interesting results. Jin and Dowson [1991] showed good agreement with other methods and showed that unlike the UHMWPE joint where the maximum shear stress was found at the surface, compliant layered joints showed a maximum at the interface between compliant layer and rigid backing, highlighting this as the most probable point of failure. Unsworth and Strozzi [1995] used a similar analysis to consider the effects of radial clearance and Poisson's ratio showing that the maximum pressure and shear stress increased as the clearance increased, and that by reducing Poisson's ratio, layer deflections increased so maintaining other parameters at a constant value. The authors demonstrated differences between the finite element model and other asymptotic solutions and so stressed the use of finite element methods in the design of joints. Strozzi and Unsworth [1994] used the same model to consider the effects of layer thickness and an optimal layer thickness of 2 mm is suggested, in agreement with experimental results [Unsworth *et al* 1988]. A formula for the minimum film thickness was also derived.

2.3.1.2 Experimental Measurement

Theoretical predictions of film thickness and contact area have been validated by comparison with values obtained by experimental measurement techniques.

The most common technique for measurement of fluid film thickness is optical interferometry where a glass surface is used against a compliant layered counterface so that a laser light can be shone through it and the fluid film to produce interference fringes. This method has been used by various workers. Varnam and Hooke [1977] used such a method for a glass plate and compliant layered cylinder to verify Hooke and O'Donoghue's [1972] theoretical predictions, showing excellent agreement for Newtonian fluids. Visscher *et al* [1993] used a similar technique to measure the roughness deformation of a rough elastomer in contact with a smooth glass plate. They showed that for lubricated contacts, after initial flattening, increasing the load did not affect the roughness deformation, since the load was carried by the fluid not the surface. They concluded that although the deformation of the elastic surface could be measured, the real area of contact between the two surfaces could not be accurately estimated due to the unknown levels of secondary and tertiary waviness which could occur.

Jin *et al* [1994b, c] used optical interferometry to measure lubricating film thickness under steady state entraining motion and squeeze film motion on a rotating disc machine. For entraining motion, the results showed good agreement with theoretical predictions [Dowson and Yao 1994 a, b] and that increasing the load (10-18.5 N) had only small negative effects (10%) on the film thickness generated. For a low viscosity fluid, the coefficient of friction was measured as 0.005 compared with a theoretical prediction of 0.003. Under squeeze film motion, both thin and thick layers showed good agreement with theory [Dowson 1970]. Measured values of film thickness were consistently slightly larger than theory due to the formation of a central pocket of fluid. Thin elastic layers were shown to produce almost uniform film thicknesses, whilst thick layers showed a large central dimple or pocket of fluid, giving a fluid film thickness very different from the theoretical prediction. With reference to the design of joints, which typically incorporate quite thin films, this result would suggest that modifying the layer thickness to incorporate larger fluid pockets would be beneficial for squeeze film action. McClure *et al* [1996] used the optical interferometry method to measure the film thickness generated for hydrogels and polyurethanes again under entraining and squeeze film actions. They again showed that for film thicknesses above 0.15 μm, the film thickness generated for entraining action showed good agreement with theory [Yao 1994, Yao and Dowson 1994], whilst under squeeze film action measured values consistently outperformed theory because of the central pocket. They showed that for longer loading periods and thinner films, fluid films on hydrogels quickly became depleted due to their porosity and so other mechanisms must be important in the low friction recorded for these materials.

The film thickness generated in knee prostheses during walking motion was determined by Murakami *et al* [1993] using an electrical resistance method. The method measured the electrical resistance between bearing surfaces, 1 being complete separation or maintenance of a fluid film, and 0 being solid-solid contact or mixed lubrication. It should be noted that this method did not differentiate between mixed and boundary regimes. Anatomical UHMWPE, cylindrical UHMWPE and anatomical compliant layered joints were considered. The anatomical UHMWPE joint showed mixed lubrication throughout, the cylindrical UHMWPE showed separation but contact at low viscosities, whilst the compliant layered joint showed separation even at the lowest viscosities.

A photographic technique was used by O'Carroll *et al* [1990] to measure the contact area between a very soft elastomer layer (E = 3 MPa) and an optically transparent indentor. Close agreement between experiment and theory was found for loads up to 300 N although at higher loads experimental values were lower than predicted. In all cases, the dry contact area was less than the lubricated contact area. Yao and Seedhom [1991] used a carbon black suspension squeezed from between bearing surfaces to measure the contact area in ankle joints. This method was used to show that the contact area increased with increasing load, load time, or decreasing elastic modulus and then to predict the contact area in an ankle joint at various stages throughout the walking cycle.

2.3.3 Medical grade polyurethanes and other possible materials

Compliant layer bearing research had considered various possibilities in the search for a suitable material. The four main contenders were [McMillin 1994]:

- silicone rubbers
- olefin based rubbers
- hydrogels
- polyurethanes.

Silicone rubbers had a proven in vivo record in many applications (including finger prostheses and tubing) [Pinchuk 1994] but due to their hydrophobic nature could be problematic in bearings. Following controversy over the safety of their use in breast implants, the main manufacturer, Dow Corning, withdrew many such materials from the market.

McMillin [1994] described a range of olefin based rubbers suitable for biomedical applications. Whilst they were biostable and possessed superior mechanical properties to silicone rubbers, they did not have a proven in vivo record and so would require extensive investigation of their biostability.

Bray and Merrill [1973] considered the use of hydrogels, as used in soft contact lenses but found them to have very poor mechanical properties (tensile modulus 0.3 - 4.6 MPa). More recent research, notably at Aston University, investigated improving their mechanical performance whilst retaining their high water content. Corkhill et al [1990] describe the introduction of an interpenetrating polymer network into the hydrophilic polymer to produce a hydrogel with a tensile modulus similar to polyurethanes (90 MPa). Caravia et al [1993a, b, c, 1995] demonstrated their superior frictional performance over polyurethanes. Their fatigue properties were still unproved, however, and so current hydrogels were not considered suitable for a compliant layered joint application.

The majority of research on compliant layered bearings focused on polyurethanes. They had superior mechanical properties to rubbers and hydrogels and had been used extensively in a wide range of in vivo applications, including catheters, heart valves and pacemaker leads. They have been reviewed in detail by various experts in the field, notably McMillin [1994], Pinchuk [1994], and Stokes et al [1995]. A brief discussion of their chemistry, their disadvantages, and the most recent technology is provided here.

2.3.3.1 Polyurethane Elastomer Chemistry

A urethane was made by the addition of an isocyanate to a hydroxyl. In this form it was unsuitable for biomedical applications. This hard segment was then reacted with a soft segment of polyester or polyether diol to give a flexible prepolymer. This prepolymer was extended by the addition of a chain extender. The three components of the polyurethane were known as the diisocyanate, the macrodiol (or macroglycol), and the chain extender. The specific chemistry and concentration of these three fractions gave the polyurethane its specific properties. Depending on the ratio of hard to soft segments, the polyurethane could be as soft as a balloon or as hard as a bristle brush [Corvita 1993, Stokes et al 1995]. Figure 2.4 gives a schematic representation of the process.

Diisocyanate

The diisocyanate formed the hard segment of the polyurethane. There were 2 classes of isocyanate: aromatic (MDI) and aliphatic (HMDI) as shown in Figure 2.5.

Aliphatic diisocyanates were more easily degraded so aromatic diisocyanates were more commonly used in biomedical applications, in spite of a questionable risk of the leaching out of carcinogens by the aromatic group [Pinchuk 1994].

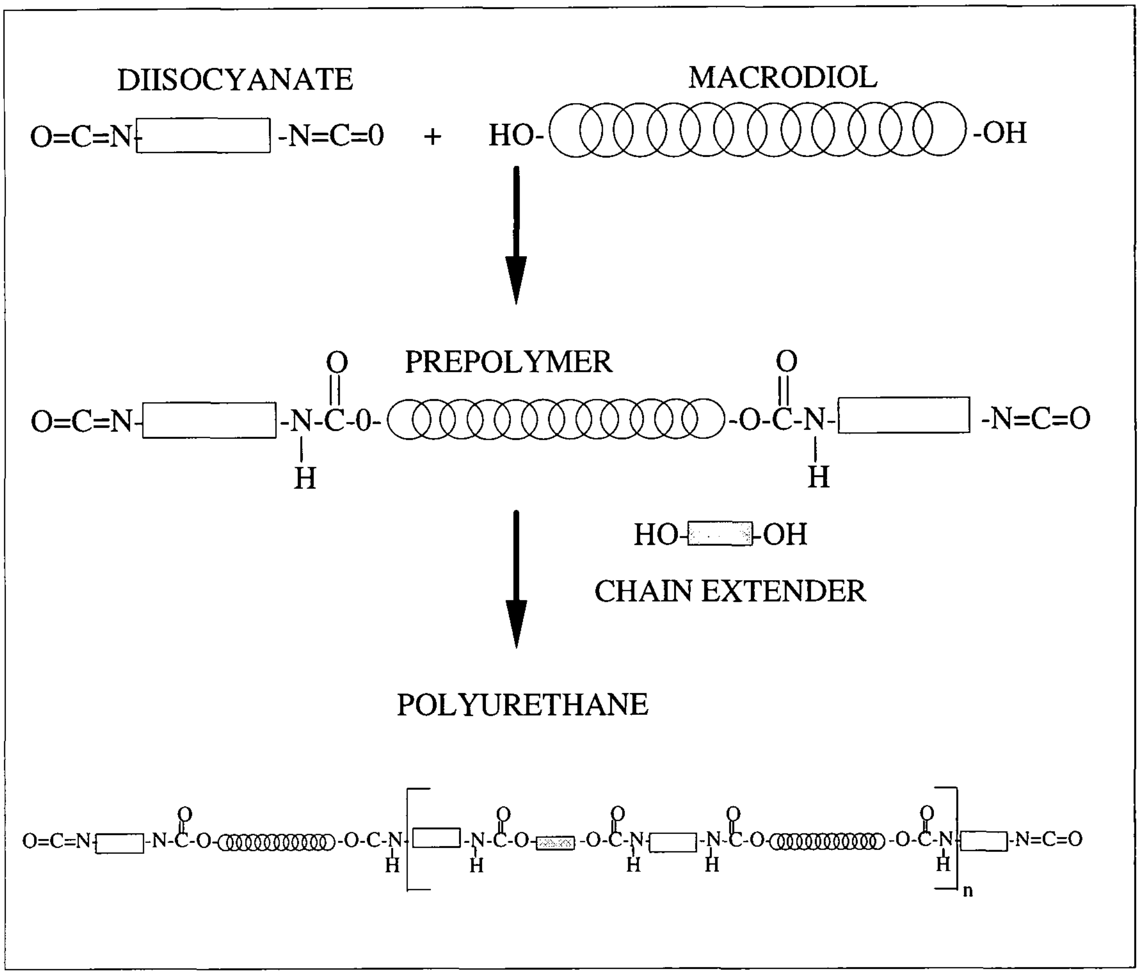
DIISOCYANATE
O=C=N-N=C=0
+
MACRODIOL
HO-OH
PREPOLYMER
O=C=N-N-C-0-O-C-N-N=C=O
HO-OH
CHAIN EXTENDER
POLYURETHANE
n

Figure 2.4 Schematic diagram of polyurethane reactions [Corvita 1993]

Macrodiols

The macrodiols (or macroglycols) represented the soft segment of the polyurethane giving them their flexibility. There were two main classes: polyesters and polyethers, both with inherent advantages and disadvantages. Polyester polyurethanes constituted the bulk of industrial polyurethane use but the ester linkages were susceptible to hydrolytic degradation and so could not be used in implants. Polyetherurethanes were not susceptible to degradation by water but did experience autoxidation when in direct contact with tissue due to the action of enzymes and oxidants. Autoxidation itself had been shown to be a surface phenomenon and so did not affect the bulk properties of the material.

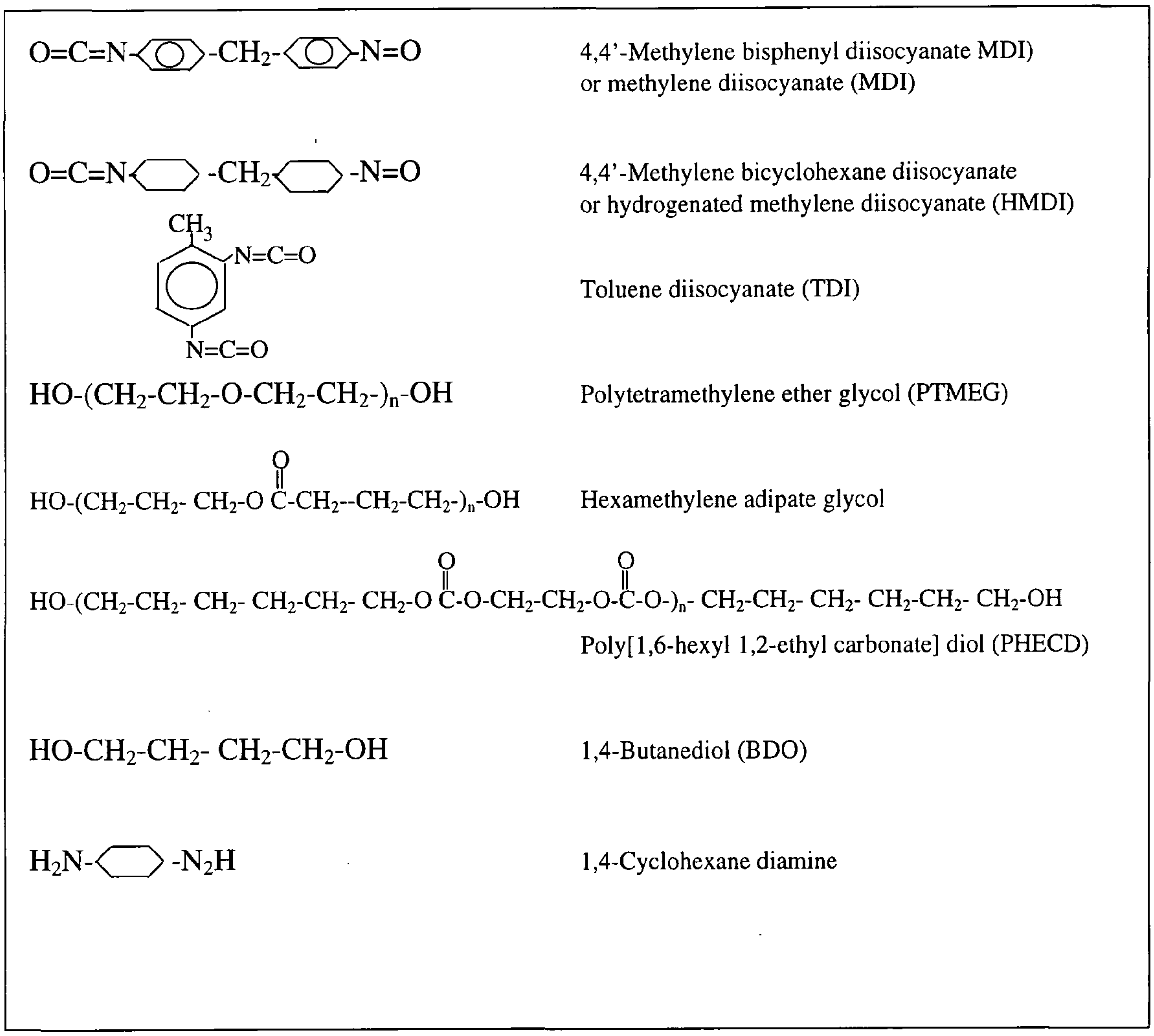
4,4'-Methylene bisphenyl diisocyanate MDI)
or methylene diisocyanate (MDI)
4,4'-Methylene bicyclohexane diisocyanate
or hydrogenated methylene diisocyanate (HMDI)
Toluene diisocyanate (TDI)
Polytetramethylene ether glycol (PTMEG)
Hexamethylene adipate glycol
Poly[1,6-hexyl 1,2-ethyl carbonate] diol (PHECD)
1,4-Butanediol (BDO)
1,4-Cyclohexane diamine

Figure 2.5 Chemical structure of constituent polyurethane monomers
[Corvita 1993]

Other factors were shown to accelerate the autoxidation and so extended its effects within the material bulk. The most notable accelerated forms were environmental stress cracking (ESC) producing deep crazed cracks where there were residual stresses in the polymer, and metal ion oxidation (MIO) where the presence of a metal accelerated the oxidation (for example in pacemaker leads) [Pinchuk 1994, Stokes et al 1995]..

Polyether urethanes were most common in implant applications and the most widely used polyether diol was polytetramethylene ether glycol (PTMEG) as shown in Figure 2.5. PTMEG was used in the most widespread early polyurethanes such as Pellethane 2363 (Dow Chemical, MI, USA). Autoxidation of such polyether urethanes however meant until recently their lack of biostability meant they too were not suitable for long-term load-bearing implants.

There was a strong market, therefore, for a 'biostable' polyether urethane which could resist the problems of ESC and MIO. The first polyurethane to meet the challenge was Corethane (Corvita Co., FL, USA). Corethane used a radically different macrodiol based on a polycarbonate glycol, PHECD as shown in Figure 2.5. It retained the same hard segment chemistry, MDI, and so excellent mechanical properties, of Pellethane [Corvita 1993, Pinchuk 1994]. As it was essentially devoid of ester and ether linkages it showed vastly improved resistance to both hydrolysis and autoxidation [Pinchuk 1994, Zhao et al; 1995], possibly partly due to its relative biological inertness [Tanzi et al 1994]. Closely following the introduction of Corethane, was a similar polycarbonate polyurethane, Chronoflex from PolyMedica Inc. It used a less stable aliphatic diisocyanate but nevertheless had shown encouraging results of in vivo and in vitro trials [Stokes et al 1995]. A third biostable polyurethane was also released by the CSIRO group based on longer chain polyester macrodiols (up to 10 carbons as compared to 4 in PTMEG), having the dual effect of stiffening the material and decreasing the number of ether linkages.

Chain Extenders

The chain extenders are small hydroxyl terminated molecules which link the diisocyanate-macrodiol prepolymer molecules. There were three chain extenders in widespread use as shown in Figure 2.5. The most common was 1,4-butanediol (BDO) which produces a thermoplastic polyurethane which was easily processed. BDO was used in Pellethane, Tecoflex (Thermedic, MA, USA) and the new biostable Corethane. The other two widespread chain extenders, ethylene diamine (EDA) and cyclohexane diamine, used in Lycra (Dupont, DE, USA) and Biomer (Ethicon, NJ, USA), were amine terminated. Whilst EDA formed urethane linkages, the amine extenders formed urea linkages which rendered the polyurethane difficult to extrude or mould so made it applicable to only thin film applications.

2.3.3.2 Adhesion of compliant layer to substrate

To maintain the form of the bearing, whilst incorporating elastohydrodynamic and micro-elastohydrodynamic effects, the elastomer layer needed to be firmly attached to a harder substrate. Early work had seen polyurethane or silicone rubber layers attached to commonly used prosthetic materials such as UHMWPE or metal. The adhesion between the substrate and layer however was frequently poor as the properties of the materials were so disparate [Blamey et al 1992, 1993, Burgess 1996].

Adhesion between two materials is described as the bonding force generated when two surfaces are in intimate molecular contact [Kinloch 1987]. There are four mechanisms of adhesion.

- mechanical interlocking
- electronic theory
- adsorption theory
- diffusion theory

Mechanical interlocking describes the interpenetration of the two surfaces either on a macro scale such as an adhesive into wood, or on a micro scale, such as occurs between chemical roughened surfaces. Electronic theory relies on different electronic bond structures on the two surfaces and so the transfer of electrons between them. The bonding is then due to the electrostatic attraction between the two surfaces. Adsorption occurs when the two surfaces are in intimate contact on an atomic scale and so interatomic or intermolecular forces occur. The strength of these forces range from relatively weak Van de Waals forces and hydrogen bonds to the very strong primary ionic, covalent or metallic bonds. None of these three adhesion mechanisms has been seen to generate a sufficiently strong adhesion of elastomers.

During the course of research at Durham University, much work has been undertaken towards achieving a strong adhesive force at the elastomer-substrate interface. Results for a polyurethane - UHMWPE bond were very poor [Blamey et al 1993]. Attempts to strengthen the bond by improving the mechanical interlocking showed some success [Burgess 1996] but the resulting bond strength was still too low for this application.

The problem of adhesion of the elastomer layer to a substrate was overcome in the work of Burgess [1996] and Smith *et al* [1996] by incorporating diffusion. Where the two materials were mutually soluble and the macromolecules mobile, excellent adhesion could be achieved by diffusion of the two materials at the interface. Having selected Corethane 80A (elastic modulus 20 MPa) as their elastomer, they used a harder grade of the same material as the substrate (Corethane 75D). The two materials were injection moulded onto one another under pressure in order to achieve a high thermal energy and a strong diffusion bond. By varying the moulding conditions, they optimised the diffusion and showed a maximum peel strength of 900 N as compared to a best value of 100 N for the UHMWPE-PU bond. The optimum moulding conditions are described in Chapter 4 [Smith *et al* 1996].

2.4 Machines for the measurement of friction and wear

The years of experimentation in the progression of understanding of the lubrication of the natural synovial joint, combined with the extensive testing of joints and materials to assess their suitability for replacement joints, has necessitated the development of methods to measure the friction and wear of joints and materials.

Studies of friction and wear of joints can be seen to fall into three categories: *in vitro* studies of materials, *in vitro* studies of joint designs, and *in vivo* or *ex vivo* measurement of joints. The interest in this research has been in *in vitro* testing and so the third category has only been considered as a validation of *in vitro* results. Various authors have undertaken work in this field, notably Charnley in the 1970s [1973] in measuring explanted examples of his own designs, and more recently Hall's extensive work in assessing the friction and wear of various explanted prostheses [Hall *et al* 1994, 1995, 1997 b, Unsworth *et al* 1995].

In vitro testing of materials and joints for use in arthroplasty is undertaken using test machines which have been defined by Clarke [1981] as falling into three classes:

- Class 1: Material testing methods with little or no attempt to simulate the physiological situation (non-physiological geometry, fluids, loading or motion)
- Class 2: Material testing methods with some attempt to simulate physiological conditions (different geometry and loading, but physiological fluids, frequency, speed, or stroke) e.g. traditional pin-on-plate or pin-on-disc type machines
- Class 3: Joint testing methods including sophisticated simulation of many physiological conditions (including geometry, loading and motion cycles) e.g. joint simulators.

Class 1 and 2 methods are frequently difficult to differentiate and so for ease of reference the machines can be divided into materials-screening methods and joint simulation methods.

2.4.1 Description of test machines

Materials screening methods typically consist of a moving component onto which a load is applied by another component. The moving component is usually a plate or a wheel and the motion typically takes the form of reciprocating sliding or rocking, or simple rotating. The load is usually constant and is applied by means of a fixed pin, a second plate, a cylindrical or spherical indentor, or a block, so that the two surfaces are in contact and their friction and wear may be measured. The motion is applied to the plate or wheel by a motor and a cam or Scotch yoke arrangement. The configuration of specimens varies from experiment to experiment but in general the plate is of a hard material and the pin or block a softer material (where dissimilar counterfaces are used).

Simulators are usually configured in a rocking arrangement with the joint at the fulcrum of the motion. The orientation of the joint differs from study to study. There has been considerable debate as to whether the joint is best tested in its *in vivo* orientation (cup uppermost), which can trap air but traps less debris, or inverted (head uppermost). One half of the joint is oscillated whilst the other is held still against it. Similarly, one of the components is loaded (usually the stationary one) so that a contact stress is applied to the joint. Various studies have attempted to estimate the normal loading and motion cycles of human joints by *in vivo* and *ex vivo* measurements. Most notable are Paul [1967], Seirig and Arvikar [1975] and English and Kilvington [1979] who measured loading cycles, and Johnson and Smidt [1969] and Swanson and Murray [1973] who estimated the motion cycle. The majority of simulators apply load and motion cycle similar to one of these or approximate the cycles as sinusoidal motion, or on-off loading.

The materials-screening apparatus and joint simulator used in the course of this research are described in detail in Chapter 3.

2.4.2 Methods of friction and wear measurement

The machines may be used to measure friction or wear or both.

Friction has been measured notably by estimating the decay in amplitude of oscillation of a joint [Charnley 1959, Jones 1936, 1937, Unsworth *et al* 1974a, b] but it was later proved that direct measurement was necessary to achieve results accurate enough to allow any useful interpretation [Unsworth 1975]. Direct measurement of friction has been carried out by measuring the forces or torque generated in the bearing using transducers, attached by means of low friction bearings to the moving parts, or by measuring the changes in the position of a particular part of the apparatus when subjected to these frictional forces. Whatever method is chosen, it is vital that the inherent friction of the measurement system is low and its accuracy in measurement high, as joints regularly demonstrate extremely low frictional forces.

There are three commonly-used methods of wear measurement [Barwell 1967]. Either the dimensions or weight of the bearing components are measured, or the weight of debris produced is monitored. Dimensional measurement of wear has been undertaken by measuring the length of the pin, which although not very accurate does allow the samples to remain in position. Alternatively, the changes in volume of the components can be assessed either by using co-ordinate measurement methods or by taking replicas of the sample. The disadvantage of these methods is they do not allow for the plastic flow of the component. More commonly now, wear is assessed by gravimetric methods, measuring the change in weight of a sample. This is more convenient than measuring the weight of debris which is often difficult to separate from the lubricant. The only disadvantage of this method is that samples frequently gain weight through fluid absorption, but this can be monitored by use of a soak control sample and pre-soaking the test samples until an equilibrium is reached.

2.4.3 Comparison of different machines

Materials-screening and joint simulator apparatus obviously represent large differences in terms of testing conditions. Joint simulation devices clearly provide the most accurate representation of the situation *in vivo*. However, both classes of test machines have their uses. McKellop [1981] summarised the advantages of the materials-screening and joint simulation methods as shown in Table 2.1.

Materials screening methods	Joint simulation methods
Inexpensive to manufacture, simple geometry specimens	exact materials (use actual prostheses), including manufacturing conditions etc.
accurate measurement of friction and wear due to simple geometry/operation	more accurate load and motion cycles, including contact areas and stresses
often multi-specimen so can quickly accumulate comparative data	can evaluate joint design as well as material (conformity, size, features)

Table 2.1 Summary of advantages of different test methods

Table 2.2 summarises some of the materials screening methods which have been described over the last 30 years of the investigation of joint replacement materials. A summary of the joint simulator machines is provided in Table 2.3. These tables do not aim to include every such work that has been published as extensive reviews have been

Machine	Motion	Speed	Stroke	Load	Contact	References
sledge microtome (1 station, F)	recip.	7-100 mm/s	19-38 mm	0-36N	ball on plate	Walker *et al* 1968 a, b Dowson *et al* 1968 Caravia 1993 a, b, c, 1995
plate-on-disc	uni.	118 mm/s	360°	900 psi	curved plate on metal disc	Rostoker, Galante 1976
tri-pin-on-disc (2 x 3 stations, F & W)	uni.	125-240 mm/s	360°	25-770N	pin on flat disc	Brown *et al* 1976 Wright *et al* 1982 Dowson, Wallbridge 1985 Caravia *et al* 1990 Cooper *et al* 1992, 1993 a, b Jin, Dowson, Fisher 1993
thrust washer bearing tester (1 station, W & F)	uni.	130 then 76 mm/s	360° then 110°	NS	flat plates	Shen, Dumbleton 1974, 1976
Plate between cylinders (1 station, F)	linear - 1 way	NS	NS	NS	plate between cylinders	Cudworth, Higginson 1976
pin-on-plate (9 station, W)	recip.	18 mm/s	19-42 mm	6-100N	pin on flat plate	Atkinson 1976 Brown *et al* 1976, 1982 Dowson *et al* 1987 Cooper *et al* 1993 a, b Derbyshire *et al* 1994, 1995
pin-on-disc (12 channel, F,W)	oscil.	0-100 mm/s	25 mm	0-445 N	flat pin on disc	McKellop *et al* 1977, 1981, 1983, Weightman & Light 1985, 1986
Pin-on-plate (1 station, W)	recip.	24-81 mm/s	NS	11-26 N	ball on plate	Medley *et al* 1980 a
Pin-on-disc (1 station, F)	uni.	3-300 mm/s	360°	6-16 N	ball on disc	Medley *et al* 1980 b Gladstone, Medley 1990
Pin-on-plate (1 station, W)	recip.	35-47 mm/s	25 mm	10N, 40N	flat pin on plate	Stokoe 1990 Sibly, Unsworth 1991 Joyce *et al* 1996
Pin-on-disc (1 station, F, W)	uni.	60 mm/s	360°	38N	flat pin on disc	Kumar *et al* 1991
Pin-on-plate (1 station, F, W)	recip.	50 mm/s	25 mm	220N	flat pin on plate	
Pin-on-plate (1 station, F)	recip.	NS	25 mm	6.83 N	flat pin on plate	Hills *et al* 1994
Pin-on-plate (3 station, F, W)	recip.	50 mm/s	25 mm	225N	flat pin on plate	Saikko 1993b, d

Table 2.2 A summary of simple materials screening machines used to study joint replacement materials.

undertaken elsewhere [McKellop 1981, Clarke 1981a] but to give an overview of the development of relevant test methods. As this development has followed (or rather preceded) the investigation of natural and artificial joints, details of individual experiments have been given in the previous sections. It is the aim of this section to describe the progression in test methods used and to outline the aims of a new test method.

In general, materials-screening and joint simulation results are not compared as their respective test conditions differ too greatly to give a useful comparison. It is more frequent for materials-screening methods to be used as a preliminary step in evaluating materials and dismissing those which are unsuitable, before the more complex and expensive task of evaluating joints is undertaken on a simulator. Only two studies have been found which directly compare results of simulator and materials-screening machines [Saikko 1993d, Derbyshire *et al* 1994] although comparisons between wear rates and coefficients of friction achieved have been drawn in other studies.

Typically, materials-screening test have shown wear factors an order of magnitude less than simulators and clinical values, which both compare well [Derbyshire *et al* 1994]. This is usually put down to the fact that abrasive wear debris is trapped within the joint *in vivo* or on the simulator but not between more simple geometries, or to the acceleration of wear by cyclic loading. This second theory suggests that researchers should probably consider their test configuration more closely as the plate in simple tests is subjected to cyclic loading, only the majority of authors have had the plate as their hard counterface. Joyce *et al* [1996] showed clearly in their reciprocating tests of cross-linked polyethylene against itself that the plate wore 20 times more than the pin and concluded this was due to the cyclic loading of the plate.

	No.	Motion cycle	Load cycle	Freq. (Hz)	References
Arthrotripsometer (ankles - F)	1	sin. FE	18N constant	0.66	Linn 1967 Linn & Radin 1968
Simulator (hips - F & W)	1	45° FE, 12° AA, 14° IE	~sin 0.5 kN on/off	0-0.83	Duff-Barclay, Spillman 1967 Scales 1969
Simulator (hips - F & W)	1	sin. 60° FE	2 peak, max. 1.6 kN	1	Walker *et al* 1968, b Walker, Gold 1971, 1973 Walker, Bullough 1973
Simulator (hips - F & W) - based on Linn's	1	sin. 60° FE	Paul, max. 3.5 kN	0.5	Weightman *et al* 1972, 1973 Simon *et al* 1975 Nusbaum *et al* 1979
Pendulum (hips - F)	1	sin. 5 ° FE	constant, max. 1.5 kN	NA	Unsworth *et al* 1974 a, b O'Kelly *et al* 1977
Simulator (hips - F)	1	sin. 60° FE	sin, max. 2.7 kN then Paul cycle	1	Unsworth *et al* 1975, 1978, 1987, 1988, 1995 O'Kelly *et al* 1977, 1978 Roberts *et al* 1982 Hall *et al* 1994, 1997 a, b
Simulator (knees - W)	1	60° Swanson/ Murray	0.8 kN Seirig/ Arkivar	1	Treharne *et al* 1981
Simulator (hips, knees - F)		sin. 60° FE	Paul, max. 5 kN	0.8	Blamey *et al* 1993 Burgess *et al* 1997
Simulator (hips - W)	5	sin. 60° FE	on/off 8000N	1	Saikko *et al* 1992, 1993a, c, d, 1994, 1995
Simulator (hips - F)	1	sin. FE	2 peak	NS	Ikeuchi *et al* 1993a
Simulator (hips - F & W)	3	46° FE, 12° AA, 14° IE	on/off 3.5 kN	1.18	Saikko 1996
Simulator (knees - W)	6	65° FE 6° AA, 5° IE	3 kN Seirig/ Arkivar	1	Burgess 1996

Table 2.3 A summary of joint simulator machines used in the investigation of replacement joints

(NS = not specified, measurement of friction = F, wear = W, uni. = unidirectional motion, recip.= reciprocating, oscil.= oscillating)

Saikko 1993d not only compared the wear of material combinations between pin-on-plate machines and joint simulators but he also compared the friction measured. He found that for the same material combination he obtained much higher coefficients of friction on the pin-on-plate machine, a range of 0.05 to 0.27, compared with the simulator, 0.02 to 0.15. In spite of this he concluded that "there is no reason to expect that a total replacement hip joint would show low friction and wear if the same is not true for its materials in the pin-on-flat test". This would seem to be an unreasonable assumption since not only do his pin-on-flat tests use two flat surfaces in contact, therefore giving no wedge effect to encourage the entrainment of fluid, but also, they employ a constant load to ensure that squeeze film effects are not incorporated either. It would seem to this author that under such entirely different lubrication regimes, not to mention the standard deviations shown between some of Saikko's results, that there is no reason to suggest that his pin-on-flat tests would give a realistic evaluation of the tribological behaviour of materials in a joint configuration.

Which brings us to the situation as it stood at the point of commencing this research. As the information in Table 2.2 clearly shows, to date tests on materials-screening machines have themselves differed greatly from one another, in the samples used, their methodology, the test conditions, the measurement techniques and way in which the results obtained have been reported. This has produced often markedly different results, as shown by Tweedale [1994] in comparing test undertaken on pin-on-plate devices run to ASTM specification [ASTM F732-82] and Leeds' own specification. Studies have shown that the frequency of a normal walking cycle is approx. 1Hz and the sliding velocity between the articulating surfaces approx. 20 mm/sec yet materials screening have employ speeds anywhere between 18 and 300 mm/sec, the ASTM standard being set, questionably, at 50 mm/sec. The lack of consistency in speeds is in addition to a lack of consistency in the type of motion used. Brown *et al* [1976], Kumar *et al* [1991] and Cooper *et al* [1993a] have all shown reciprocating motion to produce much less wear than unidirectional motion. Neither is the applied load or contact pressure used standard.

Although, joint simulators show more consistency, by their very nature they must be similar if they are all to simulate the physiological situation. Their protocols too show a high degree of variation. The disparities in materials-screening and joint testing have been highlighted many times by many sources [Dumbleton 1977, Swanson 1977, Clarke 1981b, Unsworth 1981 to name but a few] and more recent research has included the development of specified standards [ASTM F732-82]. To the author's knowledge though, there has been no attempt whatsoever to try and achieve more equivalence between simulator and materials-screening tests, although, as long ago as 1977, Dumbleton pointed out that there was no reason why screening methods could not use a simple dynamic loading pattern in order to obtain more representative results.

Research into the use of compliant layered joints is now in its advanced stages with many of parameters involved being optimised by extensive experimental and theoretical studies. There are still however some questions which must be answered before such joints can go to clinical trials. Among these, are concerns as to the start-up and creep performance of the layers and so the effects of material modifications and surface treatments or lubricants on the tribological properties of a compliant layered bearing.

The production of compliant layered acetabular cups is an expensive and elaborate procedure and so not ideally suited to frequent modification. For this reason, it would be extremely useful, in the development of soft layer technology, if a simpler and cheaper test of these bearings could be devised. The aim of this research, therefore, has been to fill the gap between materials-screening and joint simulator apparatus and provide a test method which allow a compliant layer bearing to perform as it would *in vivo* whilst still using specimens of simple geometry, and test of minimum complexity and a high degree of accuracy.

3. Apparatus

3.0 Introduction

During the course of this PhD, numerous testing apparatus have been used in order to perform the various tests described. A Lloyd R6000 universal test machine was used for the measurement of hysteresis of polyethylene and polyurethane materials, a phase shifting interferometric type surface measurement machine (Zygo) was used to assess the surface roughness of bearing surfaces, and a Fischers hardness testing apparatus with a Vickers spherical indentor was used to measure the hardness and to estimate the elastic modulus of the samples. All these apparatus were used for specific experiments using specific methods and so are described in the various sections relating to the tests in which they were used.

The majority of work on this PhD, however, has been undertaken in measuring the friction of bearing surfaces and was undertaken on two machines. The aim of this research has been to design, develop, validate and use a realistic test method for compliant layered joints. This has required familiarisation with existing test methods and development of a new method, validating its results against those of existing machines.

As described in Chapter 2, the most prevalently used machines in materials testing today fall into two categories: joint simulators and materials-screening machines. Materials-screening machines provide a very simple and low cost test method for measuring the wear (and less often the friction) occurring between material combinations but provide little representation of the situation in vivo and so consideration must be made for the test conditions in examining the results they produce. Their benefits are that the test methods are simple, provide accurate measurement of friction and wear (due to the relative simplicity of their components), and that they frequently use flat plates or discs and cylindrical pins which are easy and cheap to manufacture. Simulators provide a much more accurate representation of the situation in vivo (although still simplified) and so often allow a better assessment of whether material combinations and joint design will be successful in implantation. They are however, very expensive to develop and require complex hemispherical and spherical components for testing. The problem in testing compliant joints is that, to function with extremely low friction as they are designed to do, they require a lubrication regime which relies on the majority of the conditions seen in vivo. Soft layers have been tested with proven success on simulator machines [Unsworth 1987, 1988, Auger 1993] and with more limited success on pin-on-plate devices [Caravia 1993a, b, c, 1995].

It was thus the aim of this research to develop a test method which included the simplicity and ease of use of the pin-on-plate devices combined with the experimental conditions of the simulator so that compliant layered joints may be tested easily and under optimum conditions. In order to achieve this aim, extensive use was made of the Durham hip function friction simulator [Blamey 1993, Burgess 1996] and extensive development of a pin-on-plate friction measuring machine [Hills *et al* 1994] was undertaken.

3.1 Durham Hip Function Friction Simulator

The first Durham hip function friction simulator was commissioned in 1979 and was described by Roberts [1980] and Unsworth *et al* [1981, 1984, 1987, 1988]. A second hip function friction simulator at Durham was later commissioned by John Blamey [1993] and then modified during its extensive use in the development of a compliant layered joint by Burgess [1996]. It was the second Durham hip function friction simulator which was used in all simulator experiments undertaken during this research. As it has been described extensively elsewhere [Blamey 1993, Burgess 1996], only a brief description of its operation has been provided here.

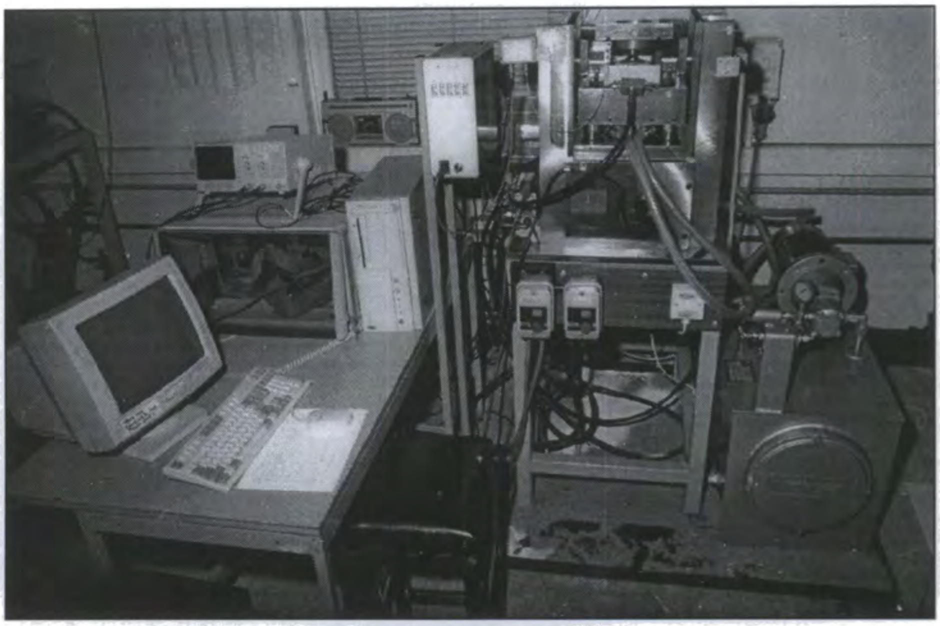

Figure 3.1 Hip function friction simulator

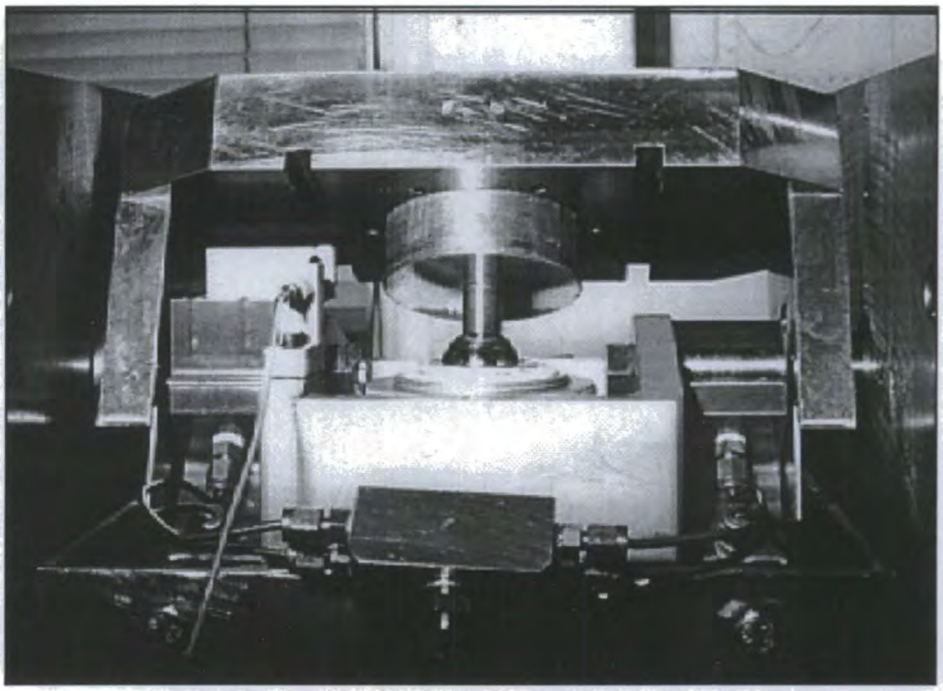

Figure 3.2 Hip joint in simulator

Figure 3.1 shows an overview of the second Durham hip function friction simulator. It consisted of a lower section, including the hydrostatic bearings which supported the friction measuring carriage, to which the acetabular or tibial component was mounted, which moved vertically to apply a loading cycle. The upper carriage, in which the femoral components were mounted, oscillated to provide the motion cycle. Its operation and design was characterised by its various functions: viz application and measurement of a loading cycle, application and measurement of a motion cycle, measurement of the frictional torque produced and the instrumentation, control and data acquisition of the machine.

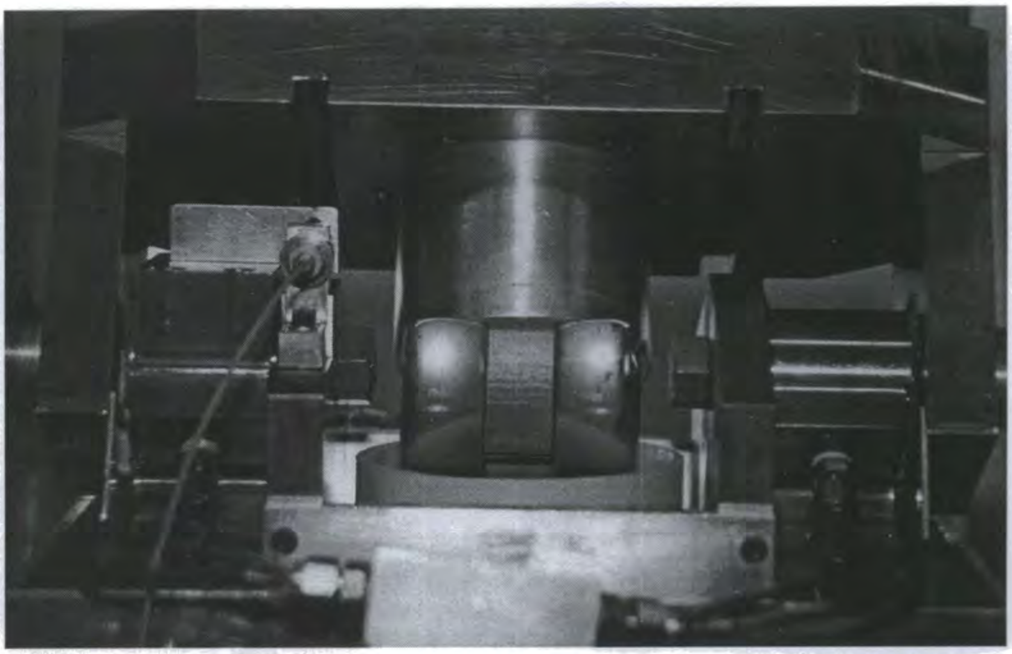

Figure 3.3 Knee joint in simulator

The second Durham hip function friction simulator was originally designed to enable artificial hip joints to be tested in both the anatomical (acetabular cup uppermost) and inverted (femoral head uppermost) positions. Since its commissioning, the simulator has undergone various modifications and improvements which have allowed it to test both hip and knee joints. In order to maintain a standard test protocol for all experiments undertaken on this machine, hip joints were mounted in the inverted orientation (femoral head uppermost, acetabular cup beneath) and knee joints (where used) in the anatomical orientation (femoral head uppermost, tibial plate beneath) as shown in Figures 3.2 and 3.3.

3.1.1 Application and measurement of load

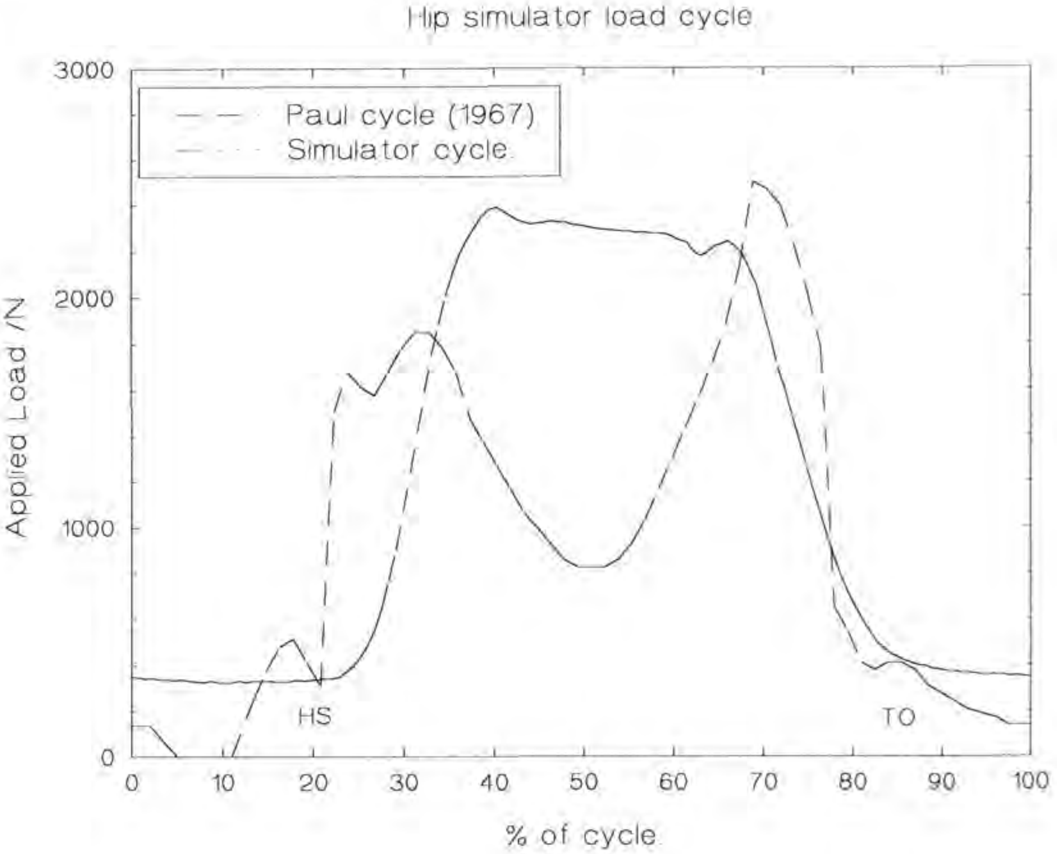

Figure 3.4 A comparison of the simulator load cycle and the Paul load cycle [1967]

While early joint testing devices used mechanical cams and weights to apply a load to the joint, the more modern machines have used servo-hydraulic systems to allow a variety of loading cycles to be applied. In its original design, the second Durham simulator used a proportional valve to control the fluid flow to a hydraulic cylinder. This raised the lower plate of a die set through four linear ball bushings moving the upper plate. The acetabular cup or tibial plate was mounted to this upper plate, and so a load was applied to the bearing which was measured by means of two strain gauged bars wired in a Wheatstone Bridge circuit. However, due to problems of electrical noise and non-linearity in this arrangement, the proportional valve was subsequently replaced with a servo-valve and the strain gauged bars by four miniature load cells (RDP, Model 13E) at the corners of the linear hydrostatic bearings. The outputs from the four load cells were amplified by a strain gauge amplifier, summed and then converted from an analogue to digital signal by an analogue to digital converter (ADC) and fed back to the controlling PC. The present loading assembly has been shown to provide excellent control and load measurement characteristics. The repeatability of the application and measurement of the applied load is discussed further in Appendix A. A cooling system to maintain a steady servo-hydraulic oil temperature has subsequently been added.

Figure 3.4 shows a comparison between the loading cycle applied on the second Durham simulator and that reported by Paul [1967] for predicted hip joint reaction forces. Whilst the loading cycle used in the simulator was simplified it did include the low load swing phase and high load stance phase which have been shown to be important if a stable lubricating regime is to be established [Unsworth *et al* 1987, 1988, Auger *et al* 1990, 1993a, 1993b]. Published work suggests that the maximum load applied to a joint in normal walking would be between 3.9 x body weight (BW) [Paul 1967] and 5.4 x BW [Seirig and Arvikar 1975] , although peak loads may be much lower for older or less active patients, especially following surgery. The design load for the second simulator was 5000N (6.75 x BW) and in standard tests undertaken on this machine, a maximum load of 2000N (2.7 x BW) and minimum load of 100N was applied. In an effort to obtain comparable results between the pin-on-plate and simulator devices, however, a range of maximum loads between 2000N and 250N were used.

3.1.2 Application and measurement of motion

Although the natural hip joint moves in three planes as shown in Figure 2.2, in order to measure the friction generated in an artificial joint directly, it was necessary to simplify this motion to flexion-extension in the sagittal plane with some movement in anterior-posterior and lateral directions allowed to ensure alignment of centres of rotation (see Section 3.1.4). The flexion-extension of the hip was approximated to a roughly sinusoidal oscillatory motion, with a frequency of 0.8 Hz as shown in Figure 3.5 where it is compared with the measured flexion-extension of a normal hip [Johnston and Smidt 1969]. The motion was provided by a 2.9 kW electric motor, driving a rack and pinion through a scotch yoke mechanism. The amplitude of oscillation was set by adjusting the maximum movement of the scotch yoke. Whilst Blamey's original design [1993] used an angular offset of +7°, the simulator had been subsequently modified to allow the angular offset to be adjusted by changing the rack length, and in all tests described here, no angular offset was used. In standard simulator protocol (and in all the experiments undertaken by this author) the amplitude of oscillation was set to +/- 25° for hip joints and +/- 35° for knee joints. An incremental encoder (Holmer) was attached to the motion system to provide a clock pulse which could be fed back to the controlling PC and a rotary potentiometer measured the angular position throughout the cycle.

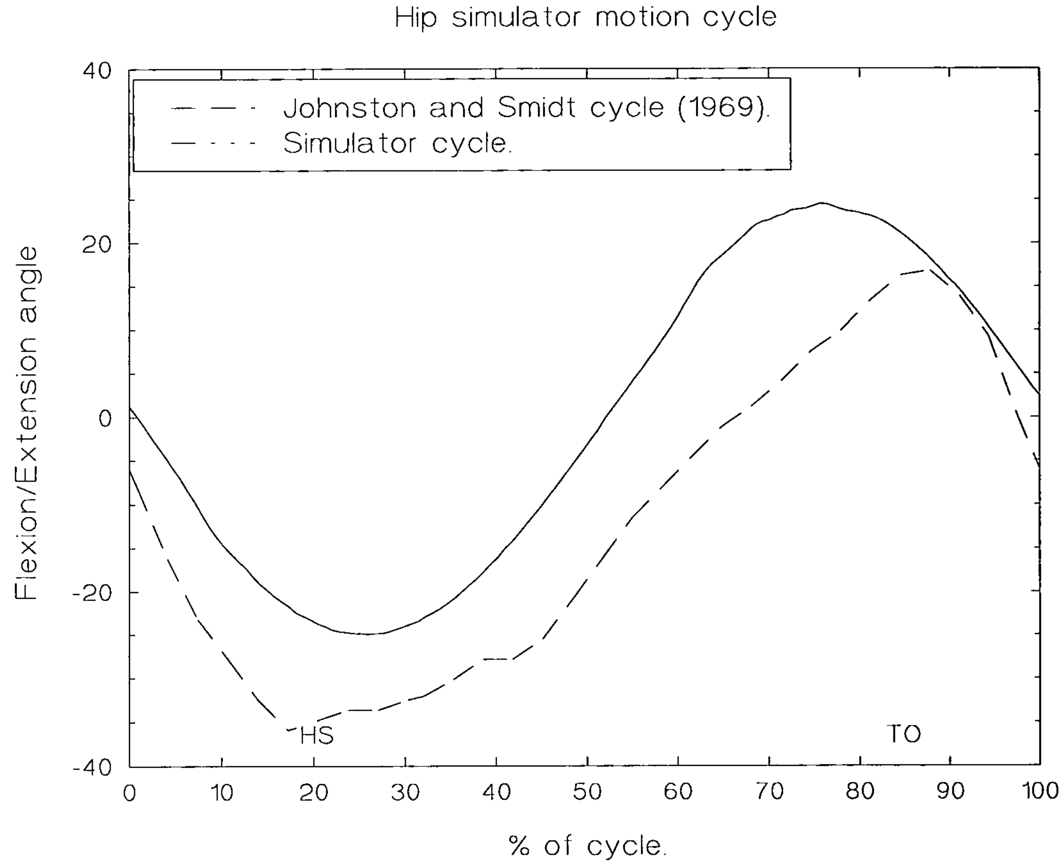

Figure 3.5 A comparison of the simulator motion cycle and the Johnson Smidt cycle [1969]

3.1.3 Measurement of frictional torque

The frictional torque generated by the motion of the femoral head within the acetabular cup (or tibial tray) was measured directly by means of a piezoelectric quartz force transducer using a method first used by Unsworth *et al* (1975). As reported earlier, the acetabular or tibial component was mounted into the friction measuring carriage which was located on the upper plate of the loading die set. The carriage was supported on two hydrostatic journal bearings which allowed rotation of the carriage in the sagittal plane which in turn were supported by two hydrostatic linear bearings which allowed some anterior-posterior and lateral translation to ensure alignment of component centres. In the case of the knee joints, which were substantially less conforming, the anterior-posterior position was fixed by locating bolts to prevent dislocation of the joint. Detailed analysis of these hydrostatic bearings [Burgess 1996] estimated the coefficient of friction generated in the hydrostatic bearings to be several orders of magnitude less than those typically measured for compliant layered joints experimentally. The only restraint on the movement of the carriage was provided by the piezoelectric transducer (Kistler 9203) which measured directly the force corresponding to the frictional torque generated as the articulation of the femoral component as its opposing bearing counterface tended to rotate the carriage. The body of the transducer was attached rigidly to the frame of the simulator, and the friction measuring carriage attached to the transducer by means of a threaded rod, which fitted into a slot on the carriage by means of washers and locking nuts. The position of the locking nut was carefully adjusted so that the transducer experienced no net force when the bearings were on and no load applied. The signal from the transducer was then amplified by a charge amplifier (Kistler 5039A) and converted from an analogue to a digital signal by an ADC and fed back to the controlling PC.

3.1.4 Instrumentation and control

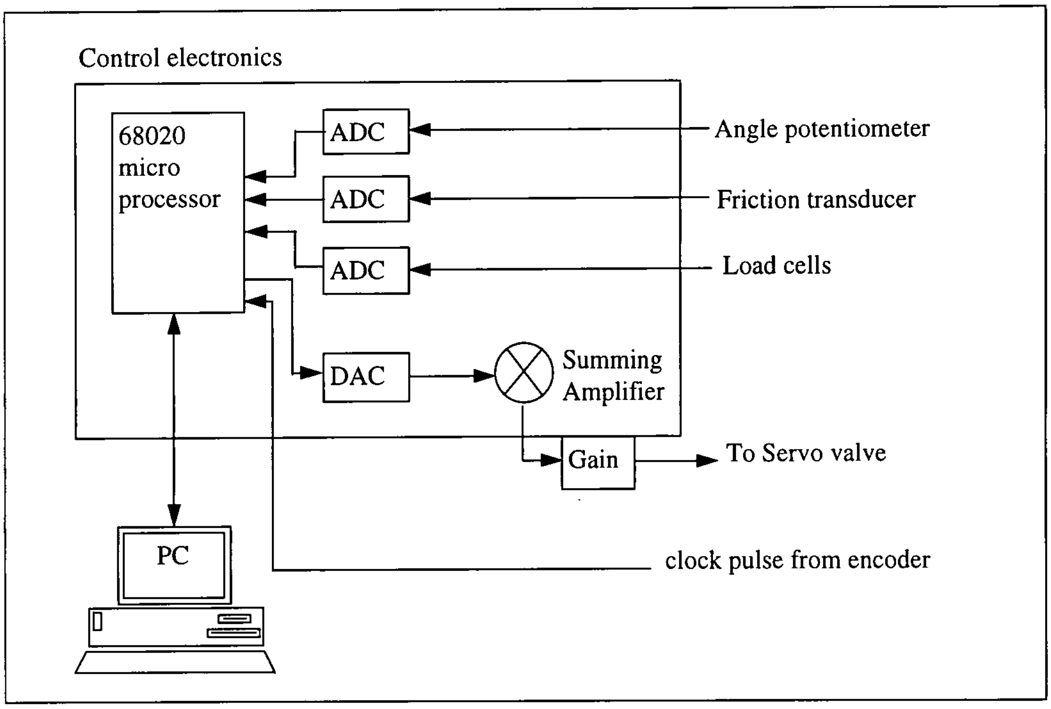
Control electronics
68020
micro
processor
ADC
ADC
ADC
DAC
Angle potentiometer
Friction transducer
Load cells
Summing
Amplifier
Gain
To Servo valve
PC
clock pulse from encoder

Figure 3.6 A schematic representation of the simulator control [Burgess 1996]

The simulator was controlled and test data collected and analysed by means of a Motorola 68020 microprocessor board built in-house with a parallel communications link to a Viglen 386 PC. Figure 3.6 shows a schematic representation of the control system. The analogue signals from the load cells, rotary potentiometer and friction transducers were converted to digital signals by means of three ADCs. The outputs from the load cells were summed to provide a feedback signal to the servo-valve so that the load could be adjusted as necessary. The incremental encoder provided a clock pulse which synchronised the applied motion cycle with the servo-hydraulically applied load cycle and the various measurement systems. A cycle consisted of 128 pulses: each clock pulse signalling the digital to analogue converter (DAC) to be updated with the load profile, and the outputs from the three ADCs to be read.

68020 software was developed by the University of Durham Microprocessor Centre to enable tests to be controlled by the PC with the test parameters inputted and included in the data files. The software also allowed calibration of the load, angle, encoder and friction measurement systems, as well as processing the collected data into a useable format.

3.2 Pin-on-plate friction measurement machine

Pin-on-plate apparatus have been used extensively for many years to measure the wear occurring between two bearing counterfaces [Sibley and Unsworth 1991, Jin *et al* 1993a, Joyce *et al* 1996] and have been adapted to measure the friction in the bearing also [Gladstone and Medley 1990, Saikko 1993b, Caravia 1993a, b, c, 1995]. The Centre of Biomedical Engineering in the University of Durham has, over the years, designed and built six pin-on-plate wear machines. One of these wear machines was subsequently adapted to measure friction. The research described here focused on extensively modifying this apparatus so that it could achieve comparable measurements of friction for compliant layered bearings to those obtained on the Durham hip function friction simulator. The original apparatus is described below along with its limitations (as used on the commencement of this research). This is followed by a detailed description of the modifications made to the original apparatus and the improvements to performance that these modifications provided.

3.2.1 The original Durham pin-on-plate friction measuring machine

The original Durham pin-on-plate measuring machine was described by Hills *et al* [1994] and is shown in Figure 3.7. A brief description of its main features is provided below.

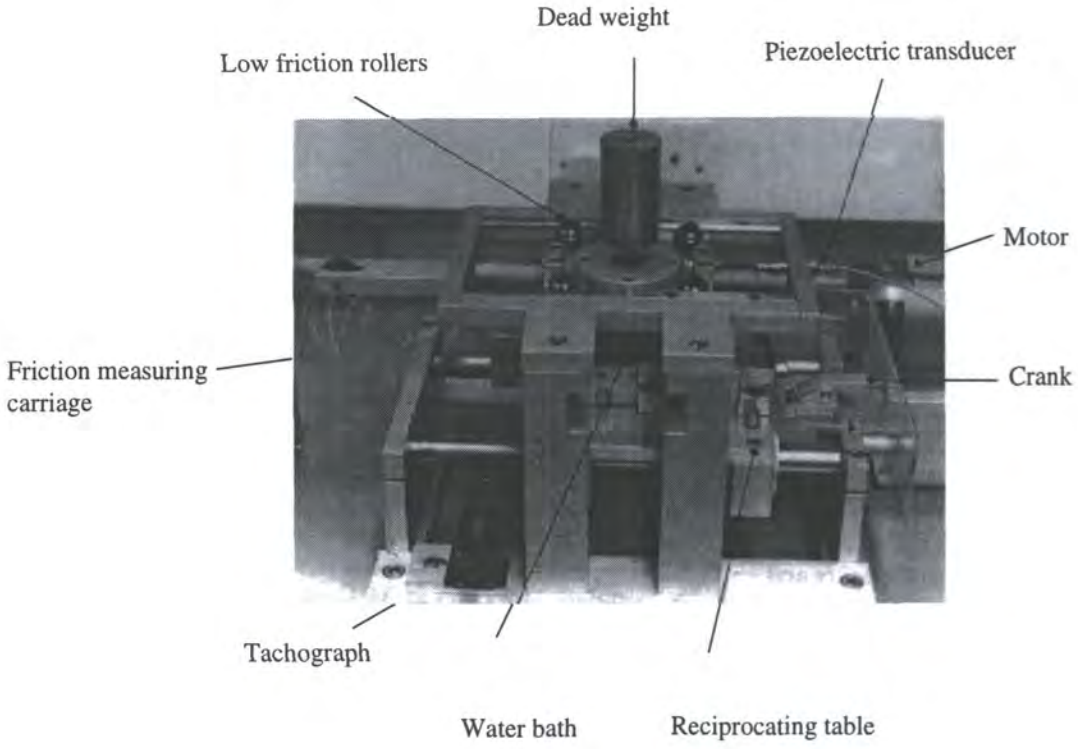
Dead weight
Low friction rollers
Piezoelectric transducer
Motor
Friction measuring carriage
Crank
Tachograph
Water bath
Reciprocating table

Figure 3.7 The original Durham pin-on-plate friction apparatus [Hills *et al* 1994]

Two side sections and two end sections were bolted together to form a rigid base to the apparatus which is firmly attached to a flat surface. The side sections held two 20 mm diameter shafts which supported the reciprocating table. A Paravalux 50W DC motor imparted a reciprocating motion to the table by means of a crank assembly and crosshead. The speed of motion of the table was controlled by a thyristor controller for DC shunt motors and the amplitude of oscillation (or stroke length) was controlled by adjusting the radius of the crank arm. The maximum sliding velocity of the pin-on-plate machine in most tests was 44 mm/sec and in all tests the stroke length was 25mm. Onto the reciprocating table was attached a stainless steel water bath which held the lubricant during tests and contained a machined sample mounting block into which the plates were positioned during testing.

A friction measuring carriage was supported above the reciprocating table, firmly bolted to four vertical columns. The carriage consisted of a rectangular frame, made up of two side and two end sections bolted together, onto the inside side edges of which 'knife edge' sections were attached. The side sections then supported two low friction V-shaped roller bearings attached to a stainless steel plate with a central bearing. A cylindrical pin attached to a cylindrical pin holder, slid freely through the central bearing to make contact with the bearing plate below. A dead weight was then applied to the top surface of the pin holder, which stood proud of the steel carriage plate, in order to apply a load to the pin-on-plate bearing. The carriage plate was restrained by a piezoelectric force transducer (Kistler 9203) which was rigidly attached to the frame of the friction measuring carriage. In this way the frictional force generated by the motion of the bearing plate against the pin could be directly measured by the force transducer as had been done in the hip function friction simulator.

The output from the piezoelectric force transducer was fed to a charge amplifier (Kistler) which amplified the signal before feeding it to an XYT plotter (RDK RW Series Model 83) which recorded the signal. The number of cycles undergone was recorded throughout testing using a tachograph.

3.2.2 Modified design

Whilst the original Durham pin on plate friction measuring apparatus was adequate for measuring the friction generated in simple bearings, it had 2 main disadvantages if used in measuring the friction of compliant layered joints.

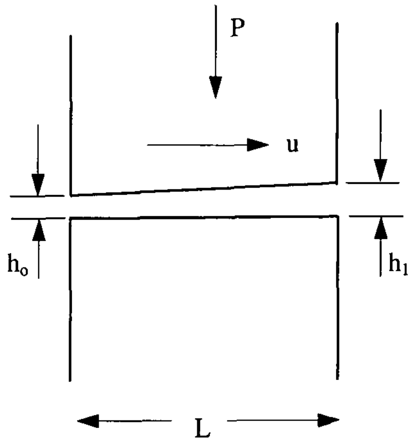

Figure 3.8 Plane inclined slider bearing

Firstly, the success of compliant layered joints depends on a fluid film being produced and maintained between the two surfaces. In vivo, and in simulators, this is achieved by the combined action of the entraining motion between the two surfaces and the squeeze film action as the bearing surfaces come together [Higginson and Norman, 1974a, b, Higginson 1977, 1978b]. Hutchings [1992] suggests that for a plane inclined slider bearing of infinite width as shown in Figure 3.8 the load per unit width supported by the entraining action, P_{ent}, would be given by

$$P_{ent} = 6\eta k u \left(\frac{L^2}{h_o^2} \right) \qquad \text{Eqn. 3.1}$$

$$\text{where } k = \ln \left(\frac{1+n}{n^2} - \frac{2}{n(2+n)} \right) \qquad \text{Eqn. 3.2}$$

whilst the normal load per unit width carried by the squeeze film action P_{sq}, would be

$$P_{sq} = 6\eta v \left(\frac{L^3}{h_o^3} \right) \qquad \text{Eqn. 3.3}$$

where v is the velocity of approach of the surfaces and n is given by $(h_l/h_0 - 1)$.

By comparing equations 3.1 and 3.3, it follows that if the velocity of approach of the surfaces is equal to or greater than h_0/L times the entraining velocity then the squeeze film becomes the most important term.

In the original design of the pin-on-plate friction measuring machine, the load was applied to the bearing statically by means of a calculated dead weight. This means that the velocity of the approach of the surfaces was zero at all times other than the initial condition when the load was first applied and so there would be minimal squeeze film contribution to the lubrication of the bearing. As h_o was typically several orders of magnitude smaller than L (in the case of the cylindrical pin, its diameter), it was deemed that the squeeze film action of the test method was likely to be very important. In order to encourage this, and so test compliant layered bearings under realistic conditions, it was necessary to incorporate application of a dynamic load into the pin-on-plate test method.

The second limitation of the original Durham pin on plate friction measuring apparatus was the low friction bearings of the friction measuring carriage. Their design suggested they should each give rise to coefficients of friction of the order of 5 x 10^{-4}, giving a total contribution to the coefficient of friction of around 0.002. Whilst this value was several orders of magnitude less than the coefficients of friction seen typically for conventional replacement joints, this could be important in measuring the friction of compliant layered bearings which had been seen to give values of friction factor on the simulator as low as 0.001. Initially, the pin on plate apparatus was used with its original low friction roller bearings but it became apparent that they were operating with excessive frictional losses and therefore could not achieve the desired level of accuracy in measuring friction. A new bearing arrangement for the friction measuring carriage was therefore also required in modifying the machine to test compliant layered bearings.

The first modification of the pin-on-plate machine was to remove the large water bath which remained from its use in wear tests where it originally held 4 samples, and so required a very large quantity of lubricant to be used if the plate was to be submerged during tests. This was replaced with a sample mounting plate and beneath it a heating plate so that the tests could be run at body temperature of 37 °C.

3.2.2.1 Dynamic loading

Following modifications, a dynamic load was applied to the pin on plate bearing pneumatically. A pneumatic cylinder was attached to the aluminium plate of the friction measuring carriage by means of a mounting platform as shown in figures 3.9 and 3.10. The rod of the pneumatic cylinder was screwed into a spacer which in turn attached to a sub-miniature load cell. The load cell (RDP Precision Miniature Load Cell Model 34) was then screwed into a modified pin holder so that the load applied by the cylinder to the pin and hence the load applied to the bearing plate could be measured. The load cell was attached to a charge amplifier (RDP Type S7DC) which amplified the signal before sending it to the XYT plotter attached to the piezoelectric force transducer.

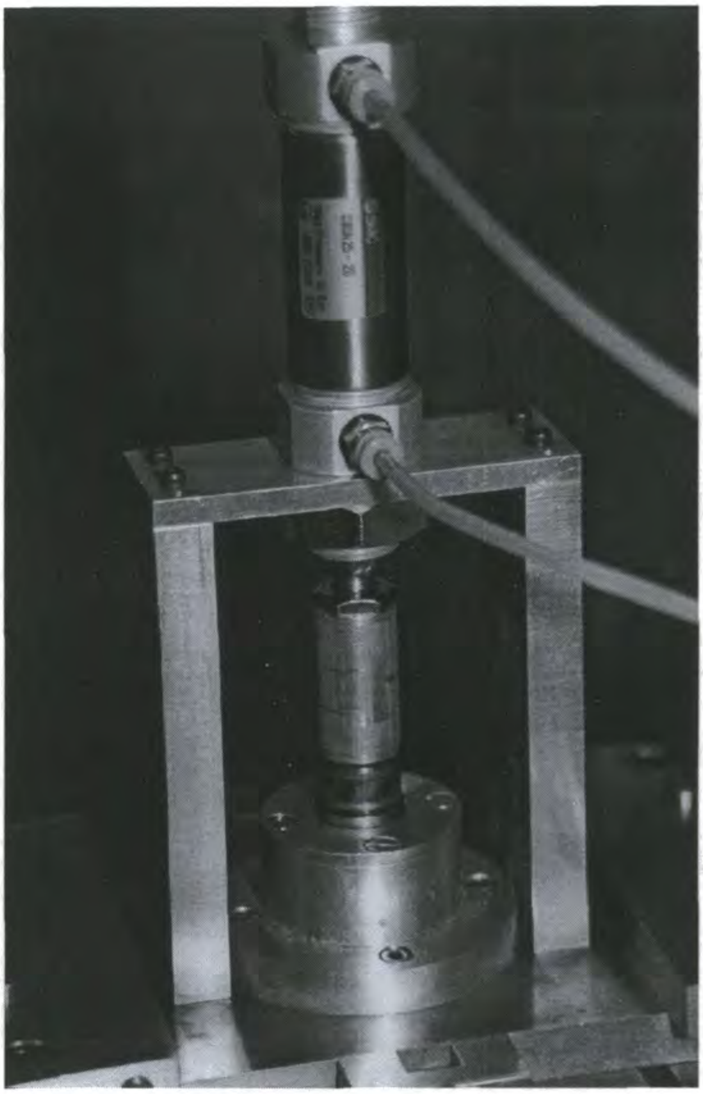

Figure 3.9 Dynamic Loading Arrangement

Subsequently, a universal joint was added to replace the spacer between the cylinder rod and the load cell to allow any out of alignment between the centre of the cylinder rod and then centre of the pin holder to be accommodated without causing friction in the movement of the pin holder in its bearing. In addition, in order to prevent the pin from tipping during the reciprocating motion, which could cause the edge of the pin to come into contact with the plate and so have a significant effect on the measured friction, the simple bearing in the aluminium plate was replaced by a linear roller bearing. This provided similarly low friction vertical motion of the pin holder but allowed a much tighter clearance between the pin holder and its bearing allowing tipping of less than 0.5°.

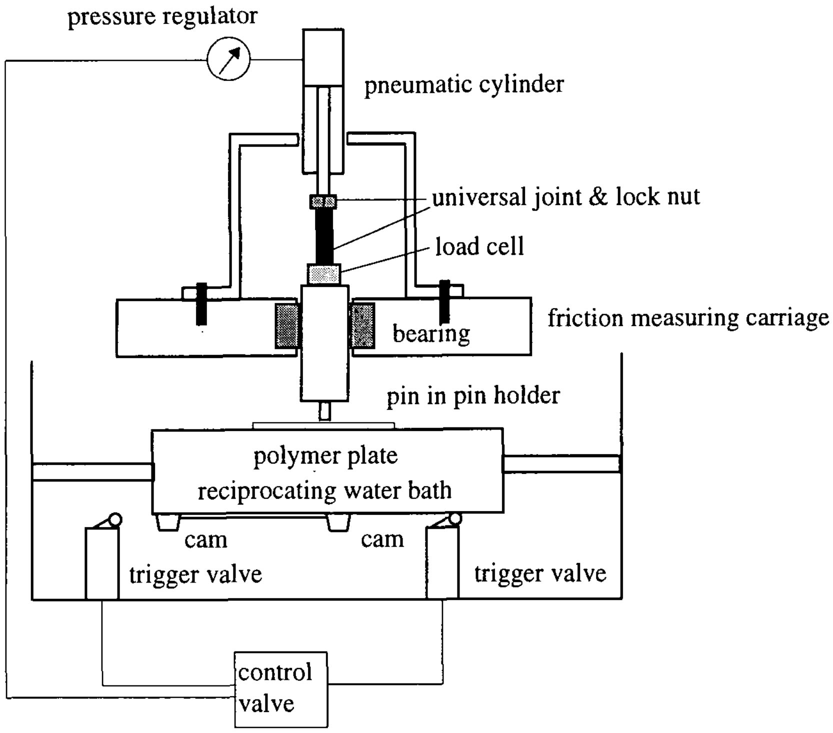
pressure regulator
pneumatic cylinder
universal joint & lock nut
load cell
friction measuring carriage
bearing
pin in pin holder
polymer plate
reciprocating water bath
cam
cam
trigger valve
trigger valve
control valve

Figure 3.10 A schematic representation of the dynamic loading arrangement on the pin-on-plate apparatus

The pressure applied to the pneumatic cylinder, and so the load applied by the pin, was controlled by means of a series of cams on the underside of the reciprocating table, two mechanical trigger valves and a control valve. A double acting pin cylinder was chosen so that by applying pressure to the top of the cylinder the pin holder would be lowered and a load applied by the pin, and by applying a pressure to the bottom of the cylinder the pin holder would be raised and the load on the pin removed. The trigger valves (Bosch Model 0820 402 102) incorporated a small roller which, when depressed and subsequently released by the movement of a cam over them, activated the control valve (Bosch Model 0820 205 003) to switch the flow of pressurised air from the top to the bottom of the cylinder or vice versa, thus raising or lowering the pin holder and applying or removing the load. The trigger valves were supported on a slotted bar so that their position could be adjusted to give the required loading cycle. By positioning the trigger valves and cams so that the switches in air flow came at either end of the stroke, a dynamic loading cycle was applied, in which a load was applied in one direction of reciprocating motion and no load applied in the other. Whilst this represented a further simplification of the *in vivo* loading cycle it still included a high load, low velocity stance phase, and a low load, high velocity swing phase. It was therefore felt to be an adequate representation of the natural loading cycle to provide the entraining and squeeze film actions required for successful lubrication of compliant layered bearings.

A cylinder with a short stroke (25mm) was chosen as little vertical motion was required. The vertical height of the pin when in its raised position was adjusted so that it was just clear of the plate (a clearance of approx. 0.5 mm) by adjusting the screw thread of the cylinder rod in the universal joint and fixing its position using a locking nut. The bore of the cylinder was chosen by calculating the cylinder area which would be required to give the necessary force under the system pressure available whilst considering the minimum operating pressure of the cylinder and so the load which it could apply (Eqn. 3.5).

$$cylinder.\ area = \frac{required.\ load}{avaliable.\ pressure} \qquad \text{Eqn. 3.5}$$

where the area is given by $cylinder.\ area = \pi\left(\frac{bore}{2}\right)^2$

The available system pressure was estimated as 5.5 bar, although it was found that it was only reliable to approx. 5 bar. Originally, a 10 mm bore cylinder (Koganei Model PDA 6x30) was chosen, which had a minimum operating pressure of 0.8 bar, providing loads in the range of 6.3 to 39.3 N. This represented a maximum contact stress on the compliant layered plate under a steel pin equivalent to that on a standard 32 mm compliant layered hip under normal test conditions. This also represented a substantial increase in load from earlier static loading tests when a dead weight of 600 g was applied. In subsequent tests, however, it became necessary to apply larger loads and so a 25 mm bore cylinder was purchased (SMC C85 N 25-25) with an operating range of 24.5 to 245.4 N. Additional mountings were then added to the apparatus to allow the larger cylinder to be attached. Unfortunately the range of the load cell used previously did not extend to the loads provided by the larger cylinder but by calibrating the cylinder up to the limits of the load cell, loads above this were extrapolated from the measured pressure, with a good degree of accuracy. The pressure to the cylinders was controlled by means of a combined filter regulator (Bosch Model 0821 300 700).

3.2.2.2 Air bearings

Whilst it had been anticipated that the low friction roller bearings would need to be replaced to allow the friction of compliant layered bearings to be measured with the required levels of accuracy, the incorporation of the dynamic loading system created a further limitation on these bearings. In order to apply the dynamic loading cycle by means of a pneumatic cylinder, the cylinder had to be mounted somewhere on the friction measuring carriage. So that the steel carriage plate was still free to move and only restrained by the piezoelectric transducer, it was necessary to mount the cylinder on the steel carriage plate. When the load was applied statically by means of a dead weight, the plate was under no load as the load was applied directly to the pin holder. However, under the new dynamic loading system, although the load was still applied directly to the pin holder, the cylinder mounting was attached to the steel carriage plate and so the plate, and therefore the roller bearings, were subjected to the upwards reaction force to the applied load.

Appendix B describes in details the testing of the roller bearings. Initially tests showed that the application of this load did not seem to increase the frictional losses in the roller bearings. However, it subsequently became apparent that this was because the losses in the roller bearings were so high that their magnitude changed little whether the plate was loaded or unloaded. This was thought to be caused either by the deterioration of the bearings under loading or the gradual deterioration of the bearing surfaces over time. By comparing the response of the transducer when subjected to a direct force and a force applied through the roller bearings (Appendix B) it was found that the roller bearings gave rise to losses of 54.3% of the measured frictional force and so must be replaced.

A hydrostatic air bearing arrangement was chosen to replace the roller bearings for its excellent low friction properties, its stiffness (when designed correctly) and so ability to support the reactive force of the load, and its cleanliness (compared to hydrostatic oil bearings).

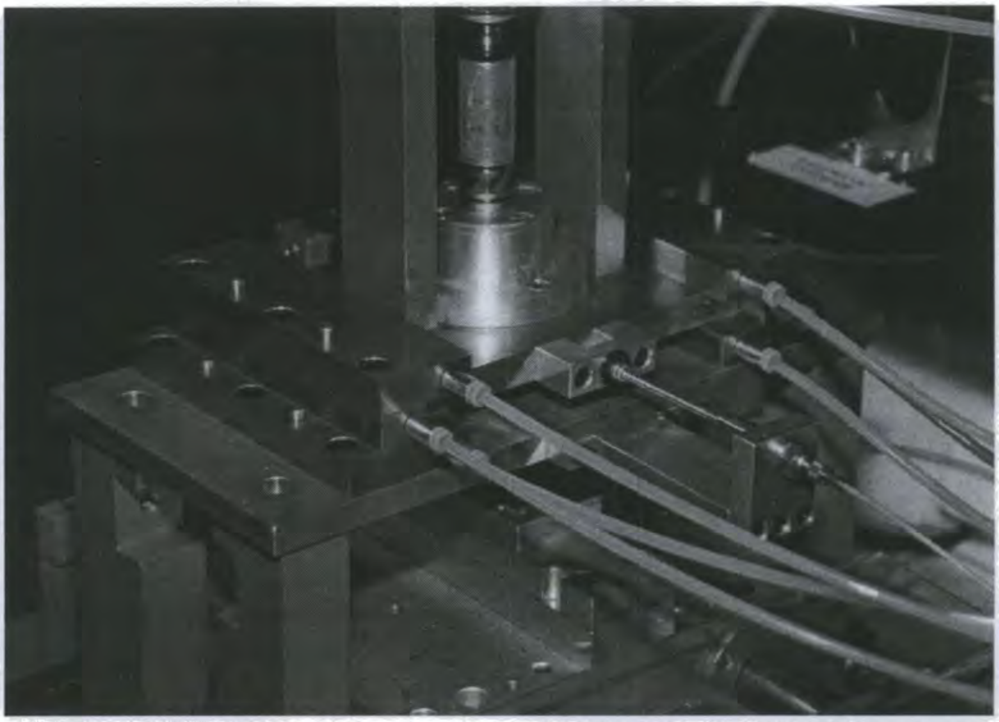

Figure 3.11 Air Bearings

The air bearing arrangement was designed to replace the previous friction measuring carriage but to attach to the supporting columns of the original pin on plate design and to be compatible with the mounting brackets of the two pneumatic loading cylinders. For this reason the air bearings were designed as two C-Section strips, replacing the knife edge sections of the roller bearings, supporting a central carriage plate. Figure 3.11 shows a photograph of the finished air bearing assembly and figure 3.12 a schematic drawing of its operation.

The calculations of the bearing dimensions required for the range of conditions used for the pin on plate apparatus are provided in Appendix C. The bearing orifice and pad dimensions required to support the reactive force using the available system pressure were calculated including a safety factor. The dimensions of the components of the original machine to which the carriage had to fit were also considered. The final design of the new friction measuring carriage included the following characteristics.

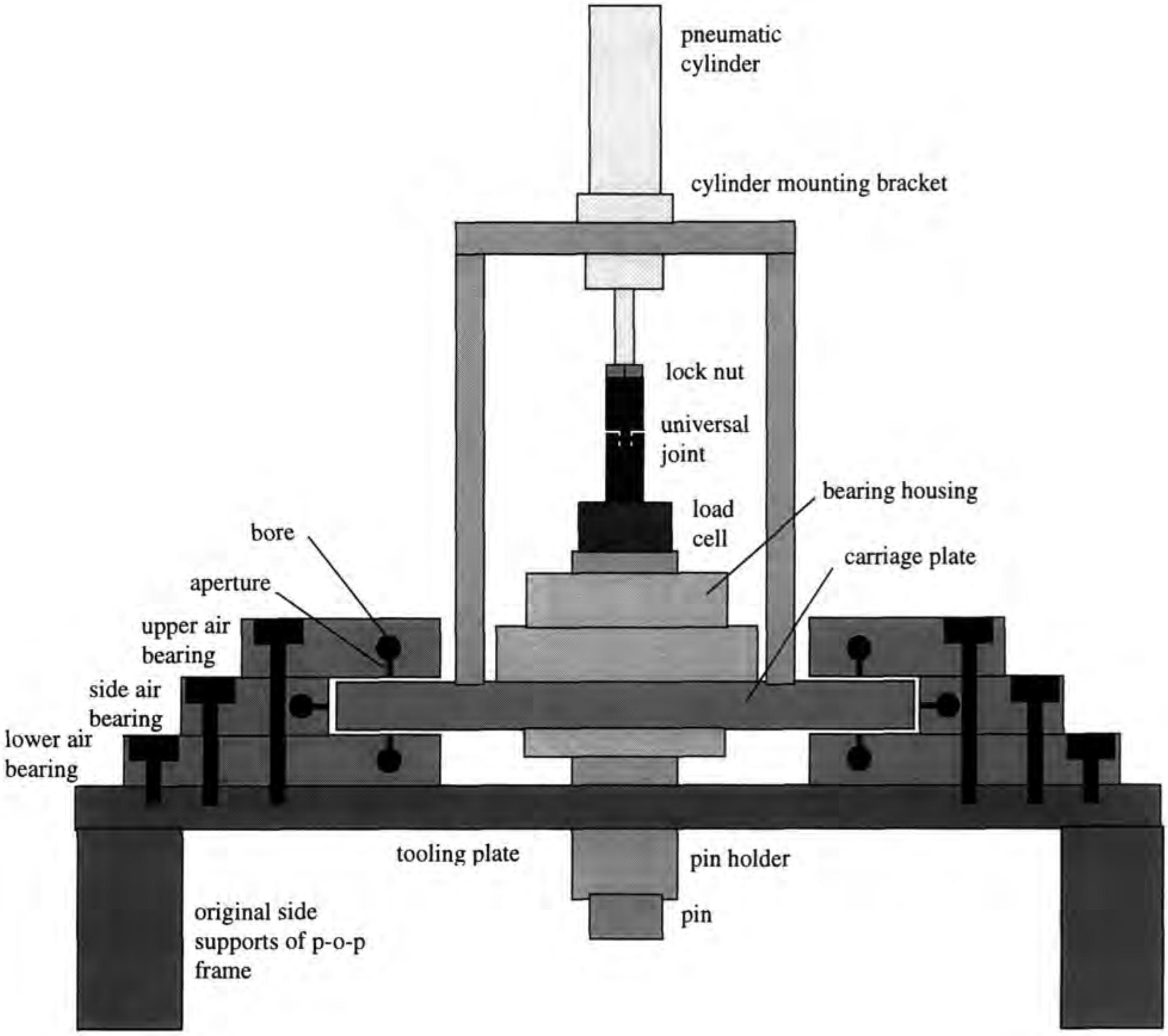
pneumatic cylinder
cylinder mounting bracket
lock nut
universal joint
bearing housing
load cell
bore
carriage plate
aperture
upper air bearing
side air bearing
lower air bearing
tooling plate
pin holder
original side supports of p-o-p frame
pin

Figure 3.12 A schematic representation of the air bearing assembly of the pin-on-plate apparatus

The two C-section sides of the air bearings where built up from lower bearing pads, side bearing pads and upper bearing pads to give the C-Section as shown in the above figures. The dimensions and pressures required for each of the three pairs of bearings two side, two lower, and two upper were all calculated (Appendix C). The critical set of bearings, however, were the upper bearings as these would have to support the upwards reaction force to the applied load. The lower bearings would only support the weight of the friction measuring carriage and its attachments, and the side bearings provide enough force to maintain the alignment of the plate within the bearings. In order to maintain symmetry and allow for future changes in the machine's use, the upper and lower bearings sets were made identical and simply operated at different pressures to give the appropriate load carrying capacities.

The three pairs of bearing pads and the carriage plate within them were all manufactured from brass plate of a standard uniform thickness of 12.00 mm. The two upper and two lower pads each measured 18.00 mm wide and 124 mm long. Each of the four pads included thirteen 0.41 mm diameter orifices along the centre of the pad's width spaced at regular intervals along its length. These orifices were bored to a depth of 3.5 mm to meet the 5 mm bore running centrally through the length of the bearing supplying the bearing pressure. The two side pads measuring 12.00 mm deep and 124 mm long, included three 0.41 mm diameter apertures at regular spacing centrally along their length connecting to an identical 5 mm bore. In each of the six bearing pads, one end of the central bore was closed off and the other threaded to a M5 thread to fit pneumatic connections.

The two C-section bearing arrangements (lower then side then upper bearing pads) were dowelled and bolted to a 125 mm long by 263 mm wide tooling plate which fitted onto to the four supporting columns of the original pin-on-plate machine. The plate ensured the alignment of the bearing sections both within the two C-sections and between them, and maintained the rigidity and fine tolerances required to ensure the minute clearances between the bearing surfaces which were necessary for effective air bearings. As air has a very low viscosity, and the stiffness of the bearings was critical in this application if the load's reactive force was to be supported without an increase in friction, the clearances between the surfaces were of the utmost importance in the design. Theoretically a clearance of 25 μm between each of the bearing surfaces was suggested to give a bearing of optimum stiffness, but in manufacture the minimum clearance which could be reliably produced was closer to 50 μm. This was therefore allowed for in the design so that the minimum film thickness under maximum load was more than three times the roughness of the surfaces. When bolted into place, the C sections had an internal height of 12.00 mm, and an internal width of 146.00 mm (100 μm thicker and wider than the carriage plate). The tooling plate had a central orifice of 50 mm to allow the vertical movement of the pin and pin holder.

A 11.90 mm thick brass carriage plate fitted into two C-section bearing assemblies, measuring 145.90 mm wide and 108 mm long, ground and polished down to a fine finish to allow the 50 μm clearances between surfaces. The carriage plate was made shorter than the bearing pad assemblies to allow a degree of adjustment of its position in the direction of the reciprocating motion, whilst ensuring that in operation, it was evenly supported by all thirteen jets of air from each upper and lower bearing pad and all three jets from each side bearing pad. The bearing pad and carriage plate assembly thus allowed very low friction movement in the direction of the reciprocating motion whilst restraining the movement of the carriage in the vertical and transverse directions using the pressure of the air bearings. The carriage plate was machined to hold the mounting bracket of the pneumatic loading cylinder as well as the bearing housing holding the linear roller bearing through which the pin holder articulated.

The carriage was restrained, as previously, by the piezoelectric force transducer. In order to reduce noise in the system further, the connection between the transducer and the carriage plate was also modified. Figure 3.13 shows the modified transducer connection.

The previous arrangement of connection used a simple threaded bar rigidly screwed into the transducer at one end and into a connection on the carriage plate of the friction measuring carriage at the other. This allowed mechanical noise to be transmitted to the transducer, and also caused bending moments in the transducer if the carriage plate moved out of alignment with the transducer (as it may have done under dynamic loading of the carriage). The new arrangement connected the transducer to carriage by means of a miniature universal joint connected at each end to a threaded bar. At the transducer end, the bar was screwed rigidly into place, but at the carriage end, it was connected to the plate by means of a slotted bracket, as in the simulator. A nylon washer was placed either side of the slot and two lock nuts were fixed either side of the washers so that a fine clearance was maintained either side of the slot. The universal joint was subsequently removed as although it allowed greater flexibility in the coupling it was not seen to provide any further benefit in reducing noise or improving the transmission of the transducer's signal, and was seen to fail at high friction.

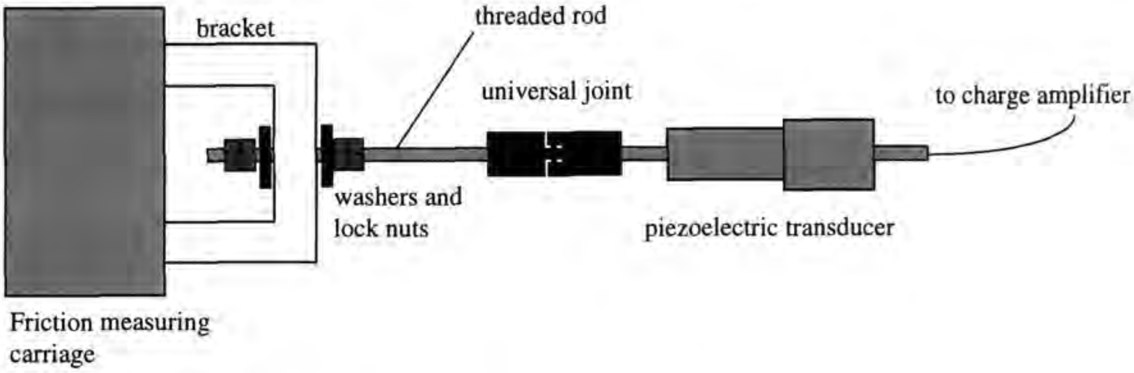

Figure 3.13 A schematic representation of the modified connection of the friction transducer on the pin-on-plate apparatus

As mentioned earlier, the bored end of each bearing pad was threaded to fit a pneumatic connector. Each of these connectors fitted to a length of 4 mm tubing and then each pair of bearing pads (lower, side and upper) was attached to a pressure regulator . In this way, the pressure supplied to each half of the bearing pair would be equal at all times, but the pressure supplied to the lower, side and upper bearing pairs could be adjusted independently, depending on the conditions of the tests. A fourth regulator was added to control the pressure supplied to the pneumatic loading cylinder and then the inputs to all four regulators were connected to a combined filter regulator so that the pressure to the entire system could be shut down without adjusting the individual regulator pressures, ensuring consistency between subsequent tests. From the calculations in Appendix C, the side and lower bearings operated at a pressure of less than 1 bar. Less than 1 bar of pressure would be required to the upper bearings to support the reactive force to a load of 40N, and under a supply pressure of 4.5 bar a load of 272N could be supported by the bearing arrangement.

Following tests, described in Appendix D, undertaken to ensure the air bearings were operating efficiently and with minimum frictional losses, even when subjected to loading forces, it was found that the new air bearing system for the friction measuring carriage gave rise to losses of between 5 and 10 %, representing a substantial improvement on the roller bearings which were found to operate under 54.3 % losses.

3.2.2.3 Instrumentation and control

The aim of this research was to produce an alternative testing method for compliant layered joints with as simple a format as possible. For this reason, it did not seem appropriate during the development stages to include in the design of the machine such additions as a closed loop electrically triggered loading system, a proportional valve to allow more complicated loading regimes, or for that matter, digital measurement of the load and friction. Contrarily, it was felt, that whilst in the long run, logging the resulting data digitally would probably save time in manipulation and analysis, it may result in a loss of accuracy in measurement in the analogue to digital conversion, and would almost certainly allow a greater chance of important aspects of the friction measurement being missed during automatic interpretation of results. If the machine, now developed, were to be used for extensive testing, it may be beneficial in terms of time to include these additions.

For the purposes of this research, however, the friction and load signals from the piezoelectric force transducer and the load cell were amplified by a charge amplifier and strain gauge amplifier respectively and fed to an XYT plotter. This meant that all aspects of the form of the friction and load traces as well as the more obvious magnitude of the forces could be easily monitored throughout testing and any inconsistencies or errors quickly diagnosed. This also facilitated adjustment of the loading cycle.

The temperature of all tests was maintained at body temperature using a thermocouple in the lubricant bath of the plate mounting attached to a temperature control unit set to 37°C. The viscosity of the lubricant and the mechanical properties of the compliant layered bearings could alter if the temperature of testing was not maintained.

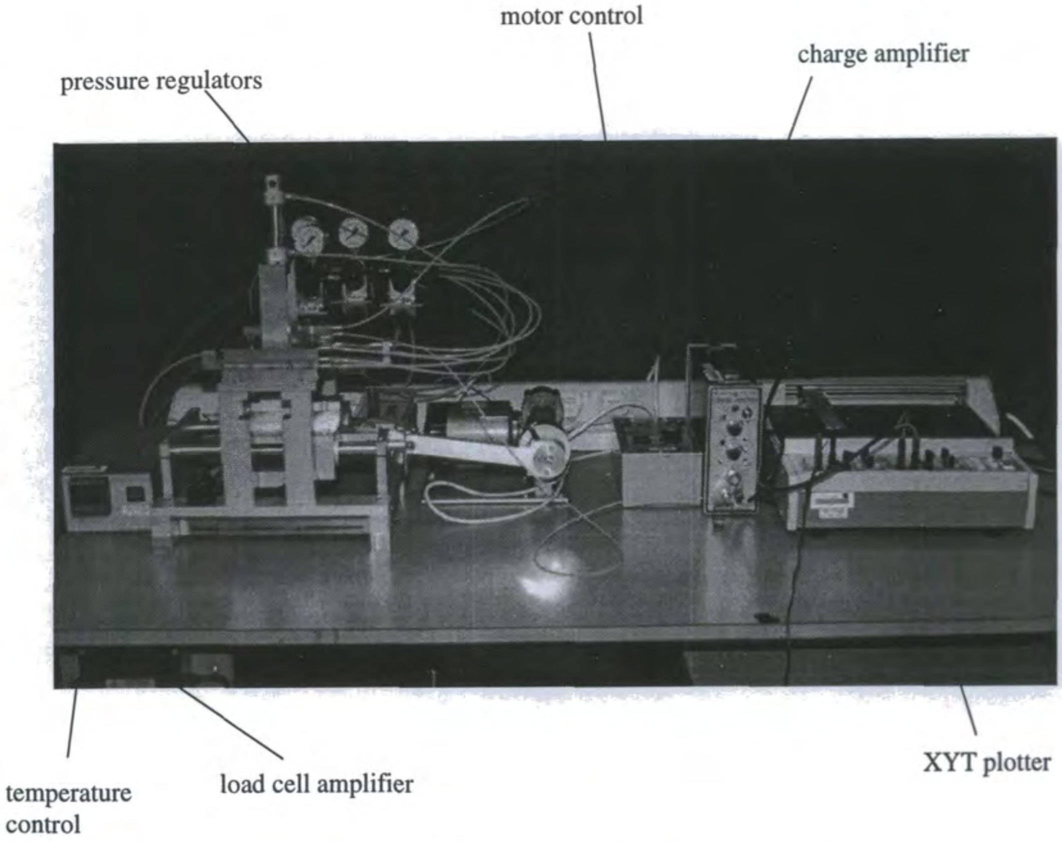
motor control
charge amplifier
pressure regulators
temperature control
load cell amplifier
XYT plotter

Figure 3.14 Instrumentation and control of the pin-on-plate friction measurement apparatus

4. Materials and Methods

4.0 Introduction

Throughout the extensive experimentation undertaken on both the hip function friction simulator and the modified pin-on-plate friction measuring machine, standard testing methods and protocols were used wherever possible to ensure as high a level of consistency as possible. In the case of the simulator which had been operated successfully for several years, a proven test protocol was used, while in the case of the pin-on-plate machine initial studies allowed a protocol to be designed so that repeatable results could be achieved. The materials and lubricants used were also standardised. In addition, the surface topography of all bearing surfaces were monitored at regular intervals over the course of the research so that the effect of bearing surface roughness could be assessed or neglected. The materials and methods used in preparing the bearing surfaces and evaluating their tribological performance are discussed in this chapter.

4.1 Materials

Two material combinations were considered in an attempt to develop a realistic test method for compliant layered joints. These were: the conventional artificial joint combination of metal against UHMWPE, and a coupling of metal against compliant layered bearing surface.

A detailed discussion of the design of compliant layered joints and the possible materials used, including medical grade polyurethanes as used here, was provided in sections 2.3 and 2.4. At the time of commencement of this research, members of the Centre for Biomedical Engineering at Durham had been investigating compliant layered bearings for more than fifteen years and so both the selection of the material and the design of the bearing were fairly advanced.

The compliant layered surfaces consisted of a thin layer of low modulus polyurethane (PU) bonded to a thicker layer of higher modulus polyurethane as a backing. The PU/PU combination had been shown [Burgess 1996] to have the advantage of a better bond integrity between the two layers than other combinations: a maximum peel force of 860N was achieved for the final PU/PU bond chosen compared to values of around 10N for an earlier combination of PU/UHMWPE. Medical grade polyurethanes, Corothane 80A and Corothane 75D, had been chosen for the soft and hard layers respectively, as they had been proven to have good biocompatibility [Pinchuk 1994]. The compliant layered bearings were produced by an injection moulding procedure, the parameters of which had all been investigated to maximise the bond strength between the two surfaces and surface finishes produced.

The optimum bond strength for PU/PU plates was given by injection moulding the low modulus layer at a temperature of 215 °C and pressure of 40 bar, removing it from the mould and allowing it to cool, then replacing it in the mould and injection moulding the higher modulus layer to the back of it at 230 °C and a pressure of 40 bar [Smith *et al* 1996]. The plates used in all tests undertaken on the pin-on-plate machine were 49 mm long by 20 mm wide, with a 3 mm compliant layer and 5 mm rigid layer, and were cut from the 100x20x8 compliant layered plates originally designed for use in peel tests. A polished metal insert was added to the original peel test sample mould so that a high surface finish could be achieved on the plates. Care was taken to place the 'hot' samples on a flat surface to cool so that the moulded plates were as flat as possible.

Acetabular cups were manufactured in a similar way but in reverse. A high modulus 75D cup was injection moulded onto a core of diameter equal to the femoral head diameter plus the required clearance plus spacers equal to the thickness of the soft layer. It was cooled and replaced in the mould against the core (the spacers now removed) and a low modulus 80A backing was moulded onto it. This inverse moulding was required to maintain the integrity of the cup shape. Tibial trays of compliant layered knee bearings were made in the same way, although knee bearings were only used in one experiment during the course of this research, namely the cylinder experiment as described in Chapter 7. All acetabular and tibial components used during this research consisted of a three mm compliant layer bonded to a 5 mm backing, so that layer thicknesses in simulator and pin-on-plate tests were standardised.

The two part injection moulding process to manufacture compliant layered bearings was undertaken at Howmedica Limerick. All polyurethane bearing surfaces were conditioned in a Ringers bath at 37 °C for a minimum of 72 hours prior to testing as this had been shown significantly to improve their frictional performance [Burgess 1996]. Figure 4.1 shows an example of each of the three compliant layered bearings used consisting of a plate for the pin-on-plate machine, an acetabular component, and a non-conforming tibial tray.

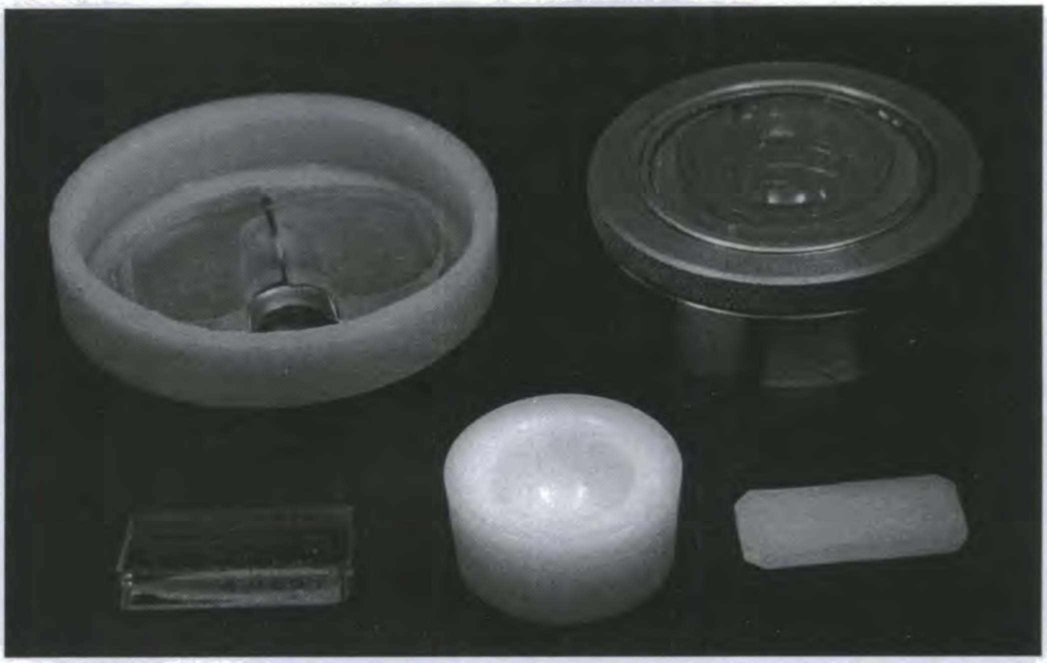

Figure 4.1 Examples of polyurethane and UHMWPE components

In addition to compliant layered bearings, experiments were undertaken on both pin-on-plate and simulator apparatus to measure the friction generated in conventional UHMWPE bearings. In the case of the simulator experiments, a standard Protek 32.4 mm diameter UHMWPE acetabular cup was used. For the pin-on-plate apparatus, plates of 49x20x4 mm were machined from standard UHMWPE (ISO 5834/2). Figure 4.1 also shows examples of the polyethylene cup and plates.

The hard counterface in all complaint layer and conventional bearings was stainless steel (medical grade 316) or cobalt chrome molybdenum (CoCrMo). In simulator tests, three femoral heads were used in hip mode tests depending on the experiment: a standard Howmedica 32 mm Exeter CoCrMo head, a Howmedica 28 mm Exeter CoCrMo head, or a mounted 30 mm ball stainless steel bearing of similar surface finish were. In the pin-on-plate apparatus, 15 mm diameter pins with bearing surfaces of a range of radii of curvature were used (10mm to 200mm). The pins were manufactured and polished to a similar surface finish to typical femoral heads at Howmedica, Limerick. Finally, in the cylinder tests described in section 5.7, stainless steel cylinders were designed for the two machines. Figure 4.2 and 4.3 shows the range of heads, pins and cylinders used in the measurement of friction on the two machines.

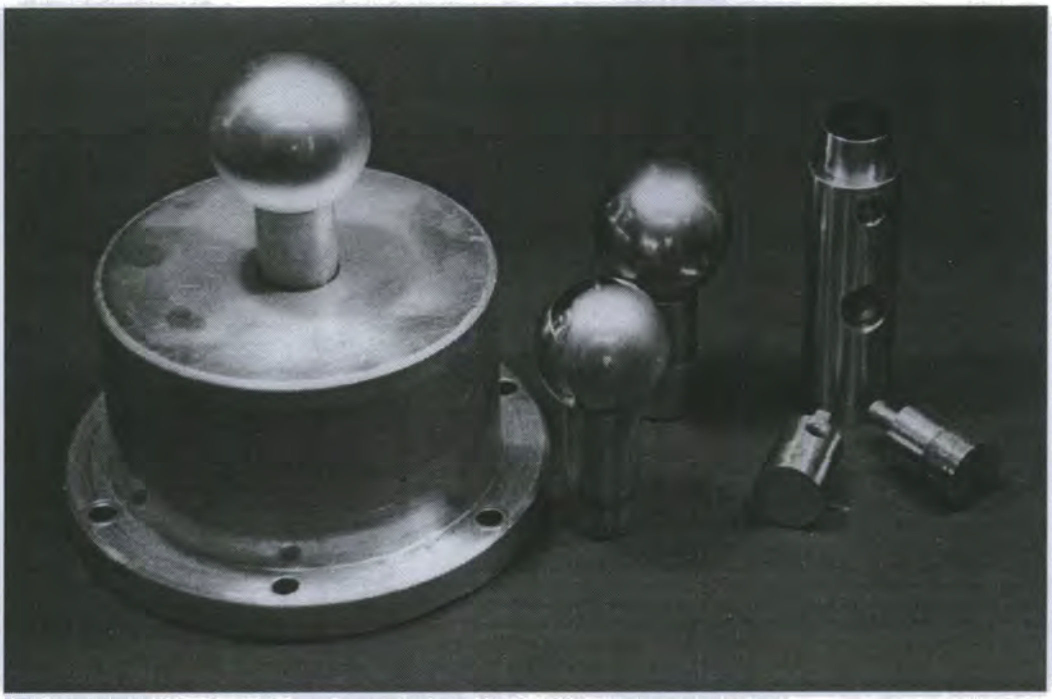

Figure 4.2 Examples of femoral heads and spherical pins

All bearings cups, plates, heads and pins were marked so that they could be tested each time in the same orientation.

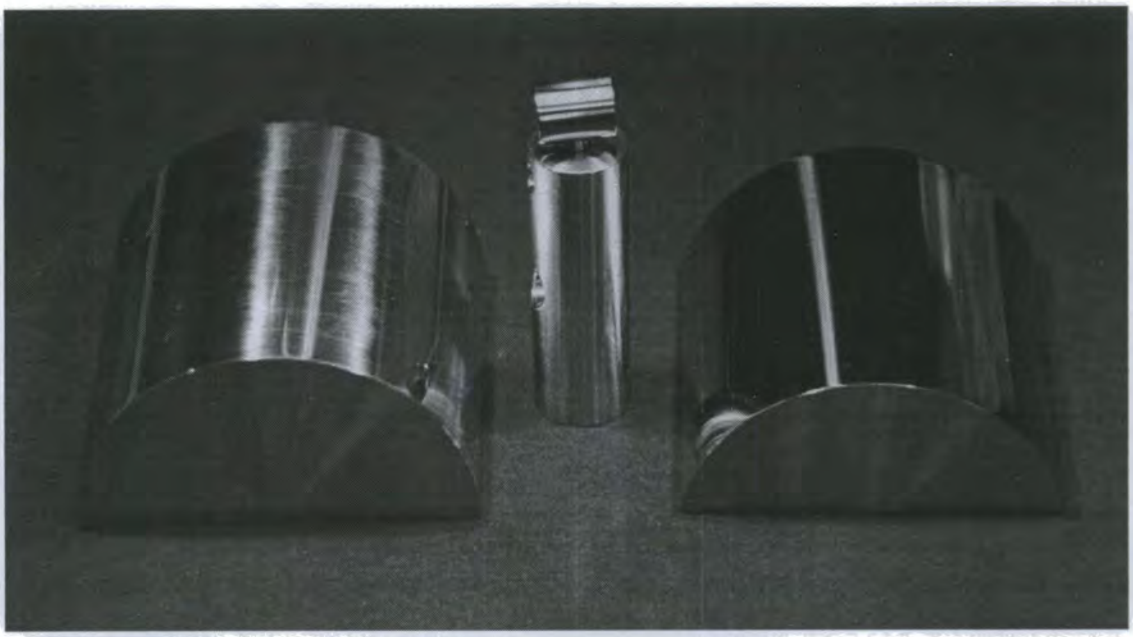

Figure 4.3 Examples of cylinders for simulator and pin-on-plate apparatus

4.2 Friction measurement on the Simulator

Extensive testing over its five years of use, by Blamey [1993] and Burgess [1996] and then during the three years of experimentation undertaken during the course of this research, had allowed a standard testing procedure to be devised. This included steps to mount the components, ensure alignment of centres and minimise misalignment torques, calibration of the various measurement systems, and use of a standard experimental protocol.

4.2.1 Mounting and elimination of misalignment errors

Various steps were undertaken to minimise misalignment of bearing components in the simulator and the inherent frictional torque errors that misalignments incur. Current experimental protocol allowed the effects of these misalignment errors to be minimised both in terms of the physical mounting of components and in terms of experimental procedures to reduce them.

In order to ensure the centre of the femoral head was aligned with the centre of rotation of the motion mechanism the assembled height of the femoral head component was set precisely. Similarly, the height of the acetabular cup (or tibial tray) was set to ensure alignment of the centre of rotation of the cup or tray with the centre of rotation of motion. For hip components, this was carried out by mounting the acetabular cup in bone cement within the test mounting using a jig. Further adjustment of the acetabular component was then allowed by adjusting a locking ring on its mounting until the correct height was reached. In the case of the tibial knee components, the alignment of centres was undertaken ensuring all components have the same overall height and by machining a 'snap-fit' to the underside of the components fitting them precisely to a common mounting.

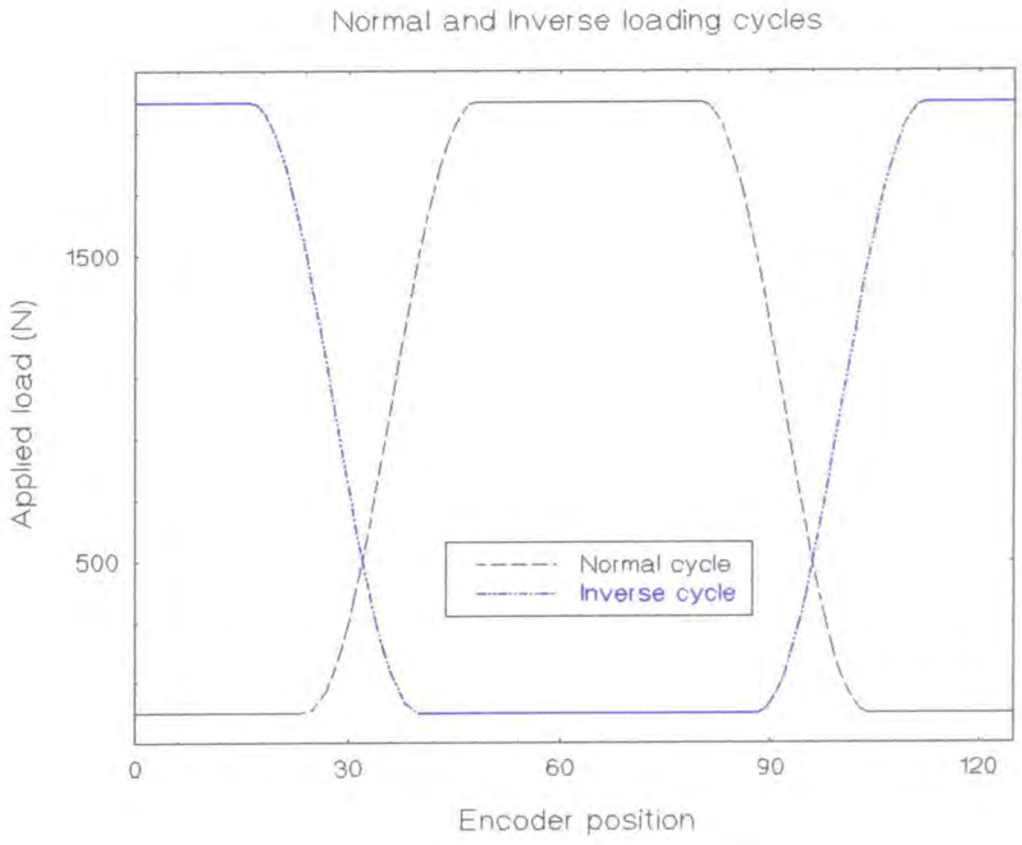

Figure 4.4 Plot of the forward and reverse loading cycles of the simulator

Anterior-posterior alignment was ensured by forward-backward motion of the hydrostatic bearings which could be checked by passing a 5 mm mandrel through holes machined in the centre of the motion assembly and hydrostatic journal bearings. In the case of the knee bearings, the hydrostatic linear bearings were disconnected and the anterior-posterior position of the tibial tray fixed by means of four bolts to prevent dislocation of the joint, the optimum alignment found by means of the mandrel.

In spite of these preventative measurements, misalignment of the acetabular cup or tibial tray with respect to the hydrostatic journal bearings was still not accommodated by the system, although it could result in an offset force and torque on the friction carriage potentially larger than those generated in the joint. In order to eliminate such torques from measurements, two phases of experimental procedure were undertaken: a forward phase, with the high load being applied in the forward direction of swing, and a reverse phase when the high load was applied in the backward direction, i.e. out of phase by half a cycle or 64 encoder pulses as shown in figure 4.4.

It was assumed that the true frictional torque, T, would have the same magnitude but opposite sign during forward and reverse loading and that the misalignment torque, T_e, would have the same magnitude and sign in both directions [Burgess 1996]. If the frictional torques measured in forward and reverse directions are T_F and T_R and are given by

$$T_F = T_e + T \qquad \text{Eqn. 4.1}$$

$$T_R = T_e - T \qquad \text{Eqn. 4.2}$$

the true frictional torque is given by

$$T = \frac{T_F - T_R}{2} \qquad \text{Eqn. 4.3}$$

Thus the misalignment torque could then be eliminated by the software in processing the test data.

4.2.2 Calibration and analysis of errors

Following every change from hip to knee mode, any extended break in testing (two weeks or more), or at regular intervals of four weeks, all measurement systems of the simulator were calibrated against known external parameters. In this way, the ADC outputs from the load cells, angular potentiometer, incremental encoder, and force transducer could be converted to real physical units. The load ADC and DAC were compared to an external load cell, the position ADC to an angular spirit level, and the friction ADC against a known torque applied to the friction measuring carriage. The resolution of the three measurement systems were 3.3 N/bit, 0.03 °/bit and 1.8 Nmm/bit for the load, angle and friction torque ADC's respectively. The calibration coefficients recorded were then fed into calibration files which were used by the software in processing the test data. Comparison of the calibration coefficients recorded over several years showed there to be very little variation and have allowed any inconsistencies to be identified quickly when they have arisen.

A detailed assessment of the precision of the simulator was undertaken by Burgess [1996]. Considering the summation of the errors in load measurement arising from ADC bit noise, load cell linearity and repeatability and strain gauge amplifier accuracy and the errors in frictional torque measurement arising from ADC bit noise, force transducer linearity and charge amplifier accuracy, he estimated the maximum error would be 4.5%, 12% and 98%, for friction factors of 0.1, 0.01, and 0.001 respectively. This would suggest that whilst the simulator provided an acceptable level of precision, of approx. 10%, for values of friction factor seen typically for conventional joints, 0.1 to 0.01, for very low friction factors as seen typically for compliant layered joints, 0.001, its precision decreased drastically. It was therefore suggested that whilst the simulator could be used effectively to demonstrate when very low friction regimes, such as full fluid film lubrication, were occurring, discerning trends in results at these very low values would be difficult.

4.2.3 Standard experimental protocol

Prior to testing, the simulator and the joint to be tested was 'warmed-up' for 400 cycles and then the cooling system to the servo-hydraulics connected. This was to allow the servo-hydraulic loading system to reach a steady temperature so that subsequent changes would be minimum, hence keeping the applied load relatively constant throughout testing (see Appendix A).

A standard test consisted of 41 cycles, during which load, angle and friction data received from the three ADCs, along with the encoder position, was recorded in digital form for typically the 1st, 21st and 41st cycles. For each test, the following parameters were entered: user i.d., cup i.d., head radius, viscosity of lubricant, loading curve (normal or inverse), number of cycles, and the cycles at which data was to be recorded. Each individual set of test data, including the inputted parameters, was saved as a numbered file which included the joint id in the title. A normal and inverse run was performed for each set of test. Tests of this form were undertaken for a range of lubricants with different viscosities in order to provide friction measurements at a range of Sommerfeld numbers (viscosity x speed /applied load per unit width). After each pair of forward and reverse runs, both components were removed from the simulator and cleaned thoroughly. Where water based lubricants were used, this was done by running them under a tap and then washing in soap and water followed by a rinse in distilled water, or by washing them thoroughly in isopropanol where oils where used. It was important to clean the components thoroughly as even small amounts of debris or dust could disrupt the very small fluid films which were expected.

Typically, each series of tests under a specific set of conditions would be repeated three times to ensure consistency of results. Table 4.1 shows the standard experimental protocol used in simulator testing.

1. Mount acetabular component in bone cement using correctly adjusted jig. Condition polyurethane components for 72 hours in Ringers bath at 37 °C.
2. Mount femoral component in holder. Check vertical height and adjust if necessary by adding spacers. Align any scratches with direction of motion.
3. Place acetabular component in mounting and ensure correct orientation. Add lubricant to cup.
4. Attach femoral head in holder to oscillating carriage and with hydrostatic bearings switched on, check vertical clearance of head in cup to ensure alignment of component centres. Adjust height of acetabular mounting using locking nuts if necessary.
5. Switch on PC and Motorola 68020, establish parallel connection and enter simulator software.
6. Switch on servo-hydraulic loading pump, and run 400 warm-up cycles. Turn on servo-hydraulic cooling system.
7. Remove both components, clean thoroughly with either soap and water (water-based lubricants) or isopropanol (oil-based lubricants). Dry using a lint-free cloth. Replace components, re-attach in position and add new lubricant.
8. Select required test conditions in software (minimum load, maximum load, joint radius, joint id, lubricant viscosity, forward/reverse loading cycle, no. of cycles, cycles to be recorded) and note file number.
9. Conduct a 'forward' run.
10. Conduct a 'reverse' run.
11. Repeat steps 7 to 10 until all viscosity lubricants have been used, using lubricants in a random order and carrying out several tests for one viscosity to assess any time-related changes.
12. When all tests in series are complete, edit and run data analysis program to process the results.
13. Repeat series of tests several times to ensure consistency.

Table 4.1 Simulator Testing Protocol

4.2.4 Analysis of Results

After all viscosities were tested, an analysis file was edited to include the appropriate file numbers and run to process the results. For the selected recorded cycles, the measured digital values of encoder position **i**, the applied load **L_i**, the measured frictional torque **T_i**, and the angle of the femoral head **A_i** were converted to real physical parameters using the measured calibration coefficients. In order to combine the values obtained for the forward and reverse loading cycles using Eqn. 4.3 it was necessary to eliminate the phase difference between the cycles. For each of the 128 points in the cycle (**i**) this was done by calculating the applied load, frictional torque, and angular position using equations 4.4, 4.5 and 4.6 respectively.

$$L_i = \frac{\left(L_{fi} + L_{r(i+64)}\right)}{2} \qquad \text{Eqn. 4.4}$$

$$T_i = \frac{\left|T_{fi} + T_{r(i+64)}\right|}{2} \qquad \text{Eqn. 4.5}$$

$$A_i = \frac{\left(A_{fi} + A_{r(i+64)}\right)}{2} \qquad \text{Eqn. 4.6}$$

Similarly the entraining velocity, **u_i**, at all 128 points i the cycle was given by equation 4.7 where f was the frequency of the flexion-extension motion (0.8 Hz), and α, the amplitude (25 ° for hips or 35 ° for knees).

$$u_i = \frac{1}{2}\left(\frac{2\pi\alpha}{360} f \cos\left(\frac{2\pi i}{128} + \frac{2\pi\alpha_0}{128}\right)\right) R_1 \qquad \text{Eqn. 4.7}$$

where R_1 was the radius of the femoral head.

The Sommerfeld number, as adapted for use on the simulator, **Z_i**, was then calculated from equation 4.8.

$$Z_i = \frac{\eta u_i R_1}{L_i} \qquad \text{Eqn. 4.8}$$

This adaptation of the original Sommerfeld number [Gumbel 1914] had been used in all previous testing on the Durham simulators and had been frequently quoted in published results. In comparing simulator and pin-on-plate results however it was effectively useless as the two machines used very different bearing geometry and so the difference in values of R_1 would give rise to very different results. For this reason, another adaptation of the Sommerfeld number, Z, was devised for pin-on-plate Stribeck results and then simulator data adjusted accordingly as described in Section 4.3.4.

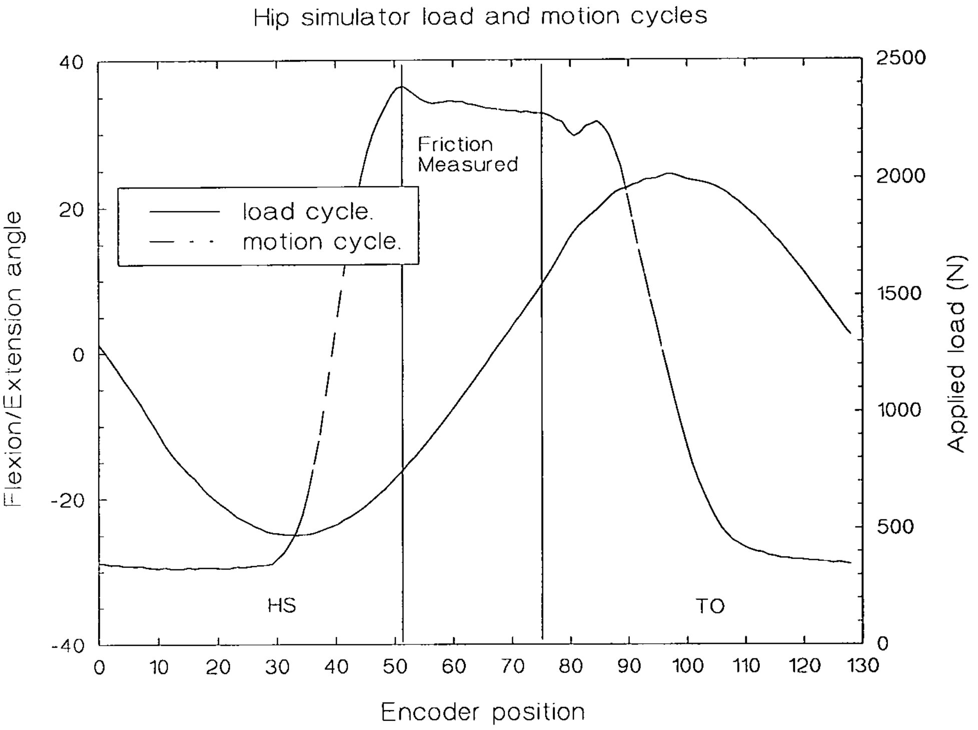

Figure 4.5 A plot of the simulator load and motion cycles showing the region over which frictional torque is measured

For each of the 128 points, the encoder position, the applied load, frictional torque, friction factor [Unsworth 1975] and Sommerfeld number were calculated. The area of interest in measuring friction was when the frictional torque would be at a maximum, during the high load stance phase of the cycle. For this reason, from the 128 data points, five points were then chosen corresponding to encoder positions of 51.5, 57.5, 63.5, 69.7, 75.5 at which the applied load and velocity were simultaneously at a maximum as shown in Figure 4.5. This is an improvement on Auger *et al*'s simulator results [1993] which only considered the one point at which load and sliding velocity were maximum.

Whilst data for the 1st, 21st and 41st cycles was processed, it was usual to consider only the 41st cycle data for purposes of analysis. These data were then plotted as a Stribeck curve (friction factor against Sommerfeld Number) to allow the lubricating regime of the tested joint to be assessed.

4.3 Pin-on-plate Tests

Whilst pin-on-plate machines have been used extensively to measure the wear in bearings, their use in measuring friction has been less commonplace. The standard practice for wear and friction testing of polymeric materials using reciprocating pin-on-flat apparatus was defined by ASTM F732-82 [1991] but whilst a clear wear testing protocol was defined, the recommendations for use of the pin-on-plate apparatus in friction testing was less specific. The Durham pin-on-plate friction measuring apparatus had been used in various studies previously [Hills 1994] but never for research of this scale. Moreover, the protocol used in achieving the results published elsewhere differed considerably, from examination of the friction during one single stroke [Caravia 1993a, 1993b, 1995] to intermittent measurement of friction throughout a several million cycle wear test [Saikko 1993b]. As the majority of the experimentation during this research would be undertaken on the pin-on-plate friction measuring machine, and that the aim of the project was to produce a realistic test method, it was therefore vital in the early stages of the project to define a standard testing procedure which could give consistently repeatable results. This included calibration of both the load cell and force transducer, the experimental protocol itself and the subsequent analysis of results.

4.3.1 Calibration and error analysis

The load cell and piezoelectric force transducer were both calibrated in situ against known external parameters at regular intervals (approx. 1 month), or following any modification to the apparatus.

The load cell was calibrated by removing the pneumatic loading cylinder in its mounting and applying dead weights directly to the load cell. By mounting the pin in the pin holder and the plate in its mounting as normal, the load cell was restrained and the response of the load cell to the loading could be measured. The load cell was connected to a strain gauge amplifier with a variable gain and zero, which were adjusted and set so that the measured displacement of the XYT plotter was within a measurable range for all applied loads. A range of loads, corresponding to the range of the load cell (0 to 50N), was applied and the displacement of the XYT plotter measured under each loading. This was repeated nine times to allow the consistency of the measurement to be considered. A calibration coefficient relating the applied load (N) to the measured displacement (mm) could then be obtained.

In the second phase of load cell calibration, the measured displacement of the XYT plotter was then related to the pressure applied to the pneumatic loading cylinder. The cylinder and cylinder mounting were replaced and a range of pressures (0.5 to 5 bar) was applied to the cylinder and the plotter displacement measured for each recorded value of pressure, repeating the measurements a minimum of 10 times to establish consistency. A calibration coefficient relating applied pneumatic pressure (bar) to the measured displacement (mm) was then calculated. In the case of the larger cylinder, this could only be accomplished for a small range of pressures (0.1 to 1.0 bar) or else the measurement range of the load cell would be exceeded. This could then be compared with the earlier calibration of applied load (N) against measured displacement (mm), so that the load applied to the bearing plate could be directly calculated from the reading of applied pneumatic pressure (bar), taking into account the extra mass of the pin and pin holder beneath the load cell. For the larger cylinder, for tests above 1 bar pressure, it was then necessary to replace the load cell with a dummy of the same dimensions to prevent damaging the fragile strain gauges, and then extrapolate the applied load from the measured pneumatic pressure.

The graphs of calibration of the load cell are provided in Appendix E. The standard deviations in the measurements achieved under each loading where typically of the order of 1.7% for the 10mm cylinder and 1.1% for the 25mm cylinder, and the correlation coefficient of the straight line calibration curves typically 0.9892 and 0.9976 respectively suggesting excellent repeatability and linearity.

The piezoelectric force transducer was calibrated in a similar manner. At the opposite end of the friction measuring carriage plate to the friction transducer was connected a thread which ran over a low friction pulley on the main frame of the machine. By hanging dead weights from this thread, tangential forces could be applied to the transducer via the carriage and its response to a known force assessed. This was the method used in measuring the losses of the roller and air bearing systems as described in Appendices B and D.

A range of loads were applied to the carriage between 0.01 N and 15 N to allow for all test conditions resulting in measured coefficients of friction in a range of 0.001 to 0.1 under applied loads between 10 N and 150 N. The transducer was attached to a charge amplifier with variable settings (time constant, gain, filter) which were adjusted to allow the full range of frictional forces to be measured by the XYT plotter and then set for all tests. Changes of sensitivity, to accommodate the range of frictional forces, were then made on the XYT plotter. For each applied force, the displacement of the plotter was measured and recorded. This repeated a minimum of ten times for each force to measure the consistency of the transducer's operation. A calibration coefficient was then calculated relating the force applied to the transducer (N) to the measured displacement (mm) for each plotter sensitivity. The standard deviations of the measurements for any particular force were of the order of 3%, and typically the correlation coefficient of the calibration curve was 0.9978. Only at very high sensitivities (frictional forces of approx. 0.01 N) were any significant errors seen, when the electrical and mechanical noise in the laboratory was frequently of an order of magnitude similar to the transducer signal. The calibration plots of the piezoelectric force transducer are given in Appendix D.

In the same way that Burgess [1996] estimated the systematic errors in the simulator measurement systems, the errors incorporating in measuring coefficient of friction on the pin-on-plate friction measuring apparatus can also be estimated. The specifications of all components of the measurement system of the pin-on-plate apparatus are given in table 4.2.

Component	Specification	Max. Error
load cell	accuracy ± 0.25% FS	0.375N for 150N load
strain gauge amplifier	linearity ± 0.02% FS	0.03N for 150N load
piezoelectric transducer	linearity ± 1% FS	0.15N for 15N force
charge amplifier	linearity ± 1% FS	0.15N for 15N force
XYT plotter	accuracy ± 0.25% FS	0.375N for 150N load 0.0375N for 15N force
	human measurement error (± 0.5mm on ruler)	0.278N for 150N load 0.0571N for 15N force

Table 4.2 Specification of the components of the measurement systems of the pin-on-plate apparatus

The total errors in the measurement of the applied load, ΔL, can be estimated as the sum of the errors in the load cell, strain gauge amplifier and XYT plotter as given by equation 4.9.

$$\Delta L = (\mathit{cell.\ accuracy}) + (\mathit{SGA.\ linearity}) + (\mathit{SGA.\ accuracy}) + (\mathit{plotter.\ accuracy}) \qquad \text{Eqn. 4.9}$$

Considering the specifications of components given in table 4.2, the maximum error in measured load would be 0.52% plus an error equivalent to ± 0.5mm displacement, that is 0.190N (0.052N + 0.137N) for an applied load of 10N and 1.06N (0.78N + 0.278N) for an applied load of 150 N.

Similarly, the total errors in the measurement of the frictional force, ΔF, can be estimated as the sum of the errors in the piezoelectric transducer, the charge amplifier (CA), and the XYT plotter as given by equation 4.10.

$$\Delta L = (transducer.\ linearity) + (CA.\ accuracy) + (plotter.\ accuracy) \qquad \text{Eqn. 4.10}$$

Using the specifications of components given in table 4.2, for a coefficient of friction of 0.001, the maximum error in measured frictional force would be 2.25% plus an error equivalent to ± 0.5mm displacement, $1.38\text{x}10^{-3}$ N ($2.25\text{x}10^{-4}$ N + $1.15\text{x}10^{-3}$ N) for a 10 N applied load and $5.63\text{x}10^{-3}$ N ($3.375\text{x}10^{-3}$ N + $2.25\text{x}10^{-3}$ N) for a 150 N applied load. For a coefficient of friction of 0.1, the maximum error in measured frictional force would be 0.339 N (0.0225 N + 0.0114 N) for a 10 N applied load and 0.395 N (0.3375 N + 0.05705 N) for a 150 N applied load.

In standard testing procedure the result of interest is the calculated coefficient of friction, defined as the ratio of frictional force to applied load. The total error in calculated coefficient of friction, Δμ, can be estimated as

$$\Delta\mu = \mu.\sqrt{\frac{\Delta L^2}{L^2} + \frac{\Delta F^2}{F^2}} \qquad \text{Eqn. 4.11}$$

The maximum error in the calculated coefficient of friction on the pin-on-plate apparatus for all conditions are given in Table 4.3. It shows that the percentage error is between 14% for a coefficient of friction of 0.001 under an applied load of 10N and 3% for a coefficient of friction of 0.1 under 150N applied load. These correspond to max. errors of $1.39\text{x}10^{-4}$, $4.88\text{x}10^{-4}$, $2.72\text{x}10^{-3}$, in coefficients of friction of 0.001, 0.01 and 0.1 respectively.

As discussed in Section 4.2.2 Burgess [1996] estimated a maximum error in calculated friction factor for each test as 3.2%, 8.3% and 69%, or for the combined results of forward and reverse runs as 4.5%, 12%, and 98% ($\sqrt{2}$ times individual errors) for calculated friction factors of 0.1, 0.01 and 0.001 respectively. From the calculated values in table 4.3, the pin-on-plate measurement system clearly operated with less systematic errors than that of the simulator. This was due to the large errors provided by the ADCs and DACs in the simulator, each having only a 2 bit precision and so giving rise to large errors in both load and frictional torque measurement. By operating an entirely analogue system, as described in Section 3.2.2.3, the errors involved in the measurement of friction have indeed been reduced as expected. This was particularly important for compliant layered bearings, operating typically at friction factors of 0.01 to 0.001, where the estimated error in the simulator recording of friction factor could be as much as 98%. Hence, if the pin-on-plate apparatus was modified to give measured friction for compliant layered bearings similar to those recorded on the simulator, it would not only be a more cheap, and easy to use method, but also a much more accurate one.

Applied Load (N)	**Friction Force (N)**	**Coeff. Friction μ**	**Comp. Error**		**Ruler Error**		**Total Error**		**Δμ**	**%Δμ**
			ΔL (N) 0.52%	**ΔF (N) 2.25%**	**ΔL (N)**	**ΔF (N)**	**ΔL (N)**	**ΔF (N)**		
10	0.01	0.001	0.052	0.0002	0.1379	0.0012	0.1899	0.0014	1.4E-04	13.9%
40	0.04	0.001	0.208	0.0009	0.1379	0.0012	0.3459	0.0021	5.2E-05	5.2%
70	0.07	0.001	0.364	0.0016	0.2776	0.0012	0.6416	0.0027	4.0E-05	4.0%
100	0.1	0.001	0.520	0.0023	0.2776	0.0023	0.7976	0.0045	4.6E-05	4.6%
150	0.15	0.001	0.780	0.0034	0.2776	0.0023	1.0576	0.0056	3.8E-05	3.8%
10	0.1	0.01	0.052	0.0023	0.1379	0.0023	0.1899	0.0045	4.9E-04	4.9%
40	0.4	0.01	0.208	0.0090	0.1379	0.0059	0.3459	0.0149	3.8E-04	3.8%
70	0.7	0.01	0.364	0.0158	0.2776	0.0059	0.6416	0.0216	3.2E-04	3.2%
100	1	0.01	0.520	0.0225	0.2776	0.0114	0.7976	0.0339	3.5E-04	3.5%
150	1.5	0.01	0.780	0.0338	0.2776	0.0114	1.0576	0.0452	3.1E-04	3.1%
10	1	0.1	0.052	0.0225	0.1379	0.0114	0.1899	0.0339	3.9E-03	3.9%
40	4	0.1	0.208	0.0900	0.1379	0.0224	0.3459	0.1124	2.9E-03	2.9%
70	7	0.1	0.364	0.1575	0.2776	0.0224	0.6416	0.1799	2.7E-03	2.7%
100	10	0.1	0.520	0.2250	0.2776	0.0571	0.7976	0.2821	2.9E-03	2.9%
150	15	0.1	0.780	0.3375	0.2776	0.0571	1.0576	0.3946	2.7E-03	2.7%

Table 4.3 Calculated systematic errors in frictional torque, measured load and calculated coefficient of friction for the pin-on-plate apparatus.

4.3.2 Standard experimental protocol

Following the completion of all modifications to the test rig to include dynamic loading and the incorporation of an air bearing supported friction measuring carriage, after careful calibration of the measurement systems, some initial tests were undertaken to establish the number of cycles of both warm-up and testing which were required in order to reach a steady state lubrication regime in which friction could be measured. The results of these tests were as follows. A warm-up of the apparatus and the pin and plate bearing to be tested was recommended for 1000 cycles prior to testing. It was also judged to be important that each series of tests should be run without any extended break in testing (more than 30 minutes) to minimise the time-dependent behaviour of the polyurethane. Furthermore, each run should consist of a minimum of 20 reciprocating cycles to ensure a steady state lubrication regime had been reached. A 40 cycle test was chosen to guarantee this situation was achieved and to comply with the simulator experimental protocol.

Pin-on-plate tests were run in a very similar way to the simulator testing, using a range of lubricants of different viscosities to produce a Stribeck curve.

The test plate was placed in its mounting on the reciprocating table, taking care that it was flat and in the correct orientation, and lubricant added to the bath. The temperature control to the bath was then switched on and the rig left to reach 37 °C. The test pin was screwed into the pin holder and the friction measuring carriage lifted into position, taking care to ensure the surface of the pin touched only the polymer plate and did not come into contact with any of the surrounding metal mountings. The carriage was then fixed to its four supports and the pressure to the air bearings and pneumatic cylinder turned on at the main filter regulator. The pressure to each of the four regulators was adjusted to give the appropriate applied load and pressure to each of the three sets of bearings. The clearance between the pin and plate was then adjusted by altering the vertical height of the pin by adjusting the position of the lock nuts and universal joint on the cylinder rod thread. The strain gauge amplifier, charge amplifier and XYT plotter were then switched on, as well as power to the DC motor and the pin-on-plate machine run for 1000 cycles. After 1000 cycles the motor was stopped immediately after the load had been removed i.e. at one end of the stroke.

1. Place test plate in mounting (ensuring sample is flat and in correct orientation), add lubricant and switch on temperature controller. Leave until lubricant temperature reaches 37 °C.
2. Attach pin to pin holder using grub screw. Place friction measuring carriage in position (taking care not to damage the pin) and attach to 4 supports.
3. Turn air supply on at main filter regulator and adjust 4 individual regulators to give required pneumatic loading and air bearing pressures.
4. Adjust vertical height of pin by altering the position of the lock nuts on the cylinder piston rod so that the pin is just clear of the plate in its raised position.
5. Switch on strain gauge amplifier, charge amplifier and XYT plotter (and power to the motor).
6. Run the pin-on-plate apparatus for 1000 warm-up cycles, switching the motor off immediately after the load is removed.
7. Detach carriage remove plate, and clean pin, plate and plate mounting thoroughly with either soap and water (water-based lubricants) or isopropanol (oil-based lubricants). Dry using a lint-free cloth. Replace components, add new lubricant and re-attach friction measuring carriage in position.
8. Zero charge amplifier and XYT plotter.
9. Switch on motor and run for 40 cycles.
10. During last 5 cycles, use XYT plotter to record the measured displacements from the load cell and force transducer.
11. Repeat steps 8 to 10 twice more to give 3x40 runs at each viscosity.
12. Repeat steps 7 to 11 until all viscosity lubricants have been used, using lubricants in a random order and carrying out several tests for one viscosity to assess any time-related changes.
13. When all tests in series are complete, analyse results
14. Repeat series of tests several times to ensure consistency.

Table 4.4 Pin-on-plate machine Experimental Protocol

Table 4.4 shows the standard experimental protocol used in pin-on-plate testing.

Following, the 1000 cycle warm-up the friction measuring carriage was detached, the pin cleaned and the plate removed from its mounting, both plate and mounting then being cleaned thoroughly. Samples were cleaned in the same way as for simulator tests, in soap and water, and then rinsed in distilled water, for water-based lubricants, and in isopropanol for oil based lubricants. The plate was replaced in its mounting, again flat and in the correct orientation, and the first lubricant added to the bath to cover the test plate. The friction measuring carriage was re-attached to its supports and the charge amplifier and XYT plotter were zeroed (briefly grounded). The motor was switched back on and the apparatus run for 40 cycles before stopping the motor when the load was removed after the 40th cycle. During the 36th to 40th cycles (the last five) the XYT plotter was used to measure simultaneously the displacements from the load cell and the piezoelectric force transducer.

The procedure was then repeated a further two times to give three sets of measured load and friction displacements for each viscosity lubricant. The friction measuring carriage was then detached again and the pin, plate and plate mounting once again cleaned before replacing them and adding another lubricant. The procedure was repeated until all lubricants had been tested three times, testing one lubricant on at least two different intervals throughout the series of tests to establish any time-dependent effects on testing. Following completion of a series of tests, the experimental conditions (pin, plate, applied load, sliding velocity) could be adjusted and another series of tests undertaken in the same way. It was normal for each series of tests under any set of conditions to be conducted three times to ensure the consistency of the results.

4.3.3 Analysis of results

For each test run, the outputs of the load cell and force transducer were recorded for the last 5 cycles. Figure 4.6 shows a typical trace from the XYT plotter.

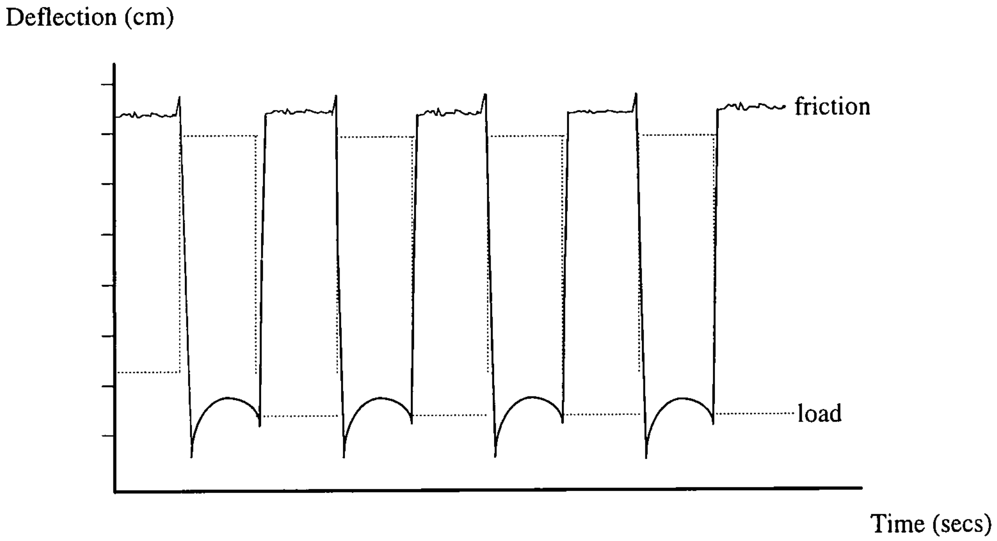

Figure 4.6 A typical trace of measured load and frictional force from the XYT plotter

For each cycle, the displacement from maximum load to zero and the displacement from maximum friction to zero was measured by hand to an accuracy of +/- 0.5 mm. This information was tabulated for tests in a series. The form of the traces was also noted for further analysis. The data were then entered into a spreadsheet and using the recorded calibration coefficients, the measured displacements of the load cell and force transducer converted into values of measured applied load (N) and frictional force (N). For each of the five cycles of each run, the coefficients of friction were then calculated as the ratio of frictional force to applied load. For each viscosity lubricant, the coefficients of friction from the three runs of five measured cycles (i.e. fifteen points) were then averaged to give one point and the standard deviations calculated.

The Sommerfeld number had originally been defined as the product of viscosity and entraining velocity, divided by load per unit width. For the purposes of simulator testing, this had been adapted over the years to become the product of viscosity, velocity and, head radius, divided by load. In order to be able to compare results from the pin-on-plate machine directly, it was necessary to define a parameter which was applicable to both machines. Various parameters were considered before deciding that a good comparison of results could be achieved by using the simulator definition of Sommerfeld number, but substituting the equivalent radius of the joint (R) for the head radius (R_1) as shown in equation 4.12. Other options were to substitute the elastohydrodynamic film thickness (h_{min}) or Hertzian contact area (a) for the femoral head radius, as they both provided a length dimension dependent on the geometry of the bearing. It was felt however, that it was better to use a dimension which was only dependent on the geometry of the bearing and not on other tribological factors so that the new definition of Sommerfeld No. could be easily understood and computed. It would also be useful if the length dimension used could be kept constant to investigate the effects of the other parameters in the Sommerfeld No.. This would not be possible for the film thickness or the contact area as they were dependent on other factors such as load, viscosity or velocity.

The equivalent radius of the joint, R, for a hip joint was given by equation 2.7 while for the pin and plate bearing it was simply equal to the radius of curvature of the pin as the plate component was nominally flat.

$$Z = \frac{\eta u R}{L} \qquad \text{Eqn. 4.12}$$

For each viscosity, the pin-on-plate Sommerfeld number, Z, was calculated. The calculated coefficient of friction could then be plotted against the calculated pin-on-plate Sommerfeld number to give a Stribeck curve which could be used to assess the operating lubrication regime of the bearing. The data from the simulator was then used to calculate the pin-on-plate Sommerfeld number and friction factor data which could be directly compared with the pin-on-plate results.

4.4 Lubricants

Two sets of lubricants were used in friction measurement tests on the simulator and pin-on-plate machines. Water-based solutions of carboxymethyl cellulose (CMC) salt (BDH, UK) were prepared by mixing different quantities of the powder into distilled water to give a range of fluid viscosities between 0.001 Pas and 0.12 Pas. In order to consider higher Sommerfeld values and the fluid film region of the Stribeck curve, a range of silicone fluids (Dow Corning 200 fluid) were also used, having viscosities between 0.00082 Pas and 29.25 Pas. The viscosity of all lubricants was measured before use on a Ferranti Shirley cone on plate viscometer using a shear rate of 3000 s^{-1} {as used by Unsworth *et al* 1987]. The silicone fluids showed essentially Newtonian properties over this range of shear rates, whereas the CMC fluid displayed markedly non-Newtonian properties, as has been shown for physiological fluids [Cooke *et al* 1978].

4.5 Measurement of surface topography of samples

All bearing counterfaces used in the measurement of friction on both simulator and pin-on-plate machines were examined using a NewView 100 optical interferometric profilometer (Zygo, Connecticut). This allowed the surface topography of the bearing counterfaces to be measured and monitored during testing, and so assess or eliminate the effects of surface roughness on measured friction. The method also allowed estimation of the curvature of samples.

The instrument had a vertical resolution of less than a nanometre and a horizontal resolution dependent on the chosen optical magnification: the number of data points remaining constant (at 320 x 240 pixels) for the area under examination, the resolution therefore changing with the size of the area. All measurements described here were undertaken using a x10 objective lens (a true magnification of x100) giving an area of examination of 730 x 550 µm and a horizontal resolution of 2.28 µm per pixel. All heads, pins, cups and plates were examined at ten positions over their articulating surface. At each position, various measurements were made: RMS roughness, Ra (arithmetic average deviation from mean plane), Peak-Valley height (the distance from the highest peak to the lowest valley), skewness Rsk (the measure of the symmetry of deviations about the mean plane). For heads and pins, the estimated radius of curvature of the surface was also measured. A full list of the roughness measurements made for all components used is provided in Appendix F.

In addition to the non-contacting profilometry measurement of the bearing surface roughnesses, each plate used on the pin-on-plate apparatus was tested against the same pin, under dry and lubricated conditions to give a standard trace for each pin. This allowed the friction measured to be compared to the measured roughness and form of the sample, but also meant that any discrepancy in friction measurement could be quickly identified if traces deviated from their normal recorded form.

5. Results and Discussion

Validation of pin-on-plate test method

5.0 Introduction

The objectives of the friction measurement tests described in this section were:

- to establish the repeatability of the new pin-on-plate test method
- to achieve results using the new method comparable with those achieved on the Durham hip function friction simulator
- to obtain values of coefficient of friction on the pin-on-plate and simulator comparable to those published in other studies under similar conditions.

Chapters 6 and 7 go on to describe the use of the new test method to draw useful conclusions on the frictional performance and design of compliant layered joints.

5.0.1 Elastohydrodynamic and micro-elastohydrodynamic theory

Elastohydrodynamic and micro-elastohydrodynamic lubrication theories were a consideration throughout the testing. The theoretical area of Hertzian contact of each bearing under all experimental conditions was estimated from equation 2.16 for spheres and 2.25 for cylinders. The elastohydrodynamic and micro-elastohydrodynamic film thickness equations given in equations 2.21, 2.22 (spheres), 2.23, 2.24 (cylinders), 2.23, 2.26 (UHMWPE) and 2.30 (micro-EHL) were then used to calculated the central and minimum film EHL thickness and minimum micro-EHL film thickness under the full range of experimental conditions. The predicted EHL and micro-EHL coefficient of friction could then be calculated from Equation 2.29 and compared with the friction measured experimentally.

The micro-elastohydrodynamic theory could only be used at low viscosities (as discussed in Chapter 2). Both elastohydrodynamic and micro-elastohydrodynamic lubrication theory were only directly applicable to full fluid film lubrication, although in the mixed regime it could be used to predict the degree of separation of bearing surfaces which was occurring. The elastohydrodynamic theory prediction of coefficient of friction therefore was compared with all experimental measurements. As micro-EHL theory was only applicable to low viscosities and the low viscosities usually showed mixed lubrication, micro-EHL film thickness and friction were calculated but were not plotted.

Lubrication theory was also important in the design of experiments. Considering the film thickness equations (Chapter 2), the following test parameters were seen to be important to the friction generated in a compliant layered bearing:

- equivalent radius of the joint, **R**
- viscosity of the lubricant, η
- adjusted elastic modulus and Poisson's ratio of the layer, **E**, ν
- entraining velocity of the bearing surfaces, **u**
- layer thickness, $\mathbf{h_T}$
- applied load, **L**

and for the micro-elastohydrodynamic film,

- the surface roughness of the hard and soft counterfaces, σ_1 and σ_2.

As the development of compliant layered joints at the University of Durham was already fairly advanced, the choice of layer thickness and compliant material had already been made and so these parameters were not altered during the course of testing. The effect of the compliance of the material was however assessed by comparing compliant layered bearings with conventional ultra-high molecular weight polyethylene (UHMWPE) bearings keeping all other experimental parameters were similar.

The effect of other design parameters was also considered. Friction was measured on both the pin-on-plate and simulator apparatus for different applied loads, equivalent radii of contact, entraining velocities, and hard and soft counterface roughness. In considering the effect of each parameter, all other conditions were held constant, and a range of lubricants of varying viscosity were used to produce a Stribeck style analysis.

This systematic consideration of test parameters allowed two assessments to be made. Firstly, it allowed the identification of the most important test parameters for achieving equivalent results between the two systems. Secondly, it allowed the importance of lubrication theory in predicting experimental results to be assessed. Lubrication theory would suggest some parameters to be more important than others and other authors have previously seen some deviation between experimental measurements and theoretical predictions [Burgess 1996]. In this way, the results obtained using the new pin-on-plate test method could be compared with those from the simulator, their equivalent theoretical predictions and those published by other authors in the field.

5.1 Repeatability of new pin-on-plate test method

Before embarking on an extensive programme of tests, it was important to establish the repeatability of the results achieved using the modified pin-on-plate test method, and that the values of coefficient of friction recorded were comparable to those found in other studies.

5.1.1 Steady-state friction for UHMWPE-metal bearings

In order to show that the pin-on-plate apparatus was giving a realistic measure of friction, a well characterised bearing combination was tested. The 200 mm radius of curvature stainless steel pin (A) was tested against an UHMWPE plate (PE2) over 900 cycles on three separate occasions using distilled water as a lubricant. An entraining velocity of 22 mm/sec and an on/off load of 10 N (corresponding to a maximum contact stress of 3.8 MPa) were applied.

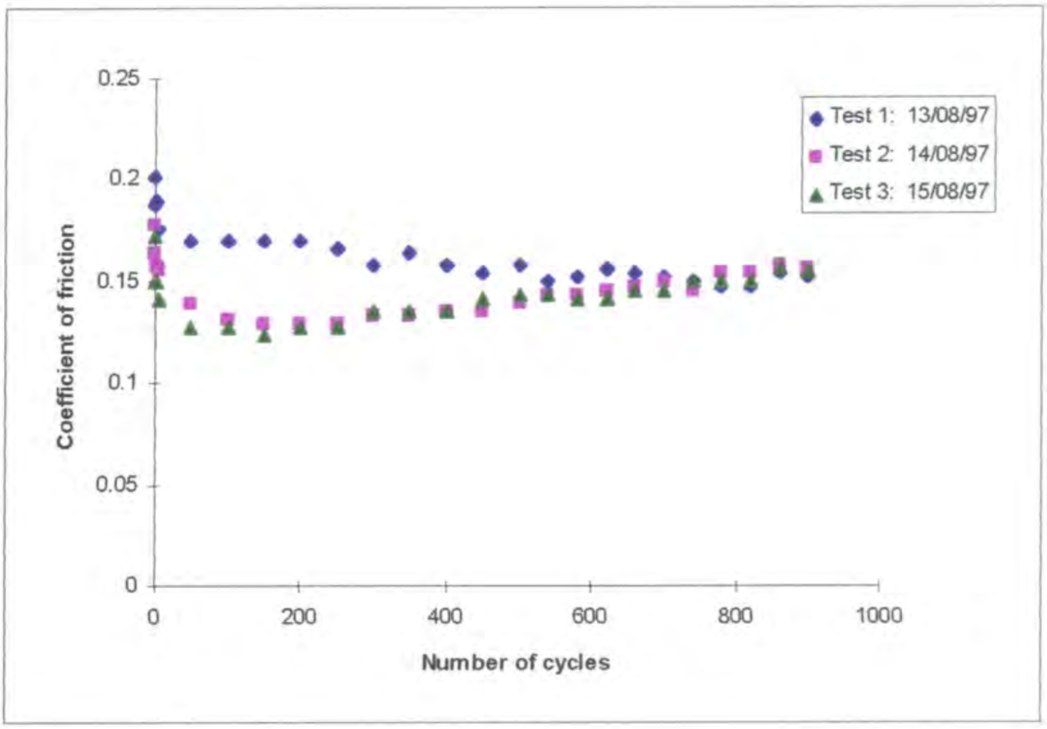

Figure 5.1 Repeatability: UHMWPE with distilled water over 900 cycles

Figure 5.1 shows the values of coefficient of friction measured for the UHMWPE - stainless steel bearing for the three runs. The graph shows that the measured friction was consistent for all three runs after about 700 cycles, which verified the need for a 1000 cycle warm-up before all tests. Before 700 cycles, there was considerable variation in the measured friction of each of the three runs; much larger values of coefficient of friction being measured on the first run than either of the two subsequent runs. This result would be consistent with the surface of UHMWPE plate undergoing some kind of semi-permanent deformation. The sample had been tested previously 6 months prior to run 1, over which time any deformation could have been recovered. After one run of 1000 cycles the surface of the plate had reached a smoother semi-permanent equilibrium which it then maintained over the following few days and two further tests.

After the 700 cycle threshold, the repeatability of the results was excellent. The average coefficient of friction recorded over the three tests was 0.153 ± 0.002, a variation of 1.32%. This value compared well with published values. Shen and Dumbleton [1974] measured coefficient of friction as 0.185 for polyethylene against 316 stainless steel under a constant 5 lb (20 N) load on a thrust washer bearing tester. McKellop *et al* [1977] measured the coefficient of friction of polyethylene vs. steel in water as between 0.1 and 0.18 under a constant 6.9 MPa contact pressure on a reciprocating pin-on-plate machine. Hitchmough [1994] used the original Durham pin-on-plate friction machine to obtain coefficients of friction between 0.14 and 0.18 for metal on UHMWPE. Caravia *et al* [1990] measured the steady state coefficient of friction of UHMWPE vs. stainless steel under a constant 2MPa (20 N) applied pressure to be between 0.05 and 0.2. Saikko [1993b] gave an average value of measured coefficient of friction of 0.10 for UHMWPE pins against Co-Cr-Mo plates under 4.8 MPa contact pressure. He measured the friction generated over 5 million wear cycles and so saw considerable variation in the friction recorded. The range of values of coefficient of friction were between 0.08 and 0.16.

5.1.2 Compliant layers

Having established that the friction recorded by the modified pin-on-plate apparatus was indeed in the expected range of values, the next stage was to assess the repeatability of the method in examining compliant layered bearings.

Three compliant layered plates (CC21A, CC25A, CC27A) were each tested on three separate occasions against the 200 mm radius of curvature stainless steel pin (A). An entraining velocity of 22 mm/sec and an on/off load of 10 N (corresponding to 1.75 MPa) were used throughout. On each occasion, friction was measured over 1000 cycles of warm-up and then a Stribeck style analysis undertaken. CMC lubricants of viscosities 0.001 to 0.15 Pa s were used to produce the Stribeck plot and distilled water (0.001 Pa s) was used as the lubricant during warm-up.

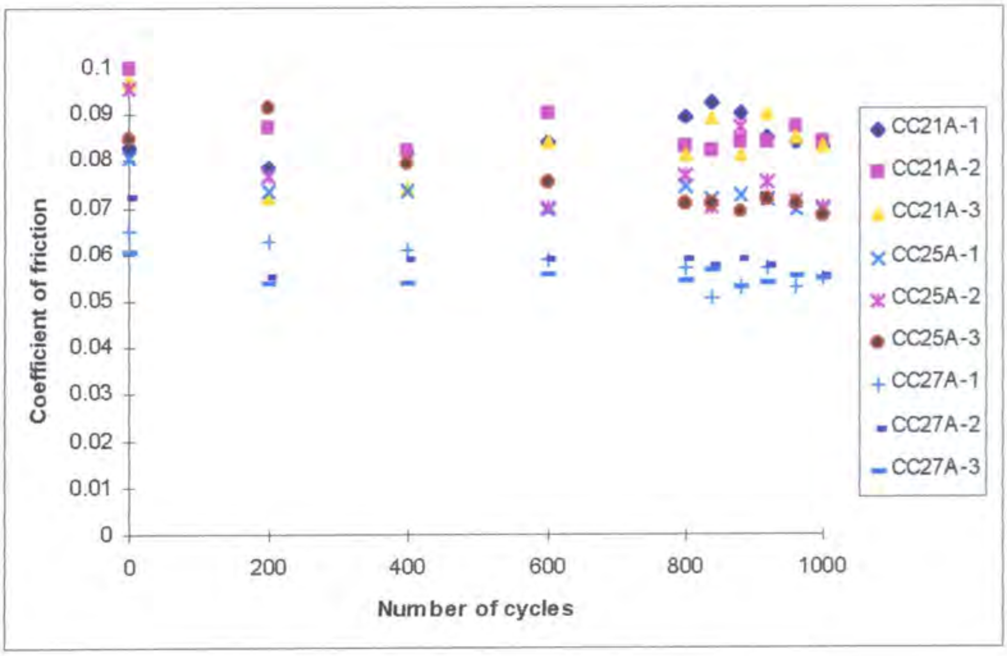

Figure 5.2 Repeatability: compliant layered samples with distilled water

Figure 5.2 shows the values of coefficient of friction recorded during the 1000 cycle warm-up for each of the three samples on each of the three occasions. Over the first 500 cycles, there was considerable variation in the coefficient of friction measured in the three runs for each individual sample. However, after 500 cycles, the friction for each sample became much more consistent over the three runs, and the data were clearly grouped within three bands representing the three samples.

After 1000 cycles, all three samples showed excellent repeatability of results over the three recorded runs. The average values of coefficient of friction were 0.0832 ± 0.0006. 0.0691 ± 0.001, and 0.0547 ± 0.0004 for samples CC21A, CC25A and CC27A respectively. This represented a variation of 0.73%, 1.57% and 0.74% in the recorded coefficient of friction after 1000 cycles for samples CC21A, CC25A and CC27A respectively.

The studies of the performance of compliant layered bearings on pin-on-plate type apparatus appeared to be few and far between and the values of friction recorded differ greatly depending on the test conditions used. Jin *et al* [1993] measured coefficients of friction of between 0.008 and 0.035 for polyurethane pins of different profiles on stainless steel discs under an 100 N applied static load. Caravia *et al* [1993a, b, c] measured higher values of coefficient of friction in their tests of spherical stainless steel indentors on polyurethane plates. The average coefficient of friction of a 50 nm Ra roughness indentor on a 20 MPa elastic modulus polyurethane plate under a contact pressure of 2 MPa, lubricated with distilled water was found to be 0.10.

The values recorded here fell between these two published results. Caravia *et al*'s study was probably the more comparable in terms of experimental conditions, using the same configuration of specimens, a similar magnitude load, a similar modulus layer and a similar roughness indentor (Ra of 200 mm pin A was 40 nm). The values recorded here were lower than Caravia *et al*'s but this was expected as the modified pin-on-plate apparatus used a dynamic on/off loading whilst Caravia *et al*'s sledge microtome used a constant load. Squeeze film effects were therefore included in these experiments but not in Caravia *et al*'s tests. In addition, Caravia *et al* used a sliding velocity of 8 mm/sec (entraining velocity of 4 mm/sec) and so the elastohydrodynamic entraining action would be less and so smaller fluid films would be generated. In a mixed lubricating regime, as expected for a lubricant of 0.001 Pa s, this meant less separation of surfaces and so more asperity contact occurred and therefore the measured friction would be higher. Coefficients of friction recorded here were therefore consistent with published results.

5.1.2.2 Stribeck Analyses

One of the most commonly used tools in assessing the tribological performance of bearings has been the Stribeck analysis, allowing the operating lubrication regime of any bearing to be assessed simply by testing it under a range of conditions (typically different lubricant viscosities). Having demonstrated that the modified pin-on-plate apparatus produced repeatable steady-state friction measurements comparable with published values, its performance in conducting Stribeck analyses was then examined.

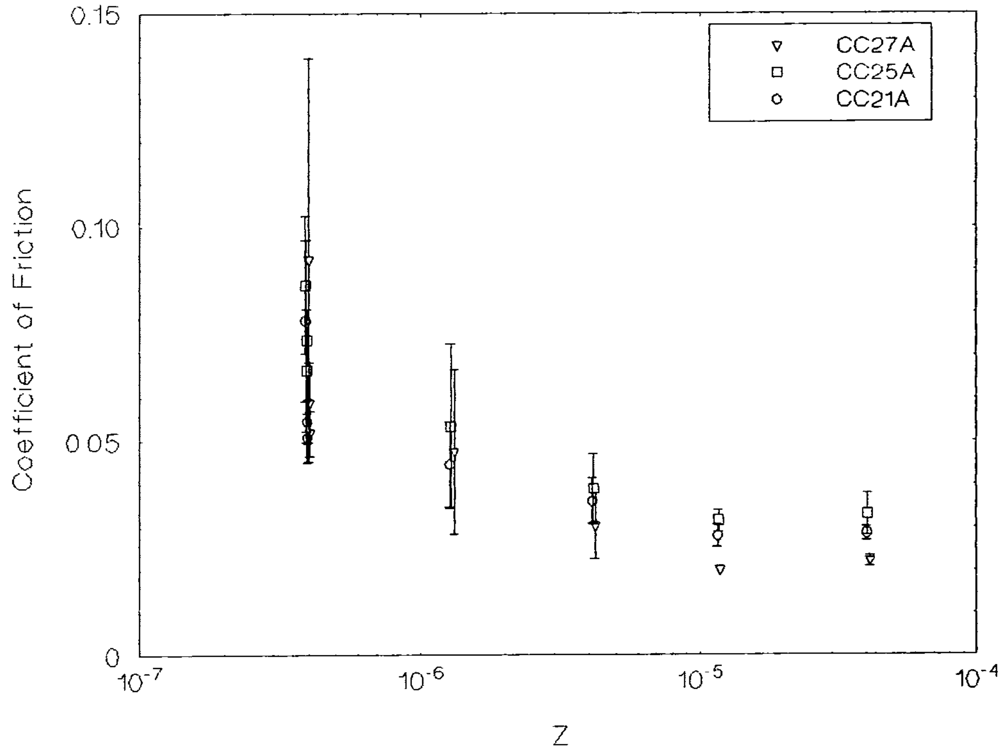

Figure 5.3 Repeatability of Stribeck analyses on pin-on-plate apparatus

(plates CC21A, CC25A and CC27A against 200mm pin A)

Figure 5.3 shows a plot of the average coefficient of friction over the three analyses against the calculated Sommerfeld parameter achieved for each of the three plates. Figure 5.4 gives a typical simulator result for three analyses over the same range of lubricants and standard simulator test conditions. The error bars show the standard deviation in the average values.

From Figure 5.3, considerable variation in the measured friction was seen for the lowest value of Z (2.5 x 10-7) when distilled water (0.001 Pa s) was used as a lubricant. Coefficients of variation of as much as 40% were typical at this viscosity. This result, however, still compared well with those obtained typically on the hip function friction simulator (Figure 5.4) which showed as much as 110% variation in measured friction factor values for distilled water.

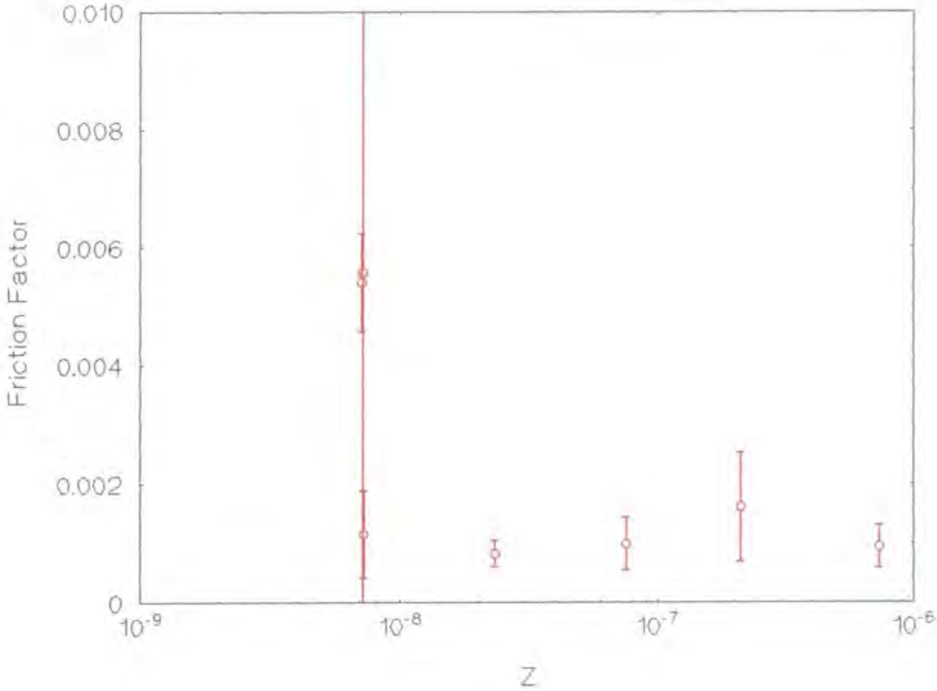

Figure 5.4 Typical simulator result (cup BB98 against 32mm Exeter head)

5.1.2.2.1 Measured friction for lowest lubricant viscosity

In a standard Stribeck analysis, the lowest viscosity lubricant was used two or three times during the course of the test so that any deviation in measurements during the course of testing could be measured. The variations quoted above relate to the deviation in coefficient of friction measured between the three separate Stribeck analyses for one of these tests in water, so the additional number of measurements at this viscosity did not explain its greater variation. It was more likely that the tribological performance of the compliant bearings was more variable for very low viscosity lubricants. At higher lubricant viscosities the separation of the surfaces was more established due to the higher film thickness. The stronger inter-molecular forces in the lubricant would also mean that the fluid film was more physically stable than for a lower viscosity lubricant. We would therefore expect to see more variability in film thickness and consequently in measured friction at the lower the viscosity of the lubricant.

Both simulator and pin-on-plate tests have shown that the friction measured for the lowest viscosity lubricant was higher in its first test than for subsequent uses. Previous authors [Burgess 1996] have recommended discarding the first 'water run' in order to reduce these deviations. Standard testing protocol, as defined in Sections 4.2.3 and 4.3.2 demanded 400 warm-up cycles for the simulator or 1000 cycles for the pin-on-plate apparatus There was no reason why the first value of measured friction should be any higher than the subsequent ones after only 6 x 40 further cycles. Indeed, friction measurement during warm-up cycles as described above, clearly showed that a steady-state value was reached by the pin-on-plate machine by this time. The decrease in the friction measured for the lowest viscosity lubricant over the period of an analysis must therefore have been in some way due to the testing protocol.

The 'test then rest' nature of the protocol was a possible factor, the standard protocol involving 3 x 40 cycle tests then a rest of around 2 minutes while the lubricant was changed. This was ruled out in the warm-up experiments (Figure 5.2) as the last 6 measurements (cycles 800 to 1000) were conducted as a series of 40 cycle test allowing one minute's rest between each. These results showed a relatively consistent coefficient of friction achieved throughout. It was therefore suggested that the decrease in friction measured at the lowest viscosity during the course of testing was due to the sample's exposure to higher viscosity lubricants between low viscosity tests. Although the surfaces of the samples and their mountings were cleaned thoroughly between each lubricant it was possible that the molecules of the higher viscosity lubricants adsorbed into the first few nm of the polyurethane sample's surface and so modified its subsequent frictional performance. Soaking overnight in a Ringers solution at 37°C caused the friction to return to its original value. This might then have been due to the re-diffusion of the adsorbed molecules and not due to the recovery of visco-elastic deformation of the polyurethane as previously supposed.

5.1.2.2.2 Repeatability

At higher viscosities, and higher values of Z, the repeatability of the results achieved on the pin-on-plate machine was very good (Figure 5.3). The variation from the average coefficient of friction at the various viscosity ranged from 4% to 40%, with an overall coefficient of variation of 12%, 22% and 17% for samples CC21A, CC25A and CC27A respectively. These results compared extremely well with those achieved on the simulator (Figure 5.4) where the standard variation in average coefficient of friction at the various viscosities ranged from 15% to 64% with an overall coefficient of variation (ratio of standard deviation to mean) of 41%. The repeatability of the load measurement on the pin-on-plate machine was excellent throughout. The average applied load was calculated as 10.8 N ± 2% compared with 2000 N ± 8% for the simulator.

5.1.2.2.3 Comparison of pin-on-plate and simulator results

The overall form of the Stribeck plot was also pleasing. All three samples produced very similar results - a downwards sloping curve reaching a minimum, and an area of zero gradient, for viscosities of 0.03 Pa s and above (Figure 5.3). The downwards trend was indicative of mixed lubrication. An increase in lubricant viscosity generated an increased fluid film, greater separation of surfaces, less asperity contact and therefore lower friction. At a certain viscosity an equilibrium point was reached at which the bearing surfaces became completely separated and so a further increase in viscosity produced no benefits in terms of frictional performance. This was the onset of full fluid film lubrication and showed a zero gradient of the Stribeck curve. At this stage the friction generated was entirely due to the shearing of the lubricant and so further increases in lubricant viscosity (and values of Z) would lead to an increase in friction. A similar result was typically seen for the simulator although the curve was less pronounced (Figure 5.4). A viscosity of 0.001 Pa s showed higher friction but fluids of higher viscosity, demonstrated extremely low friction. Over the 0.005 to 0.1 Pa s viscosity range, the measured friction factor was independent of the viscosity of the lubricant.

The differences between the friction measured on the two machines was further highlighted by considering the values of coefficient of friction and friction factor measured on the machines over the same range of viscosities. The friction factors measured on the hip function simulator ranged from a minimum of 0.00083 to a maximum of 0.0056. On the pin-on-plate machine however, the minimum coefficient of friction measured was 0.028, 0.032 and 0.020 for plates CC21A, CC25A and CC27A respectively. The maximum coefficient of friction ranged between 0.078 and 0.092. Figure 5.3 shows very little difference between the curves and coefficient of friction values obtained for the three samples. The smoothest plate, CC27A (RMS 116 nm) reached the lowest minimum coefficient of friction, 0.020 compared with the slightly rougher CC21A (RMS 146 nm) and CC25A (RMS 149 nm). Paired student's t tests on the data showed no significant differences between any 2 samples ($0.065 < P < 0.478$) over the complete range of viscosities.

Friction factors or coefficients of friction of 0.001 and below were generally attributed to the operation of a full fluid film lubrication regime. This suggested that for all viscosity lubricants, the compliant layered joint in the simulator operated under full fluid film lubrication whilst the bearing in the pin-on-plate machine operated in a mixed lubrication regime. The zero gradient of the pin-on-plate curves for viscosities of 0.03 Pa s and above would however suggest that the full fluid film regime was being reached even though the minimum coefficient of friction of 0.02 was higher than expected typically. Whilst the small differences in roughness of the pin-on-plate samples made no significant difference in the mixed regime, CC27A reached a lower minimum value of coefficient of friction as a thinner fluid film was required to achieve complete separation of the bearing surfaces, giving rise to lower shearing forces.

5.1.2.2.4 Comparison with other published results

No published studies of Stribeck analyses of compliant layered joints on reciprocating machines were found, but the simulator results shown here compared well with others published. Unsworth *et al* [1987, 1988] obtained 'coefficients of friction' of 0.018 to

0.045 for a prototype metal cup with polyurethane layer on the first Durham simulator, finding that the coefficient of friction increased as the Sommerfeld Number increased. They suggested that the rising Stribeck curve showed a full fluid film lubrication regime was in operation although their measured values of coefficient of friction were greater than 0.01, a result consistent with the pin-on-plate result above. Auger *et al* [1993] measured friction factors of between 0.003 and 0.009 for a polyurethane cup on a simulator and proposed that full fluid film lubrication was in operation throughout.

5.1.2.2.5 Summary

These initial Stribeck analyses demonstrated the possibility of achieving repeatable curves on the pin-on-plate machine that were consistent with lubrication theory and followed the trends published for simulator tests undertaken elsewhere. The form of the curves and the values of coefficient of friction measured were consistent over all nine tests and showed a downwards Stribeck mixed regime and the onset of fluid film lubrication.

The results did not, at this stage, demonstrate a good comparison between pin-on-plate and simulator results. The materials used on the two machines were nominally the same, a PU-PU compliant layer against a metal (Co-Cr-Mo in simulator, stainless steel on pin-on-plate) counterface. The geometry, however, was entirely different. The simulator bearing had a calculated equivalent radius equal to the radius of curvature of the pin (the compliant counterface being flat) of 0.2 m. The simulator joint however had a calculated equivalent radius (Eqn. 2.7) of 0.9576 m. The 'wedge effect' would encourage the entrainment of fluid between the bearing surfaces, and might therefore be much greater on the simulator than on the pin-on-plate apparatus. The geometry of the contact might therefore be an important consideration in achieving equivalent results.

5.2 Use of different lubricants

The repeatability tests and early Stribeck tests on compliant layered joints described above suggested that the onset of full fluid film lubrication could be reached on both the simulator and the pin-on-plate machines and for the simulator, extremely low friction factors (indicative of full fluid film) could be achieved. An upwards Stribeck curve showing the clear presence of full fluid film lubrication had not been achieved, though, for either machine. Previous studies on compliant layers had demonstrated such curves on simulators [Unsworth *et al* 1987, 1988, Auger *et al* 1993] and for reciprocating machines [Cudworth and Higginson 1976, Gladstone and Medley 1990]. Before commencing a large-scale test programme it was vital to establish, especially for the new pin-on-plate apparatus, that it was possible to demonstrate full fluid film lubrication in compliant layered joints if the appropriate conditions were used.

The carboxyl-methyl cellulose (CMC) water-based solutions used so far had a maximum viscosity of 0.15 Pa s. In order to test at higher Z values, and so hopefully see a rising Stribeck curve, higher viscosities were required. This could be achieved by using silicone fluids (Si) which could have a maximum viscosity of 50 Pa s. Their disadvantage was that their behaviour remained Newtonian over the range of shear stresses and so, unlike the CMC fluids, they did not behave like physiological lubricants. To investigate whether this represented an important limitation in their use in this application, tests were conducted to compare the CMC and silicone fluids and to investigate whether, by using high viscosity silicone fluids, rising Stribeck curves could be achieved.

The tests were intended as a comparison of lubricants on each machine and not as a comparison of machines and so no attempt was made to make the two systems equivalent.

Compliant layer sample CC21A was tested against 200 mm radius of curvature pin A using a range of Silicone fluid lubricants on three separate occasions. An on/off load of 10 N and a maximum entraining speed of 22 mm/sec was used throughout. The lubricant viscosities ranged from 0.000818 Pa s to 29.25 Pa s. For each viscosity the measured coefficient of friction was averaged over the three runs and the standard deviations calculated. The results were then compared with the friction measured for the range of CMC fluids. The predicted friction due to the elastohydrodynamic film thickness was also calculated.

Figure 5.5 shows a comparison of these results. The repeatability of the silicone fluid test results was excellent, particularly for lubricant viscosities of 0.048 Pa s and above. The coefficient of variation in the average value of coefficient of friction was in the range of 3.6% to 22.3%, with an average of 10.6%. The experimental results clearly showed a rising Stribeck curve for viscosities of 0.096 Pa s and above. This proved that, although the minimum measured coefficient of friction on the pin-on-plate machine was 0.022, a full fluid film lubrication regime was achieved.

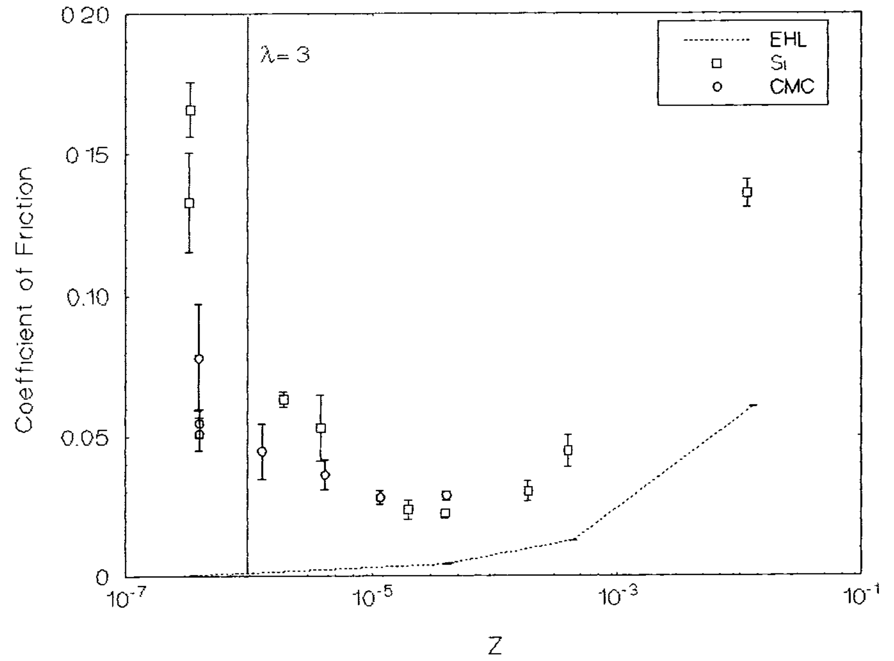

Figure 5.5 Comparison of CMC and silicone fluids on the pin-on-plate apparatus

A comparison of the results achieved for CMC and silicone fluids showed some differences. The silicone fluids gave rise to higher friction than the equivalent CMC fluid at the very low viscosities and slightly lower friction at viscosities between 0.01 and 0.1 Pa s. The lowest viscosity silicone fluid (0.000818 Pa s) was less than the lowest viscosity CMC fluid (distilled water 0.001 Pa s) and so higher coefficients of friction would be expected. Paired Student's t tests on the data showed the CMC fluids to have generated significantly lower friction than the silicone fluids over the complete range of comparable viscosities ($P = 0.013$), but ignoring the lowest viscosity, no significant difference was seen ($P = 0.162$). Roberts *et al* [1982] achieved a similar comparison of CMC and silicone fluids on simulator studies of human hip joints. For a 'low load' of 200 N they saw the onset of fluid film lubrication at viscosities of around 0.05 Pa s which is comparable with the result seen here.

5.2.2 Comparison of lubricants on the simulator

Compliant layered cup BB98 was tested against the standard 32 mm Exeter Co-Cr-Mo head on three separate occasions using a range of silicone fluid lubricants of viscosities 0.000818 Pa s to 29.25 Pa s. The maximum applied load was 2000 N and the maximum entraining velocity 11 mm/sec.

Figure 5.6 shows the comparison of experimental results for silicone fluids and CMC fluids and the corresponding elastohydrodynamic theory predictions. The important observations were as for the pin-on-plate machine above.

A rising trend was seen for viscosities of 0.096 Pa s and above, showing increasing the lubricant viscosity above this value was increasing the shear force of the lubricant and so increasing the measured friction. The average measured friction factor though was less than 0.01 for all lubricant viscosities greater than 0.000818 Pa s, reaching a minimum of 0.0012, suggesting a fluid film regime operated for all but the lowest viscosities. This was again consistent with the findings of Roberts *et al* [1982] who showed much less variation in friction factor with viscosity at higher loads (1200 N) as seen here when simulator results (2000 N) were compared with the pin-on-plate results (10 N). As for CMC fluids, much greater variability of results was seen for the lowest viscosity lubricant, but otherwise the repeatability of the results was good (deviations from average values of 8% to 51%) but not as good as for the pin-on-plate apparatus.

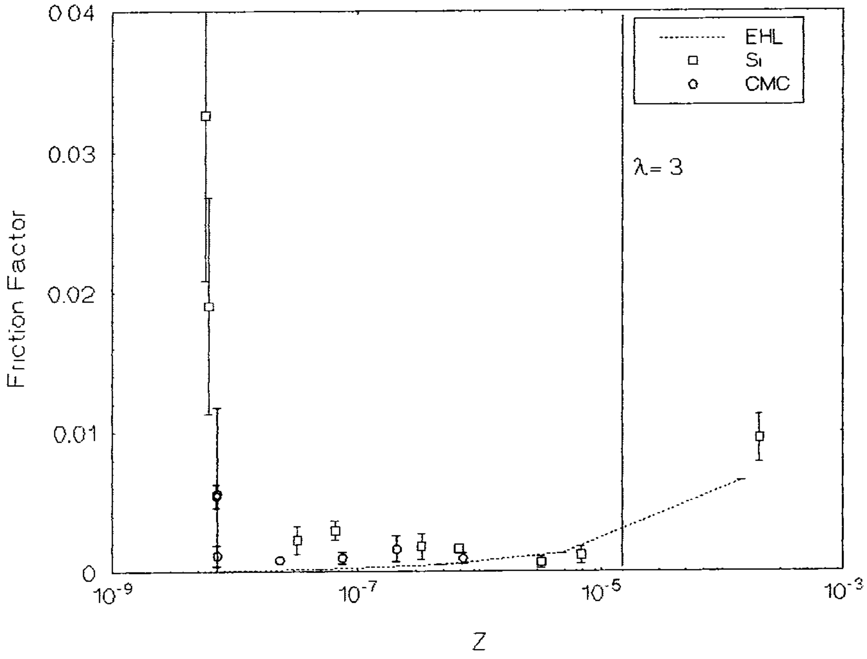

Figure 5.6 Comparison of CMC and silicone fluids on the simulator

A comparison of the results for silicone fluids and CMC fluids showed similar trends to those of the pin-on-plate apparatus. At the lowest viscosity, silicone fluids gave rise to substantially higher friction than CMC fluids. At higher viscosities though the friction factors showed very little difference between the lubricants. A paired Student's t test on the complete range of viscosities showed CMC's to give significantly lower friction than silicone fluids ($P = 0.00834$) and rejecting the lowest viscosity data, the difference was still significant although less so ($P= 0.0370$).

5.2.3 Comparison of experimental results with elastohydrodynamic theory

Pin-on-plate tests showed a poor comparison between theoretical predictions and experimental measurements, although the simulator results compared better.

Elastohydrodynamic theory could only be applied directly to the fluid film lubrication regime. The simulator results showed fluid film lubrication for most viscosities while the pin-on-plate friction results only reached fluid film for high viscosities. Elastohydrodynamic theory was less directly applicable to the pin-on-plate than the simulator situation.

Even in the fluid film regime, the theoretical predictions for the pin-on-plate apparatus suggested much lower values of coefficient of friction than those seen experimentally. The theoretical predictions for the simulator were also slightly lower than the experimental measurements of friction factor. This was consistent with previous studies on simulators which have seen experimental results for compliant layers to be higher than their predicted theoretical equivalents. Auger *et al* [1993] noticed this result and attributed the difference to 'stroke length effects', by which they meant that the stroke length to Hertzian contact width ratio was less than its theoretical optimum and hence a thinner film thickness would be formed and so more friction would be generated. That was certainly the case in these experiments where the stroke length ratio for the pin-on-plate apparatus was much lower than for the simulator, 0.0707 compared with 0.439.

Burgess [1996] saw large differences between theoretical predictions and experimental results over a variety of test conditions for compliant layered hip and knee joints on the same Durham simulator. He suggested that the theoretical prediction of elastohydrodynamic film thickness was useful in ranking joint designs, but it implied a full fluid film was maintained which was not the case under many conditions where the lubrication regime was predominately mixed. In addition, the predicted film thickness was highly dependent on the characteristics of the joint - bearing dimensions, elastic modulus etc.. Small changes in these parameters had a significant effect on the calculated film thickness and so predicted friction. Measurement of these parameters was frequently subject to error and so the theoretical predictions may have been far from the true situation in operation.

In spite of its limitations, both Auger *et al* [1993] and Burgess [1996] noted the importance of theoretical analyses in demonstrating the influence of micro-elastohydrodynamic effects. Both authors showed that full fluid film lubrication on compliant layered bearings in simulators was achieved at surface separation ratios, λ, of less than 3. The simulator tests here showed this result (Figure 5.6). Elastohydrodynamic theory predicted a lubricant viscosity of 2 Pa s for $\lambda = 3$ whilst friction factors indicative of fluid film lubrication were measured for viscosities as low as 0.005 Pa s. In contrast, the experimental conditions on the pin-on-plate apparatus (notably the much smaller load of 10 N compared with 2000 N) predicted that $\lambda = 3$ for lubricant viscosities of only 0.02 Pa s. The experimental results showed the downwards Stribeck curve flattening for viscosities of 0.048 Pa s and rising beyond 0.096 Pa s. It would therefore seem that the elastohydrodynamic and micro-elastohydrodynamic effects on the pin-on-plate machine were less effective than predicted theoretically.

5.2.4 Summary

The use of silicone fluids allowed high values of Z to be reached such that full fluid film lubrication could be demonstrated on the pin-on-plate machine and simulator. In addition, other than at the lowest viscosity of approx. 0.001 Pa s, the coefficients of friction (or friction factors) measured with silicone fluids did not differ significantly from those measured using equivalent viscosity CMC fluids. Subsequent tests on the pin-on-plate and simulator apparatus were conducted using silicone fluids to allow a Stribeck curve to be produced with a greater range of Z.

5.3 Effect of contact geometry

Testing on the pin-on-plate apparatus up to this point had been directed at establishing the repeatability of the method as well as its ability to generate the required lubrication regime (fluid film) for compliant layered joints. The only comparisons made with simulator results had concerned their relative performance in these functions. For the pin-on-plate machine to be a truly effective test method, it would have to be able to predict the in vivo performance of compliant layers. The aim was that the results from the pin-on-plate apparatus should compare with those of a simulator, which had a proven record of predicting in vivo results.

The first step in achieving equivalence between the pin-on-plate and simulator methods was to use an equivalent geometry of contact. The 32 mm compliant layered joint for the simulator gave an equivalent radius of 0.9576 m but to produce a radius of this size on a 15 mm diameter pin would be extremely difficult and costly. The obvious solution was therefore to use a joint on the simulator with an equivalent radius closer to the radius of the pin for the pin-on-plate machine. The largest radius of curvature of consistent form produced for the pin-on-plate machine was 0.2 m, and a pin of 0.1 m had also been manufactured. Using Equation 2.7, it was calculated that an equivalent radius of 0.2 m was given by a 30 mm head in a 32.4 mm diameter cup, and 0.1 m was given by a 28 mm head in the same 32.4 mm cup. Hence by using 'the wrong head in the right cup', equivalent geometry could be produced for the two systems.

Equivalent contact geometries were achieved experimentally using the previous compliant layered cup BB98 in articulation against a standard Exeter head of nominal diameter 28 mm on the simulator, and the 100mm pin against the previous compliant layered plate CC21A on the pin-on-plate machine. Table 5.1 gives a complete list of the experimental parameters for the two machines. A range of silicone fluids of viscosities 0.000818 Pa s to 29.25 Pa s was used on both machines and each joint was tested on three separate occasions.

Figure 5.7 shows the results achieved for the BB98-28 mm joint compared with the CC21A - 100 mm bearing and the previous simulator result obtained for BB98 against a 32 mm Exeter head. Each point represents the average value of the three runs and the error bars are the standard deviations from these averages. Elastohydrodynamic theory predictions for the friction generated in the three bearings are also shown.

Design Parameters	**Pin-on-plate CC21A - 100mm**	**Simulator BB98 - 32mm**	**Simulator BB98 - 28mm**
Equivalent radius, R (m)	0.100	0.9576	0.1019
Head/Pin modulus, E_1 (MPa)	2×10^5	2×10^5	2×10^5
Head/Pin Poisson's ratio, ν_1	0.3	0.3	0.3
Layer modulus, E_2 (MPa)	19.2	19.2	19.2
Layer Poisson's ratio, ν_2	0.5	0.5	0.5
Layer thickness, h_T (mm)	3.0	3.0	3.0
RMS roughness head/pin, σ_1 (nm)	55.6	47.8	47.8
RMS roughness layer, σ_2 (nm)	145.7	2100	2100
Combined RMS roughness, σ (nm)	156	2100	2100
Applied load, L (N)	10.8	2000	2000
Max. entraining velocity, u (mm/s)	22.15	11.0	9.6
Contact half-width, a (mm)	3.06	12.22	7.63
Max. contact stress, P (MPa)	0.27	0.36	1.6
Stroke Ratio, S_T	0.061	0.439	0.312
EHL film thickness, h_{min} (m)*	1.6×10^{-7}	5.4×10^{-8}	1.9×10^{-8}
EHL coefficient of friction, μ_{EHL}*	4.8×10^{-5}	5.4×10^{-5}	4.8×10^{-4}
Surface separation ratio, λ *	1.42	0.037	0.0144
μ-EHL film thickness, $h_{\mu,min}$ (m)*	4.8×10^{-8}	1.6×10^{-9}	1.5×10^{-9}
μ-EHL friction, $\mu_{\mu EHL}$ (m)*	0.00224	0.00260	0.00097

Table 5.1 Experimental conditions and contact parameters used in the comparison of 0.1 m equivalent radius systems (* when η = 0.000818 Pa s)

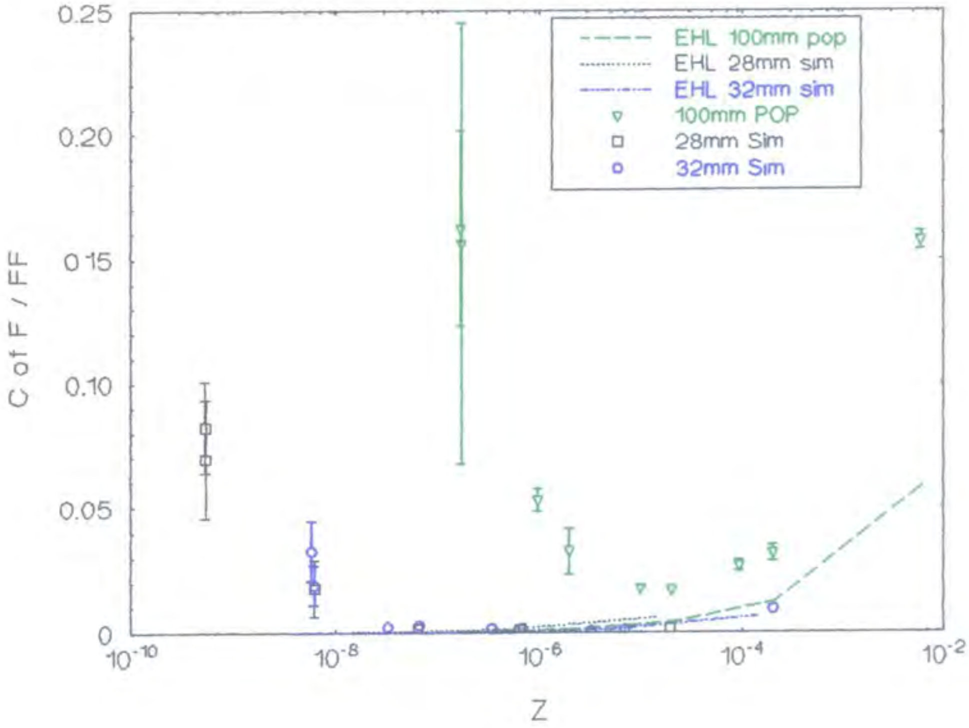

Figure 5.7 Effect of equivalent contact geometry on the pin-on-plate and simulator

The theoretical curves for the three bearings predicted that an equivalent geometry on the simulator and pin-on-plate apparatus should give rise to similar values of coefficient of friction (or friction factor) in the fluid film regime. The theoretical curve for 28 mm head bearing and the theoretical curve for the 100 mm pin-on-plate bearing were close while that of 32 mm head predicted slightly lower friction. The experimental results did not show much agreement with this theoretical prediction however. Both the simulator joint results for the 28 mm and 32 mm head were very similar in spite of the large differences in equivalent radii. (This in itself was an interesting result as it was in opposition to elastohydrodynamic theory which predicted that the clearance in the joint was very important in creating the entraining action which generated the fluid film. It is discussed in more detail in Section 5.5.) The 100mm pin on flat bearing on the pin-on-plate gave rise to significantly higher coefficients of friction in spite of having a similar equivalent radius to the 28mm head in BB98 cup on the simulator. All results showed the now familiar transition from mixed to fluid film lubrication; the transition being more marked though for the pin-on-plate bearing than the simulator joints.

Consideration of the experimental conditions in Table 5.1 provided clues to the differences between the results found on the two machines. Whilst the equivalent radii of the two bearings were the same, the very different loads used meant that Hertzian contact half-widths, contact pressures, and film thickness generated were very different. Clearly, equivalence in undeformed bearing geometry alone was not sufficient to produce similar results as this changed dramatically under load.

5.4 Effect of applied load

Comparable equivalent radii of the bearings on the pin-on-plate and simulator did not produce comparable frictional results. The next stage was to bring the other contact parameters closer together by changing the applied load on each system.

The same two bearings were used as in the previous experiment - a 28 mm head in BB98 on the simulator, and an 100 mm pin on CC21A on the pin-on-plate apparatus. Silicone fluids of viscosities 0.000818 Pa s to 29.25 Pa s were again used as lubricants and all test conditions were as for the tests described above and as given in Table 5.1. The only change in protocol was that on the pin-on-plate apparatus, the bearing was now tested under applied on/off loads of 40 N, 70 N, 100N, and 150 N and on the simulator, the bearing was tested under maximum loads of 250 N, 500 N and 1000 N (the minimum applied load on the simulator remained 100 N throughout). Each loading was used in three separate tests as previously.

Tables 5.2 and 5.3 give the calculated contact parameters for the pin-on-plate and simulator bearings respectively under the full range of loads applied (including the 10 N pin-on-plate and 2000 N simulator tests described earlier).

Figure 5.8 shows the results achieved on the pin-on-plate machine for applied loads of 10 N to 150 N. Figure 5.9 shows the simulator results for loads of 250 N to 2000 N.

Both graphs include the elastohydrodynamic theory predictions of friction for the highest applied load.

Design parameters	**10 N**	**40 N**	**70 N**	**100 N**	**150 N**
Contact half-width, a (mm)	3.06	4.09	4.60	4.95	5.39
Max. contact stress, P (MPa)	0.27	0.44	0.52	0.59	0.68
Stroke Ratio, S_T	0.061	0.082	0.092	0.099	0.108
h_{min} (m)*	$1.6x\ 10^{-7}$	$1.1x\ 10^{-7}$	$9.8x\ 10^{-8}$	$8.9x\ 10^{-8}$	$8.0x\ 10^{-8}$
μ_{EHL}*	$4.8x\ 10^{-4}$	$3.0x\ 10^{-4}$	$2.5x\ 10^{-4}$	$2.2x\ 10^{-4}$	$1.9x\ 10^{-4}$
Surface separation ratio, λ *	1.43	1.02	0.89	0.82	0.75
$h_{\mu,min}$ (m)*	$4.8x\ 10^{-8}$	$4.0x\ 10^{-8}$	$3.9x\ 10^{-8}$	$3.8x\ 10^{-8}$	$3.7x\ 10^{-8}$
$\mu_{\mu EHL}$ *	0.00224	0.00119	0.000890	0.000734	0.000592

Table 5.2 Theoretical contact parameters for 100mm pin on CC21A under various loads (* when η = 0.000818 Pa s, others conditions as in Table 5.1)

Design parameters	**250 N**	**500 N**	**1000 N**	**2000 N**
Contact half-width, a (mm)	4.93	5.71	6.60	7.63
Max. contact stress, P (MPa)	0.79	1.0	1.3	1.6
Stroke Ratio, S_T	0.20	0.23	0.27	0.31
h_{min} (m)*	3.3×10^{-8}	2.8×10^{-8}	2.3×10^{-8}	1.9×10^{-8}
μ_{EHL}*	9.7×10^{-5}	7.7×10^{-5}	6.0×10^{-5}	4.8×10^{-5}
Surface separation ratio, λ *	0.024	0.020	0.017	0.014
$h_{\mu,min}$ (m)*	1.48×10^{-9}	1.48×10^{-9}	1.48×10^{-9}	1.48×10^{-9}
$\mu_{\mu EHL}$ *	0.00324	0.00217	0.00145	0.000972

Table 5.3 Theoretical contact parameters for 28mm head in BB98 under various loads (* when η = 0.000818 Pa s, others conditions as in Table 5.1)

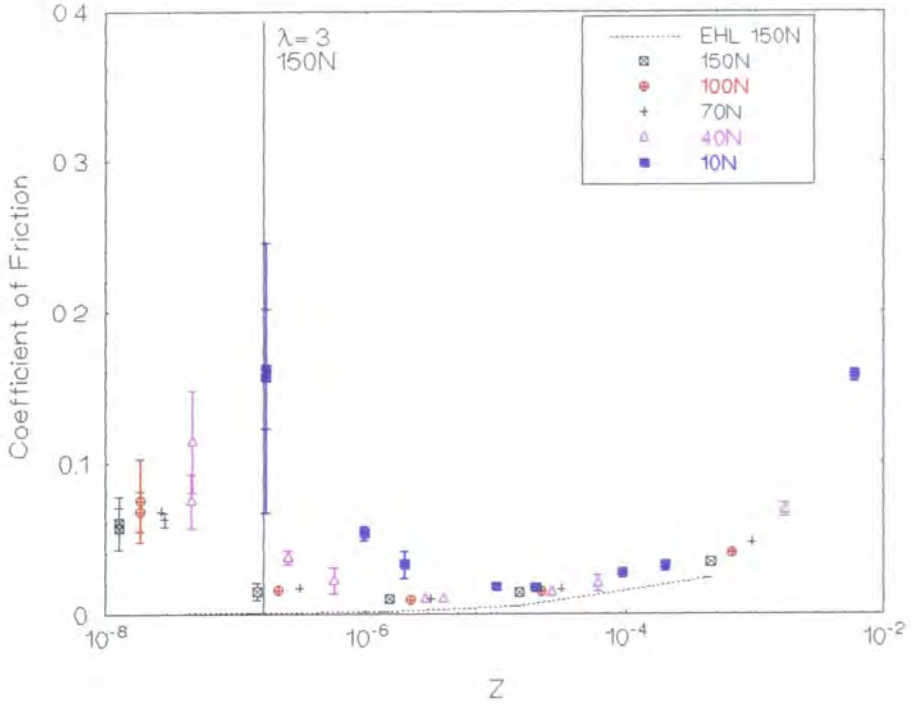

Figure 5.8 Effect of applied load measured on the pin-on-plate machine (CC21A - 100 mm pin)

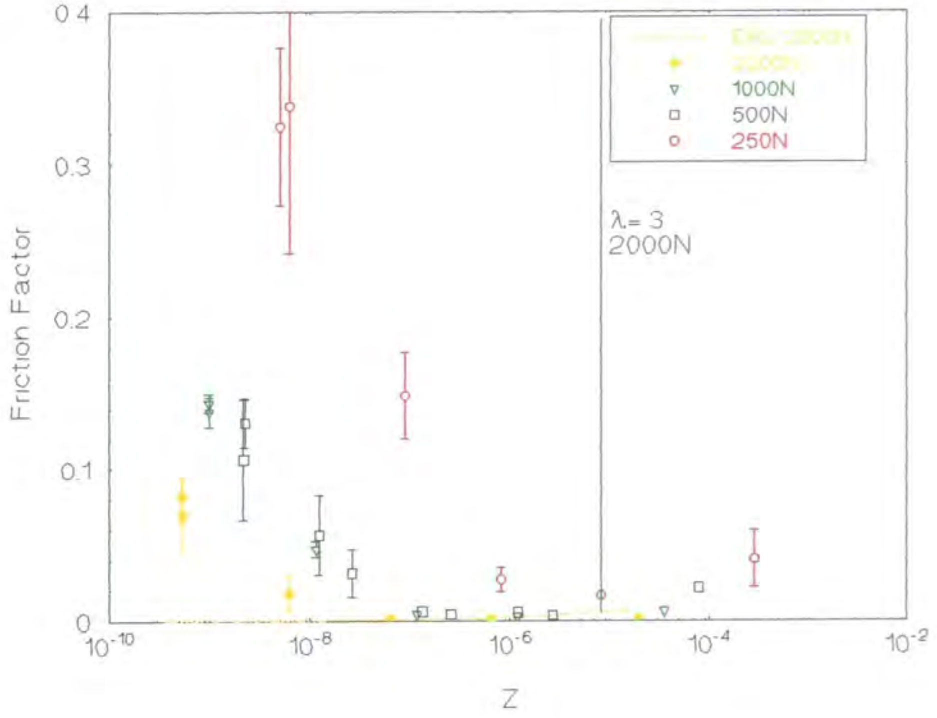

Figure 5.9 Effect of applied load measured on the simulator (BB98 - 28 mm head)

5.4.1 Observations - Effect of applied load

Two important observations were made from both of the graphs.

The measured coefficient of friction (or friction factor) in the mixed regime decreased as the applied load was increased. This trend was very obvious for both simulator and pin-on-plate results and has been noted frequently by other authors. Increasing the load increased the generated frictional force, generated higher contact stresses, causing an increase in the interaction of asperities. However the frictional force did not increase proportionally with the load, and so the calculated coefficient of friction (ratio of frictional force to applied load) decreased. Weightman *et al* [1972], Shen and Dumbleton [1974], and Hall *et al* [1994] noted a decrease in the measured coefficient of friction (or friction factor) for increasing applied load for UHMPWE-metal bearings. Cudworth and Higginson [1976] demonstrated this result for a compliant layer against a hard counterface on a rotating machine. O'Kelly *et al* [1977] and Roberts *et al* [1982] both noted the effect in simulator experiments. O'Kelly *et al* used cadaveric and artificial hip joints, and Roberts *et al* tested cadaveric joints.

The second important observation to be made from Figures 5.8 and 5.9 was that for both apparatus, all the Stribeck curves for the various loads converged in the fluid film lubrication regime. Figure 5.10 shows the elastohydrodynamic theory predication of the coefficient of friction for the various loads on the pin-on-plate and simulator apparatus. In the fluid film regime, elastohydrodynamic theory predicted one common Stribeck curve for all loads. In this regime, the friction was entirely due to the shearing of the lubricant. Increasing the load increased the Hertzian contact area and it also decreased the film thickness. The net effect was an increase in frictional force but a small decrease in the coefficient of friction (or friction factor). The calculated Sommerfeld number also decreased as the applied load decreased and so calculated coefficients of friction therefore all fell on the same curve. On this issue, there was an agreement between experimental results and theoretical predictions.

5.4.2 Comparison with elastohydrodynamic theory

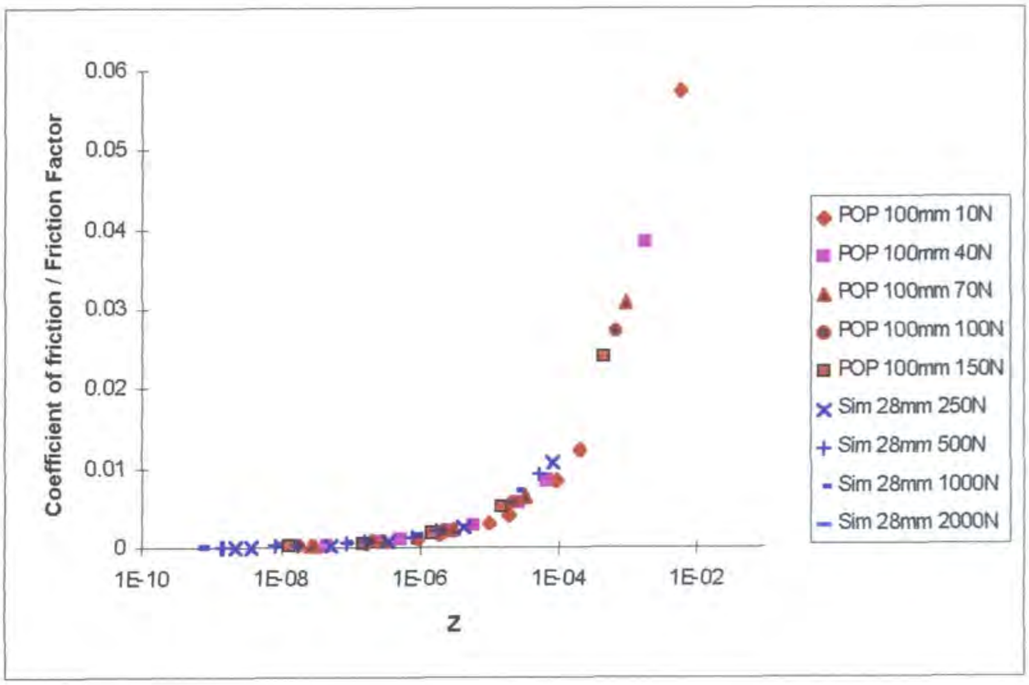

Figure 5.10 Elastohydrodynamic theory prediction of coefficient of friction for conditions used on pin-on-plate and simulator apparatus for various loads

Considering Figures 5.8 and 5.9, the experimental results on the simulator again showed a reasonable agreement with the theoretical predictions. For the higher loads, the pin-on-plate experimental results also began to show a much closer agreement with theory than seen previously (Figures 5.5 and 5.7). The elastohydrodynamic theory assumed a full fluid film and on the pin-on-plate apparatus at the higher viscosities, where a fluid film would be maintained, the experimental and theoretical results became quite close. The simulator again showed the zero gradient and then rising Stribeck curve for surface separation ratios much lower than 3, confirming micro-elastohydrodynamic lubrication to be an important effect. In the pin-on-plate machine under applied loads of 10 N and 40 N, fluid film lubrication was attained only for surface separation ratios greater than 3. For loads of 70 N and above, however, the flat area of the Stribeck curve, suggesting the onset of full fluid film lubrication, began around the predicted λ =3 value.

The improved agreement between theory and experiment at higher loads on the pin-on-plate apparatus was attributed to the effect of squeeze film lubrication. Although Smith and Medley [1986] showed the fluid film thickness to be constant throughout the walking cycle, this was due to the combination of entraining action and squeeze film effects. Under low loads, both a static or a dynamic load would have little depleting effect on the entrapped film of fluid in the bearing. A high static load would quickly deplete the fluid film, whilst a high dynamic load would have a much longer depletion time due to squeeze film effects. The work of Higginson [1978], however, showed that increasing the load applied to a bearing actually increased the time required to deplete the fluid film to a given thickness. This was because the elastic deformation of the contact gave a bigger load bearing area at higher loads. Increasing the load should therefore allow the entrapped fluid films to be maintained for longer and so less friction to be generated.

If increasing the load, increased the contact area it also increased the stroke ratio towards the optimum condition. The same reasoning followed for the simulator although the agreement between theory and experimental results was much better throughout and so the effect of the increased load was less noticeable.

5.4.3 Comparison of pin-on-plate and simulator results

Figure 5.11 represents the combined results of Figures 5.8 and 5.9 and shows the comparison of experimental results obtained on the pin-on-plate and simulator over the various loads. The graph shows two very important results.

In the fluid film regime, not only did the curves for each system under different applied loads meet, but so did the various curves for the two different machines. Figure 5.10 shows the theoretical predictions for each machine and confirmed that this result was consistent with elastohydrodynamic theory.

In the mixed lubrication regime, the 10 N pin-on-plate result still showed the highest coefficients of friction over the range of Sommerfeld numbers and the 2000 N result still showed the lowest values. In terms of the comparison of the two machines, however, the most interesting results were for the loads in between.

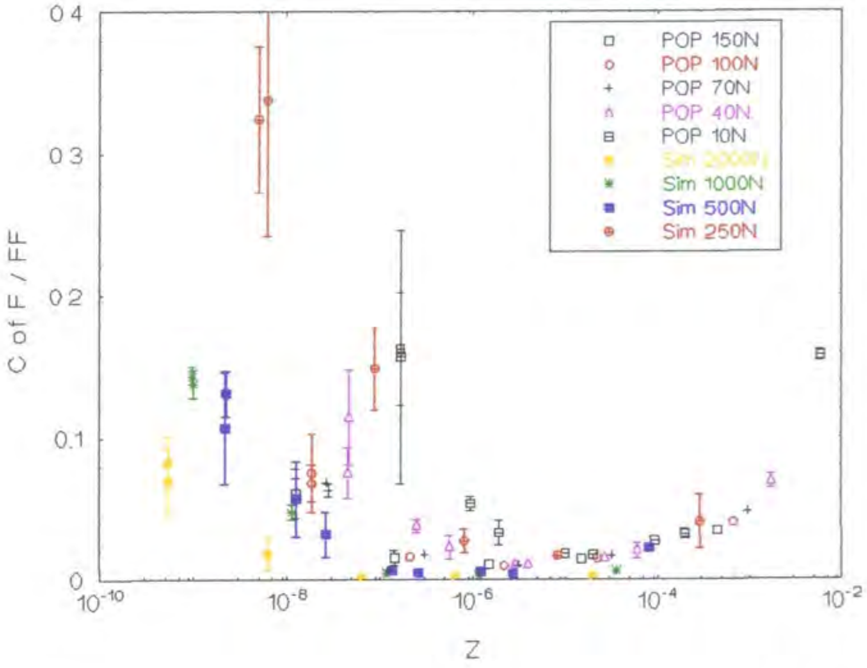

Figure 5.11 Comparison of pin-on-plate and simulator results for bearings of 0.1 m equivalent radius over a range of loads.

The Stribeck curves for the two machines showed decreasing coefficient of friction/friction factor with applied load for both machines and if curves were fitted to the data they could be ranked in the following order:

highest friction	10 N pin-on-plate curve
	250 N simulator curve
	40 N pin-on-plate curve
	70 N pin-on-plate curve
	100 N pin-on-plate curve
	150 N pin-on-plate curve ≈ 500 N simulator curve
	1000 N simulator curve
lowest friction	2000 N simulator curve

There was a distinct overlap of the experimental results of the pin-on-plate at high loads and the simulator at lower loads. This was a significant result as it showed that the pin-on-plate apparatus was capable of producing results comparable with those achieved on the hip function simulator. Another important result was that the 150 N pin-on-plate result was extremely close to the 500 N simulator result, whilst the 250 N simulator result fell between the 10 N and 40 N pin-on-plate result. The comparison of the two machines was therefore not directly related to the magnitude of the applied load. A much lower load was required on the pin-on-plate machine compared with the simulator. This in itself was reassuring as the pin-on-plate machine was designed to be small and simple in its operation and if loads of 2000 N were required to accurately assess a compliant layered joint, then no advantage could be seen and a simulator may as well be used.

5.4.4 Discussion

Considering the contact parameters given in Tables 5.2 and 5.3 provided some clues to the more important parameters in comparing bearings on the two machines. Comparison of the parameters for the two machines showed that five of the parameters were estimated as having completely different values for the two methods. These were surface separation ratio, the Stroke ratio, the micro-elastohydrodynamic film thickness, and the predicted elastohydrodynamic and micro-elastohydrodynamic coefficients of friction. The elastohydrodynamic and micro-elastohydrodynamic parameters (λ, $h_{\mu,min}$, μ_{EHL}, $\mu_{\mu EHL}$) were of little relevance in the mixed lubrication regime in any case. Of the remaining parameters, the maximum contact stress was similar for the two machines but did not 'rank' the test conditions as the experimental measurements had. The maximum contact stress predicted the pin-on-plate machine at all loads to give higher friction than the simulator.

The only comparable parameter between the two machines was the Hertzian contact half-width. For the pin-on-plate machine the predicted Hertzian contact half-widths were 3.06, 4.09, 4.60, 4.90 and 5.40 mm for applied loads of 10 N, 40 N, 70 N, 100 N, and 150 N respectively. For the simulator the predicted Hertzian contact half-widths were 4.93, 5.71, 6.6 and 7.7 mm for applied loads of 250 N, 500 N, 1000 N, and 2000 N respectively. Hence, ranking the experimental conditions in terms of the predicted Hertzian contact half-width would not give exactly the same order as seen experimentally but it did compare very closely. In particular, the Hertzian contact half-widths for the pin-on-plate 150 N test and the simulator 500 N test were 5.4 mm and 5.7 mm respectively. It would therefore appear from these results that the Hertzian contact half width was the most important parameter in achieving equivalent results for the pin-on-plate and simulator systems.

This was in direct agreement with various authors [Weightman *et al* 1973, Hutchings 1992, Hall *et al* 1994] who have noted that the frictional force was directly proportional to the Hertzian contact area for adhesive friction. Archard [1953] derived a relationship between the Hertzian contact area and the applied load depending on whether the contact was elastic or plastic, and modelled as a single or multiple asperity contact. This relationship is given in Equation 5.1. For a purely elastic single asperity contact, n had a value of 2/3, and for a purely plastic contact a value of 1. In reality, most elastic materials demonstrated a value of n between these two values ($2/3 < n < 1$) as their deformation had both plastic and elastic components.

$$a \propto L^n \qquad \text{Eqn. 5.1}$$

As the frictional force was directly proportional to the Hertzian contact area, the coefficient of friction (when adhesive friction was predominant) would be proportional to the Hertzian contact area divided by the load. The power factor in the above relation was a fraction, so the coefficient of friction of a compliant bearing in the mixed regime would therefore be expected to decrease as the applied load increased and the applied Hertzian contact area increased, as was seen experimentally.

5.5 Effect of bearing conformity

In order to verify the comparison of the two systems achieved above, the experiment was repeated for pin-on-plate and simulator bearings with an equivalent radius of 0.2 m. This also allowed the effect of changing the equivalent radius, and so the bearing conformity, to be assessed.

A 30mm head in cup BB98 was used on the simulator, and the 200 mm B pin on CC21A on the pin-on-plate apparatus. All test conditions are given in Table 5.4. Standard test protocol was used and the bearings were tested at the same loads as above (leaving out the 10 N load). Each loading was used in three separate tests as previously.

Design Parameters	**Pin-on-plate CC21A - 200mm**	**Simulator BB98 - 30mm**
Equivalent radius, R (m)	0.200	0.1979
Head/Pin modulus, E_1 (MPa)	2×10^5	2×10^5
Head/Pin Poisson's ratio, ν_1	0.3	0.3
Layer modulus, E_2 (MPa)	19.2	19.2
Layer Poisson's ratio, ν_2	0.5	0.5
Layer thickness, h_T (mm)	3.0	3.0
RMS roughness head/pin, σ_1 (nm)	66.6	69.9
RMS roughness layer, σ_2 (nm)	145.7	2100
Combined RMS roughness, σ (nm)	160	2100
Max. entraining velocity, u (mm/s)	22.15	10.3

Table 5.4 Experimental conditions used in the comparison of 0.2 m equivalent radius bearings

Tables 5.5 and 5.6 give the calculated contact parameters for the pin-on-plate and simulator bearings respectively under the full range of loads applied .

Design parameters	**40 N**	**70 N**	**100 N**	**150 N**
Contact half-width, a (mm)	4.73	5.32	5.73	6.24
Max. contact stress, P (MPa)	0.27	0.33	0.37	0.43
Stroke Ratio, S_T	0.095	0.106	0.114	0.125
h_{min} (m)*	1.5×10^{-7}	1.3×10^{-7}	1.2×10^{-7}	1.1×10^{-7}
μ_{EHL}*	3.0×10^{-4}	2.5×10^{-4}	2.2×10^{-4}	1.9×10^{-4}
Surface separation ratio, λ *	1.36	1.19	1.09	0.99
$h_{\mu,min}$ (m)*	4.5×10^{-8}	4.2×10^{-8}	4.0×10^{-8}	3.9×10^{-8}
$\mu_{\mu EHL}$*	0.0014	0.00109	0.000915	0.000748

Table 5.5 Theoretical contact parameters for 200mm pin B on CC21A under various loads (* when η = 0.000818 Pa s)

Design parameters	**250 N**	**500 N**	**1000 N**	**2000 N**
Contact half-width, a (mm)	5.67	6.56	7.59	8.78
Max. contact stress, P (MPa)	0.51	0.64	0.81	1.00
Stroke Ratio, S_T	0.217	0.251	0.290	0.335
h_{min} (m)*	4.6×10^{-8}	3.8×10^{-8}	3.2×10^{-8}	2.7×10^{-8}
μ_{EHL}*	1.0×10^{-4}	8.1×10^{-5}	6.4×10^{-5}	5.0×10^{-5}
Surface separation ratio, λ *	0.031	0.027	0.023	0.019
$h_{\mu,min}$ (m)*	1.55×10^{-9}	1.55×10^{-9}	1.55×10^{-9}	1.55×10^{-9}
$\mu_{\mu EHL}$*	0.00439	0.00294	0.00197	0.00132

Table 5.6 Theoretical contact parameters for 30mm head in BB98 under various loads (* when η = 0.000818 Pa s)

The results obtained from the tests were analysed in two ways. Firstly, the pin-on-plate and simulator results at this equivalent radius were compared with provide a second comparison of the two machines. Secondly, the pin-on-plate results at 0.2 m equivalent radius were compared with those obtained previously (Section 5.4) at 0.1 m equivalent radius. This was repeated for the simulator with the addition of the initial results obtained for an equivalent radius of 0.9576 (Section 5.2). This allowed the effect of bearing conformity (or equivalent radius) to be evaluated.

5.5.1 Comparison of pin-on-plate and simulator results for compliant layered joints with equivalent radius 0.2 m

Figures 5.12 and 5.13 show the experimental results obtained for the pin-on-plate and simulator respectively. They also include the predicted elastohydrodynamic friction for the highest load in each case.

The results showed the same trends as seen previously for the 0.1 m equivalent radius test. All curves met in the fluid film regime for each machine. In the mixed regime, the coefficient of friction/friction factor decreased as the applied load increased. This was less marked for the pin-on-plate results here than seen previously for the 100 mm pin as all the measured coefficients of friction were fairly low and so there was less contrast between high and low loads.

The simulator again showed a good agreement between theoretical and experimental values of friction factor and the pin-on-plate machine also showed a reasonable agreement as seen previously (Section 5.4). The simulator demonstrated fluid film lubrication at λ values much less than 3 as for the 28 mm head. As for the 100 mm pin, the pin-on-plate machine showed the onset of fluid film lubrication around the $\lambda=3$ mark.

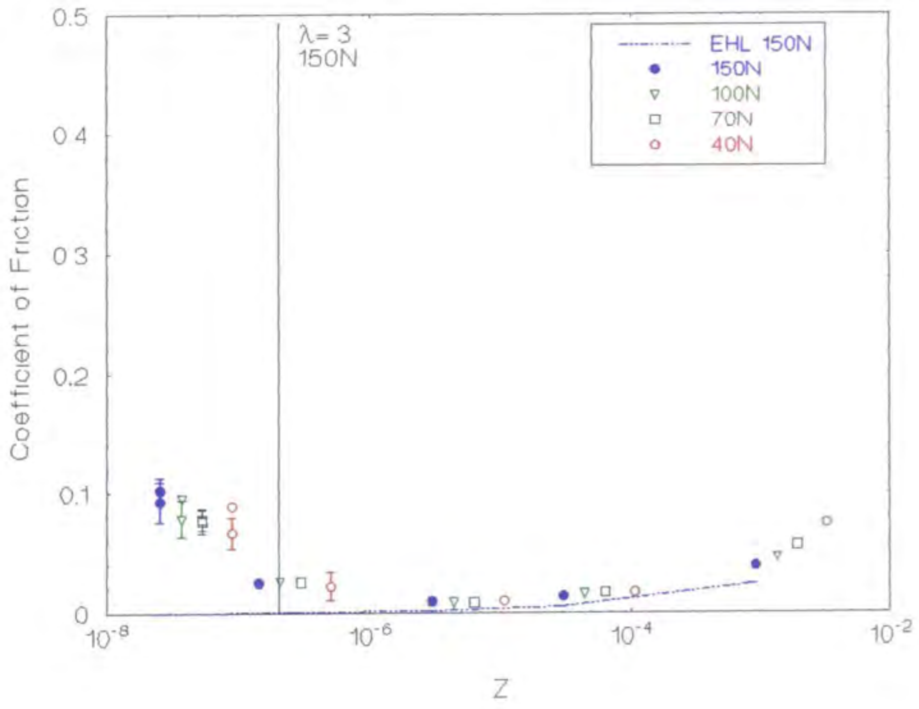

Figure 5.12 Effect of applied load on measured coefficient of friction on the pin-on-plate machine (CC21A - 200 mm B)

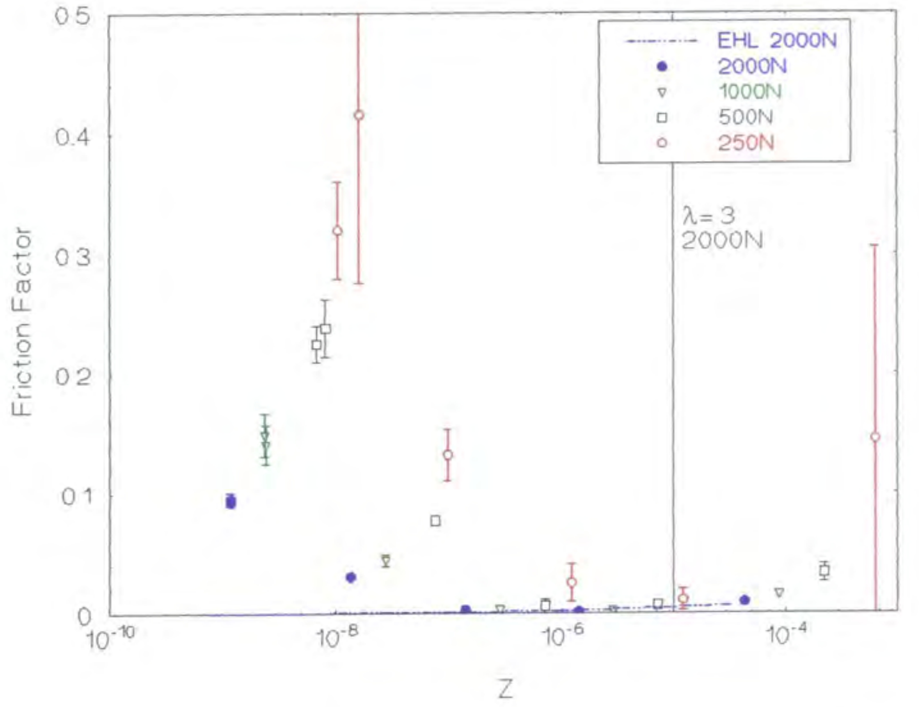

Figure 5.13 Effect of applied load on measured friction factor on the simulator (BB98 - 30 mm)

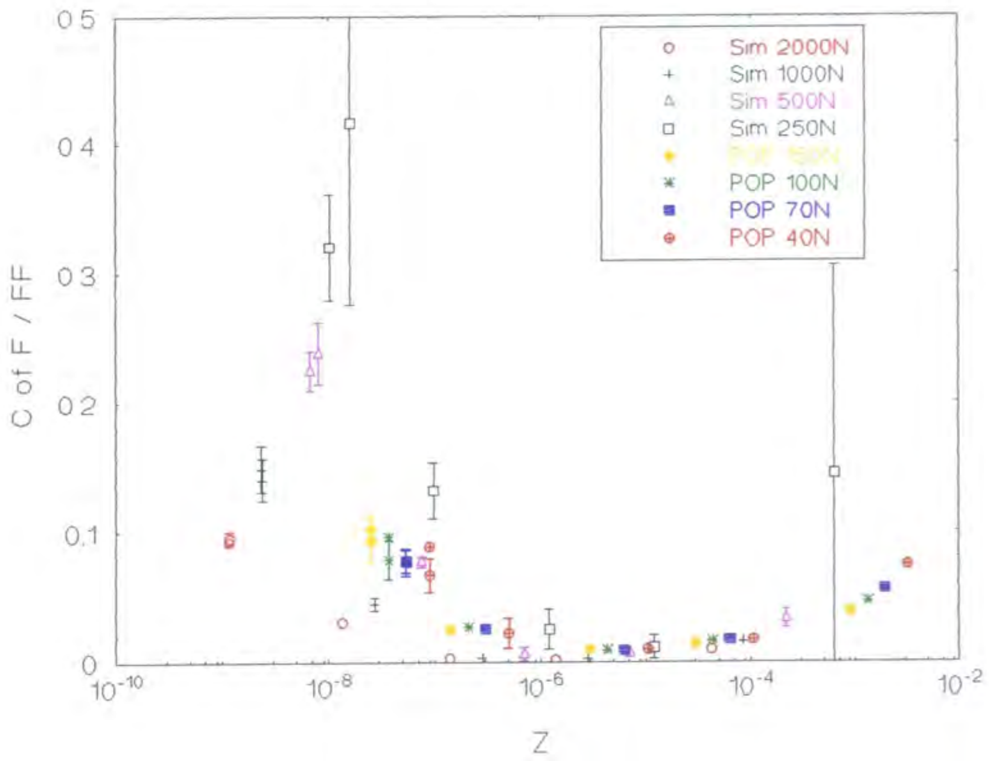

Figure 5.14 Comparison of pin-on-plate and simulator results for bearings of 0.2 m equivalent radius over a range of loads.

	Rank	Contact half-width, a (mm)
highest friction:	250 N simulator curve	5.67
	40 N pin-on-plate curve	4.73
	500 N simulator curve	5.32
	70 N pin-on-plate curve	6.56
	100 N pin-on-plate curve	5.73
	150 N pin-on-plate curve	6.24
	1000 N simulator curve	7.59
lowest friction:	2000 N simulator curve	8.78

Table 5.7 Rank of measured friction curves (in the mixed regime) compared with predicted contact half-width

Figure 5.14 shows a comparison of the results obtained on the two machines. If curves were fitted to the data points and the curves ranked in order of decreasing friction, the order would be as shown in Table 5.7:

This represented a very similar result to that of the 0.1 m equivalent radius bearings and again demonstrated the ability of the pin-on-plate apparatus to produce measurements of friction comparable to the simulator.

Considering the contact parameters given in Tables 5.5 and 5.6, the Hertzian contact half-widths showed an inverse relationship with the experimentally measured friction as shown in Table 5.7. As for the 0.1 m equivalent radius results, the lowest coefficients of friction (friction factors) were recorded for the largest predicted contact half-widths (given by the largest applied loads) and conditions with similar predicted contact half-widths on the two machines showed similar measured friction.

The tests at an equivalent radius of 0.2 m therefore reinforced the findings from the 0.1 m equivalent radius test. The pin-on-plate apparatus produced friction results in the fluid film regime which fitted the same Stribeck curve as simulator results. In the mixed lubrication regime, the measured coefficients of friction for the pin-on-plate and simulator were inversely proportional to the predicted Hertzian contact half-width, and decreased as the applied load increased. The results for the two machines coincided when the theoretical contact half-widths were similar.

5.5.2 Comparison of results for compliant layered joints with equivalent radii of 0.1 and 0.2 m for the pin-on-plate and simulator

Figures 5.15, 5.16, 5.17 and 5.18 shows the results measured for the 0.1 m and 0.2 m equivalent radius bearings on the pin-on-plate apparatus for applied on/off loads of 40 N, 70 N, 100 N, and 150 N respectively. The figures also include the elastohydrodynamic theory prediction of theory for each radius at that load.

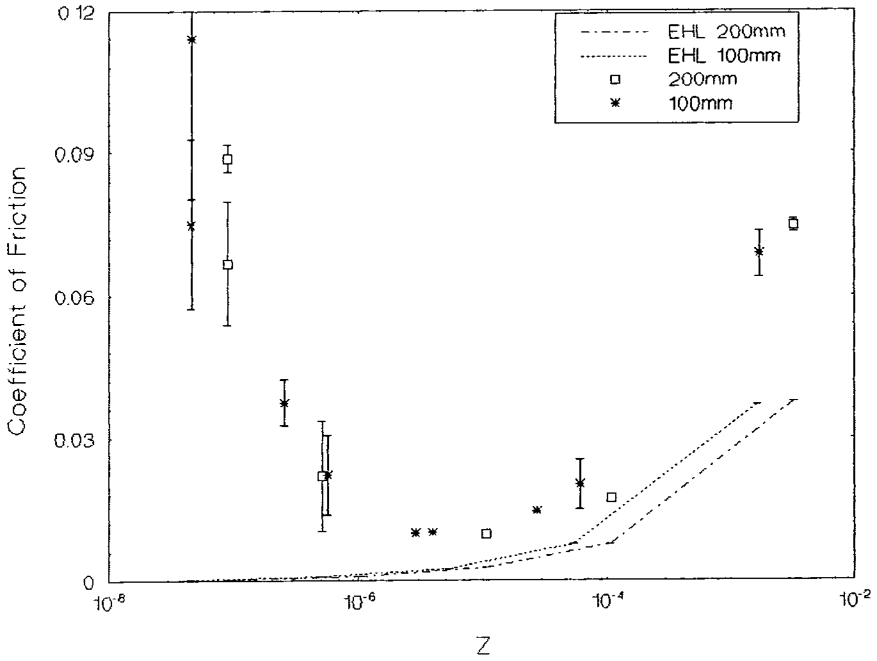

Figure 5.15 Effect of bearing conformity on the pin-on-plate apparatus under a 40 N applied load

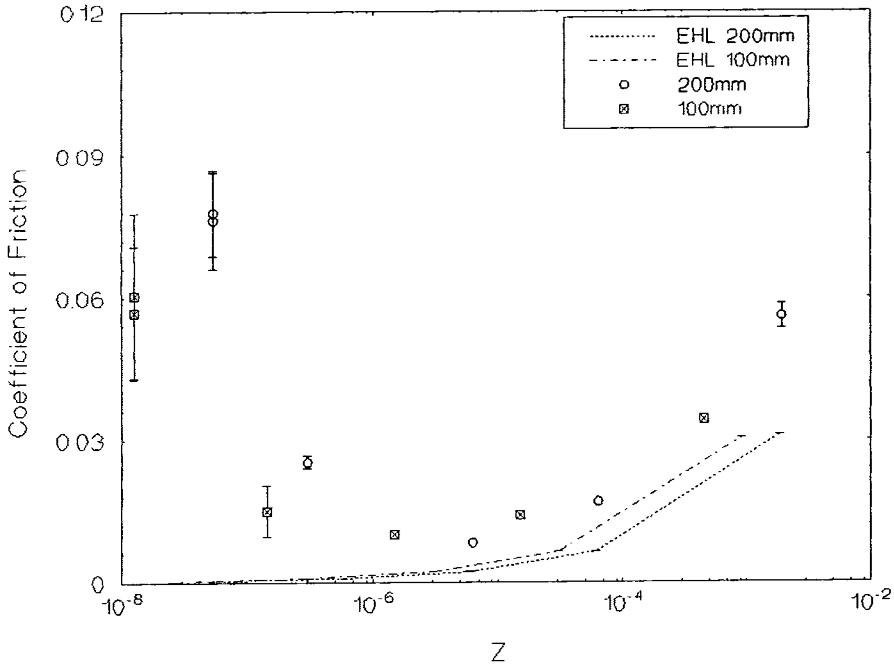

Figure 5.16 Effect of bearing conformity on the pin-on-plate apparatus under a 70 N applied load

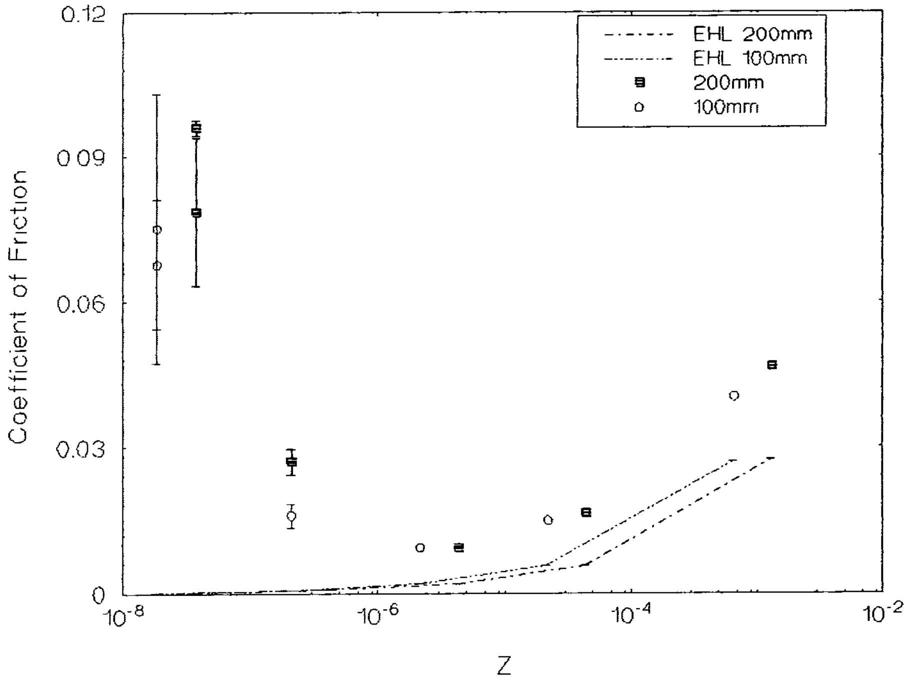

Figure 5.17 Effect of bearing conformity on the pin-on-plate apparatus under an 100 N applied load

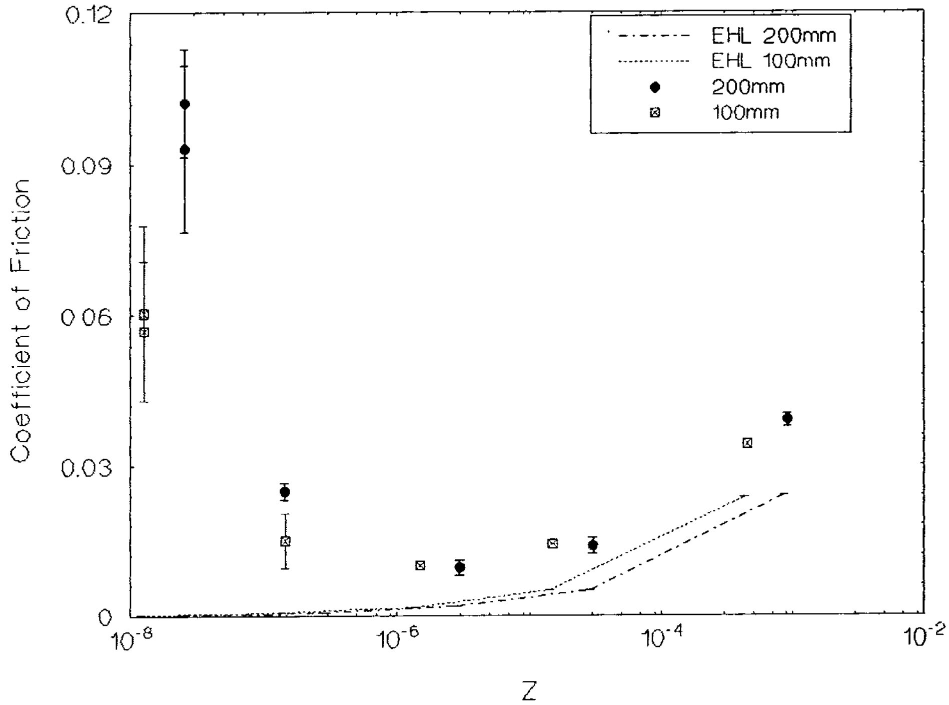

Figure 5.18 Effect of bearing conformity on the pin-on-plate apparatus under an 150 N applied load

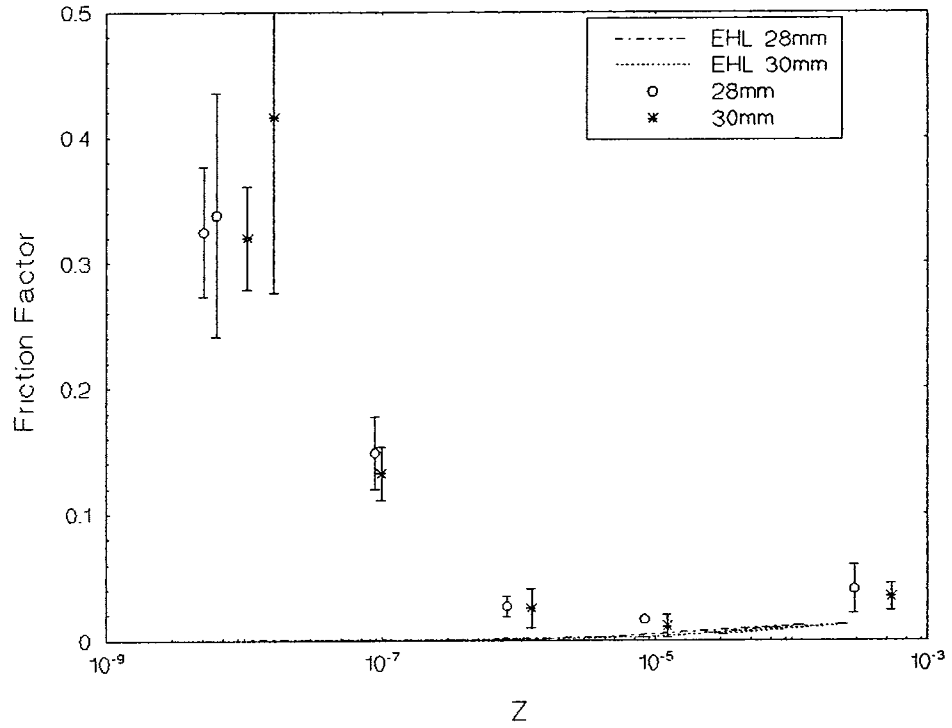

Figure 5.19 Effect of bearing conformity on the simulator under a 250 N max. applied load

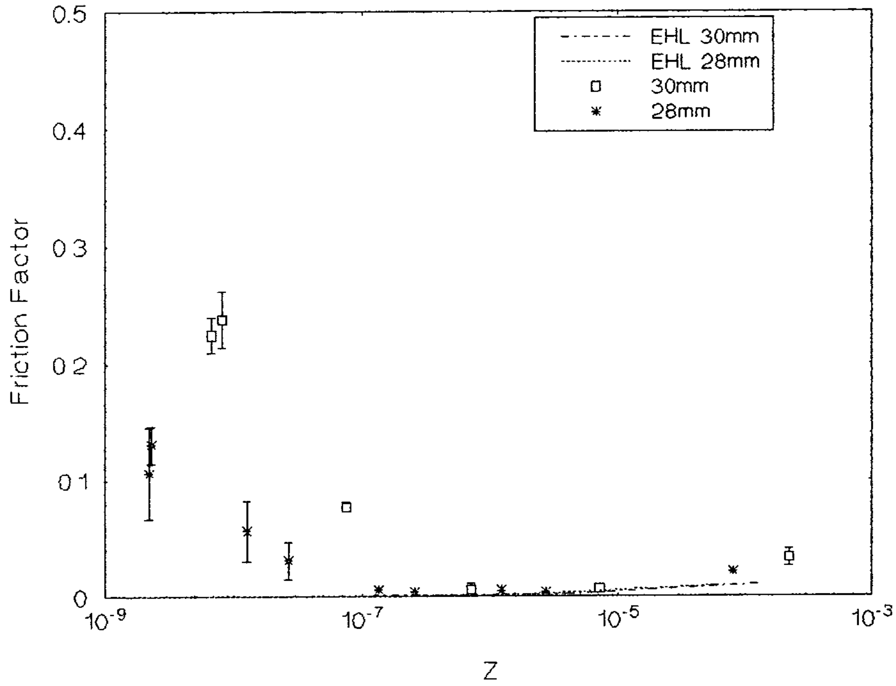

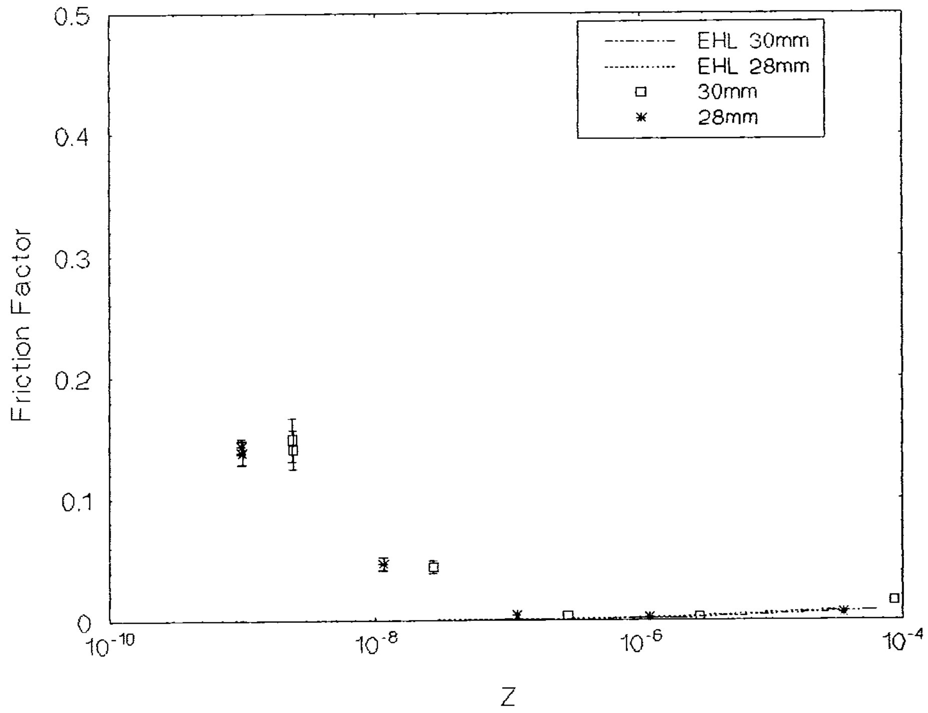

Figure 5.21 Effect of bearing conformity on the simulator under an 1000 N max. applied load

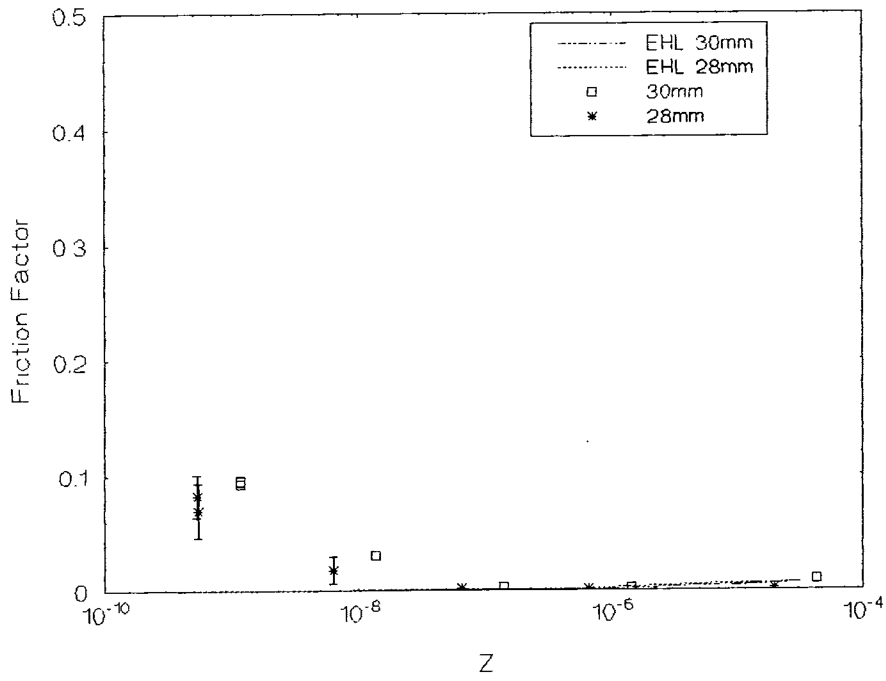

Figure 5.22 Effect of bearing conformity on the simulator under a 2000 N max. applied load

5.5.2.1 Observations

For an equivalent lubricant viscosity, the 200 mm radius of curvature pin results appeared to be at a higher value of Z than the 100 mm radius of curvature as the pin-on-plate Sommerfeld number included the equivalent radius of the joint. This can be clearly seen in the difference in the theoretically predicted curves for the two radii. This could sometimes be misleading when interpreting the results and so comparisons were made of the measured coefficient of friction of each bearing for the same viscosity.

The results showed small differences between the coefficients of friction measured for the two equivalent radii. Except for the 40 N loading condition, where the results for the two radii were very similar, the 0.2 m radius of curvature pin gave rise to slightly higher coefficients of friction than the 0.1 m radius of curvature pin in both mixed and fluid film regimes. Paired Student's t tests over all lubricant viscosities showed the 0.2 m radius results to be significantly higher than the 0.1 m radius for the 70 N, 100 N, and 150 N applied loads (P was 0.0277, 0.0235 and 0.00356 respectively). The 40 N load results did not show a significant difference. The measured surface roughness of the two pins was very similar; RMS roughness was 55.55 nm and 52.29 nm for the 100 mm and 200 mm B pins respectively and so any differences in friction measured were not likely to be caused by the hard bearing surface topography.

Figures 5.19, 5.20, 5.21 and 5.22 show a comparison of the two equivalent radius joints on the simulator for maximum applied loads of 250 N, 500 N, 1000 N, and 2000 N respectively, again including the theoretical prediction of friction. The graphs show that the simulator tests at different equivalent radii gave a very similar result to the pin-on-plate apparatus. There was very little difference in the measured friction factors using the 0.1 m and 0.2 m equivalent radius joints under applied loads of 250 N and 1000N in the mixed regime. For the 500 N and 2000 N loads, however, the 0.2 m equivalent radius joint recorded slightly higher friction than the 0.1 m equivalent radius joint in the mixed regime. At the higher viscosities in the fluid film regime, the measured friction for the 0.2 m equivalent radius joint was slightly higher than for the 0.1 m equivalent radius joint under all applied loads. Using a paired Student's t test over all viscosities, the 0.2 m radius results were found to be significantly greater than the 0.1 m radius results for the 500 N and 2000 N applied loads (P = 0.00099 and 0.0045) but the difference was not significant for 250 N and 1000 N. The RMS roughness for the 28 mm and 30 mm heads were 47.81 nm and 69.91 nm and the 28 mm head was Vitallium Co-Cr-Mo whilst the 30 mm head was stainless steel. Although this meant there were differences between the two heads, it was felt they were unlikely to be the most important factors in terms of the tribological performance of the bearings.

Considering the contact parameters for the 0.1 m and 0.2 m equivalent radius bearings given in Tables 5.2, 5.3, 5.5 and 5.6, we can see that the experimental finding on both the pin-on-plate and simulator agreed with elastohydrodynamic theory. Considering the calculated values of elastohydrodynamic coefficient of friction for each joint on each of the two machines, we can see that theory predicted that friction would have been slightly higher for the 0.2 m radius than for the 0.1 m radius. For the 150 N load and 29.25 Pa s lubricant on the pin-on-plate machine, the predicted coefficient of friction was 2.39×10^{-2} for the 0.2 m equivalent radius compared with 2.35×10^{-2} for the 0.1 m radius. For the 2000 N applied load and the same lubricant on the simulator, the predicted friction factors were 1.27×10^{-2} and 1.21×10^{-2} for the 0.2 m and 0.1 m equivalent radius joints respectively

5.5.2.2 Discussion

The decrease in measured and theoretical coefficient of friction (or friction factor) by decreasing the bearing conformity was caused by the interaction of two effects.

The decrease in equivalent radius decreased the area of contact of the bearing. The coefficient of friction (or friction factor) of the bearing had been shown to be proportional to the ratio of predicted Hertzian contact area to applied load where adhesive friction was predominant. For a constant loading, a decrease in Hertzian contact area therefore resulted in a decrease in the measured coefficient of friction in the mixed regime. In the fluid film regime, the decrease in contact area decreased the area of lubricant under shear and again decreased the measured coefficient of friction. Decreasing the bearing conformity created less of a 'wedge effect' and so reduced the entraining action of the joint. The pressure in the fluid was less and so the micro-elastohydrodynamic effects in smoothing the compliant surfaces were also smaller. In addition a decrease in bearing conformity decreased the effectiveness of the squeeze film and the films generated by the entraining action were more quickly dissipated in the less conforming bearing [Dowson *et al* 1991]. A lower equivalent radius bearing therefore generated thinner fluid films. The depletion of this film had a different effect in each of the lubrication regimes. In the mixed regime, the thinner fluid film gave less separation of the bearing surfaces and so more asperity contact. This would give rise to more friction and a later transition to the fluid film regime. In the fluid film regime, a thinner fluid film would result in a higher velocity gradient in the fluid and more shear force was generated and so the friction would be increased.

The effect of the contact angle in compliant bearing was discussed by Jin *et al* [1993a]. They showed that the wear and friction of a compliant layer were significantly increased by increasing the cone angle of the pin from 30 to 50 degrees i.e. decreasing the bearing conformity. The measured coefficients of friction went from 0.008 to 0.035. Jin *et al*'s findings [1993a] appeared to be contradictory to the theoretical and experimental results reported here but for a significant difference between the two experiments. Jin *et al* [1993a] examined the entraining effect by considering only the angle of contact and in all cases the contact area of the bearing remained unchanged. In addition, their experiments used distilled water as a lubricant and so considered only the bearing behaviour in mixed lubrication regime.

The entraining effect of the bearing was decreased in our experiments in reducing the equivalent radius of the joint from 0.2 m to 0.1 m . This could be seen in the predicted film thickness for the bearings which were less for the 0.1 m equivalent radius than for the 0.2 m equivalent radius. From Tables 5.2 and 5.5, for the150 N load and 0.000818 Pa s lubricant viscosity, the predicted film thickness for the pin-on-plate bearings were 107 nm and 80.1 nm for the 0.2 m and 0.1 m bearings respectively. From Tables 5.3

and 5.6, the predicted film thickness for the simulator bearing for the 2000 N load and 0.000818 Pa s lubricant viscosity were 20.7 nm and 19.4 nm for the 0.2 m and 0.1 m bearings respectively. The predicted micro-elastohydrodynamic film thickness were also smaller for the 0.1 m equivalent radius than the 0.2 m radius: 3.73×10^{-8} m compared with 3.95×10^{-8} m for the pin-on-plate apparatus, and 1.48×10^{-9} m compared with 1.55×10^{-9} m for the simulator..

In Jin *et al*'s experiments [1993a] the contact area remained constant, whereas in our experiments the contact area for the 0.1 m equivalent radius bearing was significantly smaller than for the 0.2 m bearing. The Hertzian contact half-width was 5.39 mm (0.1 m) compared with 6.24 mm (0.2 m) for the 150 N pin-on-plate condition, and 7.63 mm (0.1 m) compared with 8.78 mm (0.2 m) for the 2000 N simulator condition. The decrease in entraining action for the 0.1 m equivalent radius bearing compared with the 0.2 m bearing was therefore overshadowed by the decrease in theoretical Hertzian contact area.

A brief mention is required of the difference between real and theoretical contact area. The real contact area was be the sum of all the areas of asperity contact and in each case was much smaller than the theoretical contact area. The ratio of real contact area to theoretical contact area would be greater in the 0.1 m than the 0.2 m bearing as the same load was carried over a smaller area and so for the same area there would be more asperities interacting. The reduction in entraining and squeeze film actions meant that the separation was also less for the less conforming joint and so further increased the real area of contact. These effects were negligible, however, compared with the large differences in the size of the contact region. The net effect of decreasing the bearing conformity was a decrease in the real contact area. This applied only to the mixed regime. In the fluid film regime, the real area of contact was nominally zero as the bearing surfaces was completely separated by a fluid film at all times and so there should be no asperity contact.

Various authors have shown the conformity of the joint to be important in achieving optimal performance of compliant layered bearings. Dowson *et al* [1991] conducted a theoretical analysis of compliant layered joints and showed conformity to be important for maintaining the entraining and squeeze film thickness. They recommended an equivalent joint radius of 1 m to 1.5 m for optimal performance. The bearings tested here were clearly therefore far from optimal.

5.5.3 Comparison of bearing conformities on simulator

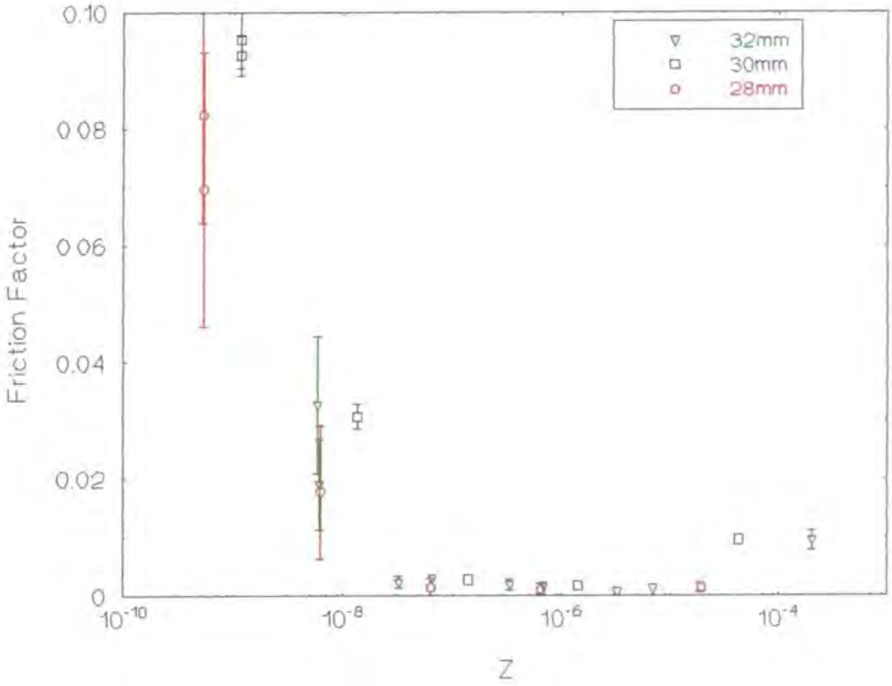

Figure 5.23 Effect of bearing conformity on simulator (BB98 against heads 28 mm, 30 mm and 32 mm under 2000 N max. load)

Figure 5.23 shows a comparison of the results achieved on the simulator for cup BB98 against heads of diameters 28 mm, 30 mm, and 32 mm (equivalent radii of 0.1 m, 0.2 m, and 0.96 m) in silicone fluids under a 2000 N load. The results provide two interesting observations in terms of the effect of bearing conformity on frictional performance.

Firstly, other than at the very lowest viscosity (0.000818 cP), the joint conformity appeared to have only a limited effect on the measured friction factors. At viscosities approaching those of physiological lubricants (0.01 Pa s), all joint conformities demonstrated low friction (friction factors of 0.02 and below) and the onset of fluid film lubrication. At viscosities above 0.01 Pa s, all joints reached a full fluid film regime. In this regime there was no discernible effect of conformity and the measured friction factor in all cases was extremely low with values around 0.002. This suggested that once a full fluid film was established, the changes in film thickness and contact area, caused by the change in bearing conformity, had little effect on the friction generated.

In the mixed regime, the most conforming joint (32 mm diameter) showed a distinct advantage in frictional performance over the less conforming joints (30 mm and 28 mm). For the 0.000818 Pa s lubricant the 32 mm diameter head recorded a friction factor of 0.019 compared with 0.095 and 0.082 for the 30 mm and 28 mm heads respectively. (This was in spite of the 32 mm head recording a significantly higher RMS roughness than the other two heads of 178.8 nm). As described above, elastohydrodynamic and micro-elastohydrodynamic theories predicted that the higher conformity would give thicker fluid films from both entraining and squeeze film actions and also an increased area of contact. The net effect theoretically was an increase in the predicted coefficient of friction. Elastohydrodynamic and micro-elastohydrodynamic lubrication theories did not, however, consider the breakdown of fluid films in the mixed regime.

For the low conformity joints, the increase in film thickness with increased equivalent radius was minimal and so was less important than the increase in contact area. In increasing the equivalent radius from 0.02 m (30 mm diameter head) to 0.9576 m (32 mm diameter head), the increase in predicted elastohydrodynamic film thickness was significant, 27 nm compared with 54 nm for the 0.000818 Pa s lubricant. The predicted micro-elastohydrodynamic film thickness increased dramatically, 1.5 nm compared with 78.3 nm for the 0.000818 Pa s lubricant. The increase in film thickness at the increased conformity led to a significant increase in degree of separation of the bearing surfaces. The predicted λ values of the three bearings reflected this: λ was 0.037, 0.019 and 0.014 for the 0.000818 Pa s lubricant for the 32 mm, 30 mm, and 28 mm diameter head joints respectively. In the mixed regime, the increased separation was very important, meaning a larger proportion of the load was supported by the lubricant and a smaller proportion supported by asperity contact. The increased conformity therefore produced a significant decrease in friction in the mixed regime as seen here. By the same reasoning, increasing the conformity of the joint allowed greater separation of bearing surfaces at lower viscosities and so advanced the onset of fluid film lubrication. Figure 5.23 shows the 32 mm head joint to show both lower friction in the mixed regime and an earlier transition to fluid film (η=0.0046 Pa s compared with above 0.0934 Pa s) than the less conforming joints.

5.5.4 Summary

From the results reported here, it would appear that the conformity of the compliant layered joint was an important factor in its tribological performance but only within certain limits and only until a full fluid film lubrication regime became established For all conformities, increasing the equivalent radius of the joint increased the elastohydrodynamic and micro-elastohydrodynamic fluid film thickness, by increasing the entraining and squeeze film effects. Increasing the equivalent radius also increased the radius of the contact region. Below a certain critical conformity, the effect of the increase in fluid film thickness was less important than the increase in Hertzian contact area and so the measured coefficient of friction (or friction factor) increased for an increased equivalent radius.

A certain critical conformity existed at which the increase in fluid film thickness in the mixed regime produced a significant increase in the separation of the bearing surfaces and so a significant decrease in the proportion of asperity contact. At this point the increase in fluid film thickness became more important than the increase in contact area and so the increase in equivalent radius produced a decrease in measured coefficient of friction (or friction factor). The increase in separation of the surfaces for a given lubricant, also meant that the onset of fluid film lubrication occurred for a lower lubricant viscosity as the bearing conformity was increased.

Burgess [1996] found that for conformities beyond this value - he tested equivalent radii of 0.96 to 2.14 - increasing the conformity of the joint provided no further benefit in terms of improved frictional performance. Indeed, if a compliant layered joint were made too conforming, it would eventually prevent the entraining of fluid and give rise to very high friction approaching a dry contact regime [Burgess *et al* 1997]. This was particularly important in considering the long-term performance of the bearing as creep could cause significant changes in the bearing conformity. Dowson *et al*'s prediction [1991] of an optimal equivalent radius of 1.0 m to 1.5 m was therefore verified by experimental measurements.

6. Results and Discussion - Verification of published results

6.0 Introduction

The tests reported in Chapter 5 successfully validated the pin-on-plate test method showing it to give results for compliant layered joints comparable with those of the simulator for conditions giving equivalent predicted Hertzian contact areas. The pin-on-plate apparatus had also been shown to record values of coefficient of friction close to published values, and demonstrated the effects of the applied load and the equivalent radius predicted by elastohydrodynamic theory and by other authors. The next experiments sought to validate further the method by using it to demonstrate widely published results.

6.1 Effect of hard counterface roughness

Counterface roughness has been shown to have a significant effect on the wear and friction of conventional joints [Dowson *et al* 1984, Weightman *et al* 1986, Dowson *et al* 1987]. Caravia *et al* [1993a] demonstrated the effect of hard counterface roughness on the measured friction against polyurethane compliant layers run dry and in deionised water. Whilst rougher counterfaces gave lower start-up friction due to their greater entrapment of fluid, they gave higher steady-state friction due to the interruption of the generated fluid film.

Two theoretically identical pins were manufactured at the start of this work. Both had a nominal radius of curvature of 200 mm, a diameter of 15 mm and were made of medical grade stainless steel with a super-finished bearing surface. Over the course of early experiments, one of the two pins (pin A) became noticeably marked and showed many scratches on its surface. Pin B had been used much less in experimentation and maintained a much better bearing surface

Pin 200 mm B had been tested in the previous experiment against plate CC21A under applied on/off loads of 40 N, 70 N, 100 N, and 150 N. These tests were repeated using pin 200 mm A against compliant layered plate CC21A under exactly the same experimental conditions. All test conditions were as given in Table 5.4. Table 6.1 gives the various surface roughness measurements for the two pins and the calculated contact parameter of the two bearings. All other contact parameters were the same for the two pins and are given for pin B in Table 5.5.

Design Parameters	**Pin-on-plate CC21A - 200mm A**	**Pin-on-plate CC21A - 200mm B**
Average Ra head roughness (nm)	42.09	39.25
Range of Ra head roughness (nm)	86.80	31.66
Average P-V head roughness (nm)	1101.06	980.24
Range of P-V roughness of head (nm)	1794.08	461.18
Average Rsk head roughness	-0.722	-1.043
Range of Rsk head roughness	2.034	2.082
Ave. RMS roughness head, σ_1 (nm)	66.57	52.29
Range of RMS roughness head (nm)	126.42	37.38
RMS roughness layer, σ_2 (nm)	145.7	145.7
Combined RMS roughness, σ (nm)	155	160
EHL coefficient of friction, μ_{EHL}*#	1.92×10^{-4}	1.92×10^{-4}
Surface separation ratio, λ *#	0.956	0.990
μ-EHL film thickness, $h_{\mu,min}$ (m)*#	3.95×10^{-8}	3.95×10^{-8}
μ-EHL friction, $\mu_{\mu EHL}$ *#	0.00748	0.00748

Table 6.1 Theoretical contact parameters for the two 200 mm pin-on-plate bearings (A and B) (# when load =150 N, * when η = 0.000818 Pa s)

Visual examination of the bearing surfaces of the pins showed in A to have a much more marked surface than pin B. The average roughness values (Ra, P-V, RMS) for the two pins, however, were very similar. Only in comparing the range of the roughness values did we demonstrate the expected difference between the two surfaces. This had important implications in the use of surface roughness measurements. Clearly it was not sufficient to consider simply an average roughness value as giving an complete description of the topography of a bearing surface. If bearing surfaces were to be compared it was important that a variety of parameters were considered and the range as well as the average value of the parameters examined. A full list of all the surface parameters measured for all the components used during this research is provided in Appendix F.

Other authors have typically used the average RMS roughness of a surface to predict micro-elastohydrodynamic fluid film thickness and the associated micro-elastohydrodynamic prediction of friction [Dowson and Jin 1986, 1987, 1992a, b, and Yao and Unsworth 1993]. This was also used here. From the values given in Table 5.7, the small difference in the measured average RMS roughness for the two pins predicted only very small differences in the micro-elastohydrodynamic film thickness and friction. The bearing surfaces of the pins however were visually very different. The question was then whether the RMS roughness value was a suitable indication of the tribological performance of a bearing surface. Would the visible difference in the surfaces have a greater effect on the measured friction than the RMS roughness value used in the micro-elastohydrodynamic theory prediction suggested?

6.1.1 Observations

Figures 6.1, 6.2, 6.3, and 6.4 compare the measured coefficients of friction for the two 200 mm radius of curvature pins (A and B) under applied loads of 40 N, 70 N, 100 N, and 150 N respectively.

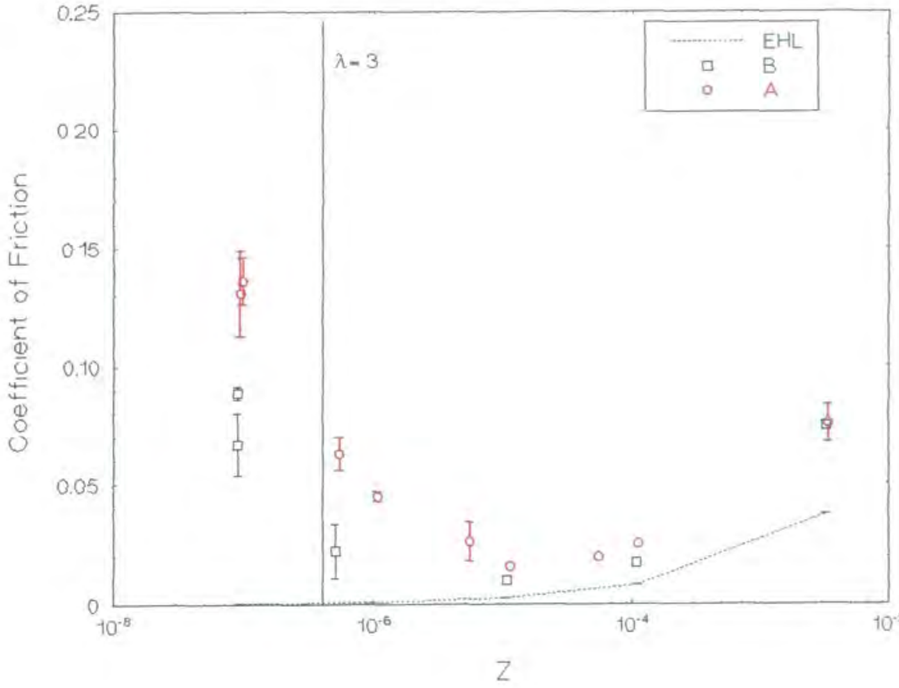

Figure 6.1 Effect of hard counterface roughness on pin-on-plate apparatus under 40 N applied load

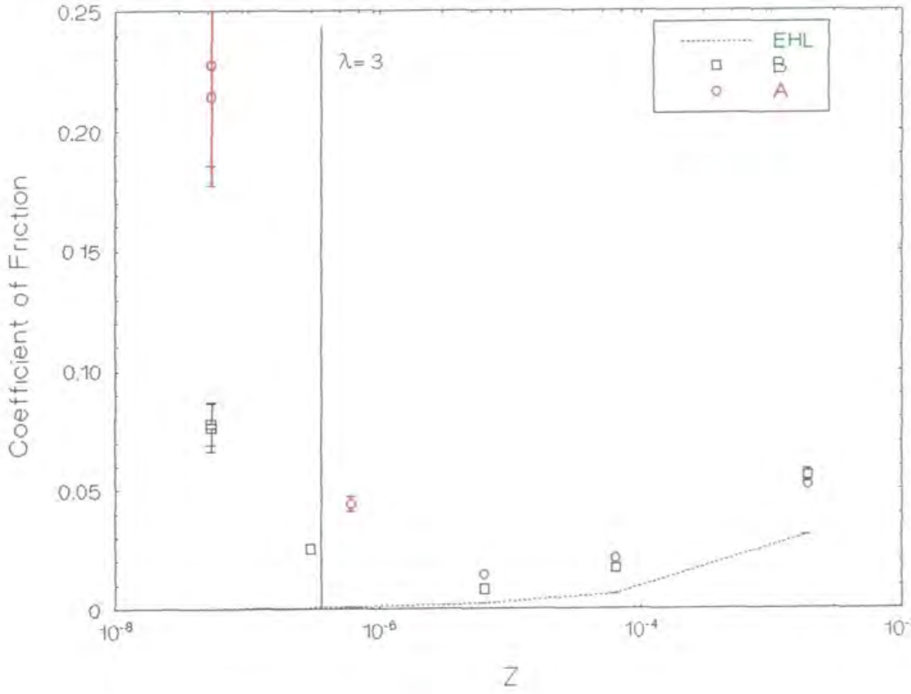

Figure 6.2 Effect of hard counterface roughness on pin-on-plate apparatus under 70 N applied load

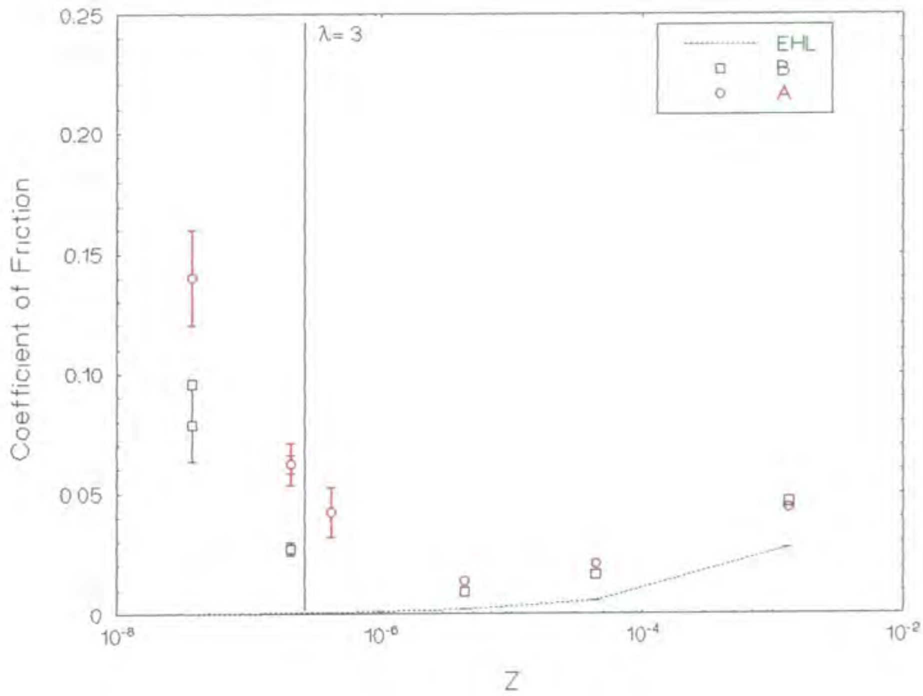

Figure 6.3 Effect of hard counterface roughness on pin-on-plate apparatus under 100 N applied load

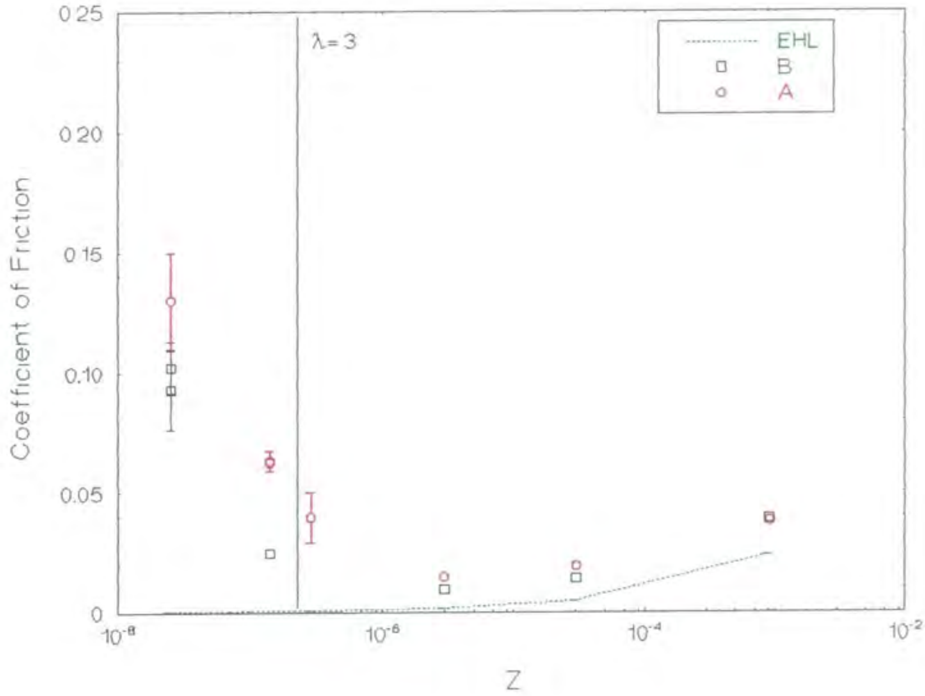

Figure 6.4 Effect of hard counterface roughness on pin-on-plate apparatus under 150 N applied load

The same observations were made from the results at all applied loads. In all cases the rougher pin A showed considerably higher coefficients of friction than the smoother pin B. Paired Student's t tests on the data obtained over all viscosities showed the coefficients of friction for pin A to be significantly higher than those of pin B for all loads. P values were 0.000217, 0.00196, 0.0314 and 0.00934 for applied loads of 40 N, 70 N, 100 N, and 150 N respectively. The difference in the hard bearing surfaces obviously had a significant effect on the frictional performance of the bearings.

The difference in measured coefficient of friction for the two bearings became less, for all loads, as the viscosity of lubricant increased. Figures 6.1 to 6.4 all show the measured coefficient of friction for the two pins at each viscosity becoming closer with increasing values of Z. For each load, at the highest viscosity (29.25 Pa s) the measured coefficient of friction for the two pins was approximately equal. The surface roughness of the hard counterface was much more important in the mixed regime than it was in a fluid film lubrication regime. Once a full fluid film had been achieved the roughness had a negligible effect on the friction generated.

6.1.2 Discussion

It would seem, therefore, that the average RMS roughness did provide an accurate estimate of the bearing surface when full fluid film lubrication had been established. In this regime, elastohydrodynamic and micro-elastohydrodynamic theories would hold. Figures 6.1 to 6.4 show a reasonably poor agreement between experimental and theoretical EHL results at all viscosities, possibly due to the very low stroke ratios in operation ($0.095 < S_T < 0.125$). The experimental measurements did agree with the elastohydrodynamic and micro-elastohydrodynamic theories in that the friction measured for the two pins in the fluid film regime was approximately equal.

In the mixed regime, however, the increased roughness of pin A significantly increased the measured coefficient of friction in a way not predicted by the average RMS roughness value. The increased roughness had a significant effect on the degree of separation of the surfaces in the mixed regime which was not shown in the λ values for the two pins which were very close (0.956 pin A and 0.990 pin B when load was 150 N and η = 0.000818 Pa s). The increased roughness of pin A increased the number of asperity contacts between the two bearing surfaces and so reduced the effective of any fluid film generated. A greater proportion of the load was then carried by the asperity contacts and less by the fluid film, and so more friction was generated. The increased roughness would also be expected to produce a later transition to the fluid film regime as thicker fluid films would be required before complete separation of surfaces would be possible. This can also be seen in figures 6.1, 6.2, 6.3, and 6.4. Once a full fluid film was established, there was theoretically no asperity contact and so the surface roughness of the bearing counterface became irrelevant.

6.1.3 Summary

The pin-on-plate machine results demonstrated the same result as Caravia *et al* [1993a]. The steady state friction of a polyurethane layer was increased by an increased counterface roughness. The results also showed an agreement in trends with elastohydrodynamic and micro-elastohydrodynamic theories, if not in the value of coefficient of friction obtained. This represented a further validation of the pin-on-plate test method. Whilst in the fluid film regime, the counterface roughness had negligible effect on the friction of a compliant layered bearing, in the mixed lubrication regime its effect was significant. This would explain why the 32 mm diameter head on the simulator produced such low friction (Section 5.5.3) in spite of its relatively rough bearing surface. Other than with the 0.000818 Pa s viscosity lubricant, the conformity of the joint had allowed it to operate in a full fluid film lubrication regime throughout and so its roughness had a negligible effect on the measured friction.

This was an important result in terms of the design of compliant layered joints. Elastohydrodynamic and micro-elastohydrodynamic theories could not predict the tribological performance of compliant bearings when the fluid film breaks down and so the counterface roughness has frequently been overlooked in considering design parameters [Dowson *et al* 1991]. Experiments have shown that for the right combination of design parameters, compliant layered joints can operate in a full fluid film lubrication regime at physiological lubricant viscosity [Unsworth *et al* 1987, 1988, Auger *et al* 1993, Burgess *et al* 1997]. Compliant layered joints may experience creep in vivo as well as possible changes in their mechanical properties and so allowances should be made in their design for the breakdown of the fluid film. It would therefore appear that, whilst the counterface roughness would be much less important in a compliant layered than in a conventional joint, a high surface finish on the hard bearing counterface would still be an important consideration in a compliant layered joint.

6.2 Comparison of compliant layers with conventional joint materials

As for the previous experiment, the pin-on-plate test method was further validated by using it to replicate another well-published result.

Since the first interest in compliant layered joints, they have been shown to provide significant benefits over conventional bearing combinations. Cudworth and Higginson [1976], Medley *et al* [1980b], Unsworth *et al* [1987, 1988], Auger *et al* [1993], and Graham *et al* [1995] had all shown compliant layered joints to give significantly lower friction than the conventional combination of UHMWPE and metal at viscosities representative of rheological lubricants. This result had been shown on both simple test machines [Cudworth and Higginson 1976, Medley *et al* 1980b, Graham *et al* 1995] and on simulators [Unsworth *et al* 1987, 1988, and Auger *et al* 1993].

The friction of compliant layered bearings against metal counterfaces had been measured on both the pin-on-plate apparatus and the simulator. Using the same counterfaces as used previously (30 mm head and 200 mm A pin), the friction of UHMWPE against metal was measured under the identical experimental conditions, as given in Table 5.4. A flat UHMWPE plate (PE4) was tested on the pin-on-plate machine and a Protek 32.4 mm diameter UHMWPE cup was tested on the simulator. Both had been previously tested extensively and so were considered 'worn in'. Applied on/off loads of 40 N, 100 N, and 150 N were used on the pin-on-plate apparatus and maximum loads of 500 N, 1000 N, and 2000 N were used on the simulator. Table 6.2 gives a comparison of the contact parameters for the compliant layered and UHMWPE bearings on the two machines.

Design Parameters	**Pin-on-plate**		**Simulator**	
	CC21A - 200mm A	**UHMWPE 200mm A**	**BB98 - 30mm**	**UHMWPE 30mm**
Equivalent radius, R (m)	0.200	0.200	0.1019	
UHMWPE modulus, E_2 (MPa)	19.2	2000	19.2	2000
UHMWPE Poisson's ratio, ν_2	0.5	0.3	0.5	0.3
UHMWPE RMS roughness σ_2(nm)	146	1260	2100	3150
Combined RMS roughness, σ (nm)	160	1260	2100	3150
Contact half-width, a (mm) #	6.24	1.23	6.56	2.85
Max. contact stress, P (MPa) #	0.43	9.4	0.64	14
Stroke Ratio, S_T #	0.125	0.025	0.251	0.109
EHL film thickness, h_{min} (m)*#	1.1×10^{-7}	1.3×10^{-8}	2.7×10^{-8}	6.3×10^{-9}
EHL coefficient of friction, μ_{EHL}*#	1.9×10^{-4}	2.1×10^{-4}	8.1×10^{-5}	7.3×10^{-5}
Surface separation ratio, λ *#	0.959	0.011	0.027	0.0020
μ-EHL film thickness, $h_{\mu,min}$ (m)*#	3.9×10^{-8}	2.0×10^{-10}	1.6×10^{-8}	5.1×10^{-11}
μ-EHL friction, $\mu_{\mu EHL}$ (m)*#	0.000748	0.0136	0.00439	0.0107

Table 6.2 Experimental conditions used in the comparison UHMWPE and compliant layered bearings (# when applied load is 150 N on the pin-on-plate or 500 N on the simulator, * when $\eta = 0.000818$ Pa s)

The experimental results obtained were analysed in two ways. The results for the UHMWPE bearing were compared to those for a compliant bearing on each machine. The results for the UHMWPE bearings on the two machines were then compared.

6.2.1 Comparison of UHMWPE and compliant layered bearing counterfaces

Figures 6.5, 6.6, and 6.7 show the comparison between the measured coefficient of friction for the UHMWPE and compliant layer plates against the 200 mm A pin on the pin-on-plate apparatus for applied loads of 40 N, 100 N, and 150 N respectively. Figures 6.8, 6.9, and 6.10 show the comparison between the measured coefficient of friction for the UHMWPE and compliant layer cups against the 30 mm head on the simulator for applied loads of 500 N, 1000 N, and 2000 N respectively. All graphs also show the predicted coefficient of friction from elastohydrodynamic lubrication theory for the two bearings under each loading. In the case of the simulator curves, the $\lambda=3$ line for the conventional joints is not shown as a lubricant viscosity above the tested range would be required. The comparisons show several general differences between the experimental measurements of friction for the two bearings as well as differences between the theoretical predictions of friction for the two bearings.

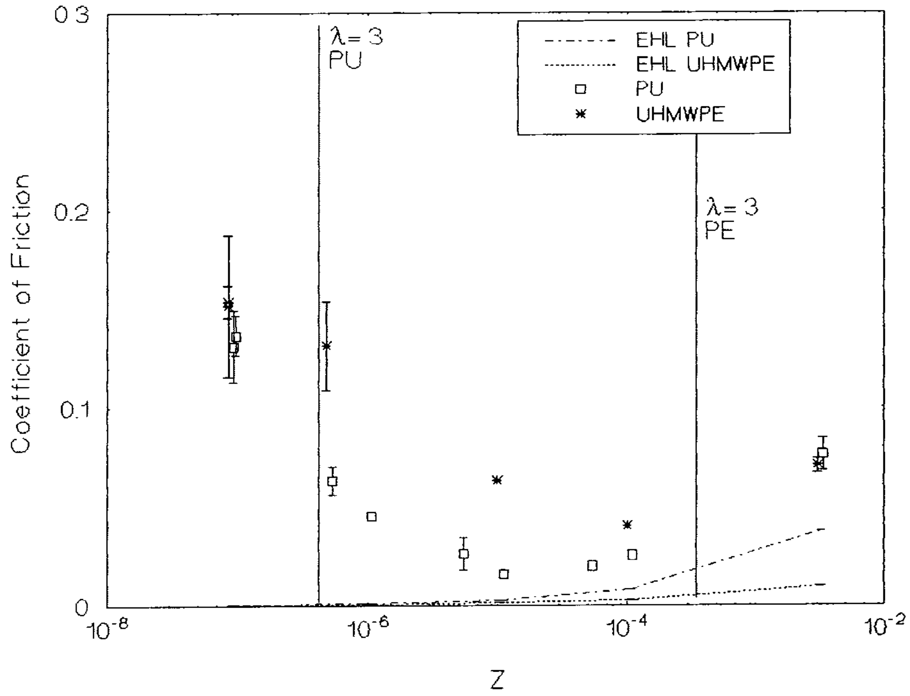

Figure 6.5 Comparison of UHMWPE and compliant layered plates under 40 N applied load on the pin-on-plate apparatus

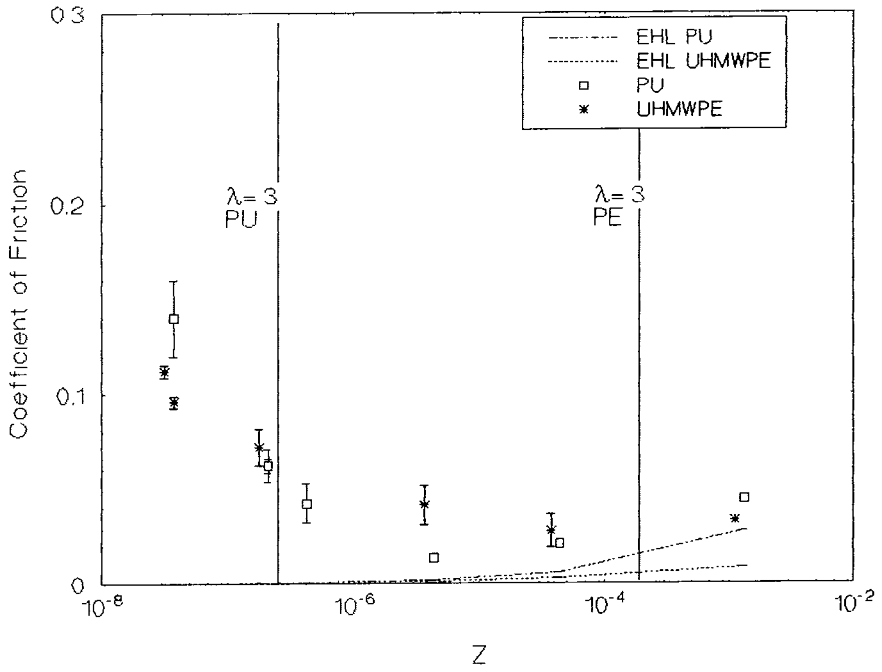

Figure 6.6 Comparison of UHMWPE and compliant layered plates under 100 N applied load on the pin-on-plate apparatus

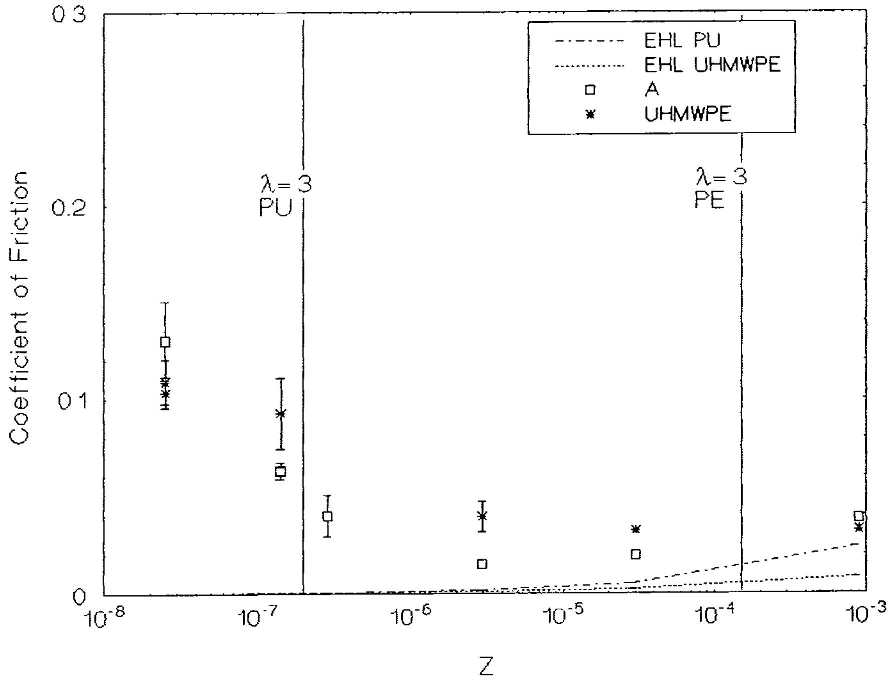

Figure 6.7 Comparison of UHMWPE and compliant layered plates under 150 N applied load on the pin-on-plate apparatus

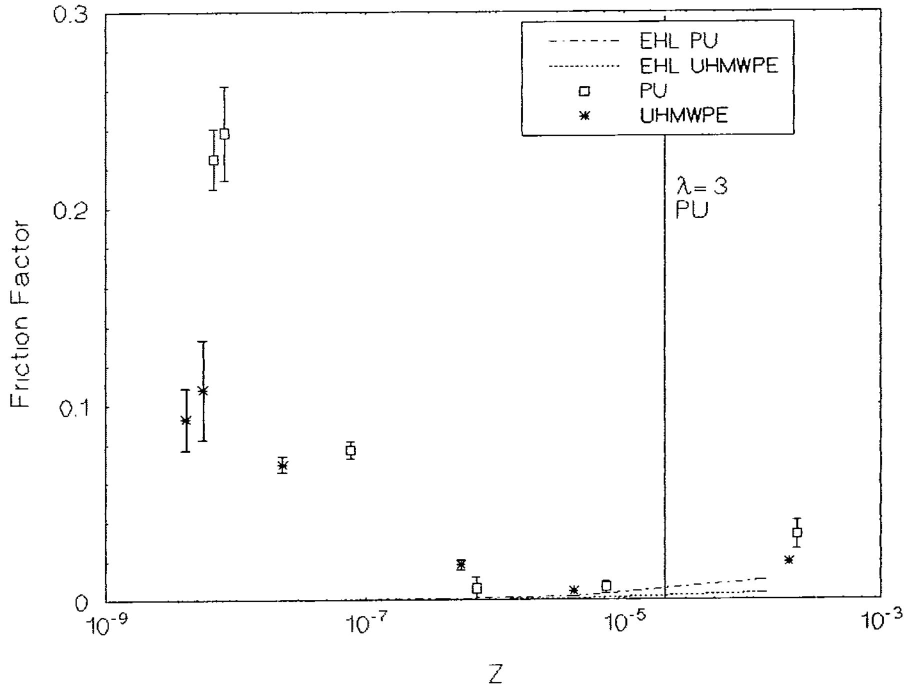

Figure 6.8 Comparison of UHMWPE and compliant layered cups under 500 N applied load on the simulator

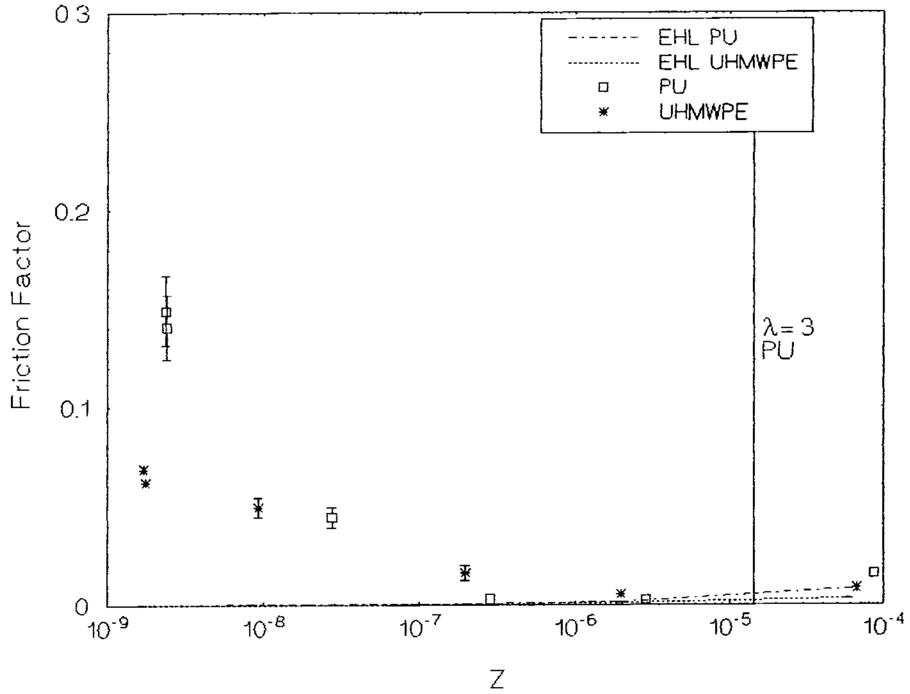

Figure 6.9 Comparison of UHMWPE and compliant layered cups under 1000 N applied load on the simulator

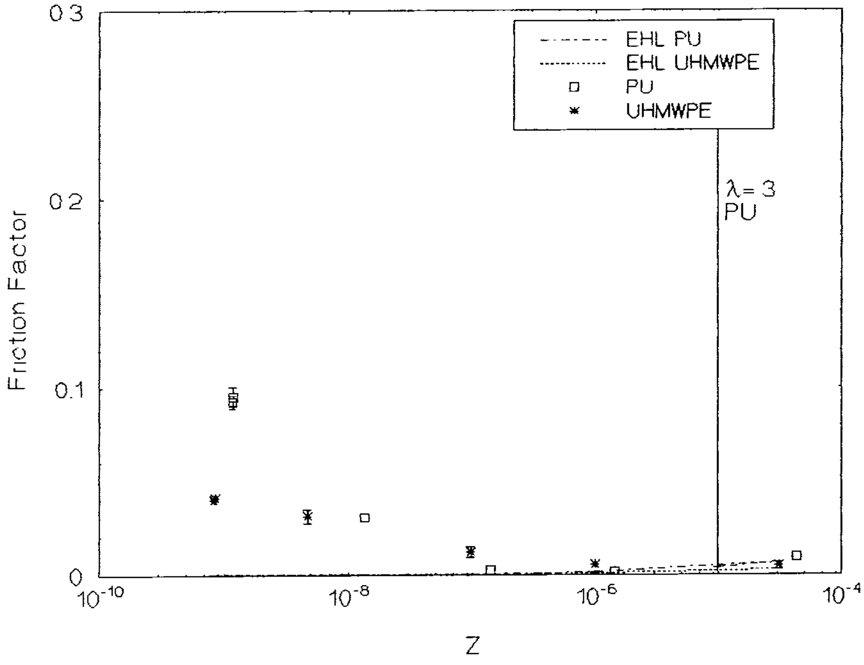

Figure 6.10 Comparison of UHMWPE and compliant layered cups under 2000 N applied load on the simulator

6.2.1.1 Observations

The first important observation made from the experimental measurements was that the results obtained for the UHMWPE bearings on the pin-on-plate and simulator apparatus were all comparable to previous published results. For the 0.000818 Pa s silicone fluid, coefficients of friction of 0.10 and 0.15 were measured on the pin-on-plate machine for loads of 40 N and 150 N respectively. For the same fluid, the measured friction factors on the simulator were 0.04 and 0.11 for maximum loads of 500 N and 2000 N respectively. The range of coefficients of friction measured on the pin-on-plate apparatus compared well with the range of published values of 0.05 to 0.2 as described in the repeatability experiments in Section 5.1.1. They also compared well with the average value of 0.153 found in the repeatability experiments for a UHMWPE-metal bearing in distilled water (0.001 Pa s) under 10 N applied load.

The simulator measurements also showed a good comparison with published results. Weightman *et al* [1973] used their 'arthrotripsometer' to measure the friction in various commercial hip replacements and measured a coefficient of friction of 0.06 for a 32 mm Charnley-Muller joint. Unsworth *et al* [1987, 1988] measured the friction of Muller UHMWPE-on-metal joints as 0.045 for a 0.002 Pa s lubricant under a 2000 N load using the first Durham simulator. Hall *et al* [1994] used the same machine to measure new Charnley prostheses and achieved an average friction factor of 0.04 in distilled water under a 2000 N peak loading. Saikko [1992b] measured 22 different cup-head combinations on a similar simulator and obtained coefficients of friction from 0.019 to 0.030 for the UHMWPE-stainless steel combination. Auger *et al* [1993] reported the coefficient of friction of UHMWPE against metal as between 0.017 to 0.042 for an average load of 1466 N. The friction factor values recorded here were similar to all these reported values.

For very low lubricant viscosities representative of a mixed lubrication regime, the UHMWPE-metal bearings gave lower measured coefficients of friction (and friction factors) than their compliant layered counterparts. As the viscosity of the lubricant increased, the measured coefficient of friction (or friction factor) of the compliant layered bearings decreased much more sharply than for the UHMWPE bearings. A fluid film lubrication regime was demonstrated by the compliant bearings at a lower lubricant viscosity than for the UHMWPE bearings (0.096 Pa s compared to 0.971 Pa s on the pin-on-plate apparatus). The minimum coefficient of friction measured was lower for the compliant layered bearings than for UHMWPE; 0.015 compared to 0.028 on the pin-on-plate apparatus and 0.002 compared to 0.004 on the simulator. Importantly, the results demonstrated clearly that it was possible to achieve a full fluid film lubrication regime for a conventional joint but not at viscosities in the range of physiological lubricants.

The measured friction of the compliant bearings remained lower than that of the conventional bearings until the Stribeck curve began to rise when the highest viscosity lubricant was used. In this full fluid film lubrication situation, when the bearing surfaces were completely separated, the coefficient of friction of the compliant layered bearings rose more sharply than that of the UHMWPE. At the highest lubricant viscosity, the polyurethane layer showed higher friction than the UHMWPE on both machines under all loads. Considering the theoretical curves, which were relevant only to the fluid film lubrication situation, the compliant layered bearing was predicted in all cases to show a higher coefficient of friction than its UHMWPE counterpart.

6.2.1.2 Discussion

These findings were completely in keeping with lubrication theory

At very low viscosities, the lubrication of the bearings was predominantly boundary lubrication, with a minimal degree of fluid film lubrication where the surfaces were separated by the lubricant. Table 6.2 shows the λ values for all the joints at the lowest viscosity were less than 1. The measured friction in this situation depended on the amount of asperity contact which was occurring and the value of dry friction for the bearing material combination.

At this viscosity where adhesive friction was predominant, the coefficient of friction was proportional to the ratio of Hertzian contact area to applied load. For the same load, the UHMWPE bearing gave a much smaller Hertzian contact area than the compliant layered bearing. From Table 6.2, the Hertzian contact half-widths on the pin-on-plate apparatus for a 150 N load were 1.23 mm for the UHMWPE bearing compared with 6.24 mm for the compliant layered bearing. In the simulator for a 500 N load, the Hertzian contact half-widths were 2.85 mm for the UHMWPE bearing compared with 6.56 mm for the compliant layered bearing. This would predict that the UHMWPE bearing would demonstrate lower friction than the compliant layered bearing for very low viscosities.

In addition, the dry contact friction of polyurethane against metal was considerably higher than that of UHMWPE against the same counterface. In a dry contact, UHMWPE-metal typically displayed coefficients of friction (or friction factor) of approximately 0.1, whilst polyurethane-metal showed significantly higher coefficients of friction (or friction factors) around 1.0 [Auger *et al* 1993, Burgess 1996]. The compliant layered bearing would have fewer asperity contacts per unit area than the UHMWPE bearing as its greater compliance allowed some asperities to be flattened. An asperity contact in the compliant layered bearing however generated significantly more friction than in the UHMWPE bearing, and the overall contact area was greater for the compliant layer. When the majority of applied load was supported by contact of asperities and the lubrication regime was towards the boundary lubrication end of the mixed regime, lower coefficients of friction (and friction factors) were generated in the UHMWPE bearing than in the compliant layered bearing.

As the viscosity of the lubricant was increased, the tribological performance of the bearings moved towards the fluid film regime. The separation of the surfaces increased and less load was supported by the interaction of asperities and more by the fluid film. At this stage the compliance of the polyurethane layers became important. The lower elastic modulus of the compliant layer allowed its surface asperities to be more easily flattened by the entraining action of the bearing producing a greater elastohydrodynamic effect. In addition, the micro-elastohydrodynamic smoothing effect of the pressure gradient produced in the lubricant was much more important in the compliant layered bearings. The fluid films generated for the compliant layered bearing were therefore thicker than in the UHMWPE-metal combination. The predicted values reflected this. For the 0.00934 Pa s lubricant viscosity and applied loads of 150N (pin-on-plate) and 500 N (simulator), the predicted elastohydrodynamic film thickness in the pin-on-plate bearings were 420 nm and 65.4 nm and in the simulator 150 nm and 30.6 nm for the polyurethane and UHMWPE bearings respectively. For the same conditions, the predicted micro-elastohydrodynamic film thickness were 39.5 nm and 0.20 nm for the pin-on-plate apparatus, and 1.55 nm and 0.051 nm for the simulator for the compliant layer and UHMWPE bearings respectively.

The thicker fluid films in the compliant layered bearing gave a greater separation of the bearing surfaces and so the dry contact values of the material combinations and the relative contact areas became less important. The λ values for the 0.00934 Pa s lubricant were 3.56 compared to 0.052 for the PU and UHMWPE bearings in the pin-on-plate apparatus under a 150 N load, and 0.100 and 0.0097 for the two bearings in the simulator under a 500 N peak load. The compliant layered bearings experienced less asperity contact than the UHMWPE bearings and so the measured coefficients of friction (and friction factors) were lower. In addition, the flattening of the compliant surface asperities meant a thinner fluid film was required to achieve complete separation of the surfaces and so the compliant bearings experienced an earlier transition to a full fluid film lubrication regime and reached a lower minimum coefficient of friction (or friction factor).

The difference between the fluid film thickness and Hertzian contact area for the two material combinations continued into the fluid film regime at which stage the experimental measurements began to show an agreement with the trends predicted by elastohydrodynamic and micro-elastohydrodynamic lubrication theory. Once the bearing surfaces had become completely separated by a film of lubricant, the increased contact area in the compliant layered bearing gave rise to greater generated friction as more lubricxant was under shear. This outweighed the decrease in friction due to the increase in film thickness. The compliant layered bearings therefore experienced higher coefficients of friction (and friction factors) than their UHMWPE counterparts. Considering again, Figures 6.5 to 6.10 brought one further observation.

On the simulator (Figures 6.8 to 6.10) a full fluid film lubrication regime was again achieved ~~of~~ λ values less than 3. This was true for both the compliant layered joints for which $\lambda = 3$ is shown and for the UHMWPE joints for which $\lambda = 3$ was off the scale. Micro-elastohydrodynamic effects were hence important on the simulator as seen previously (Section 5.2.3). The comparison between elastohydrodynamic theory predictions and experimental measurements was good.

On the pin-on-plate apparatus (Figures 6.5 to 6.7), the measured friction for the UHMWPE bearing appeared to show the onset of fluid film lubrication around the $\lambda = 3$ mark. For the compliant layered bearing, however the $\lambda = 3$ mark was still in the mixed regime of the experimentally measured Stribeck curve. Both material combinations showed significantly higher coefficients of friction than predicted by theories. Elastohydrodynamic theory was a good prediction of the onset of fluid film lubrication for the UHMWPE bearing on the pin-on-plate apparatus but less good for the compliant layer. The elastohydrodynamic effect in the compliant bearing on the pin-on-plate machine appeared to be less than predicted by theory, as we saw previously (Section 5.2.3). Although the compliant bearing benefited from the added advantage of micro-elastohydrodynamic lubrication effects it still showed higher friction and a later transition to fluid film than theory would predict.

6.2.1.3 Summary

The new pin-on-plate method demonstrated the same trends as the established simulator test. The discernible trends and the values of coefficient of friction and friction factor obtained compared excellently with other published results and extended the analysis of conventional joints over a wider range of lubricants to demonstrate a full fluid film lubrication regime. The pin-on-plate apparatus gave significantly higher values of coefficient of friction for both UHMWPE and compliant layers than would be predicted by elastohydrodynamic and micro-elastohydrodynamic theory. The difference between the results for the two material combinations was as lubrication theory would suggest.

6.2.2 Comparison of friction measured for UHMWPE-stainless steel bearings on the two apparatus

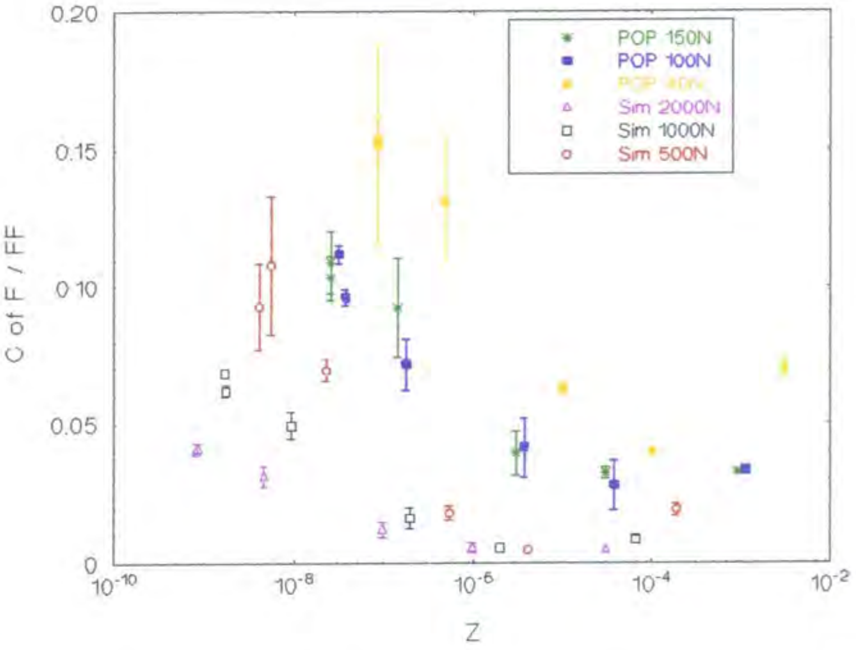

Figure 6.11 Comparison of experimental results for UHMWPE on the pin-on-plate apparatus and simulator

Figure 6.11 shows a comparison of the experimental measurements of friction for the UHMWPE bearings on the pin-on-plate and simulator apparatus under the range of applied loads. Figure 6.12 shows a comparison of the predicted friction from elastohydrodynamic theory for each condition.

6.2.2.1 Observations

In the previous tests on compliant layered joints, under an applied load of 150 N, the pin-on-plate apparatus had shown comparable friction to a bearing of equivalent radius on the simulator under a load of between 500 and 1000 N. (Section 5.4). For the conventional joint material combination of UHMWPE-stainless steel, less comparable results were seen. Considering Figure 6.11, the coefficients of friction measured on the pin-on-plate apparatus at all loads were higher than the friction factors measured on the simulator. In the fluid film regime, at the very high lubricant viscosities, the results for the two machines began to converge but not to the extent seen previously for the compliant layered joints.

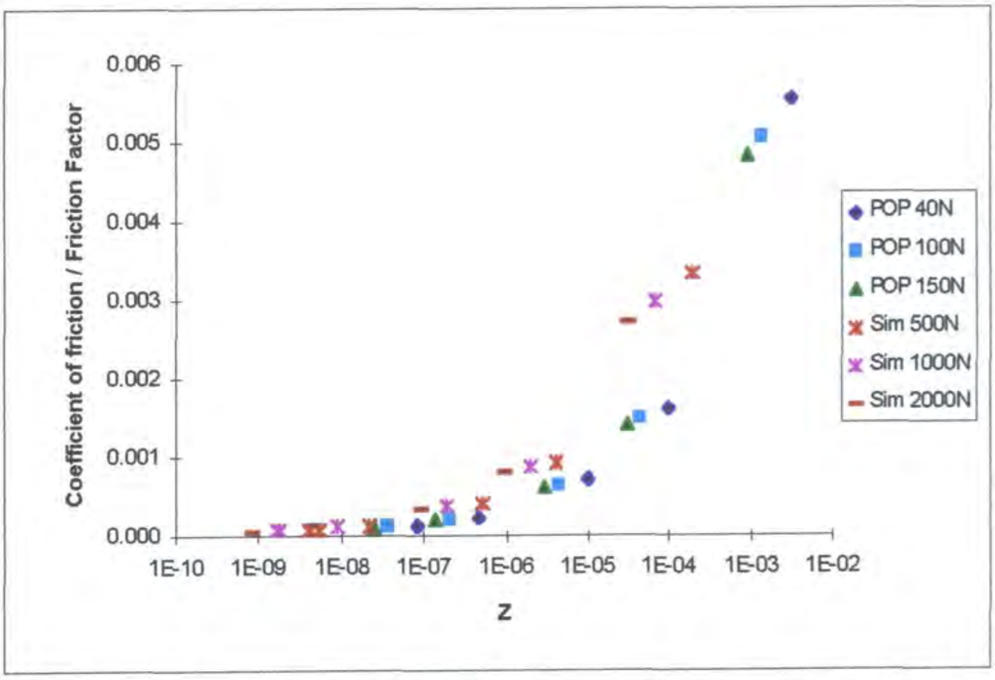

Figure 6.12 Comparison of theoretical results for UHMWPE on the pin-on-plate apparatus and simulator

The elastohydrodynamic theory predictions of friction in Figure 6.12 also showed a lack of convergence for the two machines in the fluid film regime. For the compliant layered joints theory predicted that under any load on either machine the coefficient of friction in the fluid film regime would fit the same curve if the equivalent radius of the bearing was the same (Figure 5.10 for 0.1 m equivalent radius). For the polyethylene-metal bearings, theory predicted much less comparable results for the two machines (and the various loads). As the viscosity increased, the predicted elastohydrodynamic coefficient of friction for the pin-on-plate bearings diverged from that of the simulator bearings.

6.2.2.2 Discussion

The differences between the friction results (experimental and theoretical) obtained for the two machines with UHMWPE bearings were due to differences in contact conditions. Table 6.2 showed that for the 0.000818 Pa s lubricant, the compliant layered bearings experienced similar Hertzian contact half-widths under an 150 N load on the pin-on-plate and a 500 N load on the simulator due to the elastic deformation of the material. Under the same conditions for the UHMWPE bearings the contact half-widths for pin-on-plate bearing was 1.23 mm and 2.85 mm for the simulator bearing. The stiffer material showed less elastic deformation and so gave smaller contact areas under lower loads, accentuating the difference in loading between the two machines.

Where adhesion was predominant (mixed regime), the coefficient of friction was proportional to the ratio of predicted Hertzian contact area to applied load. In Section 5.4, we saw that Hertzian contact area was proportional to applied load to a power of 2/3 (purely elastic) to 1 (purely plastic). Hence, the relationship between coefficient of friction and applied load is shown in Equation 6.1.

$$\mu = A.\, L^{B} \qquad \text{Eqn. 6.1}$$

where B was equal to -1/3 for a purely elastic contact and 0 for a purely plastic contact.

The compliant layered bearing represented a more elastic contact than the UHMWPE, and so B had a more negative value for the compliant layer than the UHMWPE. The same increase in applied load would therefore result in a greater increase in contact area for the compliant layered bearing than for the UHMWPE bearing. As a result, the decrease in coefficient of friction due to an increased load would be greater for the compliant layered bearing.

Contact conditions which had shown comparable friction results for the two machines for compliant bearings, showed significantly higher friction on the pin-on-plate for UHMWPE bearings. The difference in elastic modulus of the two polymers meant that loads which gave equivalent contact areas for the two machines for compliant layered bearings gave significantly different contact areas for UHMWPE bearings If the applied load on the pin-on-plate bearing was increased beyond 150 N and the applied load on the simulator decreased beyond 500 N, comparable Hertzian contact half-widths could be achieved. In this situation, we would see comparable friction results for the two machines.

Saikko [1993d] was the only published work found where the measured friction on pin-on-plate and simulator machines was compared. He measured the friction of UHMWPE against various counterfaces on a reciprocating machine and a simulator. He found the pin-on-plate machine gave significantly higher coefficients of friction than the simulator, a range of 0.05 to 0.27 compared with 0.02 to 0.15. He attributed this difference to the 'static' measurement of friction on the pin-on-plate at the reversal of the reciprocating motion. He also suggested the flat geometry and static loading of his pin on plate method could have made lubricant entrapment more difficult. The friction also increased during the course of testing on the pin-on-plate due to the occurrence of wear.

6.2.2.3 Summary

The test on conventional bearing materials showed a worse comparison between the pin-on-plate and simulator apparatus than the previous compliant layered bearing tests. This was attributed to less comparable contact conditions in these experiments. The higher elastic modulus of the UHMWPE gave less contact under lower loads and so highlighted the difference in loading conditions between the two machines. It is envisaged that comparable measurements of friction could be obtained for UHMWPE-metal combinations on the two machines but for more closely comparable loads than was necessary for compliant bearings.

7 Results and Discussion

Cylinder experiment - a line contact condition

7.0 Introduction

The performance of the new pin-on-plate test method for spherical contacts has been well-established by the previous experiments described in Chapters 5 and 6. Whilst this was applicable to hip joint prostheses, the knee joint might be more accurately modelled as a line contact. Over the course of the development of compliant layered bearings at the University of Durham, the hip function friction simulator had been modified to allow the friction of knee prostheses to be measured. It therefore seemed appropriate that the final stage in the validation of the new pin-on-plate test method was to assess line contacts.

Standard femoral knee components have a complex geometry. They often consist of two separate condyles which articulate against bearings on a tibial tray, and have two axes of curvature - the major medial-lateral radius and the minor anterior posterior radius. In order to simplify the contact geometry, a simple cylinder was used with a single radius of curvature in the direction of motion. The cylinders' lengths were greater than the widths of the counterfaces so that edge effects were not a problem.

Cylindrical components were manufactured from stainless steel for use on the pin-on-plate apparatus and simulator. The cylinders were designed so that the contact stress on each machine would be the same as on a normal knee prosthesis. A much larger load was applied by the simulator than by the pin-on-plate machine, so the pin-on-plate cylinders were much smaller than the simulator cylinders. The contact area had previously been shown to be the most important parameter in achieving comparable friction results on the two machines. It was felt, however, that the other contact parameters should be properly investigated. By using the same contact stress on both machines, its effect could be assessed. In addition, for similar contact stresses the entraining velocity of the pin-on-plate machine was varied. This changed the values of the predicted film thickness and coefficient of friction and allowed assessment of their relationship with the measured friction.

Two cylinders were manufactured for each machine. One cylinder was kept 'as manufactured' with a normal finish and the other was polished to give a super finish. This allowed a further assessment of the effect of the roughness of the hard counterface. The manufactured cylinders were used in place of the usual femoral component on the simulator or the spherical pin on the pin-on-plate. Flat compliant layered knee bearings were used as the soft counterface on both machines. In the simulator, a pair of knee bearings were fixed in the normal mounting. The maximum contact width on the simulator was equal to twice the maximum width of each bearing. On the pin-on-plate apparatus, a single knee component was cut down to give the required contact width. Three different compliant layered bearings (or pairs of bearings) were tested on each machine. The measured RMS roughness of the various bearings was slightly different and so the effect of the roughness of the compliant layer was also assessed.

The peak applied load on each machine was set to give the same contact stress of 3.2 MPa. A load of 43 N was applied on the pin-on-plate apparatus and 2000 N on the simulator (1000 N to each half of the bearing). In addition, one bearing pair was tested on the simulator under an 1000 N load. The entraining velocity on the simulator was set by the frequency of oscillation and the amplitude. Two different entraining velocities were used on the pin-on-plate apparatus. The usual range of silicone fluids were used as lubricants and standard test procedure was followed throughout.

Table 7.1 gives a complete list of the experimental conditions for the various components on the two machines. A full description of line contact theory is given in Chapter 2.

Design Parameters	**Pin-on-plate**	**Simulator**
Cylinder radius, R (mm)	6.0	38.4
Bearing width, w (mm)	10.1	2 x 37
Applied load, L (N)	43	i: 2 x 1000 ii: 2 x 500
Contact half-length , a (mm)[1]	5.05	18.5
Contact half-width , b (mm)	1.18	i: 7.53 ii: 5.32
Max. contact stress, P (MPa)	3.25	i: 3.23 ii: 2.29
Stroke ratio, S_T	0.101	0.197
Max. entraining velocity, u (mm/s)	I: 25 II: 4.5	34.6
EHL film thickness, h_{min} (nm) *	I: 170 II: 63	i: 230 ii: 380
EHL coefficient of friction, μ_{EHL} *	I: 3.2×10^{-4} II: 1.4×10^{-4}	i: 1.5×10^{-4} ii: 2.2×10^{-4}
RMS cylinder roughness, σ_1 (nm)	normal: 71.14 super: 48.01	normal: 102.93 super: 62.07
RMS layer roughness, σ_2 (nm)	C1: 259 C3: 196 C4: 87.6	M1/M2: 139 M3/M4: 220 M5/M6: 157
Comb. RMS roughness, σ (nm) #	269	243
Surface separation ratio, λ	I: 1.27 II: 0.35	i: 1.42 ii: 2.26

Table 7.1 Experimental parameters for cylinder tests (where * is $\eta = 0.000818$ Pa s, # is normal cylinder and C1 or M3/M4).

---

[1] Note, for this condition the predicted half-length of the contact is the half the width of the compliant bearing,

7.1 Effect of entraining velocity

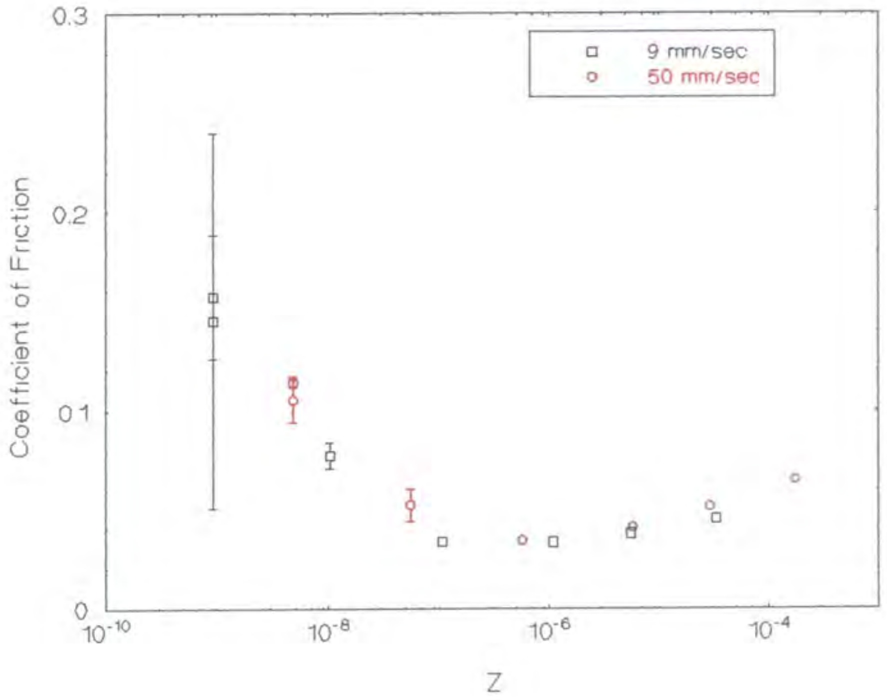

Figure 7.1 Effect of entraining velocity (super-finished cylinder against C1)

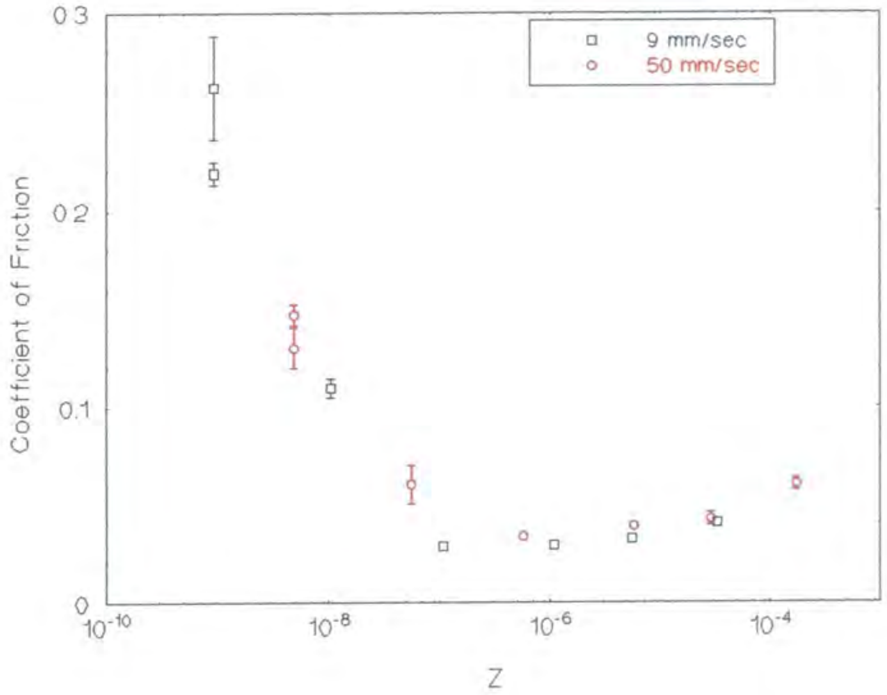

Figure 7.2 Effect of entraining velocity (super-finished cylinder against C3)

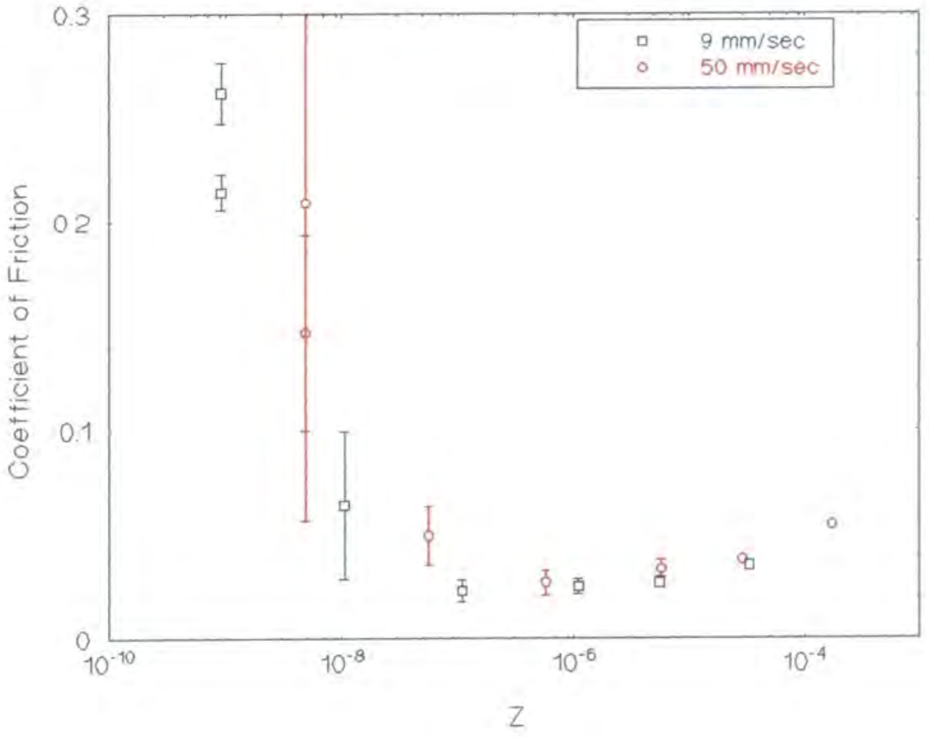

Figure 7.3 Effect of entraining velocity (super-finished cylinder against C4)

Figures 7.1, 7.2, and 7.3 show the coefficients of friction measured on the pin-on-plate apparatus testing the super-finished cylinder at entraining velocities of 9 mm/sec and 50 mm/sec against the three compliant bearings C1, C3, and C4 respectively. The results for the normal cylinder showed the same effect of entraining velocity and so are not shown here.

All three compliant bearings showed the same results. The Stribeck curves were of the now familiar form showing mixed lubrication for low lubricant viscosities and full fluid film lubrication at the highest viscosities. The repeatability of the friction measurement on both machines was comparable with that of the spherical contacts.

Higher coefficients of friction were generated at the lower entraining velocity than at the higher velocity. This was the expected result, Auger et al [1993] saw the same for UHMWPE. If all other parameters were constant, the lower entraining velocity would give rise to smaller fluid films. There would therefore be less separation of surfaces in the mixed regime, and higher velocity gradients in the lubricant films in the fluid film regime. The interesting observation in terms of this research was that the measured coefficients of friction for both speeds fitted the same Stribeck curve. For a given viscosity, the coefficient of friction at the lower velocity was higher but the value of the Sommerfeld parameter was lower.

The difference in experimental protocols for pin-on-plate and simulator apparatus was discussed in Section 2.4. The entraining velocity of the articulating surfaces of a human hip had been shown to be approximately 10 mm/sec [Johnson and Smidt 1969]. The Durham simulator had an entraining velocity of 11 mm/sec for a 32 mm diameter femoral head. The ASTM standard for pin-on-plate tests however was 25 mm/sec [ASTM F372-82]. The entraining velocity used in the majority of pin-on-plate tests in this research was just less than the ASTM standard at 22 mm/sec.

During this research, the pin-on-plate and simulator apparatus were compared in terms of the full Stribeck curves achieved on each machine. In this type of comparison the difference in entraining velocity between the two machines was not important as the same Stribeck curve was achieved independently of the entraining velocity used. If the absolute values of the coefficients of friction (or friction factors) measured were to be compared for a particular condition, the difference in entraining velocity would then become important. It is recommended that future testing using the pin-on-plate method, and in the future definition of materials testing protocols, entraining velocities should be standardised for all tests.

7.2 Effect of compliant layer roughness

The effect of the roughness of the compliant layer was investigated for the line contact situation on both the pin-on-plate apparatus and simulator.

7.2.1 Pin-on-plate Apparatus

Figures 7.4 and 7.5 show a comparison of the results obtained for the three compliant knee bearings (C1, C3, C4) on the pin-on-plate machine against the normal finished cylinder at entraining velocities of 9mm/sec and 50 mm/sec respectively. Figures 7.6 and 7.7 show the results of the same tests using the super-finished cylinder. The elastohydrodynamic theory prediction of friction is also shown.

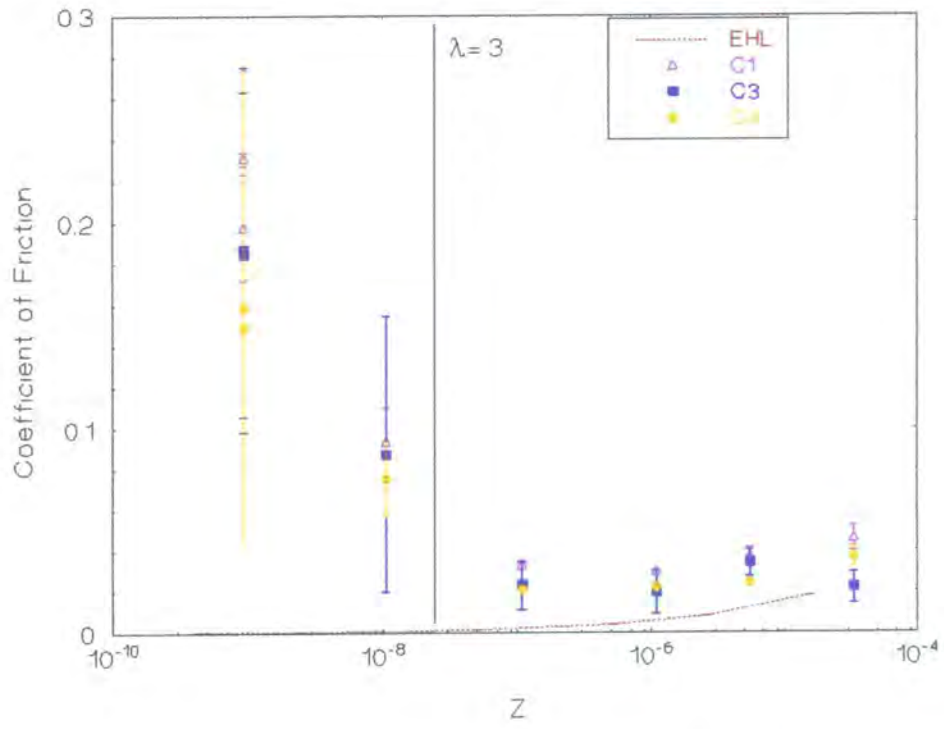

Figure 7.4 Effect of compliant layer roughness (normal finish cylinder at 9 mm/sec on the pin-on-plate apparatus)

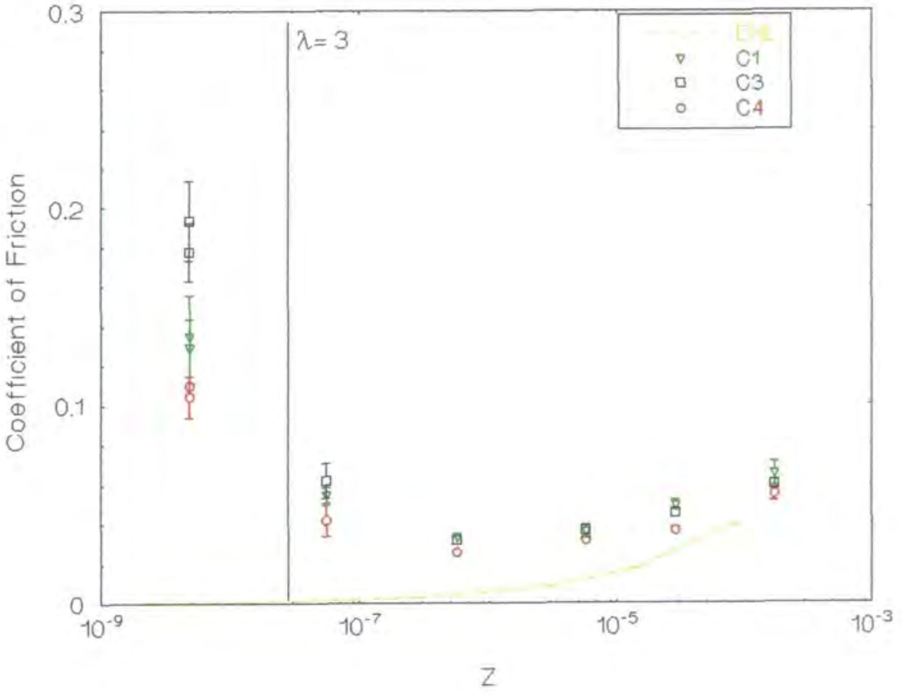

Figure 7.5 Effect of compliant layer roughness (normal finish cylinder at 50 mm/sec on the pin-on-plate apparatus)

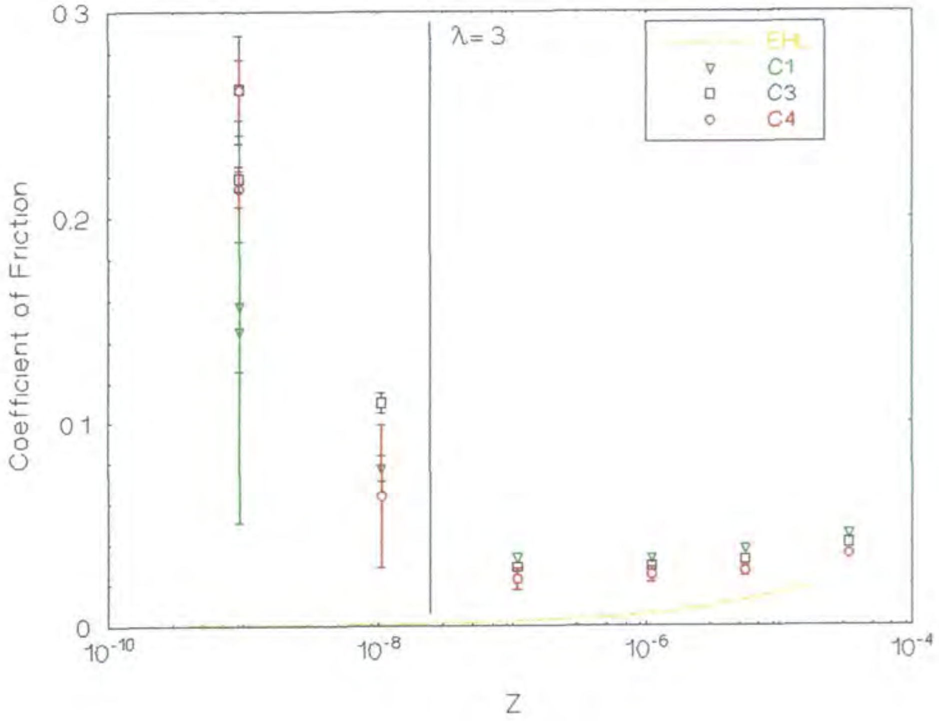

Figure 7.6 Effect of compliant layer roughness (super finish cylinder at 9 mm/sec on the pin-on-plate apparatus)

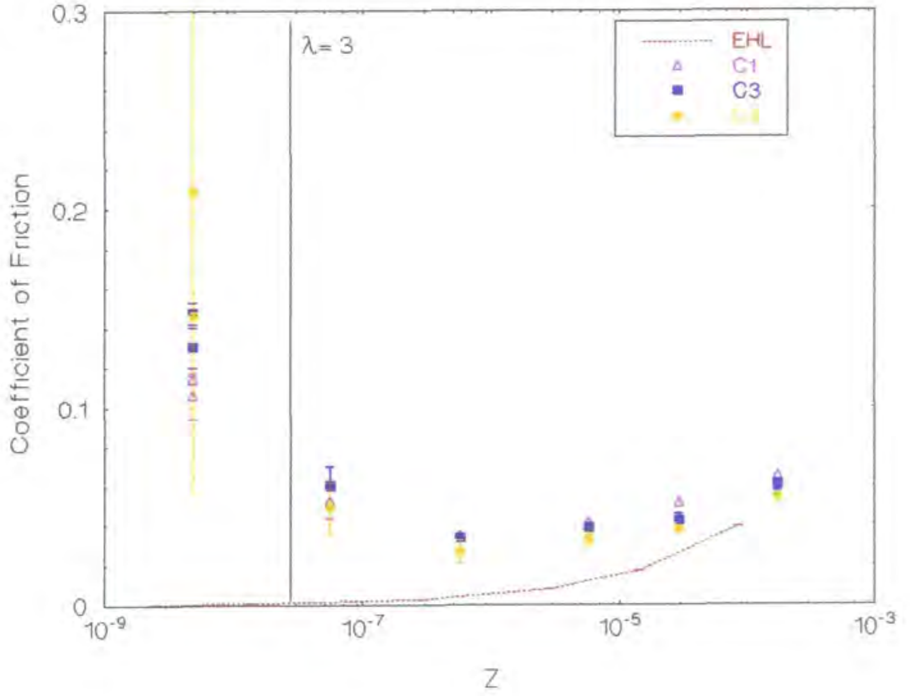

Figure 7.7 Effect of compliant layer roughness (super finish cylinder at 50 mm/sec on the pin-on-plate apparatus)

In general there was very little difference between the friction measured for the three compliant layered bearings. Paired Student's t tests were performed on the measured coefficients of friction of all bearing pairs (C1 vs. C3, C1 vs. C4, C3 vs. C4) for both cylinders and both entraining velocities over the full range of lubricant viscosities. The majority of tests (7 of 12) showed no significant differences between the friction measured for any of the compliant bearings. There were several significantly different results.

- For the normal cylinder at 9 mm/sec C1 showed significantly higher coefficients of friction than C4 ($P = 0.0363$).
- For the normal cylinder at 50 mm/sec, the coefficient of friction of C3 was significantly higher than C1 ($P = 0.027$) and C4 ($P = 0.004$), and the coefficient of friction of C1 was significantly higher than C4 ($P = 0.00057$) i.e. μ (C3)>μ (C1)>μ (C4)
- The only significant difference for the super-finished cylinder was at 9 mm/sec when C3 again showed significantly higher coefficients of friction than C1 ($P = 0.0408$).

The RMS roughness of the three samples are given in Table 7.1 as 259 nm, 196 nm, and 87.6 nm for samples C1, C3, and C4 respectively. A full list of the measured roughness parameters for the samples is given in Appendix F. The significant differences observed between measured coefficients of friction did not show any correlation with the roughness values other than the smoothest sample C4 showing the lowest friction for the normal cylinder at 50 mm/sec. C3 was measured as being less rough than C1 and yet showed significantly higher coefficients of friction in two experiments. Over all lubricant viscosities, the roughness of the compliant layer seemed to have little effect on the measured friction on the pin-on-plate apparatus.

An interesting effect can be seen in the measured coefficients of friction in 7.4, 7.5, 7.6, and 7.7 for the lowest viscosity lubricant. 7.4 and 7.5 show the results for the normal finish cylinder. In both graphs, sample C4 showed the lowest coefficient of friction for the 0.000818 Pa s lubricant. The friction for C1 and C3 were higher although the order differed at the different velocities. Figures 7.6 and 7.7 show the measured coefficients of friction for the super-finished cylinders. In both graphs, C4 demonstrated the highest coefficients of friction and C1 the lowest. C1 had the highest RMS roughness and C4 had the lowest RMS roughness.

Whilst these differences did not hold for all viscosities, the graphs showed a clear difference in the effect of compliant layer roughness at the lowest lubricant viscosity depending on the roughness of the counterface. When the counterface was very smooth, there appeared to be some benefit from a rougher compliant layer. This was presumed to be due to fluid entrapment. When the hard counterface had some irregularities (normal finish cylinder) fluid could be trapped within them. A smooth compliant layer was then optimal to minimise asperity contact. When the hard counterface was very smooth (super-finished cylinder) the fluid could no longer be entrapped by the hard counterface, and so a rougher compliant layer then became optimal, providing areas of fluid entrapment between the asperities of the compliant bearing surface. At higher lubricant viscosities, the bearing surfaces were separated by a film of lubricant and these fluid entrapment effects were no longer important. Caravia *et al* [1993] found that rough indentors on compliant layers generated lower start-up friction but smooth indentors generated lower friction in the steady-state conditions. The benefit of the rough indentors was ascribed to the importance of fluid entrapment when films were low (start-up).

7.2.2 Simulator

Figure 7.8 shows the measured friction factors for three bearing pairs, M1/M2, M3/M4, and M5/M6 against the normal finish cylinder on the simulator. The elastohydrodynamic theory prediction of friction is also shown.

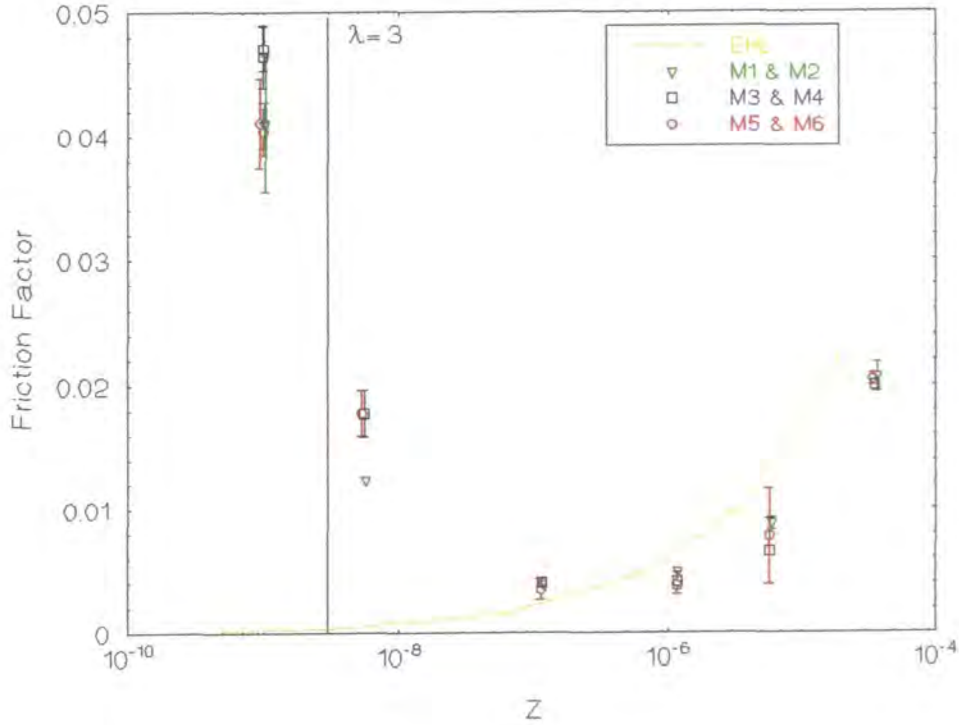

Figure 7.8 Effect of compliant layer roughness (normal finish cylinder on simulator)

A typical Stribeck curve was achieved on the simulator for the line contact situation. Higher friction factors and a more mixed regime was seen at low viscosities than had previously been seen for point contacts. The simulator results showed even less difference between the measured friction factors for the three bearing pairs than seen on the pin-on-plate apparatus. The average RMS roughness of the bearing pairs were 139 nm , 220 nm, and 157 nm for M1/M2, M3/M4, and M5/M6 respectively as given in Table 7.1. A full list of roughness parameters is given in Appendix F. Paired Student's t test were again performed on results and no significant differences were found between the measured friction factors of any two bearings ($0.0596<P<0.365$).

7.2.3 Summary

It was concluded that the roughness of the compliant layer had very little effect on the measured friction of the bearing over the full range of lubricant viscosities. There could be some benefit, however, in using rougher layers against very smooth counterfaces if there was a high degree of contact between the bearing surfaces.

7.3 Comparison of experimental and theoretical results

Figures 7.4, 7.5, 7.6, 7.7, and 7.8 also allowed a consideration of the relationship between experimental measurements and theoretical predictions.

For the point contact, the pin-on-plate results had typically shown a poor comparison with elastohydrodynamic theory and the simulator measurements a much better comparison. As elastohydrodynamic theory was only directly applicable to the fluid film situation, this was attributed to the lubrication regime in the simulator being much closer to fluid film throughout. The pin-on-plate apparatus demonstrated predominantly mixed lubrication for many conditions.

A similar result was seen here for the line contact situation. The pin-on-plate friction measurements (Figures 7.4 to 7.7) were much higher than the simulator measurements (Figure 7.8) throughout. This was in spite of the simulator friction factors being considerably higher for the line contact than previously seen for a point contact demonstrating a predominantly mixed lubrication for manyof the lubricants. At the very highest viscosities (4.585 and 29.25 Pa s) the pin-on-plate results show the upwards Stribeck curve indicative of full fluid film lubrication. At these viscosities, the theoretical and experimental results begin to converge. As for the point contact, the simulator experimental measurements showed a much closer agreement with elastohydrodynamic theory. The stroke ratios were 0.101 and 0.197 for the pin-on-plate apparatus and simulator respectively. Stroke ratio effects could have been a factor in the closer match between theory and experiment seen for the simulator compared to the pin-on-plate apparatus.

Interestingly, at the highest lubricant viscosities, elastohydrodynamic lubrication theory overestimated slightly the experimentally measured friction factors on the simulator. This was attributed to the contact half-length used in the theoretical calculations. The predicted half-length of the line contact was greater than the width of the bearing and so the bearing half-width of 18.5 mm was used in theory calculations. This value represented the width of the bearing at its widest point (it was kidney-shaped) and so would give an over-estimation of the contact in general.

Another consideration was the use of a surface separation ratio, λ, of 3 to predict the onset of fluid film lubrication. For point contacts, the simulator demonstrated fluid film lubrication for Z values far below that for $\lambda = 3$, demonstrating the importance of micro-elastohydrodynamic effects. The pin-on-plate apparatus, contradictorily, did not demonstrate fluid film lubrication until Z values far above $\lambda = 3$ were attained, suggesting elastohydrodynamic and micro-elastohydrodynamic effects were less effective than theory predicted.

The pin-on-plate apparatus showed a better comparison for the line contact. The transition to full fluid film lubrication was achieved for values of Z only slightly greater than predicted for $\lambda = 3$. The results for the simulator showed a marked contrast to those for the point contact. $\lambda = 3$ was predicted for values of Z around that of the 0.000818 Pa s lubricant viscosity and far lower than the onset of friction achieved in the experimental results. The elastohydrodynamic and micro-elastohydrodynamic effects appeared to be less effective than theory would predict for the simulator.

7.4 Effect of hard counterface roughness

Figures 7.9 and 7.10 show a comparison of the coefficients of friction measured for the normal and super finish cylinders against sample C1 for the two entraining velocity. Figure 7.11 shows a similar comparison of results for bearing pair M3/M4 against the two cylinders on the simulator. The results were representative of those obtained for all the compliant bearings.

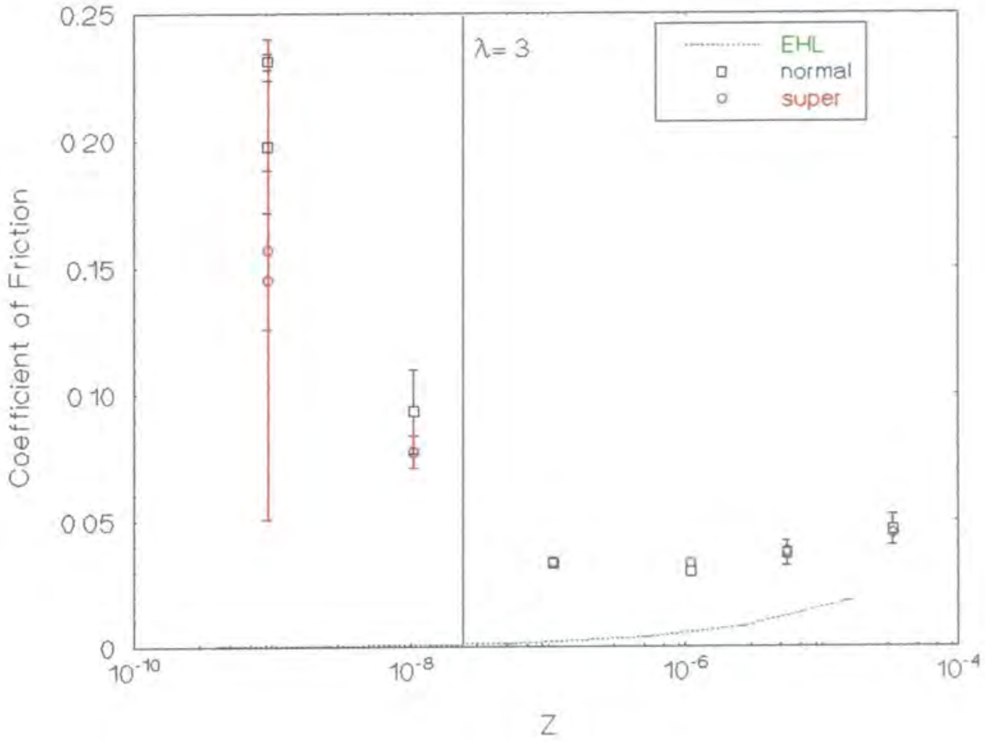

Figure 7.9 Effect of hard counterface roughness (C1 at 9 mm/sec) on the pin-on-plate apparatus

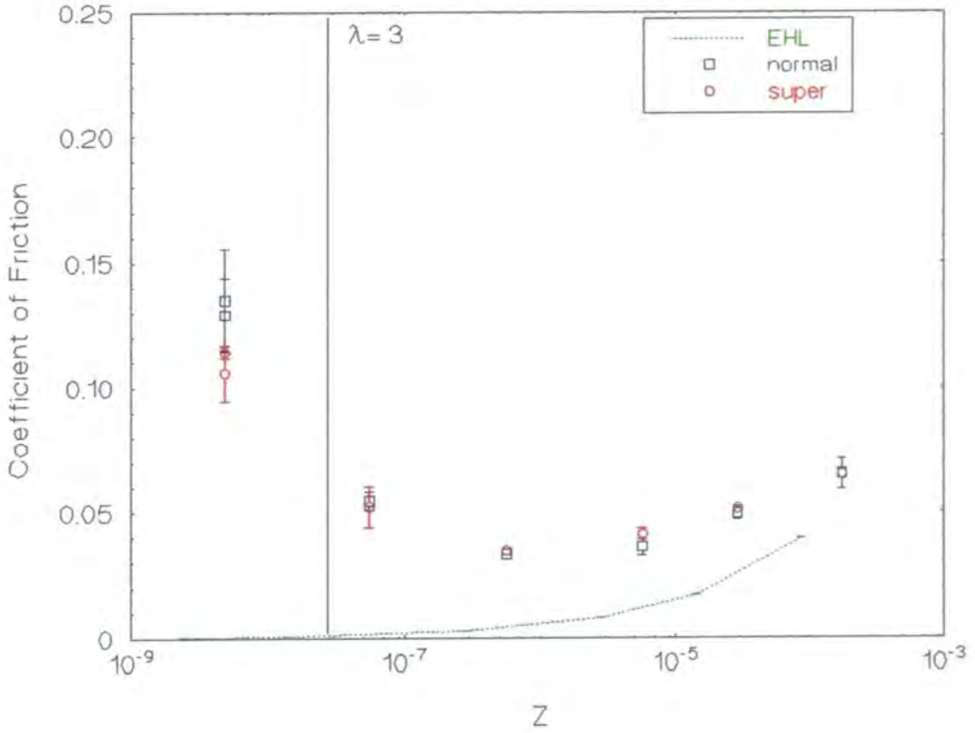

Figure 7.10 Effect of hard counterface roughness (C1 at 50 mm/sec) on the pin-on-plate apparatus

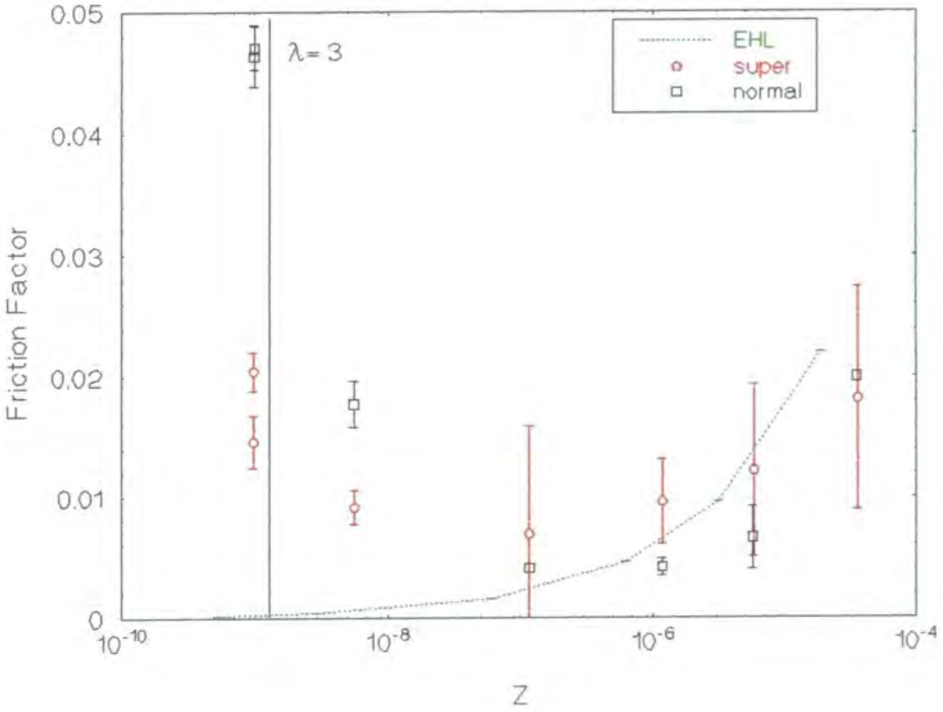

Figure 7.11 Effect of hard counterface roughness (M3/M4) on the simulator

On the pin-on-plate apparatus the results showed little difference between the coefficients of friction measured for the two cylinders over the full range of viscosities. The super-finished cylinder generated marginally lower coefficients of friction at both entraining velocities for the lowest lubricant viscosities (0.000818 Pa s and 0.00934 Pa s) where the lubrication was mixed. The measured friction factors on the simulator showed the same trend. The super-finished cylinder gave lower friction for the two lowest viscosity lubricants. At higher viscosities where the bearing showed full fluid film lubrication, the friction recorded for the two cylinders was very close. The average RMS roughness of the cylinders are given in Table 7.1.

Paired student's t tests were performed on the results for the two cylinders against each compliant layered bearing (or pair) at both entraining velocities. Over the full range of lubricant viscosities, no significant difference in measured coefficient of friction (friction factor) was found on either the simulator or the pin-on-plate apparatus ($0.0548 < P < 0.107$).

The result reinforced the findings in Section 6.1. The roughness of the hard counterface was important in the mixed regime. When the fluid films were thin, a rougher bearing gave less separation of surfaces and more asperity contact. Once complete separation of the surfaces was achieved, the roughness of the hard counterface was no longer important.

7.5 Comparison of pin-on-plate and simulator results

Figure 7.12 shows a comparison of the typical results obtained on the pin-on-plate apparatus at both entraining velocities (sample C1 normal cylinder) and the simulator (M3/M4 normal cylinder). The result for simulator bearing under an 1000 N load is also shown. The graph includes the elastohydrodynamic theory prediction of friction for one of the conditions on each the pin-on-plate and simulator.

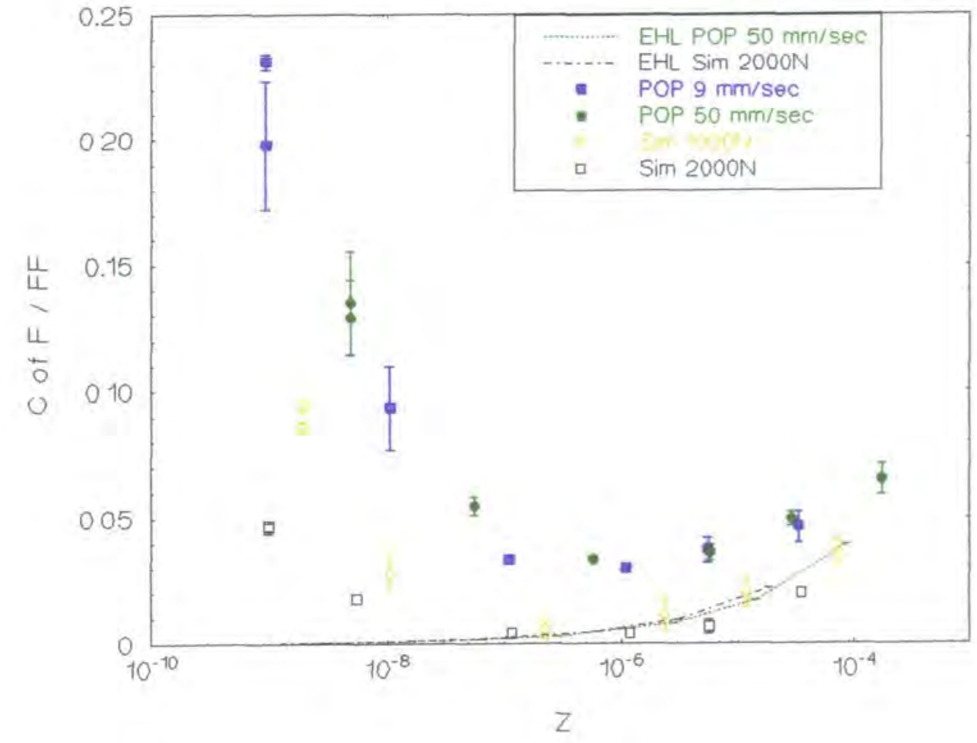

Figure 7.12 Comparison of results obtained for a line contact on pin-on-plate apparatus and simulator

The theoretical predictions showed that the measured coefficients of friction (or friction factors) on the two machines would be expected to fit the Stribeck curve in the full fluid film regime. The values given in Table 7.1 demonstrated this. For the 29.25 Pa s viscosity lubricant, the predicted elastohydrodynamic coefficient of friction 4.0×10^{-2} at 50 mm/sec, and 1.8×10^{-2} at 9 mm/sec on the pin-on-plate apparatus and 2.2×10^{-2} on the simulator.

The experimental results for the two machines compared less favourably. At all viscosities, the coefficients of friction measured on the pin-on-plate apparatus were much higher than the friction factors measured on the simulator. The measurements for the two machines began to converge for the very high values of Z ($\eta > 4.585$ Pa s) but not to the degree seen previously for compliant layered bearings under point contacts. This was in spite of the contact stresses, elastohydrodynamic fluid film thickness, and elastohydrodynamic coefficients of friction for the two machines all being much closer for line contacts than they were previously for point contacts.

The major difference between contact parameters for the bearings on the two machines was the Hertzian contact area. For a line contact, this was modelled as being a long thin rectangle, half-length, a and half-width, b. On the simulator the predicted half-length of the contact was greater than the half-width of the bearing and so this was the limiting dimension and was used in the analysis. The predicted values of a and b were 5.05 mm (9.31 mm predicted) x 1.18 mm for the pin-on-plate apparatus and 18.5 mm (48.5 mm predicted) x 7.53 mm. This meant that the predicted Hertzian contact areas for the two machines would be 23.84 mm^2 and 557.22 mm^2 respectively.

The contact area had been shown both by this research to be the most important factor in achieving comparable measurements of friction by different test methods. Equating the contact stress or the elastohydrodynamic and micro-elastohydrodynamic parameters did not, in this experiment, give comparable measurements of friction because the bearing contact areas on the two machines were too different.

The effect of contact area was reinforced by one final experiment. The same bearing on the simulator was tested under half the original load (500N on each half of the bearing pair). The contact stress was lower, 2.3 MPa, and the predicted Hertzian contact half-length and half-width smaller: 18.5 mm (38.6 mm predicted) and 5.32 mm. The predicted contact area was then 393.7 mm^2. Figure 7.12 shows that halving the applied load, increased the measured friction factor. This was in keeping with the results seen for the point contact and demonstrated again the relationship between coefficient of friction (friction factor) and the predicted contact area.

7.6 Summary

Tests under line contact conditions demonstrated similar trends for both the pin-on-plate and simulator test methods. The roughness of the compliant layer was seen to have a negligible effect on measured coefficient of friction (and friction factor), while the roughness of the hard counterface was important in the mixed regime but not in the full fluid film regime. Pin-on-plate tests also showed higher friction measured for lower entraining velocities but that the measured coefficients of friction fitted the same Stribeck curve for all velocities. The measured values of coefficient of friction on the pin-on-plate and friction factor on the simulator did not compare well but this was attributed to the difference in Hertzian contact area. The line contact experiments verified the results obtained on the pin-on-plate apparatus under the point contact condition and reinforced earlier findings that comparable measurements of friction would be given by different test methods for comparable Hertzian contact areas.

8. Summary of Results and Discussion

8.0 Introduction

The results described in Chapters 5, 6, and 7 represented extensive testing of the new pin-on-plate method and extensive comparisons with a proven test method, the relevant theories, and with the work of other authors. The experiments described validated the new pin-on-plate test method and allowed several interesting relationships to be observed.

8.1 Validation of pin-on-plate method

The modified pin-on-plate test method was validated by proving that its results were repeatable, within reasonable experimental errors, and comparable with a proven test method. In addition, each individual experiment showed comparable trends and comparable measured values of coefficient of friction with those in other published studies under similar conditions.

8.1.1 Repeatability

The results of pin-on-plate test method were shown to be more repeatable than those of the simulator. The average coefficient of variation of the measured coefficients of friction (or friction factors) was 17% in the pin-on-plate apparatus compared to 41% in the simulator. The application of the load was also more repeatable. The lowest load of 10.8 N ± 2% in the pin-on-plate machine compared with 2000 N ± 8% in the simulator. The highest variation was seen for the lowest viscosity as this was the least stable situation in terms of lubrication. At this viscosity, the pin-on-plate machine showed a variation of up to 40% whilst the simulator demonstrated as much as 110%. Repeated runs at the lowest lubricant viscosity during the course of testing showed the measured friction to decrease. This was thought to be due to some residual effect of the high viscosity lubricants used between the tests.

The accuracy of friction measurement of the pin-on-plate method was also calculated as being an improvement on that of the simulator. The major systematic error in the measurement of friction on the simulator was from the analogue-digital and digital-analogue converters which were not used in the pin-on-plate method. The maximum systematic error on the simulator was 98% while on the pin-on-plate only 13.9%.

8.1.2 Comparison with the simulator

All results obtained by the pin-on-plate test method led to the same conclusion. The friction results obtained on the pin-on-plate apparatus were comparable with those on the simulator when the predicted Hertzian contact areas of the bearings on the two machines were similar. This held for both mixed and full fluid film lubrication. The result applied to both point contacts and line contacts, as well as compliant layered bearings and bearings of conventional joint materials. The experimental conditions required to give equivalent contact areas depended on the equivalent radius of the bearing, the adjusted elastic modulus of the materials, and the applied load. For compliant layered bearings of the same equivalent radius, the same result was achieved for a pin-on-plate bearing under 150 N to a simulator bearing under a load between 500 N and 1000 N. For a conventional UHMWPE-metal combination, a much higher load was required on the pin-on-plate machine as the elastic deformation of the polyethylene was much lower. In line contacts, both Hertzian contact half-length and contact half-width had to be considered in equating the predicted contact area.

Comparable results were achieved in the two machines in spite of some differences between the methods. These were the simplified on/off loading on the pin-on-plate apparatus, the difference in entraining velocity, the difference in point of friction measurement, the difference in sliding/rolling action.

The simplification of the loading cycle on the pin-on-plate apparatus was not thought to jeopardise the significance of its results as it included a high load stance phase and a low load swing phase as did the simulator. The difference in entraining velocity had been shown in these experiments to affect the individual values of coefficient of friction measured but not the overall Stribeck curve.

Point of measurement of friction

The point of measurement of friction had been constant throughout testing on both machines. The simulator measured frictional torque during the maximum loading part of its cycle but also when the velocities were maximum. Typical traces of the measured frictional torque obtained during a cycle on the simulator are shown in Figure 8.1 for a 0.000818 Pa s viscosity lubricant.

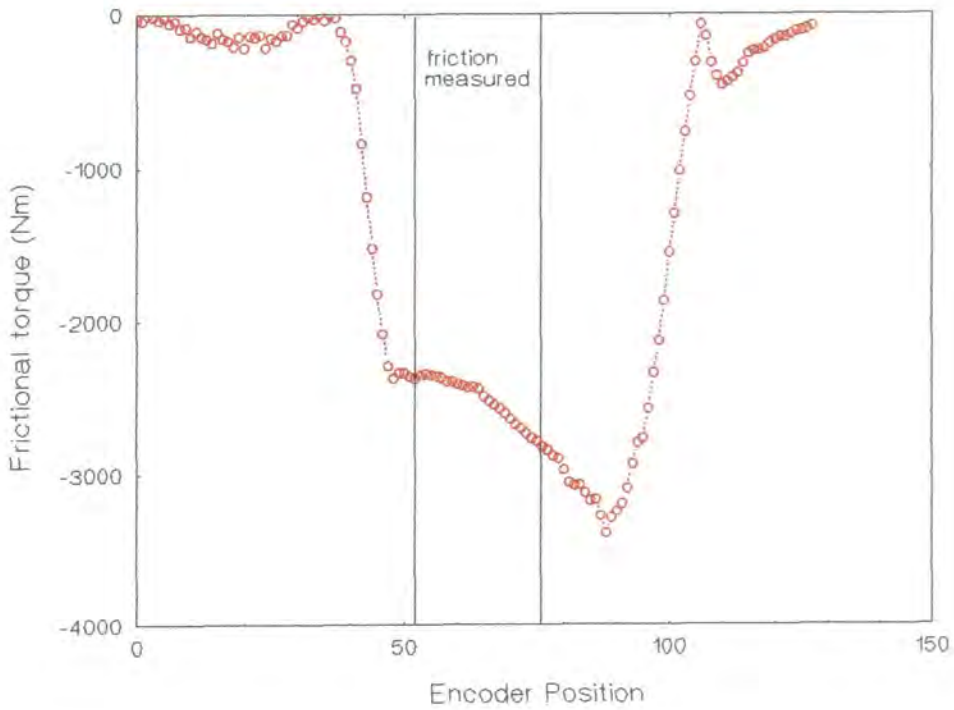

Figure 8.1 A typical simulator trace of frictional torque (0.000818 Pa s)

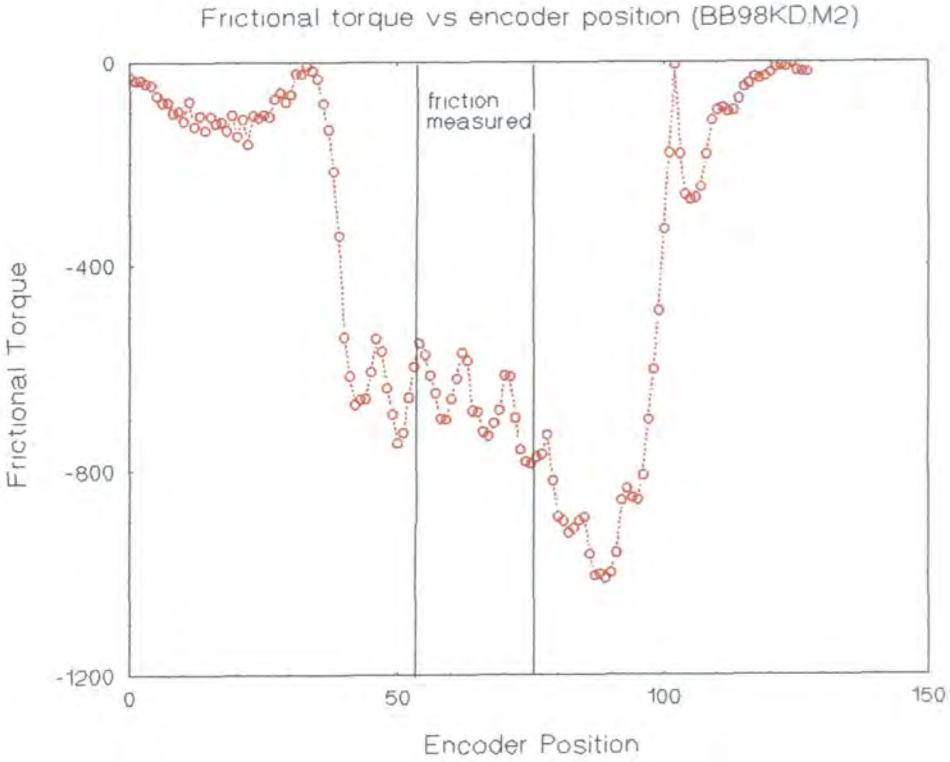

Figure 8.2 A typical simulator trace of frictional torque (0.00934 Pa s)

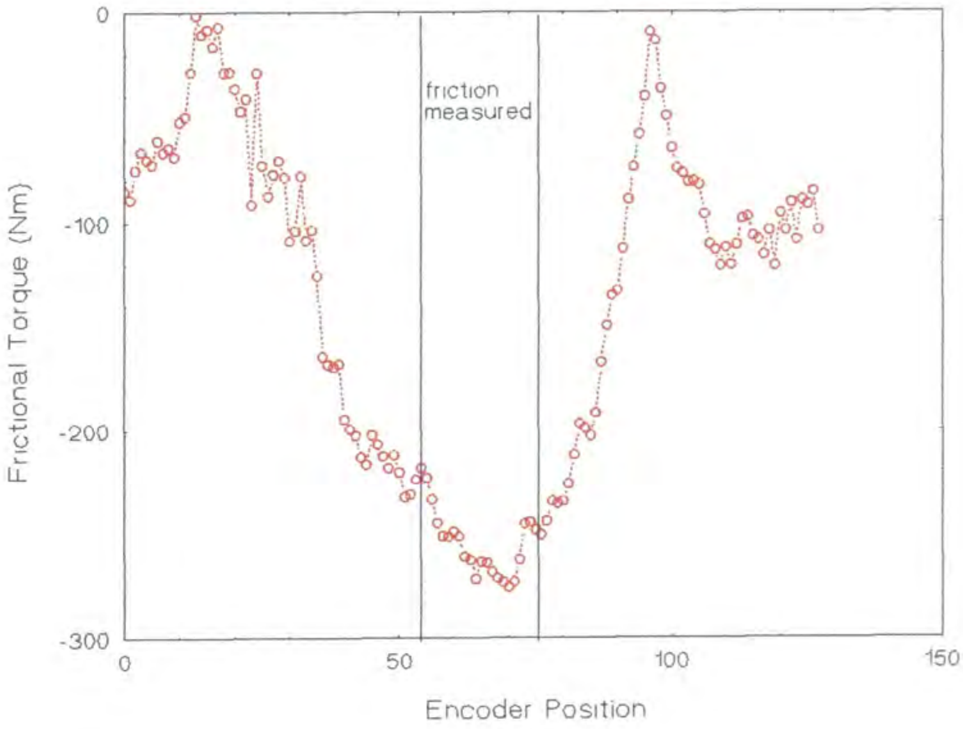

Figure 8.3 A typical simulator trace of frictional torque (29.25 Pa s)

Figures 8.2 and 8.3 show the measured frictional torque at 0.00934 Pa s and 29.25 Pa s. The area of interest, in terms of the lubrication of the bearing, was the high load phase between encoder positions of 48 and 88 DAC units. The friction factor showed a slightly different form due to the variation in the loading cycle during this phase. The traces of friction factor are given in Appendix G.

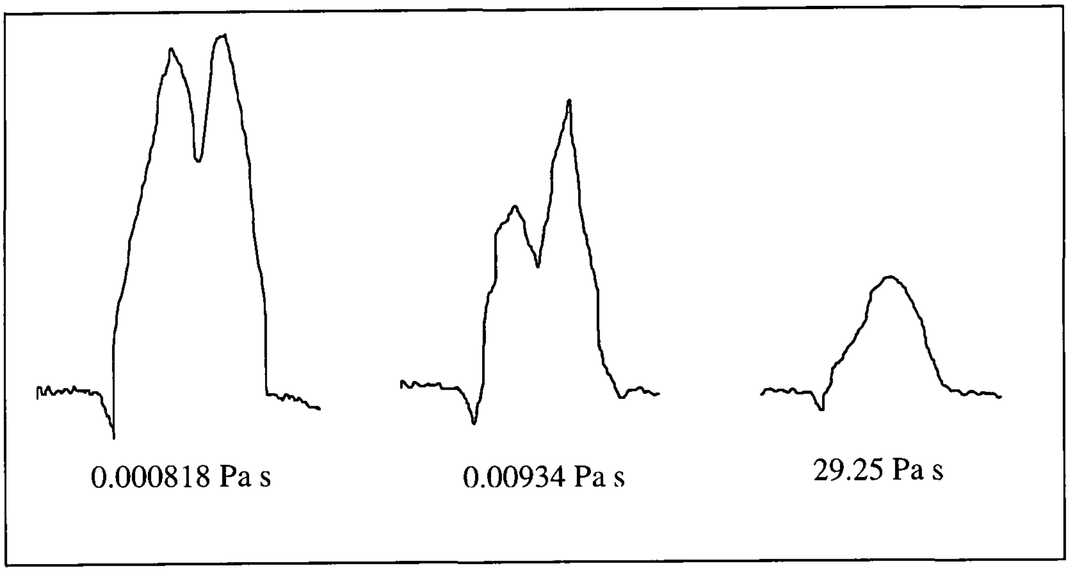

Figure 8.4 Typical pin-on-plate traces of frictional force

Figure 8.4 shows the typical trace of frictional force obtained for the same three viscosities on the pin-on-plate apparatus (coefficient of friction traces showed the same form as the magnitude of load was constant during the loading phase). Unlike the simulator, the pin-on-plate apparatus showed zero friction for half the cycle as the load was removed completely while on the simulator a minimum load of 100 N was applied in its low load phase.

The traces showed the expected results.

At the lowest viscosity on the pin-on-plate apparatus, the measured friction in the loading phase was minimum for the highest entraining velocity. The lubrication of the bearing at this point was mixed and so the highest entraining velocity produced the thickest films and so the greatest separation of the bearing surfaces. This occurred in the middle of the loading cycle. The friction rose either side of this minimum to a maximum value at the lowest entraining velocities when the reciprocating motion of the machine reversed.

At the highest viscosity, the measured friction in the loaded phase was maximum for the highest entraining velocity on both machines. In this situation, the friction was generated by the shearing of the lubricant, and so the highest velocity would produce the maximum shear force.

At the 0.00934 Pa s lubricant viscosity (and the 0.000818 Pa s viscosity on the simulator), the situation was somewhere in between. The measured friction was again highest for the lowest entraining velocity (mixed lubrication) but the friction at the start of the loading cycle was lower than at the end of the loading cycle although the same entraining velocity was in operation at the two instances. This was attributed to the advantage of greater load bearing area due to greater elastic deformation which allowed an increased load to give a longer fluid film depletion time. This was not seen for the 0.000818 Pa s on the pin-on-plate apparatus which implied the increase in load bearing area due to elastic deformation was more effective on the simulator than on the pin-on-plate machine, due to the higher loads as discussed in Chapter 5.

Standard test protocol on the pin-on-plate apparatus measured the frictional force at its maximum value during the loading cycle for five separate runs. On the simulator, friction was measured for five points between 51.5 and 71.5 which were then averaged and used to calculate a single value of friction factor. From Figures 8.1, 8.2, and 8.3 it can be seen that this the frictional torque was not always at its maximum during the period of measurement.

The differences between the friction at the point of measurement on the simulator and its maximum were small but nevertheless, the pin-on-plate apparatus measured friction under more extreme conditions than the simulator.

Difference in sliding/rolling

The other difference in the two test methods was the difference in the articulation of the surfaces. On the simulator, the femoral component rocked against its counterface with some anterior-posterior sliding. On the pin-on-plate apparatus, the action was purely sliding as the pin moved linearly along the plate. The result was that the area of contact on the simulator remained fairly constant, whilst on the pin-on-plate apparatus it was moved along the length of the sample during the course of a stroke. This was shown in the difference in stroke ratios of the two machines.

In moving the contact area along the length of the stroke on the pin-on-plate, the effect of any hysteresis in loading and unloading the plate would be included in the measured values of friction. The magnitude of its effect and its significance in terms of the measured friction is investigated in Chapter 9.

8.1.3 Comparison with theory

In all experiments, Hertzian contact theory and elastohydrodynamic and micro-elastohydrodynamic lubrication theories were used to calculate the contact and lubrication parameters predicted for the particular experimental conditions.

8.1.3.1 Hertzian Contact theory - relationship between load and friction

Hertzian contact theory was shown to be extremely significant. The single most important parameter in achieving comparable results by the two methods was found to be the contact area. As discussed earlier, this was consistent with Hertzian contact theory.

The frictional force caused by adhesive friction was directly proportional to the area of contact. The area of contact was shown to be proportional to the applied load to a power factor depending on the material and the contact regime [Archard 1953]. The coefficient of friction was defined as the ratio of frictional force to applied normal load. This then gave the relationship described in equation 6.1 that μ is proportional to the (applied load)^{B}. Table 8.1 gives the theoretical values of B for the various conditions of contact [Archard 1953]. In most elastic materials such as compliant layers, B was likely to be less than predicted as some plastic deformation would also occur.

Deformation	**Single area of contact**	**Multiple area of contact**
Elastic	-0.333'	-0.2
Plastic	0	0

Table 8.1 Theoretical values of friction-load power factors, B

In the experiments described here, various bearings have been tested under a range of loads under a variety of conditions. The measured coefficient of friction (or friction factor) in each experiment has been plotted against the load applied and a curve fitted to the results of the form in equation 6.1.

Bearing	**Average B** ($0.000818<\eta<0.096$ Pa s)
CC21A - 200 mm A	-0.1533
CC21A - 200 mm B	-0.04854
CC21A - 100 mm	-0.29983
PE4 - 200 mm A	-0.33377
BB98 - 30 mm	-0.683
BB98 - 28 mm	-0.736
Protek - 30 mm	-0.4839

Table 8.2 Average experimental friction-load power factors, B

Considering only the results for lubricant viscosities of 0.096 Pa s and less (where the lubrication would be mixed), the average values of B found for each experiment are given in Table 8.2.

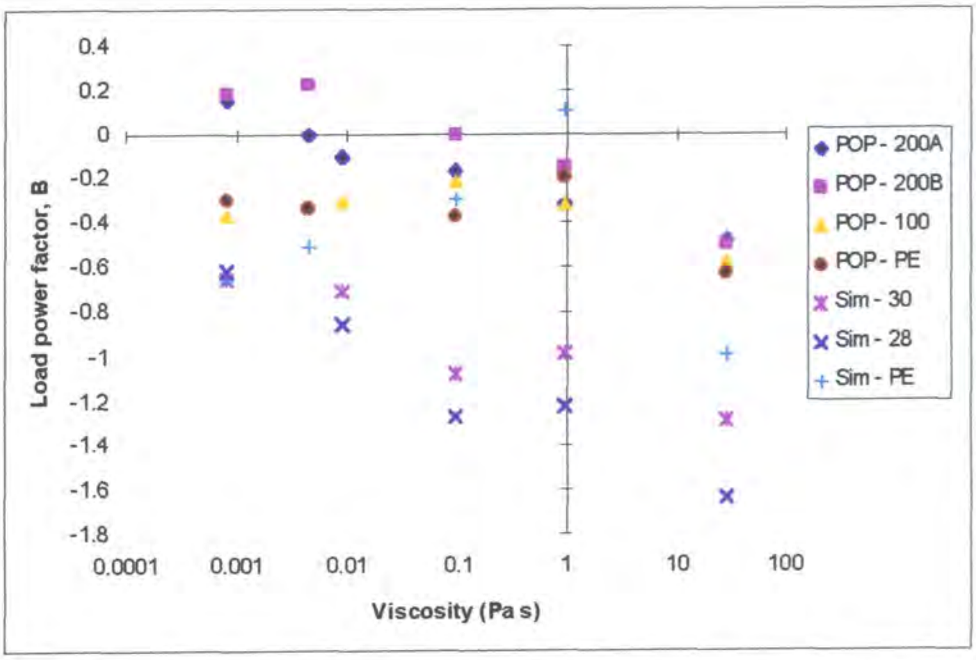

Figure 8.5 Relationship between friction-load power factor, B, and lubricant viscosity

Figure 8.5 shows the relationship between B and the lubricant viscosity. Table 8.2 and Figure 8.5 both show that the results on the pin-on-plate apparatus showed a much closer agreement with the theoretical predictions of B than those of the simulator. This was because, under the conditions used, the simulator frequently showed full fluid film lubrication for all lubricant viscosities and so the adhesive friction predictions no longer held. The pin-on-plate apparatus showed mixed lubrication for higher viscosities and so the theory held better. The simulator polyethylene results had lower power factors than the simulator compliant layered bearing results, consistent with this reasoning as polyethylene tests had shown more mixed lubrication. Figure 8.5 also shows that as the viscosity increased so did the numerical value of the power factor B, deviating further from its predicted values as the bearings moved towards the fluid film regime. Hall *et al* [1994]. tested new and explanted Charnley prostheses under a range of loads on a simulator and also found B to be higher than predicted. He achieved an average value of B of -0.898 for the lubricated condition.

Overall, the results of the pin-on-plate experiments showed a good correlation with Hertzian contact theory predictions which were invaluable in predicting equivalent conditions between the two machines.

8.1.3.2 Elastohydrodynamic and micro-elastohydrodynamic lubrication theories

Both Auger *et al* [1993] and Burgess [1996, Burgess *et al* 1997] have discussed the relevance of elastohydrodynamic and micro-elastohydrodynamic lubrication theories in predicting the tribological performance of compliant layered bearings. The elastohydrodynamic and micro-elastohydrodynamic lubrication theories were only directly applicable to the fluid film regime but provided a useful indication of the degree of separation of the bearing surfaces in the mixed regime. The micro-elastohydrodynamic lubrication theory was even less applicable as it was only valid for viscosities of 0.096 Pa s or less, at which fluid film lubrication seldom occurred.

Both authors found only limited comparisons between their theoretical predictions and their experimental results. They gave different reasons for the differences as discussed in 5.2.3. They did both find, however, that using elastohydrodynamic theory to calculate the surface separation ratio, they could demonstrate the effects of micro-elastohydrodynamic lubrication in compliant layered bearings.

The experimental measurements of friction obtained here have again shown only limited agreement with the lubrication theories. On the simulator, the agreement was as seen by Auger et al [1993] and Burgess [1996]: theoretical friction was lower than experimental but experimental results gave a transition to fluid film for λ values much less than 3.

On the pin-on-plate apparatus, there was less agreement. The theoretical predictions were much lower than their experimental counterparts. In addition, in most cases, the onset of fluid film lubrication was not seen until λ was much greater than 3. It appeared that the elastohydrodynamic and micro-elastohydrodynamic effects were less effective the pin-on-plate apparatus than the simulator, and less effective on the pin-on-plate apparatus than theory would predict.

The lack of agreement between theoretical and experimental results on the simulator was attributed to several factors: the lubrication regime in operation, squeeze film effects, and stroke ratio effects (and hysteresis).

The compliant layered bearings in the simulator had operated with full fluid film lubrication for most viscosities. In the pin-on-plate apparatus, the compliant layered bearings demonstrated mixed lubrication for many viscosities. The elastohydrodynamic and micro-elastohydrodynamic lubrication theories were therefore less applicable to the pin-on-plate apparatus than to the simulator for many experimental conditions.

The larger applied loads on the simulator gave rise to greater squeeze film effects. The fluid films were generated by the entraining actions of the bearings, which were often comparable for the two machines. The smaller elastic deformation of the surfaces under lower loads would give smaller load bearing areas and so the fluid films would be more quickly depleted. This would explain why the theoretical predictions of friction were often the same for the two machines even when the experimental measurements of friction differed. The lubrication theories used here calculated only the fluid films generated by entraining action.

The stroke ratios also differed between the two machines. The pin-on-plate apparatus had a lower stroke ratio and so was expected to demonstrate larger deviations between experimental results and theory. In addition, the hysteresis effects (mentioned earlier) would not be allowed for in the theoretical prediction of friction.

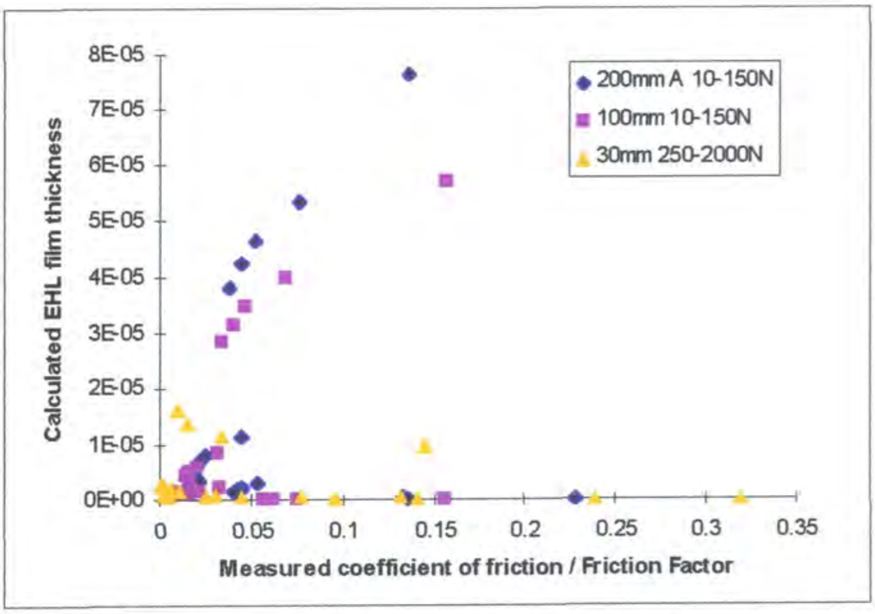

Figure 8.6 **Predicted elastohydrodynamic film thickness vs. measured coefficient of friction**

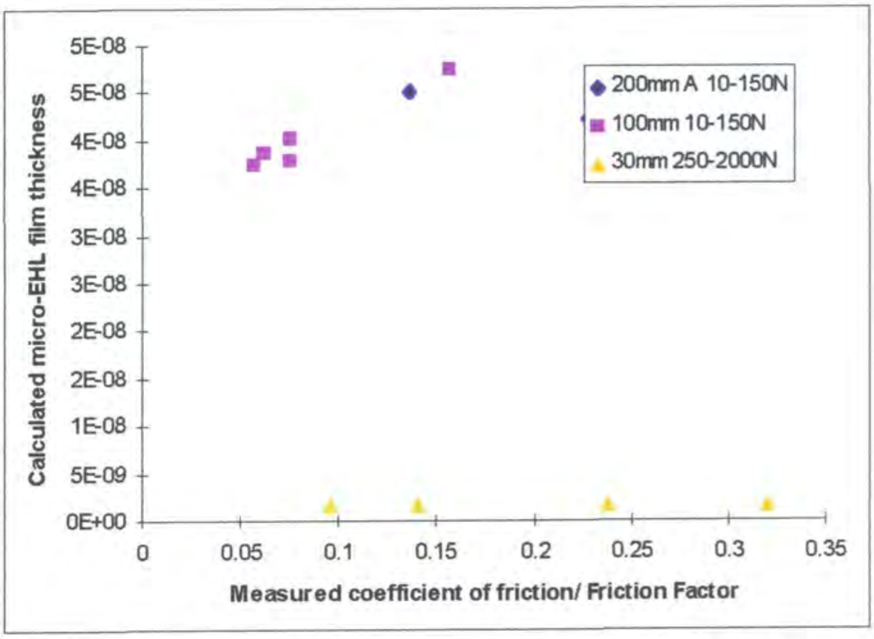

Figure 8.7 **Predicted micro-elastohydrodynamic film thickness vs. measured coefficient of friction**

Figures 8.6, and 8.7 show the predicted elastohydrodynamic film thickness and predicted micro-elastohydrodynamic film thickness plotted against the measured coefficients of friction and friction factors obtained experimentally for the various bearings. The elastohydrodynamic film thickness was calculated for all lubricant viscosities whilst the micro-elastohydrodynamic film thickness was calculated for viscosities of 0.096 Pa s and below. The graphs showed some agreement between the measured friction and predicted film thickness. For the EHL film thickness, the measured friction fell into two bands, one representing the results under fluid film and the other the results under mixed lubrication. The micro-EHL film thickness showed an increase in friction with decreasing film thickness as expected. The correlation was limited however, as seen by Burgess [1996].

Although, the values predicted by theory and the values found experimentally differed, the experimental friction measurements did follow the trends predicted by theory. Lubrication theories did therefore have a use in predicting the frictional performance of compliant layered bearings on the pin-on-plate apparatus.

8.2 Effect of design parameters

The various contact and lubrication theories predicted various design parameters would be important in terms of the frictional performance of a compliant layered joint. Having validated the pin-on-plate test method, it was then used to assess the effects of these parameters.

The effects of applied load, and entraining velocity have already been discussed. In addition, the effects of bearing conformity, the hard counterface roughness, the compliant layer roughness, and the elastic modulus of the soft counterface were also assessed.

8.2.1 Bearing conformity

For low bearing conformities (R of 0.1 m and 0.2 m), the most important effect was found to be the change in Hertzian contact area. By increasing the bearing conformity, the entraining action of the bearing and so the fluid film thickness was increased, but this was found to be a negligible effect compared to the increase in area of contact. The higher conformity bearing was found to give rise to higher coefficients of friction in both mixed and fluid film regimes. This showed agreement with the trend predicted by elastohydrodynamic theory.

A critical bearing conformity existed at which the increase in fluid film thickness in the mixed regime became more important than the change in Hertzian contact area. When this was reached, increasing the bearing conformity gave rise to a sufficient increase in the separation of the surfaces so as to reduce the measured coefficient of friction in the mixed regime (seen for joints with R of 0.9576 m). In the fluid film regime, the change in conformity had no discernible effect on the measured friction.

The bearing conformity was found to be important only in the mixed lubrication regime and only above a certain value.

8.2.2 Hard counterface roughness

The effect of the roughness of the hard counterface on the measured coefficient of friction was assessed for both point and line contacts. The results showed that an increase in the counterface roughness gave rise to higher coefficients of friction in the mixed regime but had no effect on the measured friction once fluid film lubrication was achieved. This was consistent with the steady-state results of Caravia *et al* [1993]. Results also showed that the use of an average value of RMS roughness in lubrication theory calculations did not give an accurate estimate of the roughness of the surface or its effect on lubrication in the mixed regime.

8.2.3 Compliant layer roughness

The roughness of the compliant layer was again assessed in both point and line contacts. In both cases, the roughness of the counterface showed a limited correlation with measured coefficient of friction in the mixed regime. The smoothest sample often gave rise to the lowest coefficient of friction. Once complete separation of surfaces had been achieved, the roughness had no significant effect on the friction generated. One further observation was that when the hard counterface was very smooth, a tribological advantage was gained at very low viscosities by using a slightly rougher compliant layer enabling better fluid entrapment in the bearing.

8.2.4 Comparison of compliant layered bearings and conventional materials

The effect of the elastic modulus of the soft counterface was assessed by comparing compliant layered joints to similar UHMWPE bearings. The compliant layered bearings showed a tribological advantage over the conventional joint materials under all test conditions, except the lowest lubricant viscosity (0.0008181 Pa s) and the highest lubricant viscosity (29.25 Pa s). At the lowest viscosity, separation of the bearing surfaces was negligible and so the compliant bearing demonstrated higher friction due to the larger area of contact and higher dry coefficient of friction. At lubricant viscosity values above the minimum (including values comparable with physiological lubricants), the lower elastic modulus of the compliant bearing allowed greater elastohydrodynamic and micro-elastohydrodynamic effects and so gave thicker fluid film thickness and lower coefficients of friction. The compliant layered joints also showed transition to fluid film at lower lubricant viscosities and lower minimum values of coefficient of friction. At the highest lubricant viscosity once complete separation of surfaces was achieved, the thicker fluid films in the compliant layer became unimportant, and the much larger area of contact actually gave rise to higher coefficients of friction (friction factors). These results were consistent with other published studies on compliant layered bearings.

8.3 Use of a new Sommerfeld Parameter

In order to directly compare the pin-on-plate apparatus and the simulator it was necessary to define a new Sommerfeld parameter as described in equation 4.12. The original Sommerfeld No. had used the unit length of the bearing as its length parameter and previous simulator tests had used the femoral head radius. Conducting a dimensional analysis of the expression for the friction generated revealed that the equivalent radius of the joint, the fluid film thickness, or the contact half-width would all have been equally appropriate choices for the length parameter. In order to keep the simple form of the original Sommerfeld parameter as discussed in Chapter 4, the equivalent radius of the joint was chosen for the tests reported here.

To verify that the definition of Sommerfeld parameter using the equivalent radius was appropriate it is worthwhile to briefly consider how the results obtained would appear if plotted against other 'Sommerfeld parameters'.

Figure 8.8 shows the results for an 0.1m equivalent radius bearing from the pin-on-plate apparatus and simulator when plotted against $\eta ua/L$. Figure 8.9 shows the same results plotted against $\eta uh_{cen}/L$. The original results plotted against the pin-on-plate Sommerfeld No., Z ($\eta uR/L$), were given in Figure 5.11.

Close examination of the three figures shows very little difference between them. The two alternative parameters seem to show negligible benefit over the Sommerfeld parameter chosen and have the added disadvantage of using a length parameter which is dependent on factors other than simply the bearing's geometry. The chosen new definition of Sommerfeld No. would therefore seem to be justified.

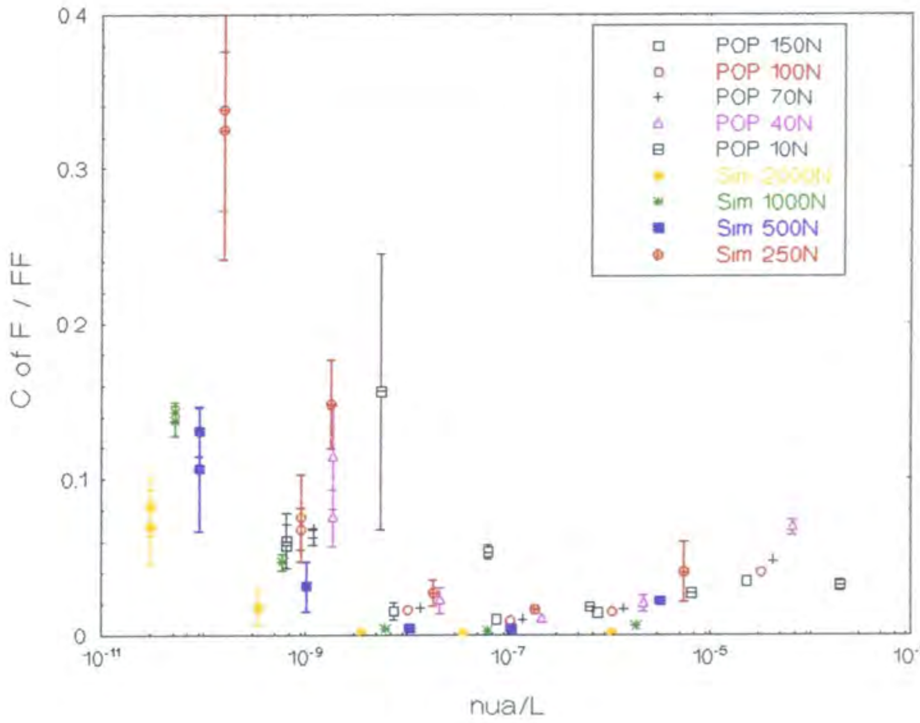

Figure 8.8 Results for pin-on-plate machine and simulator plotted against ηua/L

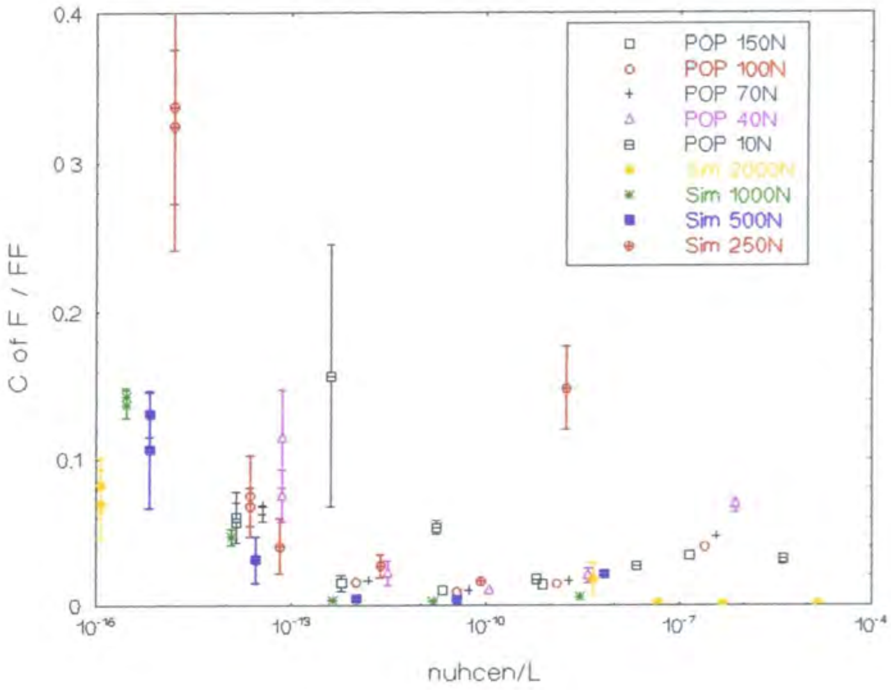

Figure 8.9 Results for pin-on-plate machine and simulator plotted against $\eta uh_{cen}/L$

9. Investigation of the Mechanical Properties of Polyurethane

9.0 Introduction

The mechanical properties of the polyurethane were vital to its function in a compliant layered bearing. Authors in the compliant bearing field had often considered the mechanical properties of the materials in their studies and the properties of the commercially available polymers are well documented [Unsworth *et al* 1987, 1988, Blamey *et al* 1993, Burgess 1996]. Commercially used polymers, a compliant layer of Corethane 80A on a hard Corethane 75D substrate, were used in these experiments and their mechanical properties were investigated in depth by Burgess [1996].

Three sets of tests were undertaken during this research to assess the mechanical properties of the Corethane 80A-Corethane 75D compliant layered material. These tests were:

- Hardness testing using a ball indentation method
- Hysteresis measurement of actual specimens and counterfaces
- Creep measurement of compliant layered cups.

9.1 Hardness testing

In order to give a fair comparison of friction results, it was felt important that the compliant layered samples used in the course of this research showed comparable mechanical properties to previously reported values. The hardness and elastic modulus are the most commonly reported properties and so experiments were undertaken to measure these for the samples used here.

A Fischer hardness testing programme was used, with a Vickers indentor and depth of indentation was measured in ten 1 second increments until an applied load of 5 MN was reached. The depth of indentation continued to be measured as the sample was unloaded to allow for any hysteresis. The method was used to assess the positional variation of hardness across the layer and the effect of conditioning solutions on the hardness of the polyurethanes.

9.1.1 Positional repeatability

Measurement of the positional variation of hardness was undertaken for 3 samples, a newly manufactured single layer sample of Corethane 80A (CH192), an aged bonded layer sample of 80A-75D (C30A), and a conditioned and aged bonded layer sample of 80A-75D (D3). The ISE corrected hardness values measured are given in the following diagrams and tables.

	1	2	3	4	5	6	7	8	9
A	x2.1								x2.25
B			x1.71				x2.32		
C					x2.41	x3.03			

Figure 9.1 Positional reproducibility of hardness across a new unbonded sample

Position	ISE Corrected Hardness (N/mm^2)
A1	2.1 ± 0.0041
B3	1.71 ± 0.073
C5	2.41 ± 0.06
C6	3.03 ± 0.051
B7	2.32 ± 0.03
A9	2.25 ± 0.107
average	**2.30 ± 0.43**

Table 9.1 Positional reproducibility of hardness of a new unbonded sample

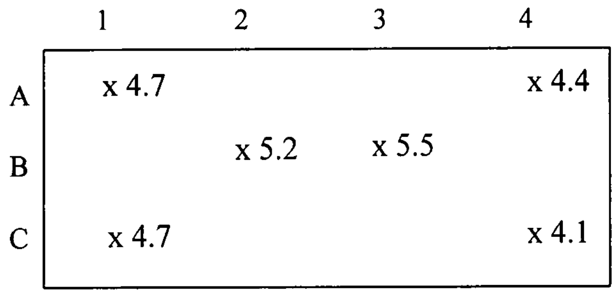

Figure 9.2 Positional reproducibility of hardness of an aged bonded sample

Position	ISE Corrected Hardness (N/mm^2)
A1	4.7 ± 0.0041
C1	4.7 ± 0.073
C4	4.1 ± 0.06
A4	4.4 ± 0.051
B2	5.2 ± 0.03
B3	5.5 ± 0.107
average	**4.77 ± 0.51**

Table 9.2 Positional reproducibility of hardness of an aged bonded sample

Position	ISE Corrected Hardness (N/mm^2)
A1	2.39 ± 0.16
B3	2.48 ± 0.63
Average	**2.44 ± 0.06**

Table 9.3 Hardness of a conditioned and aged bonded sample

The above results suggest the following observations.

Although there was much variation in the values of hardness measured within the newly manufactured Corethane 80A sample, there appeared to be no direct correlation with the position at which the measurement was taken. In contrast, the aged double layer sample was clearly harder in the centre of the sample than at the edges, presumably due to the strength of the interface between the two layers.

The bonded Corethane 80A-75D sample was considerably harder than the un-bonded 80A sample in an unconditioned state: 4.77 ± 0.51 N/mm^2 compared 2.30 ± 0.43 N/mm^2. The conditioned bonded sample was considerably less hard than the unconditioned sample, reaching a value of ISE corrected hardness comparable with a single layer sample, 2.44 ± 0.06. These values demonstrated a reasonable comparison with those reported by Burgess [1996] for a similar experiment. He achieved slightly higher values for the Corethane 80A layer but attributed this to the fact that the measurement technique of Waters [1965] recommended a layer thickness of 4 mm while in his experiments only 2.3 mm layers were used. All layers in this research have been 3 mm thick which would explain the slightly lower hardness values obtained.

Using the method described by Waters [1965] the measured indentation depth could be used to estimate the elastic modulus of the material. This gave an estimated modulus for the unconditioned bonded sample of approx. 14.9 MPa, slightly lower than typically reported.

9.1.2 Effect of conditioning treatments

Burgess [1996] showed polyurethane compliant layered bearings to demonstrate much improved frictional performance if they were conditioned in an aqueous solution prior to testing. It was thought that this was due to both surface absorption of some water, and the softening of the material. Comparison above of the limited hardness measurements made for a conditioned and an unconditioned bonded Corethane 80A-75D sample showed some evidence of this reduction in hardness.

To assess the mechanical effects of conditioning polyurethane layers further, sixteen pairs of samples were measured daily as they underwent various conditioning treatments

Three sets of four newly manufactured samples underwent the following conditioning treatments:

Set A (pairs 1-4) in air
Set B (pairs 5-8) in deionised water
Set C (9-12) in a phosphate-buffered solution

Each sample was measured 3 times on each occasion at the centre of the sample , and at 0.5 mm either side of the centre. Each sample was cut in the same way from the as-manufactured Corethane 80A piece (see Figure 9.3), all four in one set from a particular moulded piece.

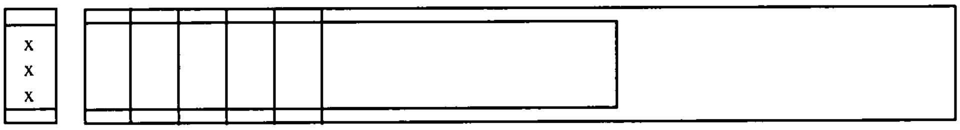

Figure 9.3 Preparation of samples for conditioning

The average values of hardness of the samples before and after 72 hours of conditioning are detailed in Table 9.4.

Set	Conditioning treatment	Average initial hardness N/mm^2	Average final hardness (after 72 hours) N/mm^2
A	air	2.298 ± 0.109	2.615 ± 0.209
B	deionised water	2.79 ± 0.449	2.66 ± 0.361
C	phosphate buffered	2.903 ± 0.137	2.783 ± 0.292

Table 9.4 Effect of conditioning on hardness of polyurethanes

72 hours ageing in air appeared to increase the polyurethane layer hardness from an average values of 2.298 to 2.615 N/mm^2. Soaking in aqueous solutions seemed to decrease the hardness of the Corethane 80A over the same period, 2.847 to 2.722

N/mm^2. This result agreed with the result seen above for the bonded layer and suggested an elastic modulus for the un-bonded layer of slightly less than 7 MPa.

The hardness and the elastic modulus values recorded here compare reasonably well with other published values and showed that for a compliant layer bonded to a rigid substrate the maximum hardness would be in the middle of the sample where the adhesion would be most effective.

9.2 Hysteresis measurement

Measurement of friction on the pin-on-plate apparatus and hip function friction simulator had highlighted differences in the articulation of the bearing surfaces. On the simulator, the area of contact, and hence area of deformation, remained reasonably constant throughout oscillation. On the pin-on-plate apparatus, the stroke ratio was much smaller and the deformed area under the loaded pin moved along the compliant layered plate during the stroke. Figure 9.4 shows a diagrammatic representation of this process.

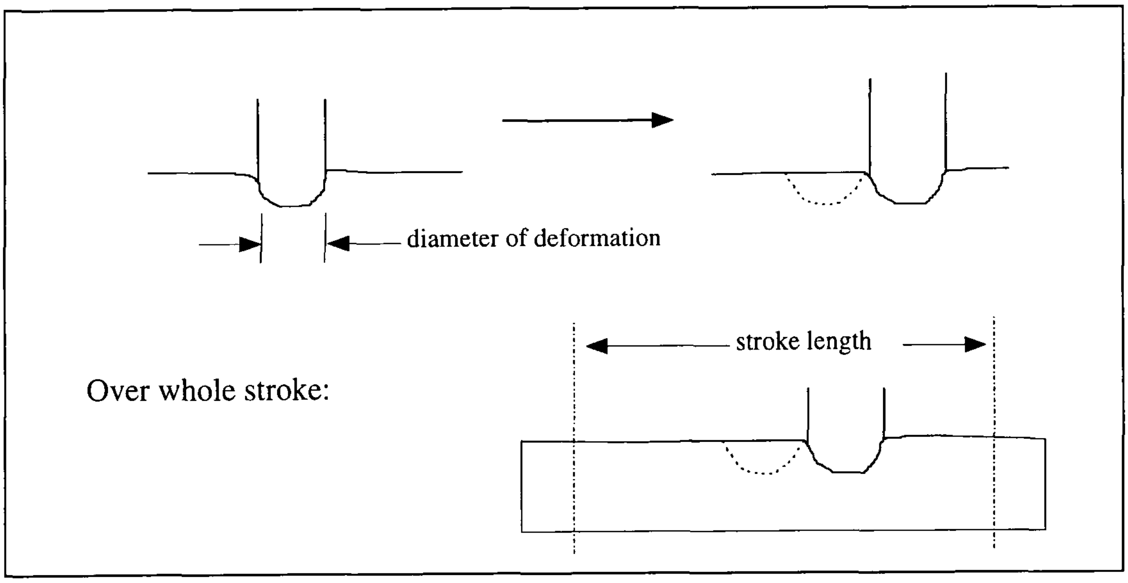

Figure 9.4 Deformation of plate during testing

In the course of one stroke on the pin-on-plate apparatus, the plate would be deformed and then recovered along the whole length of the stroke as the area under the pin was deformed and then recovered as the pin moved along. This meant that the pin on plate friction measurements also included a force representative of the energy lost in the hysteresis of the compliant layered sample over its stroke length. The hysteresis effect on the simulator was much smaller as the stroke ratio was much larger and the area under deformation did not change much throughout the loading cycle.

A Lloyds R6000 Universal Testing machine was used to measured the energy dissipated through hysteresis of the material when the test pins were applied to the test plates under the various loads used in friction measurements. The deflection of the compliant layered plate was measured as the pin was loaded and then unloaded to give two curves (deformation and recovery). The area between the two deflection-load curves represented the energy dissipated through hysteresis for one contact area. Figure 9.5 shows a typical result.

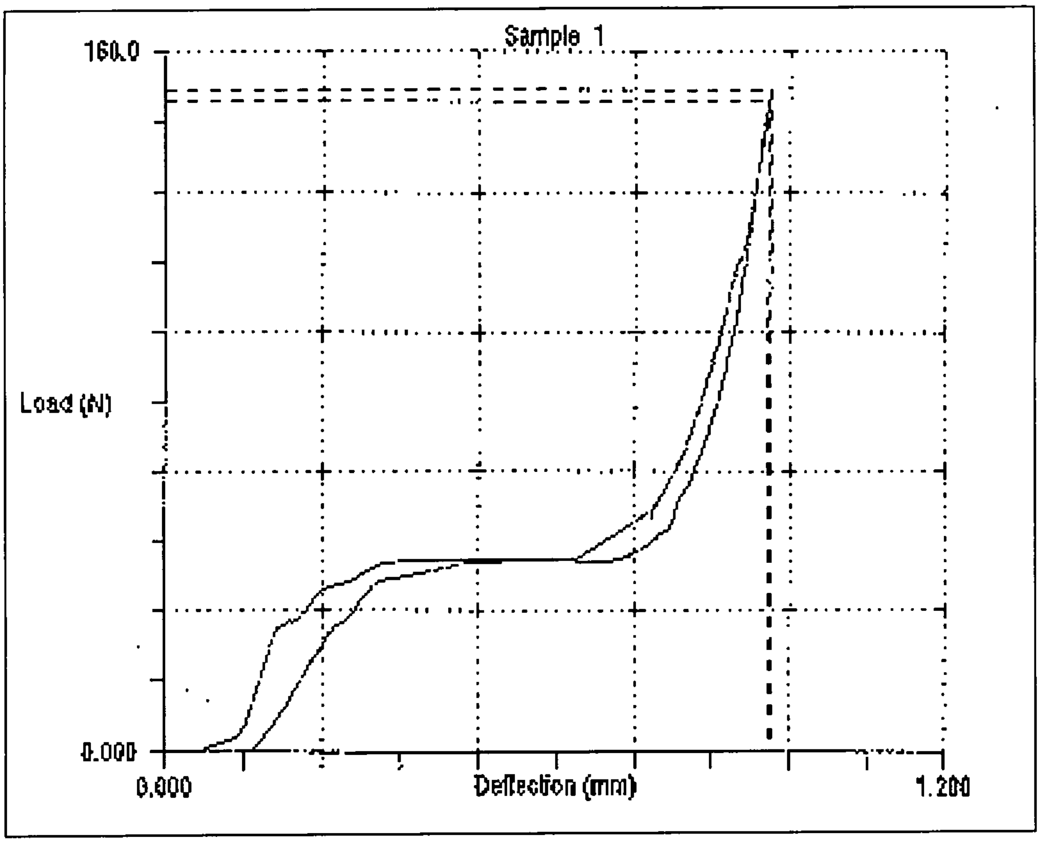

Figure 9.5 A typical hysteresis measurement

In the pin on plate friction measurements, the load was applied for half the total cycle, that is across the whole stroke length. The energy dissipated through hysteresis of the compliant layer during one stroke would then be given by:

Energy dissipated through hysteresis in one stroke = energy dissipated for one contact area x no. of contact areas

Eqn. 9.1

$$\text{where the no. of contact areas} = \frac{\text{stroke length} + 1\ \text{diameter of contact}}{\text{diameter of contact}} \qquad \text{Eqn. 9.2}$$

This assumed that the energy used to move an area of deformation through the plate was similar to the energy required to deform the whole plate area by area.

The frictional force generated by hysteresis was then given by:

$$\begin{aligned}\text{Frictional force} &= \frac{\text{Energy dissipated in 1 stroke}}{\text{stroke length} + 1\ \text{diameter of contact}}\\ &= \frac{\text{Energy dissipated in 1 contact area}}{\text{diameter of contact}}\\ &= \frac{\text{Measured area between curves}}{\text{diameter of contact}} \qquad \text{Eqn. 9.4}\end{aligned}$$

The effective hysteresis contribution to the measured coefficient of friction could then be calculated by dividing the frictional force by the applied load.

Table 9.5 gives the average values of energy, force and effective coefficient of friction for conditioned and unconditioned compliant layered samples as well as UHMWPE under a range of loads using the 200mm A pin as the indentor in all cases. Each measurement was taken a minimum of 5 times and an average value calculated.

Sample	Applied load	Energy (Nmm)	Frictional Force (N)	Coefficient of Friction
Conditioned PU	40 N	1.536	0.162	0.00406
	70 N	3.305	0.311	0.00444
	100 N	3.934	0.343	0.00343
	150 N	6.032	0.483	0.00322
Unconditioned PU	150 N	4.667	0.473	0.00249
UHMWPE	150 N	5.518	1.441	0.00961

Table 9.5 Hysteresis measurements

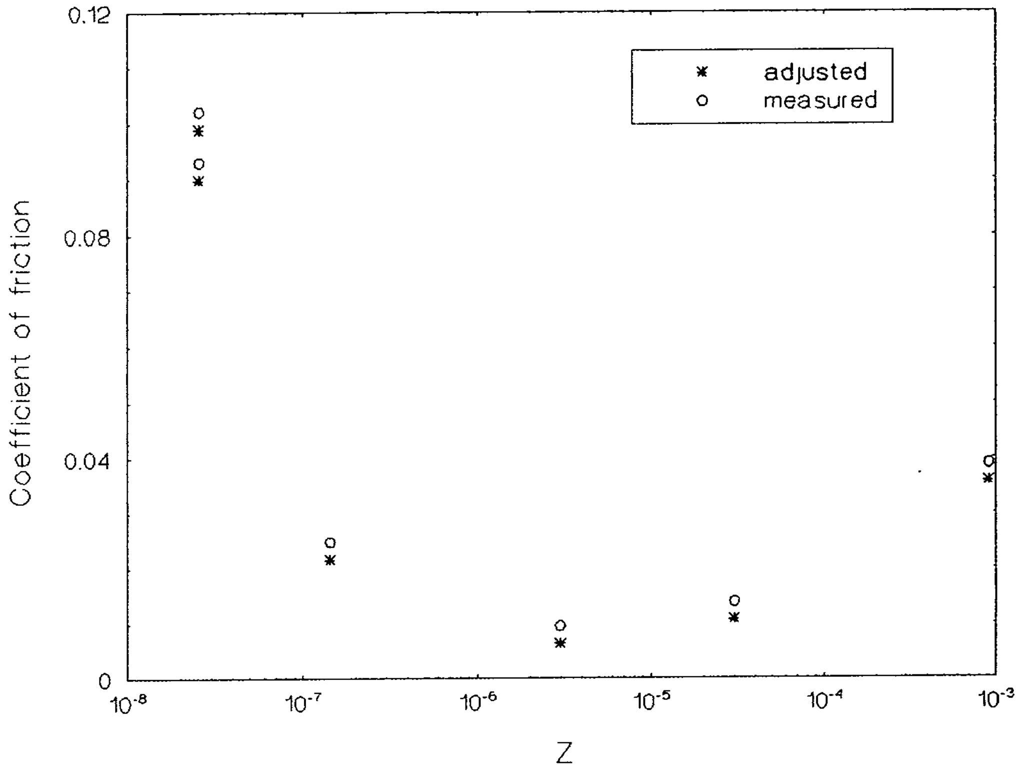

Figure 9.6 Effect of hysteresis on measured friction results for compliant layers (CC21A 200mm B 150N)

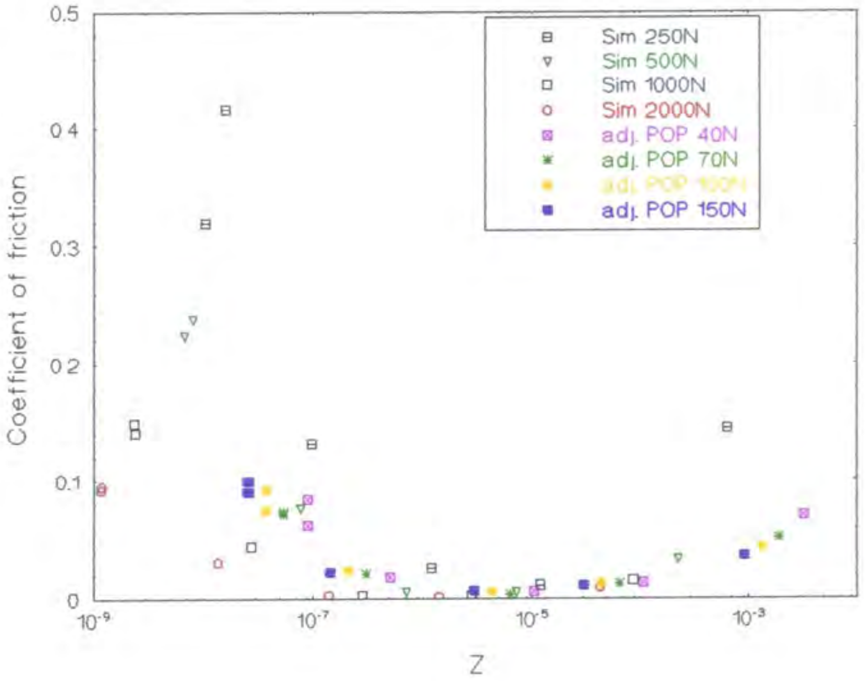

Figure 9.7 Comparison of pin on plate and simulator measured friction results after adjustment for hysteresis of compliant layer

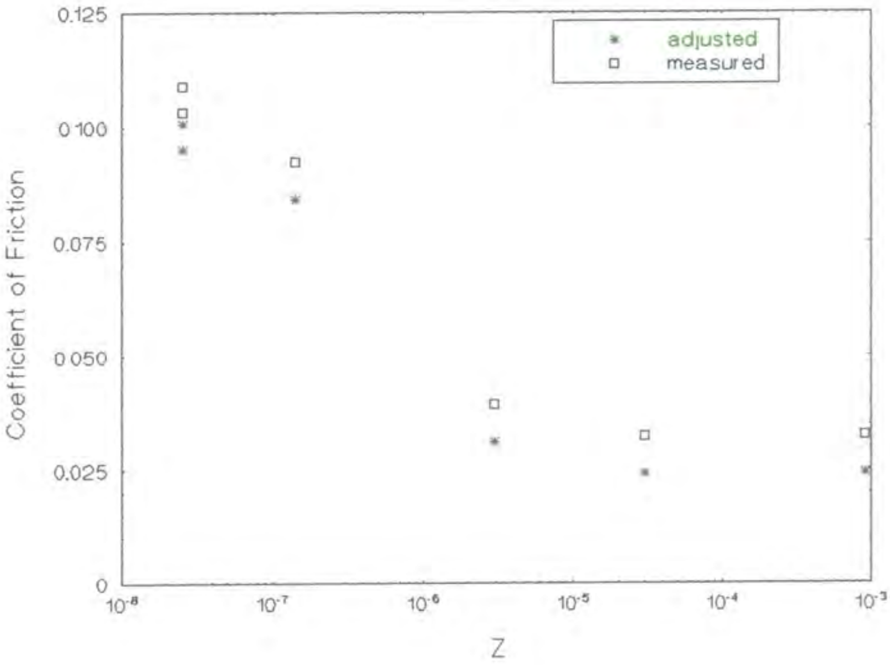

Figure 9.8 Effect of hysteresis on measured friction results for UHMWPE (PE4 200mm B 150N)

Figure 9.6 shows the difference the hysteresis of the compliant layer made to the measured friction. The measured values of coefficient of friction are as reported previously whilst the adjusted values represent the same values minus the effect of hysteresis as given in Table 9.5. Figure 9.7 shows a comparison of the adjusted pin-on-plate values for the 200mm B pin and the measured simulator values for the 30 mm femoral head. These results were shown in their unadjusted form in Figure 5.14 of Chapter 5. Figure 9.8 shows the measured and adjusted friction results for the UHMWPE tests.

The hysteresis of the compliant layer typically gave rise to an increase in coefficient of friction of the order of 0.003. Whilst this was consistent and did bring the pin on plate friction measurements closer to the very low values of friction factor typically recorded on the simulator, it was relatively small compared with the absolute values of coefficient of friction typically measured on the pin on plate apparatus. The unconditioned compliant layered sample showed less deformation and so less effect of hysteresis consistent with the increased hardness seen in Section 9.1.

The effective coefficient of friction due to the hysteresis of the UHMWPE plate was much larger, with an average value of 0.00961. This was because the area of contact of the indentor was smaller for the UHMWPE than for a compliant layered sample under the same load. The measured coefficients of friction for the UHMWPE were also much larger than for the polyurethane layers and so Figure 9.8 shows that the effect of the hysteresis was still small.

The difference in articulation of the bearing surfaces on the pin on plate apparatus and on the simulator, and the inherent differences in deformation of the soft counterfaces that this entailed, was shown to be a factor in the difference between the friction measured on the two machines. The effect of greater material hysteresis incorporated in the pin on plate friction measurements was found to be small however and so was not thought to be one of the more important factors in achieving comparable results on the two apparatus.

9.3 Creep measurement

Experiments in Chapter 5 had shown the conformity of a bearing to have various effects on its measured friction. At low conformities, increasing the conformity increased the area of contact and so increased the measured coefficient of friction, but at a certain critical conformity, the increased entrainment of fluid in the mixed regime became more important than the increased contact area and the measured friction decreased for low lubricant viscosities . Burgess [1996] had shown that at joint conformities above this value (R of 0.9576) the conformity of the joint was relatively unimportant.

One possible important consideration in examining the effect of bearing viscosity on measured friction, was the creep behaviour of the compliant bearing. This was commonly thought to be one of the more significant disadvantages of using a compliant material for a load bearing application such as in the hip or knee joint.

An experiment was devised to measure both the elastic and plastic deformation of a compliant layered cup and the effect this creep behaviour had on the friction generated when it was tested in the simulator against a standard femoral head. Nine compliant layered cups were obtained, three moulded from each of three different cores known as C1, C2, and C3. The diameters of the three cores were 32.346 mm, 32.696 mm and 32.424 mm respectively. The cups were BB77, BB78, and BB79 (C1), BB98, BB99, and BB100 (C2), and BB74, BB75, and BB76 (C3). Two femoral heads were used in the tests: the standard 32 mm Exeter head as was previously used in friction tests, and an identical head with a different mounting used as an indentor in creeping the samples. All simulator friction tests were undertaken using a range of CMC fluids as lubricants and an applied loading cycle of 2000 N max. and 100 N min. The load applied during creep was also 2000 N.

The changes in cup dimensions were assessed using a replica method which was shown by Burgess [1996] to have a systematic error of approx. 0.2%. A fast-setting dentists replica making material (Provil, Bayer, UK) was used. It was dimensionally stable and cured in less than 60 seconds. A replica was made of each cup in its 'as manufactured' state (I). It was then soaked for 7 days in Ringer's solution at 37 °C and a further replica made (II). The cup was friction tested on the simulator (A). It was then placed under a 2000N constant applied load in distilled water at 37 °C in a Hounsfield tensile test machine and the deflection of the cup was measured over a 7 day period. After 7 days, the load was removed and the cup was immediately friction tested (B) to assess the effect of any dimensional changes on its tribological performance. When removed from the simulator, a further replica was made of the cup (III). After six months had passed, all nine cups were then friction tested once more (C) to assess whether any of the changes noted were temporary.

9.3.1 Friction results

Figures 9.9, 9.10, and 9.11 show the average friction results recorded for the three different sets of cups (C1, C2, C3) at the three different stages of measurement (A, B, C). Figure 9.12 shows the deformation of the nine samples over their seven days loading.

The first point to notice was that when tested initially, the differences in bearing conformity appeared to have no significant effect on their frictional performance. Set A results for all cups, C1, C2 and C3 (equivalent radius 2.116 m, 0.9576 m, and 1.792 m respectively) showed extremely low friction factors, μ less than 0.01 in all cases. This was consistent with the findings of Burgess [1996].

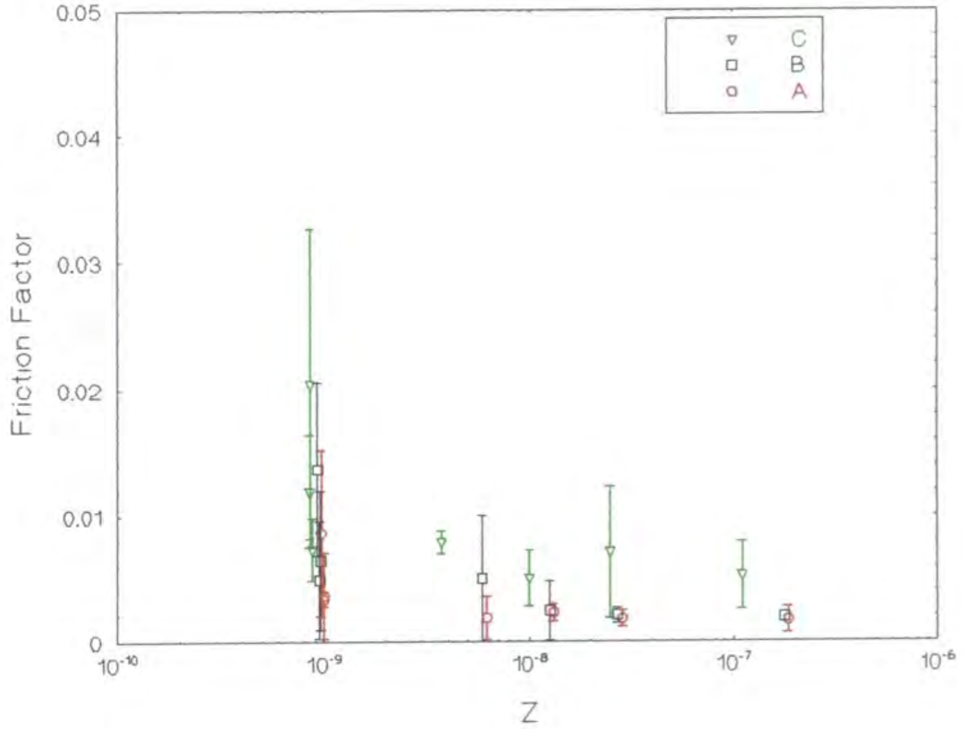

Figure 9.9 Average measured friction for C1 cups in creep tests

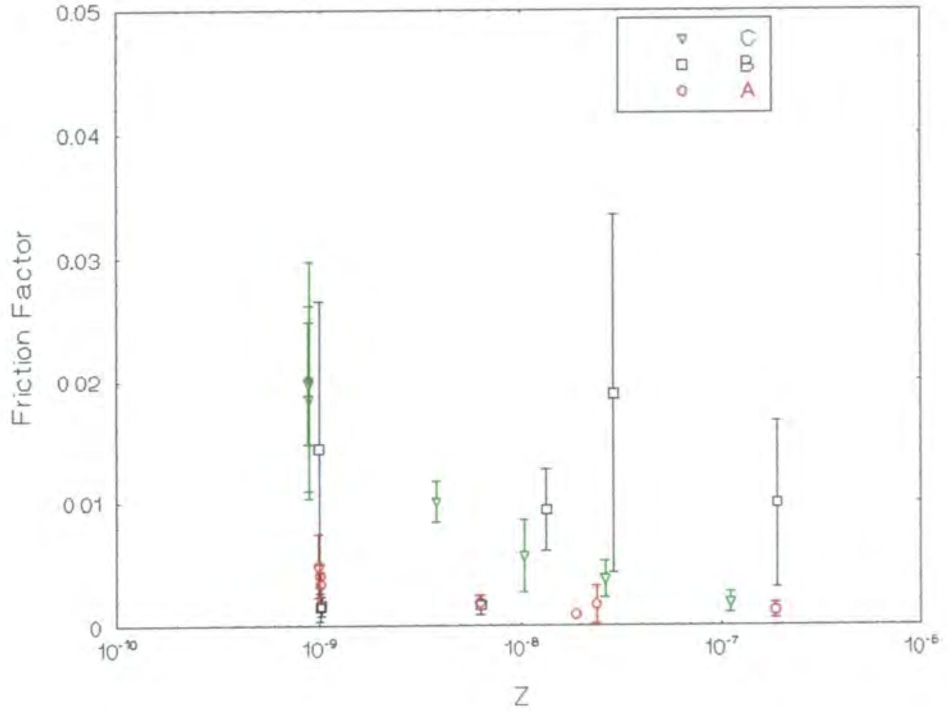

Figure 9.10 Average measured friction for C2 cups in creep tests

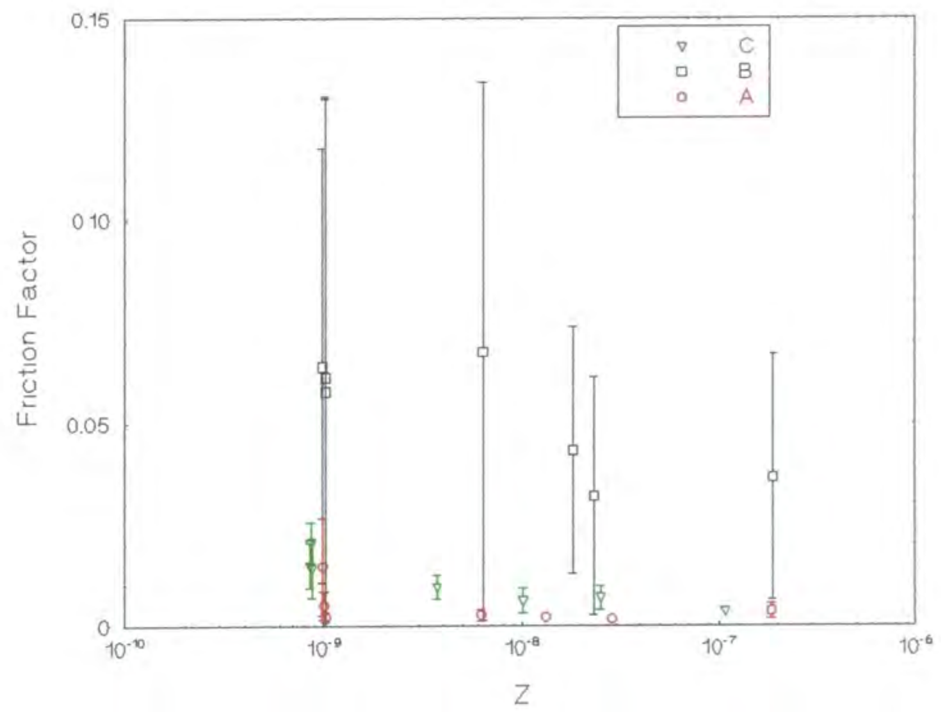

Figure 9.11 Average measured friction for C3 cups in creep tests

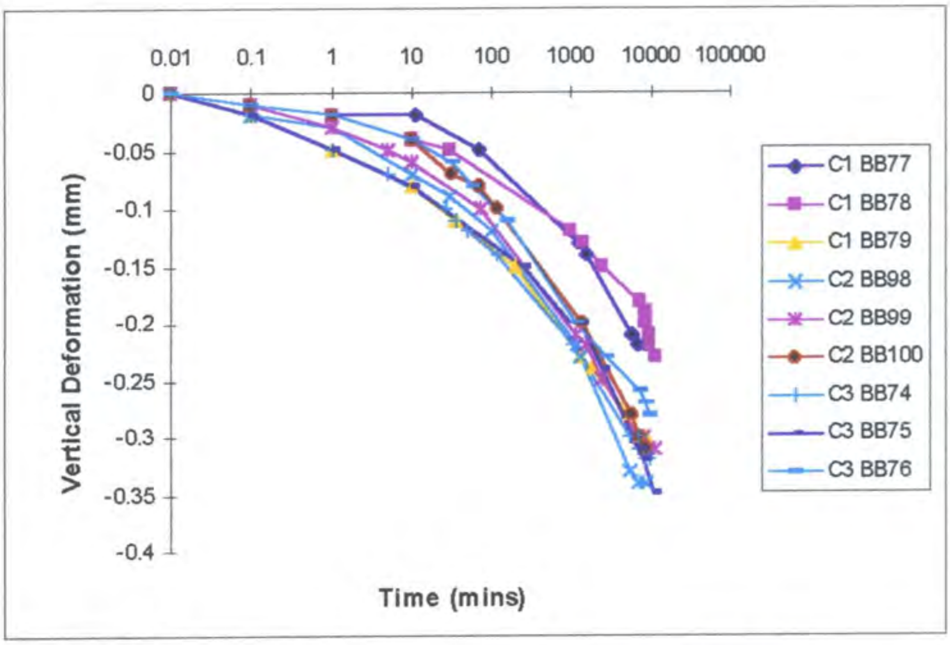

Figure 9.12 Deformation of creep cups over 7 days loading

After seven days loading, the three sets of cups showed different frictional performance (B). The C1 cups showed very little change in the measured friction after loading (Figure 9.9) . The C1 cups also underwent the smallest deformations (Figure 9.12). The C2 cups showed a slight increase in measured friction after the loading period, but μ was still around 0.02 or less (Figure 9.10). The C3 cups showed a significant increase in the measured friction immediately after loading (Figure 9.11). BB74 in particular showed friction factors around ten times the original measured values. After six months recovery, the measured friction factors for all three sets of cups (C) had returned to close to their initial values.

Following from these results, one of each set of cups was re-tested. It was re-soaked for a further seven days in Ringer's solution and then re-loaded at 2000 N for a further 7 days. Friction measurements in the simulator were taken after soaking (D) and after loading (E) as previously. Replicas were made of the cups after soaking (IV), after loading (V), and after loading and friction testing (VI).

Figures 9.13, 9.14, and 9.15 show the full set of friction results (A to E) recorded for the three cups BB78 (C1), BB100 (C2), and BB76 (C3) respectively. Figure 9.16 shows the measured deflection of the three cups during their second loading period (re-creep) compared to the first loading period (creep).

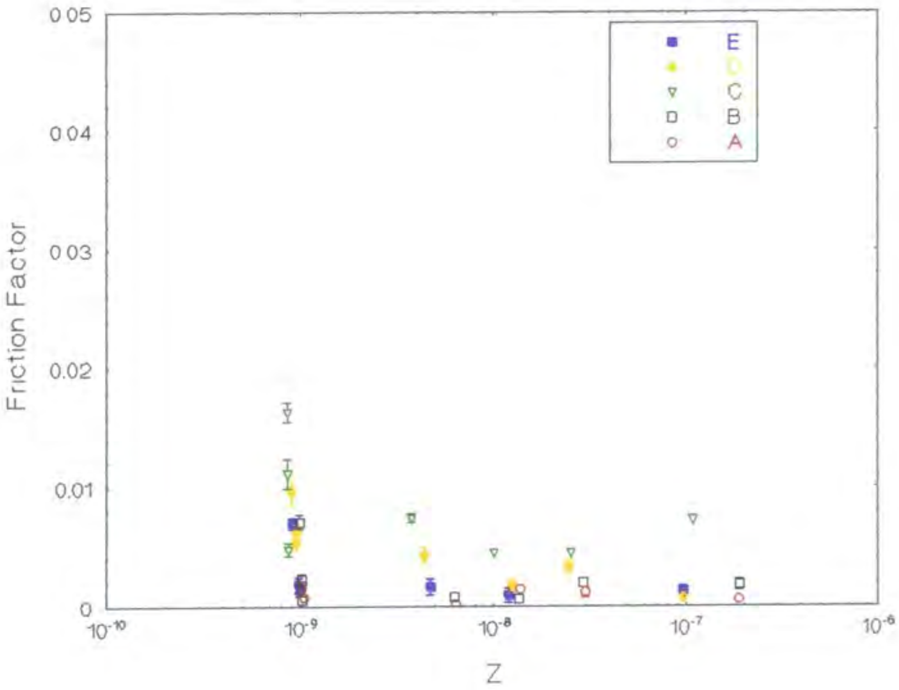

Figure 9.13 Friction results for creep and re-creep of cup BB78 (C1)

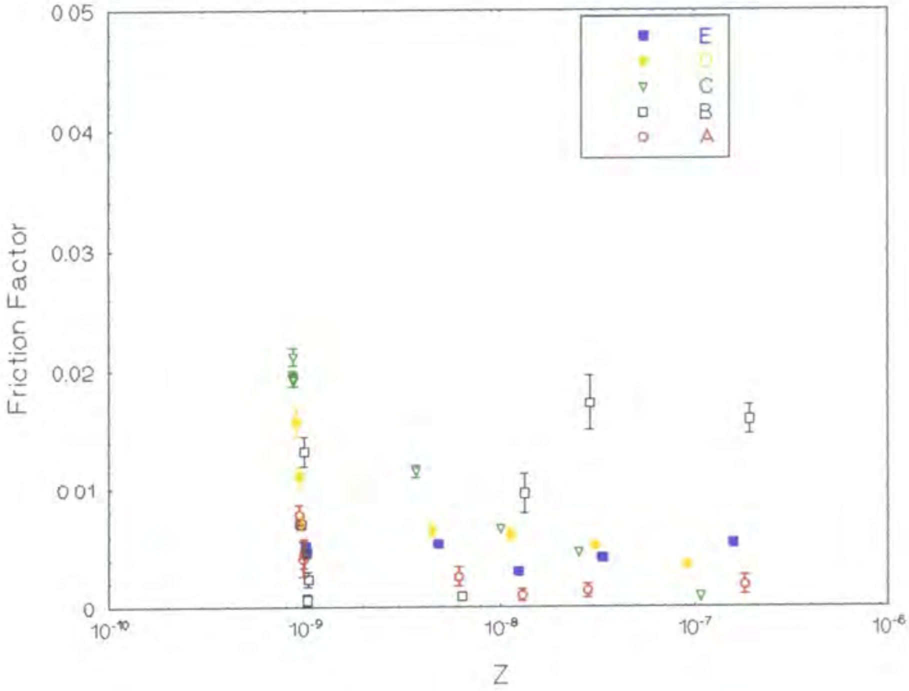

Figure 9.14 Friction results for creep and re-creep of cup BB100 (C2)

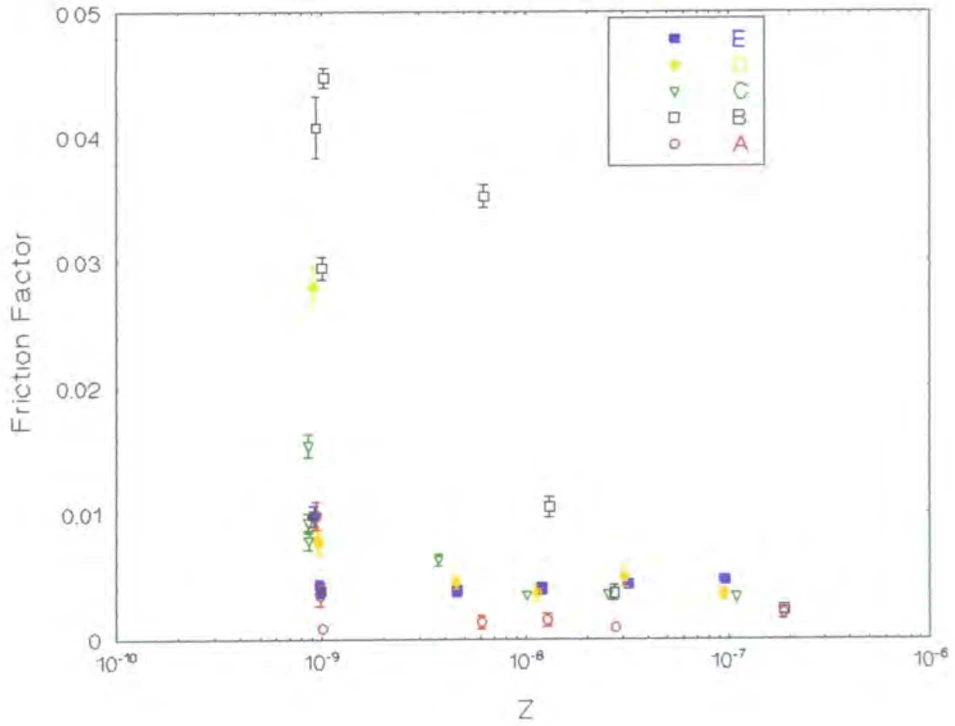

Figure 9.15 Friction results for creep and re-creep of cup BB76 (C3)

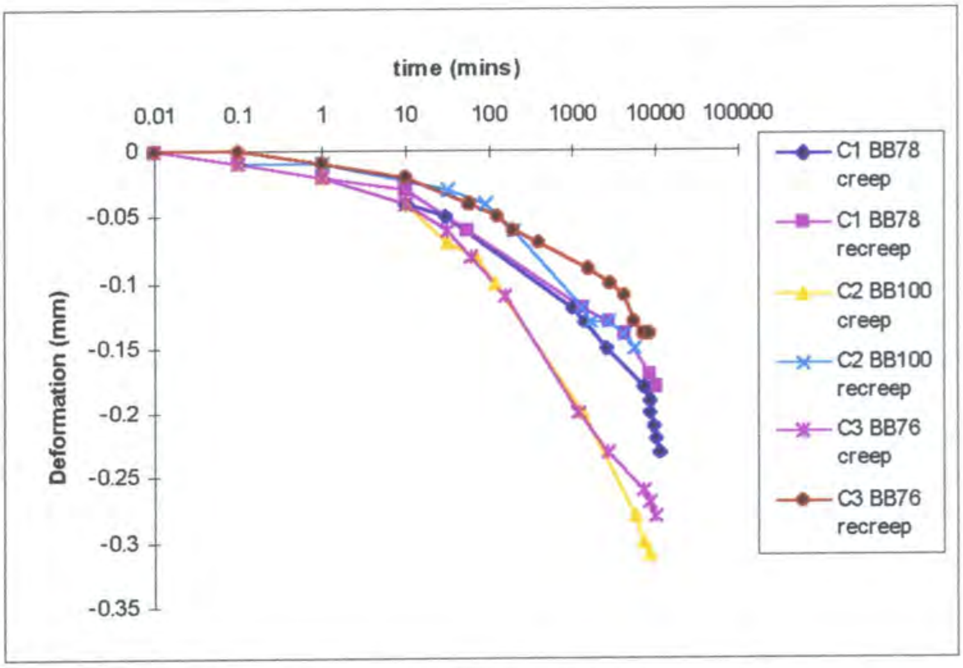

Figure 9.16 Deformation of cups BB78 , BB100, BB76 during creep and re-creep

The graphs show that when re-loaded none of the cups showed any significant change in their frictional performance. The measured friction factors following the re-creep period for all three cups was less than 0.01 as had been seen initially. All three cups also showed less deformation due to the 2000 N load the second time as shown in Figure 9.16.

9.3.2 Replica measurements

The replicas made were sent to be measured on a co-ordinate measuring machine (CMM) in Howmedica, Limerick. The diameter of each replica (ϕ) and the deviation from this diameter (Δ) are given in Table 9.6. To recap, symbols I to VI represent replicas taken at the following stages:

I	as manufactured
II	following 7 days soak
III	following 7 days loading at 2000N and subsequent friction testing
IV	following 7 days re-soak
V	following 7 days re-loading at 2000N
VI	following 7 days re-loading at 2000N and subsequent friction testing.

The replicas showed C1 and C3 cups to have very similar internal diameters initially while C2 cups were measured as having larger internal diameters. This was consistent with measurements made of the moulding cores and of cups retained in Limerick. Cup BB80 (C1) was used as a control and both the cup and a replica made in the usual way were measured. The measured diameters showed a 4.6% difference slightly larger than the 2% systematic error suggested by Burgess [1996].

All cups showed a decrease in internal diameter following soaking (shown by an decrease in replica diameter) as the polyurethane expanded. Following loading, the internal diameters of the cups decreased as the cups deformed to fit the femoral head. The max. deviation from the measured diameter also typically decreased. The C2 replicas showed the greatest decrease in diameter as they had the largest initial diameter.

	Size	Cup	I	II	III	IV	V	VI
ϕ	C1	BB77	31.95	31.932	31.796			
Δ			0.0338	0.0191	0.0289			
ϕ		BB78	32.053	31.988	31.901		32.051	31.881
Δ			0.0784	0.0556	0.0357		0.1489	0.1327
ϕ		BB79	32.005	32.006	31.877			
Δ			0.0589	0.0667	0.048			
ϕ	C1	BB80	replica	32.215	cup	32.352		
Δ	control			0.0365		0.0501		
ϕ	C2	BB98	32.178	32.138	31.898			
Δ			0.1597	0.1850	0.0389			
ϕ		BB99	32.258	32.111	31.907			
Δ			0.1313	0.1850	0.0611			
ϕ		BB100	32.218	32.226	32.034	32.165	32.051	32.149
Δ			0.0957	0.0687	0.0700	0.0721	0.1175	0.2277
ϕ	C3	BB74	31.927	32.004	31.806			
Δ			0.0613	0.1033	0.0403			
ϕ		BB75	31.876	31.971	31.793			
Δ			0.0447	0.0869	0.0338			
ϕ		BB76	32.082	32.014	31.803	31.990	31.874	31.956
Δ			0.0335	0.0102	0.0500	0.1106	0.1521	0.1107

Table 9.6 CMM measurement of replicas in creep and re-creep experiments

Following loading, the measured diameters of all replicas were much closer than initially (as they had all deformed to fit the same femoral head). The re-creep measurements showed similar results. The measured values after the second seven days soaking (IV) were again smaller than the initial I values and loading again decreased the internal diameters of the cups further to fit the femoral head. The deformation the second time (V) was however less than seen previously (III). After the second loading, replicas were made immediately after the load was removed (V) and after friction testing (VI) whilst the first time, replicas were made only after friction testing. Comparing the V and VI measured diameters showed that some of the deformation of the cups was recovered during the friction testing period.

9.3.3 Discussion

The CMM measurements suggested that C1 and C3 cups were dimensionally very similar and yet they showed significantly different frictional performance following loading (B). The CMM measurements of both groups of cups after loading (III) did however show the C3 cups to have the smallest internal diameters. During friction testing following the first loading period, the C3 cups were seen to 'grip' the head which was not seen for the C1 cups at all and to a much lesser extent for C2 cups. This would explain the significantly higher friction after loading demonstrated by the C3 cups.

The deformation caused by the loading was shown to be temporary as after six months recovery, the measured friction had returned to its initial low value. Re-loading of the cups produced significantly less deformation the second time and so the significant increases in friction seen previously were not repeated. Although the C3 cup again had the smallest internal diameter after loading (V), it was not as small as seen previously and so did not cause the cup to grip the head as before.

As a final stage in this experiment, all the cups were examined under a x10 magnification on a microscope. All the cups showed common imperfections due to the injection moulding procedure such as a central mark from the gating and concentric grooves. The C3 cups also showed an imperfection not seen on the other cups thought to be a form of surface tearing of the compliant layer due to the higher friction generated as the cup had gripped the head and prevented the entrainment of lubricant. An example of this tearing is shown in Figure 9.17.

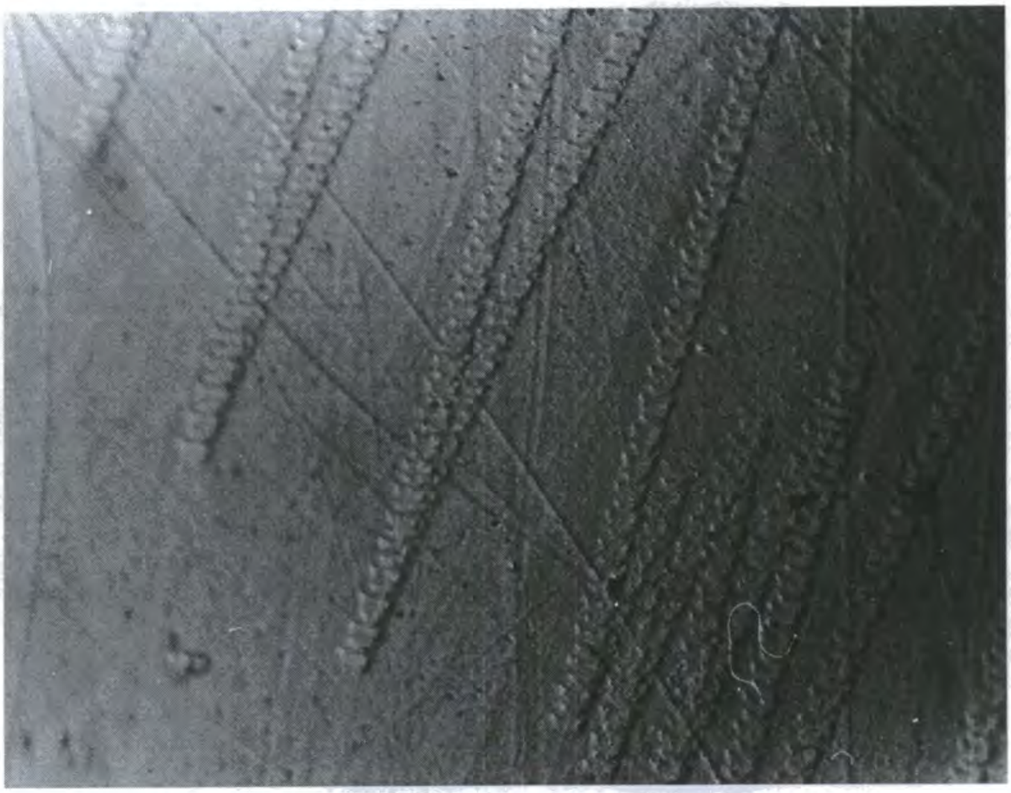

Figure 9.17 A microscope photograph of tears on the surface of a C3 cup

All cups were manufactured by the same method and using the same material. The only differences in the three sets of cups should therefore have been their internal diameter. The frictional performance and dimensional changes of the cups following loading would suggest otherwise. As the internal diameters of the C1 and C3 cups were very similar, the differences in the degree of deformation and so subsequent changes in friction seen must have been due to another factor outside of those investigated here.

This gives rise to two conclusions as to the design of compliant layered joints for implantation. Firstly, above a certain value, the conformity of the joint is not important so long as it does become too tight and prevent fluid entrainment. Secondly, all factors in the design and manufacture of compliant layered joints must be carefully monitored and controlled if they are to perform as they are designed.

In general, it would appear that if the case of 'gripping' of joints of too tight conformity is avoided, the creep of compliant layered joints would not limit the excellent frictional performance of these bearings.

10. Conclusions

10.0 Introduction

Conventional replacement joints, of UHMWPE and metal couplings, can give their recipient as much as 20 years of pain-free use. However, the success of such joints is becoming their downfall. As they are implanted in ever younger patients, a demand is growing for replacement joints which will last longer than 20 years. Currently, the majority of replacement joints fail because of excessive wear of the UHMWPE component which leads to osteolysis and subsequent removal of the prosthesis. To prevent such failures engineers and surgeons are turning to alternative materials to replace the UHMWPE component. One approach has been to investigate the use of a compliant layered bearings, as has been undertaken at Durham.

The development of compliant layered bearings at Durham had reached a fairly advanced stage. Materials for the compliant layer and for its rigid backing had been selected and a process for injection moulding such a bearing finalised [Smith *et al* 1996]. The design of the bearing had also been thoroughly examined [Burgess 1996, Burgess *et al* 1997]. Before such a bearing could go to clinical trials, however, it still needed extensive testing.

At the point of commencing this research, all tests on compliant layered bearings at Durham had been undertaken on a joint simulator which meant each modification to the compliant bearing required a new injection moulding. To optimise the bearing design and to test surface modifications, a simplified test method would therefore be extremely useful. Ideally the method should use a simple specimen geometry but incorporate a load, motion and bearing form such that the compliant layered bearing performs as it would *in vivo*.

The aims of this research were to develop a simplified test method, validate its results against a known method (the Durham hip function friction simulator), and use the new test to draw useful conclusions as to the tribological performance of compliant layered bearings.

10.1 Development of a simplified test method

A machine was developed to measure the friction generated in compliant layered bearings. It was based on a reciprocating pin-on-plate materials-screening apparatus. It was modified to include a dynamic loading cycle. The load was applied by means of pneumatic cylinder triggered mechanically by the motion of the carriage to produce a square load waveform. The maximum load which could be applied was 245N. Hydrostatic air bearings were designed and incorporated such that loads up to 272N could be supported on the central carriage whilst still allowing the carriage to float freely with negligible friction.

Stainless steel pins were designed and manufactured to have radii of curvature of 100 mm and 200 mm. These radii represented the equivalent radii of a 28 mm femoral head and a 30 mm femoral head in a 32 mm acetabular cup respectively. A flat plate with a 3 mm thick compliant polyurethane layer attached to a rigid polyurethane backing was used as the soft layer counterface. Plates of UHMWPE were also used for validation. These components produced bearing configurations with equivalent radii which could be replicated by standard hip prostheses on the hip function friction simulator. Whilst hip joints could be modelled as point contacts, knee joints might be modelled better by line contacts and so they were also considered. Simple cylinders were designed and manufactured for both machines and were tested in articulation with prototype non-conforming compliant layered knee bearings (Howmedica Int).

A new Sommerfeld parameter was defined to allow the results of different test methods to be compared directly. The new parameter, Z, was defined as the product of lubricant viscosity, entraining velocity and equivalent radius, divided by the applied load. It was used in all analyses of results to give Stribeck style curves.

10.2 Validation of the simplified test method

The new test method was validated by comparing its results with those of the hip function friction simulator, theoretical predictions of Hertzian contact and elastohydrodynamic and micro-elastohydrodynamic friction, and with the published results of other authors.

The systematic errors in friction measurement and the repeatability of the results obtained were assessed first. The errors in friction measurement of the pin-on-plate apparatus were found to be significantly lower than those of the simulator.

The repeatability of the pin-on-plate test method was evaluated in three ways. The steady-state measurement of the friction of UHMWPE against stainless steel with distilled water was measured. The steady-state friction of compliant layers against stainless steel with distilled water was then measured in the same way for three separate samples. Finally, the repeatability of the Stribeck analyses produced by the test method was assessed. The steady-state tests showed repeatability within 2% and comparable results to other published values. The Stribeck analyses showed the standard deviation of results of the simplified test method to be a third of those of the simulator results.

Silicone fluids and carboxymethyl cellulose were compared as lubricants. Over the full range of viscosities there was no significant difference in the results obtained for the two lubricants. Subsequently, silicone fluids were used as the lubricant in all testing as they offered a larger range of viscosities and so a greater range of the Sommerfeld parameter.

The equivalent radius of the bearings on each of the machines was made equal. This alone did not produce equivalent results on the two machines as the contact geometry deformed under loading. The applied load to each machine was adjusted until the Stribeck analyses of the two apparatus converged in the mixed regime.

Hertzian contact theory and elastohydrodynamic and micro-elastohydrodynamic theories were used to predict the contact half-width, maximum contact stress, stroke ratio, EHL minimum film thickness, EHL coefficient of friction, surface separation ratio, micro-EHL minimum film thickness, and micro-EHL coefficient of friction. Of all these parameters, it was found that the Hertzian contact half-width was most important in achieving equivalent results on the two machines. If the predicted Hertzian contact half-width was similar for the bearing on each of the apparatus, the measured coefficient of friction (or friction factor) would also be similar. A 150N load on the pin-on-plate apparatus was found to give a Stribeck curve equivalent to a 500N load on the joint simulator.

There was considerable deviation between the coefficients of friction measured experimentally and those predicted by EHL and micro-EHL theories. Theory consistently under-estimated the values of the coefficient of friction seen experimentally. This had been seen previously by other authors [Auger *et al* 1993, Burgess 1996]. Theoretical predictions were made for all lubricant viscosities although strictly EHL and micro-EHL theory only applied to the full fluid film regime which could explain the disagreement. The theoretical predictions did, however predict the trends and the effects of the design parameters seen experimentally.

10.3 Effect of design parameters

Once validated, the simplified test method was used to assess the effects of various parameters on the coefficient of friction measured for the compliant layered bearings.

The coefficient of friction in the mixed lubrication regime decreased as the applied load increased. Theory predicted that frictional force was proportional to the contact area which in turn was proportional to the applied load to a power of n. The coefficient of friction was therefore proportional to the load to the power of B where B had a value between 0 and -1/3 [Archard 1953]. Values of B calculated from the results of the pin-on-plate apparatus were within this range. In the fluid film regime, the Stribeck curves for all loads on both machines converged to one curve.

The conformity of the bearing had a mixed effect on the coefficient of friction measured. At very low conformities (as for equivalent radii of 100 mm and 200 mm) increasing the bearing conformity led to an increase in the measured coefficient of friction in the mixed regime. Once a critical conformity was reached, the increase in conformity caused a decrease in coefficient of friction. Beyond this critical value, the bearing conformity had a negligible effect on the coefficient of friction measured as the elastic deformation of the surface under load absorbed any changes. The only exception was if the bearing became conforming enough to allow 'gripping' of the femoral head which caused a significant increase in the measured coefficient of friction. In the same way, creep was not found to limit the bearing's performance, unless it caused 'gripping' to occur. Once full fluid film lubrication was achieved, the friction generated was independent of the bearing conformity.

An increase in the roughness of the hard counterface produced an increase in the coefficient of friction measured in the mixed regime. Once full fluid film lubrication was achieved, the roughness of the hard counterface was no longer important. The results also raised questions over the use of an average RMS roughness as an estimate of the effect of roughness on a bearing's tribological performance.

The compliant layer roughness was found to have a limited effect on the coefficient of friction measured. The smoothest sample often gave the lowest friction. There could be some benefit however in using a rougher compliant layer against a very smooth counterface at low lubricant viscosities, as it might allow greater entrapment of fluids.

Increasing the entraining velocity decreased the measured coefficient of friction. It also increased the value of Z, however, and so all measured results fitted the same Stribeck curve irrespective of the entraining velocity used.

Compliant layered bearings were shown to have significant benefits in terms of tribological performance over the conventional bearing materials of UHMWPE and stainless steel. The compliant layered bearings demonstrated a transition to fluid film lubrication at lower lubricant viscosities and lower measured coefficients of friction at all but the very lowest lubricant viscosity.

10.4 Recommendations for future work

This thesis hoped to illustrate just some of the benefits and possibilities for a simplified test method for compliant layered joints. Having brought the development of the apparatus to this stage, there are still various possibilities to develop the machine further and numerous opportunities to use it in other experiments to further the understanding of compliant layer and other bearings.

Whilst the analogue measurement system adopted has proved excellent in this research, the apparatus could be further developed to include servo-hydraulic load and motion control and digital logging of results. Although this would limit the accuracy of the measurement system, as seen for the simulator, it would increase the usability of the machine and allow much faster processing of results. It may therefore be an advantage if large-scale testing was planned.

The load range of the apparatus could be extended so that results equivalent to those under physiological loads could be achieved. It is estimated that this would require a load on the pin-on-plate apparatus of the order of 500N. This could be achieved with the present apparatus if a compressor with a higher pressure range was incorporated.

The geometry of the hard counterfaces could be developed further. During the course of this research, the radius of curvature of the pins has been limited by the manufacturing facilities available. This meant the maximum radius of curvature which could be realistically achieved was 200 mm. Ideally, a radius of curvature of approximately one metre would be used to approximate a typical joint replacement. Whilst this may not be achievable, investigation of larger equivalent radii would be useful.

Surface modification of the compliant layer is a possibility in compliant layer bearings, to improve the 'wettability' of the bearing and to limit start-up friction. The simple geometry of the test specimens would facilitate the production of many iterative modifications. Such modifications could include coatings or treatments. The effect of physiological lubricants and pre-treatments on the frictional performance of compliant layered bearings could also be investigated.

The apparatus could be used to measure the friction of other materials. Hydrogels are an option for a porous compliant bearing surface and their friction could be measured using this apparatus, coupled with wear tests to assess their long-term mechanical stability. The apparatus could also be used to aid the re-investigation of hard bearing surfaces such as metal-metal and ceramic-ceramic. It may also prove to be a useful addition to long-term wear studies of UHMWPE to assess the effect of changes in the bearing on the friction generated in the joint.

References

Archard J. F. (1953). Contact and rubbing of flat surfaces. *Journal Applied Physics*, Vol. 24, No. 8, pp. 981-988.

ASTM F732 - 82 (1989). Standard practice for reciprocating pin-on-flat evaluation of friction and wear properties of polymeric materials for use in total joint prostheses. (Annual Handbook of ASTM standards; American Society for Testing and Materials; Philadelphia; 212-217; 13.01)

Atkinson J. R. (1976). An investigation into the wear of ultra-high molecular weight polyethylene when a polyethylene wear pin is loaded against a reciprocating polyethylene counterface lubricated by bovine synovial fluid at ambient temperature (18oC). Investigation by Metallurgy Dept, Leeds University.

Atkinson J. R., Dowson D., Isaac G. H., Wroblewski B. M. (1985a). Laboratory wear tests and clinical observation of the penetration of femoral heads into acetabular cups in total replacement hip joints. II: A microscopic study of the surfaces of Charnley polyethylene acetabular sockets. *Wear*, Vol. 104, pp. 217-224.

Atkinson J. R., Dowson D., Isaac J. H., Wroblewski B. M. (1985b). Laboratory wear tests and clinical observations of the penetration of femoral heads into acetabular cups in total replacement hip joints. III: The measurement of internal volume changes in explanted charnley sockets after 2-16 years in vivo and the determination of wear factors. *Wear*, Vol. 104, pp. 225-244.

Auger D. D., Dowson D., Fisher J., Jin Z.-M. (1993). Friction and lubrication in cushion form bearings for artificial hip joints. *Proc. Instn. Mech. Engrs.*, Vol. 207H, pp. 25-33.

Auger D. D., Dowson D., Fisher J. (1995a). Cushion form bearings for total knee replacement. Part 1: Design, friction and lubrication. *Proc. Instn. Mech. Engrs.*, Vol. 209H, pp. 73-82.

Auger D. D., Dowson D., Fisher J. (1995b). Cushion form bearings for total knee replacement. Part 2: Wear and durability. *Proc. Instn. Mech. Engrs.*, Vol. 209H, pp. 83-91.

Barbour P. S. M., Barton D. C., Fisher J. (1995). The influence of contact stress on the wear of UHMWPE for total replacement hip prostheses. *Wear*, Vol. 181, pp. 250-257.

Barnett C. H., Cobbold A. F. (1962). Lubrication with living joints. *J. B. J. S.*, Vol. 44B, pp. 662.

Bartel D. L., Burstein A. H., Todam D., Edwards D. L. (1985). The effect of conformity and plastic thickness on the contact stresses in metal-backed plastic implants. *Journal of Biomechanical Engineering - Transactions of the Asme*, Vol. 107, pp. 193-199.

Bartel D. L., Bicknell V. L., Wright T. M. (1986). The effect of conformity, thickness and material on stresses in ultra-high molecular weight polyethylene components for total joint replacement. *J. Bone Joint Surg. [Am]*, Vol. 68A, pp. 1041-1051.

Barwell T. (1967). Friction and wear, detection and measurement. *Symposium lubrication and wear in living and artificial human joints. 7th April 1967. I Mech E. London*, Vol. Paper 11, pp. 1-9.

Ben Abdallah A., Treheux D. (1991). Friction and wear of ultrahigh molecular weight polyethylene against various new ceramics. *Wear*, Vol. 142, pp. 43-56.

Blamey J., Rajan S., Unsworth A., Dawber R. (1991). Soft layered prostheses for arthritic hip joints - a study of materials degradation. *Journal of Biomedical Engineering*, Vol. 13, pp. 180-184.

Blamey J. M., Mullin P. J., Seaton J., Unsworth A., Parry T. V. (1992). Bonding of soft layers to rigid backings. In: Dowson D. et al., Eds. *19th Leeds-Lyon Symposium.* Elsevier Science, Amsterdam, .

Blamey J. M. (1993a). Improved tribology and materials for a new generation of hip prostheses. *PhD Thesis.* University of Durham.

Blamey J. M. (1993b). Measurements of elastic modulus and hardness of biocompatible polyurethanes and the effects on contact area within the hip prosthesis. In: Dowson D. et al., Eds. *Thin Films in Tribology.* Elsevier Science, Amsterdam, 535-540.

Bonfield W. (1987). Materials for the replacement of osteoarthritic hip joints. *Metals and Materials. Prosthetics*, Vol. December, pp. 712-716.

Brandwood A., Noble K. R., Schindhelm K., Meijs G. F., Gunatillake P. A., Chatelier R. C., Mccarthy S. J., Rizzardo E. (1992). Influence of stress on novel biomedical polyurethanes. Clinical Engineering. Proc. 9th European Soc. Conf. Biomaterials.

Bray J. C., Merrill E. W. (1973). Poly(vinyl alcohol) hydrogels for synthetic articular cartilage material. *Journal of Biomedical Materials Research*, Vol. 7, pp. 431-443.

British Standard; BS 7251 (1990). Orthopaedic Joint Prostheses; Part 4. Specification for bearing surfaces of hip joint prostheses. (British Standards Institution, London).

British Standard; BS 7251 (1990). Orthopaedic Joint Prostheses; Part 8. Guide to laboratory evaluation of change of form of bearing surfaces of hip joint prostheses. (British Standards Institution, London).

Brown K. J., Atkinson J. R., Dowson D., Wright V. (1976). The wear of ultra high molecular weight polyethylene and a preliminary study of its relation to the in vivo behaviour of replacement hip joints. *Wear*, Vol. 40, pp. 255-264.

Bruck S. D., Mueller E. P. (1988). Radiation sterilization of polymeric implant materials. *J. Biomed. Mat. Res.*, Vol. 22, pp. 133-144.

Burgess I. C. (1996). Tribological and mechanical properties of compliant bearings for total joint replacements. *PhD Thesis*, University of Durham.

Burgess I. C., Cunningham J. L., Unsworth A. (1997). Polyurethane acetabular components incorporating a compliant surface layer, for new generation hip prostheses. Internal Document, University of Durham, publication suppressed.

Caravia L., Dowson D., Fisher J., Jobbins B. (1990). The influence of bone and cement debris on counterface roughness in sliding wear tests of ultra-high molecular weight polyethylene on stainless steel. *Proc. Instn. Mech. Engrs.*, Vol. 204H, pp. 65-70.

Caravia L., Dowson D., Fisher J. (1993a). Start up and steady-state friction of thin polyurethane layers. *Wear*, Vol. 160, pp. 191-197.

Caravia L., Dowson D., Fisher J., Corkhill P. H., Tighe B. J. (1993b). Friction and mixed lubrication in soft layer contacts. In: Dowson D. et al., Eds. *Thin Films in Tribology*. Elsevier Science, Amsterdam, .

Caravia L., Dowson D., Fisher J., Corkhill P. H., Tighe B. J. (1993c). A comparison of friction in hydrogel and polyurethane materials for cushion-form joints. *Journal of Materials Science: Materials in Medicine*, Vol. 4, pp. 515-520.

Caravia L., Dowson D., Fisher J., Corkhill P. H., Tighe B. J. (1995). Friction of hydrogel and polyurethane elastic layers when sliding against each other under a mixed lubrication regime. *Wear*, Vol. 181, pp. 236-240.

Charnley J. (1959). The lubrication of animal joints. *Proc. Instn. Mech. Engrs.*, Vol. Symposium on Biomechanics, London 1959, pp. 12-19.

Charnley J. (1960). How are our joints lubricated? *Nature*, Vol. 4 (5), pp. 175-179.

Charnley J. (1961). Arthroplasty of the hip. A new operation. *Lancet*, Vol. May, pp. 1129-1132.

Charnley J. (1966). An artificial bearing in the hip joint: implications in biological lubrication. *Fed. Proc*, Vol. 25, pp. 1079-1081.

Charnley J., Kamangar A., Longfield M. D. (1969). The optimum size of prosthetic heads in relation to the wear of plstic sockets in total replacement of the hip. *Med. and Biol. Engng.*, Vol. 7, pp. 31-39.

Charnley J., Cupiz Z. (1973). The nine and ten year results of the low-friction arthroplasty of the hip. *Clin. Orthop.*, Vol. 95, pp. 9-25.

Charnley J. (1979). Low Friction Arthroplasty of the Hip. Spinger-Verlag, New York.

Charnley J. (1995). The long-term results of low-friction arthroplasty of the hip performed as a primary intervention. *J. Bone Joint Surg. [Br]*, Vol. 54B, pp. 61-76.

Chittenden R. J., Dowson D., Taylor C. M. (1986a). Elastohydrodynamic film thickness in concentrated contacts. Part 1: Experimental investigation of lubricant entrainment aligned with the major axis of the contact ellipse. *Proc. Instn. Mech. Engrs.*, Vol. 200C, pp. 207-217.

Chittenden R. J., Dowson D., Taylor C. M. (1986b). Elastohydrodynamic film thickness in concentrated contacts. Part 2: Correlation of experimental results with elastohydrodynamic theory. *Proc. Instn. Mech. Engrs.*, Vol. 200C, pp. 219-226.

Cipera W. M., Medley J. B. (1996). A friction based study of cobalt-based alloys for metal-metal hip implants. In Proc. Fifth World Biomaterials Congress, May 29- June 2, 1996, Toronto, Canada, pg 781.

Clarke I. C. (1981a). Wear of artificial joint materials. I: Friction and wear studies: validity of wear-screening protocols. *Engineering in Medicine*, Vol. 10, No. 3, pp. 115-122.

Clarke I. C. (1981b). Wear of artificial joint materials. IV: Hip joint simulator studies. *Engineering in Medicine*, Vol. 10, No. 4, pp. 189-198.

Cooper J. R., Dowson D., Wright V. (1992). Mechanisms of generation of wear particles of ultra high molecular weight polyethylene. In: Dowson D. et al., Eds. *Wear Particles.* Elsevier Science, London, 29-39.

Cooper J. R., Dowson D., Fisher J. (1993a). The effect of transfer film and surface roughness on the wear of lubricated ultra-high molecular weight polyethylene. *Clinical Materials*, Vol. 14, pp. 295-302.

Cooper J. R., Dowson D., Fisher J. (1993b). Macroscopic and microscopic wear mechanisms in ultra-high molecular weught polyethylene. *Wear*, Vol. 162, pp. 378-384.

Corkhill P. H., Trevetta A. S., Tighe B. J. (1990). The potential of hydrogels as synthetic articular cartilage. *Proc. Instn. Mech. Engrs.*, Vol. 204H, pp. 147-155.

Corvita Co. (1993). Corethane Product Literature. Corvita Co., Miami, USA.

Cudworth C. J., Higginson G. R. (1976). Friction of lubricated soft surface layers. *Wear*, Vol. 37, pp. 299-312.

Davidson J. A., Poggie R. A., Mishra A. K., Salehi A., Harbaugh M. E. (1992). Increased wear and contact stress from increased polyethylene stiffness in prosthetic knee and hip articulation. 7th International Conference on Biomedical Engineering. Dec 2-4, 1992, Singapore.

Derbyshire B., Fisher J., Dowson D., Hardaker C., Brummitt K. (1994). Comparative study of the wear of UHMWPE with zirconia, ceramic and stainless steel femoral heads in artificial hip joints. *Medical Engineering & Physics*, Vol. 16, pp. 229-236.

Derbyshire B., Fisher J., Dowson D., Hardaker C. S., Brummitt K. (1995). Wear of UHMWPE sliding against untreated, titanium nitride-coated and hardcor-treated stainless steel counterfaces. *Wear*, Vol. 181, pp. 258-262.

Dintenfass L. (1963). Lubrication in synovial joints: a theoretical analysis - a rheological approach to the problems of joint movements and joint lubrication. *J. Bone Joint Surg. [Am]*, Vol. 45A, p. 1241.

Dowson D. (1961). Inertial effects in hydrostatic thrust bearings. *Trans ASME. J. Basic Engineering*, Vol. June, pp. 227-234.

Dowson D. (1962). A generalized Reynold's equation for fluid film lubrication. *Int. J. Mech. Sci.*, Vol. 4, pp. 159-170.

Dowson D. (1967). Modes of lubrication in human joints. *Proc. Instn. Mech. Engrs.*, Vol. 181, pt. 3J, p. 45.

Dowson D., Longfield M. D., Walker P. S., Wright V. (1968). An investigation of the friction and lubrication in human joints. *Proc. Instn. Mech. Engrs.*, Vol. PE, pp. 70-78.

Dowson D., Unsworth A., Wright V. (1970). Analysis of boosted lubrication in human joints. *J. Mech. Eng. Sci.*, Vol. 12, No. 5, pp. 364-369.

Dowson D., Walker P. S., Longfield M. D., Wright V. (1970). A joint simulating machine for load bearing joints. *Med. and Biol. Engng.*, Vol. 8, pp. 37-43.

Dowson D., Wright V., Unsworth A., Gvozdanovic D. (1975). An overall view of synovial joint lubrication. *Annals of the Rheumatic Diseases*, Vol. 34. Suppl., pp. 94-97.

Dowson D., El-Haby Diab M. M., Gillis B. J., Atkinson J. R. (1984). The influence of counterface topography on the wear of ultra-high molecular weight polyethylene under wet and dry conditions. In Proc. Int. Symp. on Polymer Wear and its Control, St Louis (American Chemical Society, New York) pp226-32.

Dowson D., Wallbridge N. C. (1985). Laboratory wear tests and clinical observations of the penetration of femoral heads into acetabular cups in total replacement hip joints. Part 1. Charnley prostheses with polytetrafluoroethylene acetabular cups. *Wear*, Vol. 104, pp. 203-215.

Dowson D., Jin Z.-M. (1986). Micro-elastohydrodynamic lubrication of synovial joints. *Engineering in Medicine*, Vol. 15, No. 2, pp. 63-65.

Dowson D., Jin Z.-M. (1987). An analysis of micro-elastohydrodynamic lubrication in synovial joints considering cyclic loading and entraining velocities. In: Dowson D., Ed. *13th Leeds-Lyon Symposium.* Elsevier Science, Amsterdam, 375-386.

Dowson D., Taheri S., Wallbridge N. C. (1987). The role of counterface imperfections in the wear of polyethylene. *Wear*, Vol. 119, pp. 277-293.

Dowson D. (1990). 29. Bio-tribology of natural and replacement synovial joints. In: Mow, Ratcliffe, Woo, Eds. *Biomechanics of diarthrodial joints. Vol. 2* Springer Verlag, New York, 305-345.

Dowson D., Yao J. (1990). A full solution to the problem of film thickness predication in natural synovial joints. In: Dowson D. et al., Eds. *16th Leeds-Lyon Symposium.* Elsevier Science, Amsterdam, 91-102.

Dowson D., Fisher J., Jin Z. M., Auger D. D., Jobbins B. (1991). Design considerations for cushion form bearings. *Proc. Instn. Mech. Engrs.*, Vol. 205H, pp. 59-68.

Dowson D. (1992). Developments in lubrication - the thinning film. *Journal of Physics. D - Applied Physics*, Vol. 25, pp. A334-A339.

Dowson D. (1992). 35th Anniversary issue of wear - Novel aspects of wear - Introduction. *Wear*, Vol. 153, pp. 1-7.

Dowson D. (1992). Engineering at the interface. *Proc. Instn. Mech. Engrs.*, Vol. 206C, pp. 146-165.

Dowson D., Jin Z. M. (1992a). Microelastohydrodynamic lubrication of low elastic modulus solids on rigid substrates. *Journal of Physics. D - Applied Physics*, Vol. 25, pp. A116-A123.

Dowson D., Jin Z.-M. (1992b). A full numerical solution to the problem of microelastohydrodynamic lubrication of a stationary compliant wavy layered surface firmly bonded to a rigid substrate with particular reference to human synovial joints. *Proc. Instn. Mech. Engrs.*, Vol. 206H, pp. 185-193.

Dowson D. (1993), Ed. Thin films in Tribology. Elsevier Science, Amsterdam, .

Dowson D., Yao J. Q. (1994a). Elastohydrodynamic lubrication of soft-layered solids at elliptical contacts. Part 1: elasticity analysis. *Proc. Instn. Mech. Engrs.*, Vol. 208J, pp. 31-42.

Dowson D., Yao J. Q. (1994b). Elastohydrodynamic lubrication of soft-layered solids at elliptical contacts. Part 2: film thickness analysis. *Proc. Instn. Mech. Engrs.*, Vol. 208J, pp. 43-52.

Dowson D. (1995). Elastohydrodynamic and microelastohydrodynamic lubrication. *Wear*, Vol. 190, pp. 125-138.

Duff-Barclay I., Spillman D. T. (1967). Total human hip joint prostheses - a laboratory study of friction and wear. *Proc. Instn. Mech. Engrs.*, Vol. 181. Pt. 3J, pp. 90-103.

Dumbleton J. H. (1977). Joint simulators. In: Dowson D., Wright V., Eds. *Evaluation of artificial joints.* Biological Engineering Society, London, 47-49.

Dumbleton J. H. (1978). Wear and its measurement for joint prosthesis materials. *Wear*, Vol. 49, pp. 297-326.

English T. A., Kilvington M. (1979). In vivo records of hip loads using a femoral implant with telemetric output (a preliminary report). *Journal of Biomedical Engineering*, Vol. 1, No. 2, pp. 111-115.

Fein R. S. (1967). Are synovial joints squeeze film lubricated? *Proc. Instn. Mech. Engrs.*, Vol. 181, pp. 125-128.

Fisher J., Dowson D. (1991). Tribology of total artificial joints. *Proc. Instn. Mech. Engrs.*, Vol. 205H, pp. 73-79.

Fisher J., Dowson D., Hamdzah H., Lee H. L. (1994). The effect of sliding velocity on the friction and wear of UHMWPE for use in total artificial joints. *Wear*, Vol. 175, pp. 219-225.

Geigy (1970), Ed. Geigy Scientific Tables. 7th ed. J. R. Geigy S. A., Basle, Switzerland, .

Gladstone J. R. (1988). The tribology of elastomeric layers for use in hemiarthroplasty [Thesis]. *University of Waterloo*, .

Gladstone J. R., Medley J. B. (1990). Comparison of theoretical and experimental values for friction of lubricated elastomeric surface layers under transient conditions. In: Dowson D. et al., Eds. *16th Leeds-Lyon Symposium.* Elsevier Science, Amsterdam, 241-250.

Gore T. A., Higginson G. R., Kornberg R. E. (1981). Some evidence of squeeze-film lubrication in hip prostheses. *Engineering in Medicine*, Vol. 10, pp. 89-94.

Graham R. M., Joseph P. F., Dooley R. L., Laberge M. (1995). Effect of lubricant viscosity and bearing surface stiffness on the lubrication mechanism of a point contact as a total hip arthroplasty model. 21st Annual Meeting of Society for Biomaterials. March 18-22, 1995, San Fransisco.

Grassam, Powell (1964), Eds. Gas lubricated bearings. Butterworths, London, .

Greenwood J. A., Tripp J. H. (1967). The elastic contact of rough spheres. *J. Appl. Mech.*, Vol. March, pp. 153-159.

Greenwood J. A. (1988). Film thickness in circular elastohydrodynamic contacts. *Proc. Instn. Mech. Engrs.*, Vol. 202, C1, pp. 11-17.

Greenwood J. A., Johnson K. L. (1992). The behaviour of transverse roughness in sliding elastohydrodynamically lubricated contacts. *Wear*, Vol. 153, pp. 107-117.

Grinnell S. K., Richardson H. H. (1955). Design study of hydrostatic gas bearing with inherent orifice compensation. *Trans ASME. J. Basic Engineering*, Vol. November, pp. 11-21.

Hall R. M., Unsworth A., Wroblewski B. M., Hardaker C. (1993). Long term changes in the frictional behaviour and wear in implanted Charnley prostheses. *J. Bone Joint Surg. [Br]*, Vol. 67B Supp III, p. 267.

Hall R. M., Unsworth A., Wroblewski B. M., Burgess I. C. (1994). Frictional characterisation of explanted Charnley hip prostheses. *Wear*, Vol. 175, pp. 159-166.

Hall R. M., Unsworth A., Craig P. S., Hardaker C., Siney P. S., Wroblewski B. M. (1995). Measurement of wear in retrieved acetabular sockets. *Proc. Instn. Mech. Engrs.*, Vol. 209H, pp. 233-242.

Hall R. M., Unsworth A. (1997). Friction in hip prostheses: A review. *Biomaterials*, Vol. 18, pp. 1017-1026.

Hall R. M., Unsworth A., Wroblewski B. M., Siney P., Powell N. J. (1997). The friction of explanted hip prostheses. *British Journal of Rheumatology*, Vol. 37, p. In Press.

Hamrock B. J. (1994). Fundamentals of Fluid Film Lubrication. International ed. McGraw-Hill, New York, .

Hamrock B. J., Dowson D. (1976a). Isothermal elastohydrodynamic lubrication of point contacts. Part 1 - Theoretical formulation. *J. Lub. Tech.*, Vol. April, pp. 223-229.

Hamrock B. J., Dowson D. (1976b). Isothermal elastohydrodynamic lubrication of point contacts. Part 2 - Ellipticity parameter results. *J. Lub. Tech.*, Vol. 98. Series F, pp. 375-383.

Hamrock B. J., Dowson D. (1976c). Isothermal elastohydrodynamic lubrication of point contacts. Part 3 - Fully flooded results. *J. Lub. Tech.*, Vol. April, pp. 264-276.

Hamrock B. J., Dowson D. (1977). Isothermal elastohydrodynamic lubrication of point contacts. Part 4 - Starvation results. *J. Lub. Tech.*, Vol. January, pp. 15-23.

Hamrock B. J., Dowson D. (1978). Elastohydrodynamic lubrication of elliptical contacts for materials of low elastic modulus. Part 1 - fully flooded conjunction. *J. Lub. Tech.*, Vol. 100, pp. 237-245.

Higginson G. R., Norman R. (1974a). The lubrication of porous elastic solids with reference to the functioning of human joints. *J. Mech. Eng. Sci.*, Vol. 16, No 4, pp. 250-257.

Higginson G. R., Norman R. (1974b). A model investigation of squeeze-film lubrication in animal joints. *Phys. Med. Biol.*, Vol. 19, No. 6, pp. 785-792.

Higginson G. R. (1977). Elastohydrodynamic lubrication in human joints. *Proc. Instn. Mech. Engrs.*, Vol. 191. No. 33, pp. 217-223.

Higginson G. R. (1978a). Elastohydrodynamic lubrication in human joints. *Engineering in Medicine*, Vol. 1, pp. 35-41.

Higginson G. R. (1978b). Squeeze films between compliant solids. *Wear*, Vol. 46, pp. 387-395.

Higginson G. R., Unsworth A. (1981). The lubrication of natural joints. In: Dumbleton, JH Ed., *Tribology of Natural and Artificial Joints* .,Elsevier Science, Amsterdam, pp. 47-73.

Hills R. J., Unsworth A., Ive F. A. (1994). A comparative study of the frictional properties of emollient bath additives using porcine skin. *British Journal of Dermatology*, Vol. 130, pp. 37-41.

Hitchmough K. (1994). The frictional properties of cross-linked polyethylene. Final Year Undergraduate Project, University of Durham.

Hlavacek M., Novak J. (1995a). The role of synovial fluid filtration by cartilage in lubrication of synovial joints. Part 3 - squeeze film lubrication: axial symmetry under low loading conditions. *Journal of Biomechanics*, Vol. 10, pp. 1193-1198.

Hlavacek M. (1995b). The role of synovial fluid filtration by cartilage in lubrication of synovial joints. Part 4 - squeeze film lubrication: The central film thickness for normal and inflammatory synovial fluids for axial symmetry under high loading conditions. *Journal of Biomechanics*, Vol. 28, No.10, pp. 1199-1205.

Hooke C. J., O'Donoghue J. P. (1972). Elastohydrodynamic lubrication of soft highly-deformed contacts. *J. Mech. Eng. Sci.*, Vol. 14, No 1, pp. 34-48.

Howie D. W., Haynes D. R., Rogers S. D., McGee M. A., Pearcy M. J. (1993). The response to particulate debris. *Orthopedic Clinics of North America*, Vol. 24, pp. 571-581.

Hutchings I.M. (1992). Tribology: Friction and wear of engineering materials. Edward Arnold, Kent.

Ikeuchi K., Goto S., Isobe K., Oka M. (1993a). An experimental study of contact conditions and friction in hip prostheses. In: Dowson D., Ed. *Thin Films in Tribology.* Elsevier Science, Amsterdam, 521-527.

Ikeuchi K., Oka M. (1993b). A model analysis of squeeze film effect in a hip joint. In: Dowson D., Ed. *Thin Film in Tribology.* Elsevier Science, Amsterdam, 513-520.

Jin Z. M., Dowson D. (1991). Stress analysis of cushion form bearings for total hip replacements. *Proc. Instn. Mech. Engrs.*, Vol. 205H, pp. 117-124.

Jin Z. M., Dowson D. (1992). The effect of porosity of articular cartilage on the lubrication of a normal human hip joint. *Proc. Instn. Mech. Engrs.*, Vol. 206H, pp. 117-124.

Jin Z. M., Dowson D., Fisher J. (1993a). Wear and friction of medical grade polyurethane sliding on smooth metal counterfaces. *Wear*, Vol. 162, pp. 627-630.

Jin Z. M., Dowson D., Fisher J. (1993b). Minimum and central film thickness formulae for an elastic layer firmly bonded to a rigid cylindrical substrate under entraining motion. *Wear*, Vol. 170, pp. 281-284.

Jin Z. M., Dowson D., Fisher J. (1993c). Fluid film lubrication in natural hip joints. In: Dowson D. et al., Eds. *Thin Film in Tribology. 19th Leeds-Lyon Symposium.* Elsevier Science, Amsterdam, 545-555.

Jin Z. M., Dowson D., Fisher J. (1994a). A parametric analysis of the contact stress in ultra-high molecular weight polyethylene acetabular cups. *Medical Engineering & Physics*, Vol. 16, pp. 398-405.

Jin Z. M., Dowson D., Fisher J., Rimmer D., Wilkinson R., Jobbins B. (1994b). Measurement of lubricating film thickness in low elastic modulus lined bearings, with particular reference to models of cushion form bearings for total joint replacements. Part 1: steady state entraining motion. *Proc. Instn. Mech. Engrs.*, Vol. 208J, pp. 207-212.

Jin Z. M., Dowson D., Fisher J., Rimmer D., Wilkinson R., Jobbins B. (1994c). Measurement of lubricating film thickness in low elastic modulus lined bearings, with particular reference to models of cushion form bearings for total joint replacements. Part 2: Squeeze film motion. *Proc. Instn. Mech. Engrs.*, Vol. 208J, pp. 213-217.

Jin Z.-M., Dowson D., Fisher J. (1995). Contact pressure prediction in total knee joint replacements. Part 1 - general elasticity solution for elliptical layered contacts. *Proc. Instn. Mech. Engrs.*, Vol. 209H, pp. 1-8.

Jin Z.-M., Stewart T., Auger D. D., Dowson D., Fisher J. (1995). Contact pressure prediction in total knee joint replacements. Part 2: application to the design of total knee joint replacements. *Proc. Instn. Mech. Engrs.*, Vol. 209H, pp. 9-15.

Johnson K. L., Greenwood J. A., Poon S. Y. (1972). A simple theory of asperity contact in elastohydrodynamic lubrication. *Wear*, Vol. 19, pp. 91-108.

Johnson R. C., Smidt G. L. (1969). Measurement of hip joint motion during walking *Journal ogf Bone and Joint Surgery (American)*, Vol. 51A, pp. 1083-1094.

Jones E. S. (1934). Joint Lubrication. *Lancet*, Vol. 1, p. 1426.

Jones H. P., Walker P. S. (1968). Casting techniques applied to the study of human joints. *Symposium lubrication and wear in living and artificial human joints. 7th April 1967. I Mech E. London*, Vol. 14, p. 57.

Jones W. R., Hady W. F., Crugnola A. (1981). Effect of irradiation on the friction and wear of ultra-high molecular weight polyethylene. *Wear*, Vol. 70, pp. 77-92.

Joyce T. J., Ash H. E., Unsworth A. (1996). The wear of cross-linked polyethylene against itself. *Proc. Instn. Mech. Engrs.*, Vol. 210H, pp. 11-16.

Judet J., Judet R. (1950). The use of an artificial femoral head for arthroplasty of the hip joint. *J. Bone Joint Surg. [Br]*, Vol. 32, p. 166.

Judet R., Judet J. (1952). Technique and results with the acrylic femoral head prosthesis. *J. Bone Joint Surg. [Br]*, Vol. 34, No. 2 .

Kinloch (1987). Adhesion and adhesives: science and technology. Chapman and Hall, London.

Kumar P., Oka M., Ikeuchi K., Shimizu K., Yamamuro T., Okumura K., Kotoura Y. (1991). Low wear rate of UHMWPE against zirconia ceramic (y-psz) in comparison to alumina ceramic and sus 31 alloy. *Journal of Biomedical Materials Research*, Vol. 25, pp. 813-828.

Lancaster J. K. (1990). Material-specific wear mechanisms: relevance to wear modelling. *Wear*, Vol. 141, pp. 159-183.

Lemm W. (1984). Biodegradation in polyurethanes. In: Planck H., Egbers G., Syre I., Eds. *Polyurethanes in biomedical engineering.* Elsevier Science, Amsterdam, 103-108.

Lewis P. R., McCutchen C. W. (1959). Experimental evidence for weeping lubrication in mammalian joints. *Nature*, Vol. 184, pp. 1285-1286.

Ling F. F. (1974). A new model of articular cartilage in human joints. *J. Lub. Tech.*, pp. 449-507.

Linn F. C. (1967). Lubrication of Animal Joints. Part 1 - The arthrotripsometer *J. B. J. S.* Vol. 49A, pp. 1079-1098.

Linn F. C., Radin E. L. (1968). Lubrication of Animal Joints. Part 3 - The effect of certain chemical alterations of the cartilage and lubricant. *Arth. Rheum*, Vol. 2, No. 5 .

Little T., Freeman M., Swanson A. (1969). Experiments on friction in the human hip joint. In: Wright V., Ed. *Lubrication and wear in joints.* Sector, London, 110-115.

Livermore J., Ilstrup D., Morrey B. (1990). Effect of femoral head size on wear of the polyethylene acetabular component. *J. Bone Joint Surg. [Am]*, Vol. 72A, pp. 518-528.

MacConnaill M. A. (1932). The function of intra-articular fibro-cartilages. *J. Anatomy.*, Vol. 66, pp. 210.

Maroudas A. (1967). Hyaluronic acid films. *Proc. Instn. Mech. Engrs.*, Vol. 181, pp. 122-124.

Maroudas A. (1969). Studies on the formation of hyaluronic acid films. In: Wright V., Ed. *Lubrication and wear in joints.* Sector Publishing Ltd., London, 125-133.

McClure G., Jin Z. M., Fisher J., Tighe B. J. (1996). Determination of lubricating film thickness for permeable hydrogel and non-permeable polyurethane layers bonded to a rigid substrate with particular reference to cushion form hip joint replacements. *Proc. Instn. Mech. Engrs.*, Vol. 210H, pp. 89-93.

McCutchen C. W. (1959). Mechanism of animal joints. Sponge-hydrostatic and weeping bearings. *Nature*, Vol. 184, pp. 1284-1285.

McCutchen C. W. (1962). The frictional properties of animal joints. *Wear*, Vol. 5, pp. 1-17.

McCutchen C. W. (1966). Boundary lubrication by synovial fluid: demonstration and possible osmotic explanation. *Fed. Proc*, Vol. 25, pp. 1061-1168.

McCutchen C. W. (1967). Physiological lubrication. *Proc. Instn. Mech. Engrs.*, Vol. 181, Pt. 3J .

McKellop H., Clarke I. C., Markolf K. L., Amstutz H. C. (1977). Polyethylene wear in prosthetic joints. In: Dowson D., Wright V., Eds. *Evaluation of artificial joints.* Bioengineering Society, London, .

McKellop H. (1981). Wear of artificial joint materials II. Twelve-channel wear screening devices: correlation of experimental and clinical results. *Engineering in Medicine*, Vol. 10, pp. 123-136.

McKellop H., Clarke I. C., Markolf K., Amstutz H. (1983). Friction and wear properties of polymer, metal and ceramic prosthetic joint materials evaluated on a multichannel screening device. *Journal of Biomedical Materials Research*, Vol. 15, pp. 619-653.

McKellop H., Clarke I. (1988). Wear of artificial joint materials in laboratory tests. *Acta Orthopaedica Scandinavica*, Vol. 59, pp. 349-352.

McMillin C. R. (1994). Elastomers for biomedical applications. *Rub. Chem. Tech.* , Vol. 67, pp. 417-446.

Medley J. B., Pilliar R. M., Wong E. W., Strong A. B. (1980a). The breakdown of fluid film lubrication in elastic iso-viscous point contacts. *Wear*, Vol. 63, pp. 25-40.

Medley J. B., Pilliar R. M., Wong E. W., Strong A. B. (1980b). Hydrophilic polyurethane elastomers for hemiarthroplasty: a preliminary in vivo wear study. *Engineering in Medicine*, Vol. 9, No. 2, pp. 59-65.

Medley J. B., Dowson D., Wright V. (1984a). Transient elastohydrodynamic lubrication models for the human ankle joint. *Engineering in Medicine*, Vol. 13, No 13, pp. 137-152.

Medley J. B., Dowson D. (1984b). Lubrication of elastic iso-viscous line contacts subject to cyclic loads and entrainment velocities. *J. Lub. Tech.*, Vol. 27, 3, pp. 243-251.

Medley J. B. (1994). Some background theory for the cushion bearing concept in joint replacement implants. *Wear*, Vol. 175, pp. 9-16.

Morscher E. W. (1992). Current status of acetabular fixation in primary total hip-arthroplasty. *Clin. Orthop.*, Vol. 274, pp. 172-193.

Mow V. C. (1969). The role of lubrication in biomechanical joints. *Trans. ASME. J. Trib.*, Vol. April, pp. 320-328.

Murakami T., Ohtsuki N., Higaki H. (1993). The adaptive multimode lubrication in knee prostheses with compliant layer during walking motion. In: Dowson D., Ed. *Thin Films in Tribology*. Elsevier Science Publishers, Amsterdam, 673-682.

Murray D. W., Carr A. J., Bulstrode C. J. (1995). Which primary hip replacement? *J. Bone Joint Surg. [Br]*, Vol. 77B, pp. 520-527.

Nusbaum H. J., Rose R. M., Paul I. L., Crugnola A. M., Radin E. L. (1979). Wear mechanisms in UHMWPE in total hip prostheses. *J. Mech. Eng. Sci.*, Vol. 23, pp. 777-789.

O'Carroll S., Jin Z. M., Dowson D., Fisher J., Jobbins B. (1990). Determination of contact area in cushion form bearings for artificial joints. *Proc. Instn. Mech. Engrs.*, Vol. 204H, pp. 217-223.

Ogston A. G., Stanier J. E. (1950). On the state of hyaluronic acid in synovial fluid. *Biochem. J.*, Vol. 46, pp. 364-376.

O'Kelly J., Unsworth A., Dowson D., Jobbins B., Wright V. (1977). Pendulum and simulator for studies of friction in hip joints. In: Dowson D., Wright V., Eds. *Evaluation of artificial joints*. Bioengineering Society, London, 19-29.

O'Kelly J., Unsworth A., Dowson D., Hall D. A., Wright V. (1978). A study of the role of synovial fluids and its constituents in the friction and lubrication of human hip joints. *Engineering in Medicine*, Vol. 7, pp. 73-83.

Paul J. P. (1967). Forces transmitted by joints of the human body. *Proc. Instn. Mech. Engrs.*, Vol. 181, pp. 8-15.

Pinchuk L. (1994). Review: A review of biostability and carcinogenicity of polyurethanes in medicine and the new generation of biostable polyurethanes. *J. Biomater. Sci.*, Vol. Polymer Edn., Vol. 6, No. 3, pp. 225-267.

Poss R., Brick G. W., Wright R. J., Roberts D. W., Sledge C. B. (1988). The effects of modern cementing techniques on the longevity of total hip arthroplasty. *Orthopedic Clinics of North America*, Vol. 19, pp. 591-598.

Radin E. L., Paul J. P. (1972). A consolidated concept of joint lubrication. *J. Bone Joint Surg. [Am]*, Vol. 54, No. 3, pp. 607-616.

Roberts B. J., Unsworth A., Mion N. (1982). Modes of lubrication of human hip joints. *Nature*, Vol. 41, pp. 271-274.

Roe R. J., Grood E. S., Shastri R., Gosselini C. A., Noyes F. R. (1981). Effect of radiation and sterilization and aging ultrahigh molecular weight polyethylene. *J. Biomed. Mat. Res.*, Vol. 15, pp. 209-230.

Rose R. M., Radin E. L. (1982). Wear of polyethylene in total hip prostheses. *Clin. Orthop.*, Vol. 170, pp. 107-115.

Rose R. M., Goldfarb H. V., Ellis E., Crugnola A. M. (1983). On pressure dependence of wear of UHMWPE. *Wear*, Vol. 92, pp. 99-111.

Rostoker W., Galante J. O. (1976). Some new studies of the wear behaviour of ultrahigh molecular weight polythylene. *Journal of Biomedical Materials Research*, Vol. 10, pp. 303-310.

Rostoker W., Galante J. O. (1979). Contact pressure dependence of wear rates of UHMWPE. *Journal of Biomedical Materials Research*, Vol. 13, pp. 964-975.

Saikko V., Paavolainen P., Kleimol M., Slatis P. (1992a). A five station hip joint simulator for wear rate studies. *Proc. Instn. Mech. Engrs.*, Vol. 206H, pp. 195-201.

Saikko V. (1992b). A simulator study of friction in total replacement hip joints. *Proc. Instn. Mech. Engrs.*, Vol. 206H, pp. 201-211.

Saikko V. O. (1993a). Wear of polyethylene acetabular cups against alumina femoral heads -5 prostheses compared in a hip simulator for 35 million walking cycles. *Acta Orthopaedica Scandinavica*, Vol. 64, pp. 507-512.

Saikko V. (1993b). Wear and friction properties of prosthetic joint materials evaluated on a reciprocating pin-on-flat apparatus. *Wear*, Vol. 166, pp. 169-178.

Saikko V. O., Paavolainen P. O., Slatis P. (1993c). Wear of the polyethylene acetabular cup - metallic and ceramic heads compared in a hip simulator. *Acta Orthopaedica Scandinavica*, Vol. 64, pp. 391-402.

Saikko V. (1993d). Tribology of total replacement hip joints studied with new hip joint simulators and a materials-screening apparatus. *Acta Orthop. Scanda.*, Vol. 110, pp. 1-44.

Saikko V. (1994). Wear of polyethylene acetabular cups against zirconia femoral heads studied with a hip-joint simulator. *Wear*, Vol. 176, pp. 207-212.

Saikko V. O. (1995). Wear of the polyethylene acetabular cup - the effect of head material, head diameter, and cup thickness studied with a hip simulator. *Acta Orthopaedica Scandinavica*, Vol. 66, pp. 501-506.

Saikko V. (1996). A three axis hip joint simulator for wear and friction studies on total hip prostheses. *Proc. Instn. Mech. Engrs.*, Vol. 210H, pp. 175-185.

Scales J., Kelly P., Goddard D. (1969). Friction torque studies of total hip replacements - the use of a simulator. In: Wright V., Ed. *Lubrication and Wear in Joints.* Sector Publishing Ltd, London, 88-102.

Scholes S. C., Hall R. M., Unsworth A., Scott R. (1997). The effects of material combination. and lubricant on the friction of total hip prostheses. Abstract. *J. B. J. S.* (British).

Seedhom B. B., Dowson D., Wright V. (1973). Wear of solid phase formed high density polyethylene in relation to the life of artificial hips and knees. *Wear*, Vol. 24, pp. 35-51.

Seirig A., Arvikar R. J. (1975). The predication of muscular load sharing and joint forces in the lower extremities during walking. *J. Biomechanics*, Vol. 8, pp. 89-102.

Semlitsch M. (1993). CoCr metal-metal articulation as a solution to the problem of wear of total joint replacements. Proc. SERC/I.Mech.E Annual Expert Meeting on Failure of Joint Prostheses, Mech. Engrs. Pub. Ltd., Bury St. Edmunds, pp. 40-43.

Shanbhag A. S., Jacobs J. J., Black J., Galante J. O., Glant T. T. (1994). Macrophage/particle interactions: Effect of size, composition and surface area. *Journal of Biomedical Materials Research*, Vol. 28, pp. 81-90.

Shen C., Dumbleton J. H. (1974). The friction and wear behaviour of irradiated very high molecular weight polyethylene. *Wear*, Vol. 30, pp. 349-364.

Sibly T. F., Unsworth A. (1991). Wear of cross-linked polyethylene against itself - a material suitable for surface replacement of the finger joint. *Journal of Biomedical Engineering*, Vol. 13, pp. 217-220.

Simon S. R., Paul I. L., Rose R. M., Radin E. L. (1975). "Stiction-friction" of total hip prostheses and its relationship to loosening. *J. Bone Joint Surg. [Am]*, Vol. 57A, pp. 226-230.

Smith T. J., Medley J. B. (1986). Development of transient elastohydrodynamic models for synovial joint lubrication. In: Dowson D. et al., Eds. *13th Leeds-Lyon Symposium.* Elsevier Science, Amsterdam, 361-374.

Smith N., Doyle C., Jones E. (1996). Prosthetic bearing element and process for making such element *European Patent* EP 0698382AZ..

Spikes H. A. (1996). Mixed lubrication - An overview. 10th International Colloquiem on Tribology - Solving friction and wear problems. Essingen, Germany. Pages 1713-1735.

Stewart T. D., Fisher J. (1996). Composite cushion form knee joint replacements. Fifth biomaterials world congress. May 29 - June 2 1996. Toronto, Canada.

Stokes K. (1984). Environmental stress cracking in implanted polyether polyurethanes. In: Planck H., Egbers G., Syre I., Eds. *Polyurethanes in biomedical engineering.* Elsevier Science, Amsterdam, .

Stokes K. B. (1988). Polyether polyurethanes: Biostable or not? *J. Biomat. Appl.*, Vol. 3, pp. 228-259.

Stokes K., McVenes R., Anderson J. M. (1995). Polyurethane elastomer biostability. *J. Biomat. Appl.*, Vol. 9, pp. 321-354.

Stokoe S. M. (1990). A finger function simulator and surface replacement prosthesis for the metacarpal-phalangeal joint [Dissertation]. *University of Durham*, .

Stout K. J. (1985). The effect of manufacturing variations on the performance of externally pressurized gas-lubricated journal bearings. *Proc. Instn. Mech. Engrs.*, Vol. 199. C4, pp. 299-309.

Strozzi A., Unsworth A. (1994). Axisymmetric finite element analysis of hip replacement with a elastic layer. The effects of layer thickness. *Proc. Instn. Mech. Engrs.*, Vol. 208H, pp. 139-149.

Swanson A. (1977). Limitations of joint simulators. In: Dowson D., Wright V., Eds. *Evaluation of artificial joints.* Bioengineering Society, London, 35-49.

Tabor D. (1981). Friction - the present state of our understanding. *J. Lub. Tech.*, Vol. 103, pp. 169-179.

Tanner R. I. (1966). An alternative approach to the problems of joint movements and joint lubrication. *Phys. Med. Biol.*, Vol. 11, pp. 119-121.

Tanner R. I. (1996). An alternative mechanism for the lubrication of synovial joints. *Phys. Med. Biol.*, Vol. 11, No. 1, pp. 119-127.

Tanzi M. C., Mantero S., Freddi G., Motta A., Sada A., Peluso G. (1994). Cytocompatibility of two segmented biomedical polyurethanes. *Journal of Materials Science: Materials in Medicine*, Vol. 5, pp. 705-710.

Timoshenko S. P., Goodier J. N. (1970), Eds. Theory of Elasticity. 3rd ed. McGraw-Hill Book Co, Singapore, .

Torrance A. A., Parkinson A. (1993). Towards a better surface finish for bearing materials. In: Dowson D. et al., Eds. *Thin Films in Tribology.* Elsevier Science, Amsterdam, 91-98.

Treharne R. W., Young R. W., Young S. R. (1981). Wear of artificial joint materials. Part 3 - simulation of the knee joint using a computer controlled system. *Engineering in Medicine*, Vol. 10, No. 3, pp. 137-142.

Tweedale P. J. (1994). A comparison of the ASTM and Leeds screening test protocols. Internal report. National Centre of Tribology, AEA Technology.

Unsworth A., Dowson D., Wright V. (1974a). The frictional behaviour of human synovial joints - Part 1: Natural joints. *J. Lub. Tech.*, Vol. 96, pp. 1-8.

Unsworth A., Dowson D., Wright V., Koshal D. (1974b). The frictional behaviour of human joints. Part II: Artificial joints. *J. Lub. Tech.*, Vol. 96 .

Unsworth A., Dowson D., Wright V. (1975). Some new evidence on human joint lubrication. *Annals of the Rheumatic Diseases*, Vol. 34, pp. 277-285.

Unsworth A. (1978). The effects of lubrication in hip joint prostheses. *Phys. Med. Biol.*, Vol. 23, pp. 253-268.

Unsworth A. (1981). Artificial Joints. In: Wright V., Dowson D., Eds. *An introduction to the biomechanics of joints and joint replacement.* MEP, London, 134-139.

Unsworth A., Pearcy M. J., White E. F. T., White G. (1987). Soft layer lubrication of artificial hip joints. In: *Proc. I.Mech.E. Int. Conf. on Tribology, friction, lubrication and wear, 50 years on.* Mech Engrs Pub Ltd, London, 715-724.

Unsworth A., Pearcy M. J., White E. F. T., White G. (1988). Frictional properties of artificial hip joints. *Engineering in Medicine*, Vol. 17, pp. 101-104.

Unsworth A. (1991). Tribology of human and artificial joints. *Proc. Instn. Mech. Engrs.*, Vol. 205H, pp. 163-171.

Unsworth A. (1993). Failure of joint prostheses. *Proc. Instn. Mech. Engrs.*, Vol. 207H, pp. 263-266.

Unsworth A. (1995). Recent developments in the tribology of artificial joints. *Tribology International*, Vol. 28, pp. 485-495.

Unsworth A., Hall R. M., Burgess I. C., Wroblewski B. M., Streicher R. M., Semlitsch M. (1995). Frictional resistance of new and explanted artificial hip joints. *Wear*, Vol. 190, pp. 226-231.

Unsworth A., Strozzi A. (1995). Axisymmetric finite element analysis of hip replacement with a elastic layer. The effects of clearance and Poisson's Ratio. *Proc. Instn. Mech. Engrs.*, Vol. 209H, pp. 59-64.

Varnam C. J., Hooke C. J. (1977). Non-Hertzian elastohydrodynamic contacts: an experimental investigation. *J. Mech. Eng. Sci.*, Vol. 19, No 5, pp. 189-192.

Visscher M., Hendrius C. P., Struik K. G. (1993). The real area of contact measured on elastomers. In: Dowson D. et al., Eds. *Thin films in tribology.* Elsevier Science, Amsterdam, 705-714.

Walker P. S., Dowson D., Longfield M. D., Wright V. (1968a). Boosted lubrication in synovial joints by fluid entrapment and enrichment. *Nature*, Vol. 27, pp. 512-520.

Walker P. S., Dowson D., Longfield M. D., Wright V. (1968b). Rheological behaviour of human joints. Conference on Experimental Rheology, University of Bradford, April 17-19 1968.

Walker P. S., Sikorski J., Dowson D., Longfield M. D., Wright V. (1970). Features of the synovial fluid film in human joint lubrication. *Nature*, Vol. 225, No. 5236, pp. 956-957.

Walker P. S., Gold B. L. (1971). The tribology (friction, lubrication and wear) of all metal artificial hip joints. *Wear*, Vol. 17, pp. 285-299.

Walker P. S., Gold B. L. (1973). Comparison of the bearing performance of normal and artificial human joints. *J. Lub. Tech.*, Vol. 95, pp. 333-341.

Walker P. S., Bullough P. G. (1973). The effects of friction and wear in artificial joints. *Symposium lubrication and wear in living and artificial human joints*, Vol. 14, No 2, pp. 275-293.

Wang D.-S., Lin J.-F. (1991). Effect of surface roughness on elastohydrodynamic lubrication of line contacts. *Tribology International*, Vol. 24, No.1, pp. 51-62.

Wang A., Sun D. C., Stark C., Dumbleton J. H. (1995). Wear mechanisms of UHMWPE in total joint replacements. *Wear*, Vol. 181, pp. 241-249.

Waters N. E. (1965). The indentation of thin rubber sheets by spherical indentors. *Journal Applied Physics*, Vol. 16, pp. 557-563.

Weightman B., Simon S., Paul I., Rose R., Radin E. (1972). Lubrication mechanism of hip joint replacement prostheses. *J. Lub. Tech.*, Vol. 94, pp. 131-135.

Weightman B. O., Paul I. L., Rose R. M., Simon S. R., Radin E. L. (1973). A comparative study of total hip replacement prostheses. *Journal of Biomechanical Engineering - Transactions of the Asme*, Vol. 6, pp. 229-311.

Weightman B., Light D. (1985). A comparison of RCH 1000 and Hi-fax 1900 ultra-high molecular weight polyethylenes. *Biomaterials*, Vol. 6, pp. 177-183.

Weightman B., Light D. (1986). The effect of the surface finish of alumina and stainless-steel on the wear rate of UHMW polyethylene. *Biomaterials*, Vol. 7, pp. 20-24.

Willert H. G., Semlitsch M. (1975). Reaction of the articular capsule to plastic and metallic wear products from joint endoprostheses. Congress of Dutch-Swiss Orthopaedic Socieities. Lausanne. May 1994. (Sulzer Technical Review; 2; 119-131)

Willert H. G., Semlitsch M. (1977). Reactions of the articular capsule to wear products for artificial joint prostheses. *Journal of Biomedical Materials Research*, Vol. 11, pp. 157-164.

Williams J. A. (1994), Ed. Engineering Tribology. 1st ed. Oxford University Press, Oxford, .

Wong E. (1981). Development of a biomedical polyurethane. Orthopedic implant applications. *Am. Chem. Soc. Symp.*, Vol. 172. No. 31, pp. 489-504.

Wright K. W. J., Dobbs H. S., Scales J. T. (1982). Wear studies of polymeric materials using a pin-on-disc machine. *Biomaterials*, Vol. 3, pp. 41-48.

Yao J. Q., Seedhom B. B. (1991). A new technique for measuring contact areas in human joints - the 3S technique. *Proc. Instn. Mech. Engrs.*, Vol. 205H, pp. 69-72.

Yao J. Q., Unsworth A. (1993). Asperity lubrication in human joints. *Proc. Instn. Mech. Engrs.*, Vol. 207H, pp. 245-254.

Yao J. Q. (1994). Contact mechanics of soft layer artificial hip joints. Part 1 : General solutions. *Proc. Instn. Mech. Engrs.*, Vol. 208H, pp. 195-205.

Yao J. Q., Dowson D. (1994). Elastohydrodynamic lubrication of soft-layered solids at ellpitical contacts. Part 1: elasticity analysis. *Proc. Instn. Mech. Engrs.*, Vol. 208J, pp. 31-41.

Yao J. Q., Parry T. V., Unsworth A., Cunningham J. L. (1994). Contact mechanics of soft layer artificial hip joints. Part 2: Application to joint design. *Proc. Instn. Mech. Engrs.*, Vol. 208H, pp. 206-215.

Zhao Q., Casas-Bejar J., Urbanski P., Stokes K. (1995). Glass wool -H2O2/CoCl2 tests system for in vitro evaluation of the biodegradative stress cracking in polyurethane elastomers. *Journal of Biomedical Materials Research*, Vol. 29, pp. 467-475.

Appendix A - Repeatability of load application on simulator

During the early testing of soft layer joints on the simulator, it became apparent that the coefficient of friction measured by the simulator was in some way related to the period of time over which the simulator had been running on that particular occasion. For constant loading conditions, joint, and lubricant, the coefficient of friction measured appeared to decrease with continued testing. As expected, the hydrostatic bearing oil and servo-hydraulic oil increased in temperature during the testing period.

It was suggested that the decrease in measured coefficient of friction may have been due to changes in the actual load applied by the system (although the requested load was maintained constant). By carrying out a series of tests, it was found that over a period of testing under constant conditions, the measured minimum and maximum loads applied by the system would gradually decrease in spite of the requested load being held constant. It was felt that it was the decrease in minimum load which was having the most significant effect as the minimum load had been seen to have a greater effect on the frictional torque produced than the maximum load had.

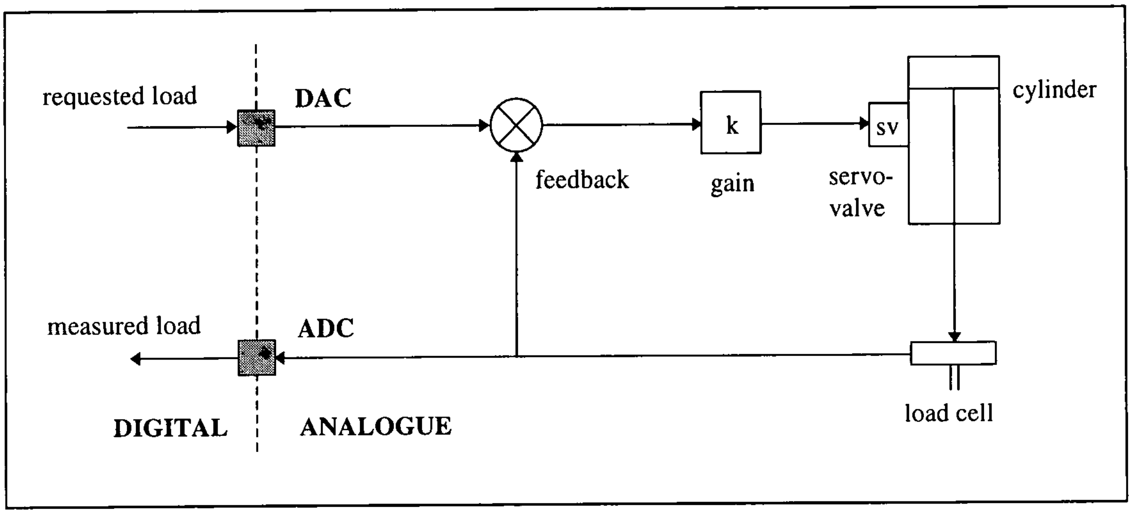

Figure A.1 Block diagram of the load control system of the simulator

To identify which part of the system was affecting the actual load applied, the simulator's load cells were calibrated at six different temperatures, 'warming up' the simulator by 400 cycles between calibrations. The temperature of the servo-valve (controlling the load cells) was recorded using a thermocouple.

Figures A.2 and A.3 show the ADC and DAC calibrations for the six different temperatures. The ADC calibration shows little change with temperature, proving that the applied load measurement systems were independent of temperature, and that the load measured was indeed the load being applied. The DAC calibration showed a linear relation between the calibration coefficients (gradient and intercept) with the measured temperature of the servo-valve. Considering Figure A.2, this meant that either the DAC and other electronic components, the load cells, or the servo-hydraulic pump-valve-cylinder system were affecting the closed loop feedback signal and were thus responsible for the temperature dependent decrease in the applied load. Further work showed the servo-hydraulic system to be responsible.

Figures A.4 and A.5 show the linear relationship between the DAC calibration coefficients and the servo-valve temperature. As the temperature of the servo-hydraulic oil increased, the intercept and gradient of the DAC calibration became more negative , and so the load decreased for any fixed requested value as had been seen experimentally.

In order to reduce these temperature-dependent effects, two alterations were made to simulator test protocol. Firstly, a cooling system was been fitted to the servo-hydraulic oil pump so that the oil was continually cooled throughout testing. Temperatures recorded during a testing period were seen to rise much more slowly and to reach a fairly steady value by the end of a series of tests. Secondly, the simulator was run for a minimum of 400 'warm up' cycles prior to testing as suggested and all tests in a series were run at approximately the same servo-valve temperature. These measures have allowed more repeatable results to be produced, such as those described here.

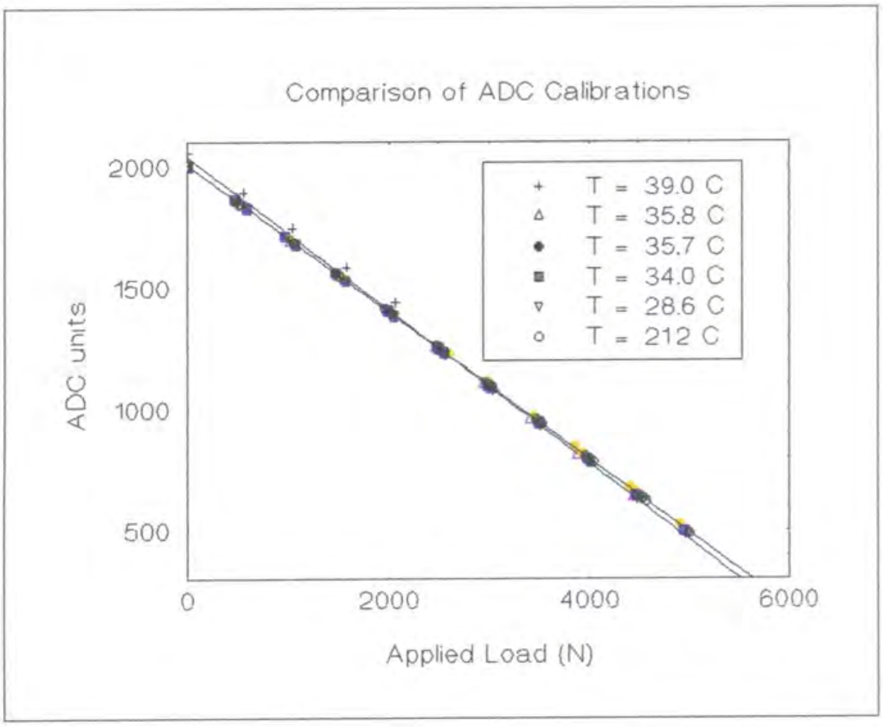

Figure A.2 ADC calibration curves for six different temperatures

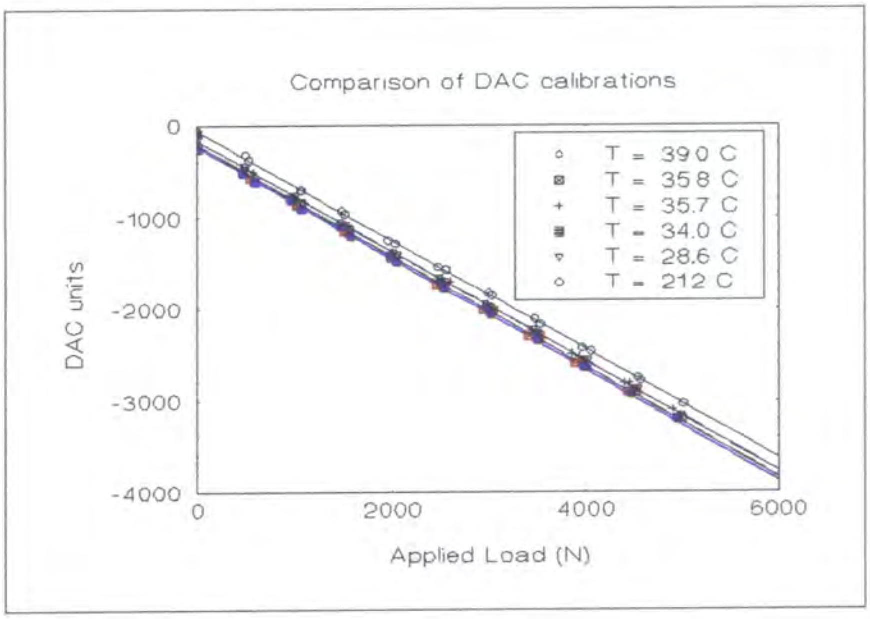

Figure A.3 DAC calibration curves for six different temperatures

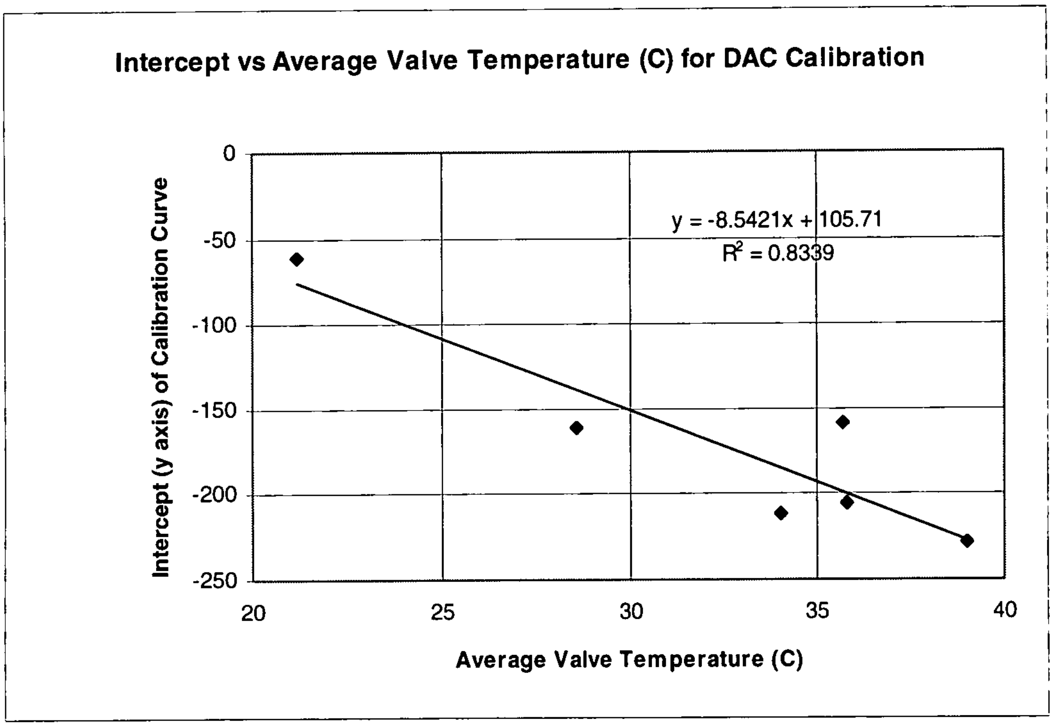

Figure A.4 Relationship between the intercept of the DAC calibration curve and servo-valve temperature

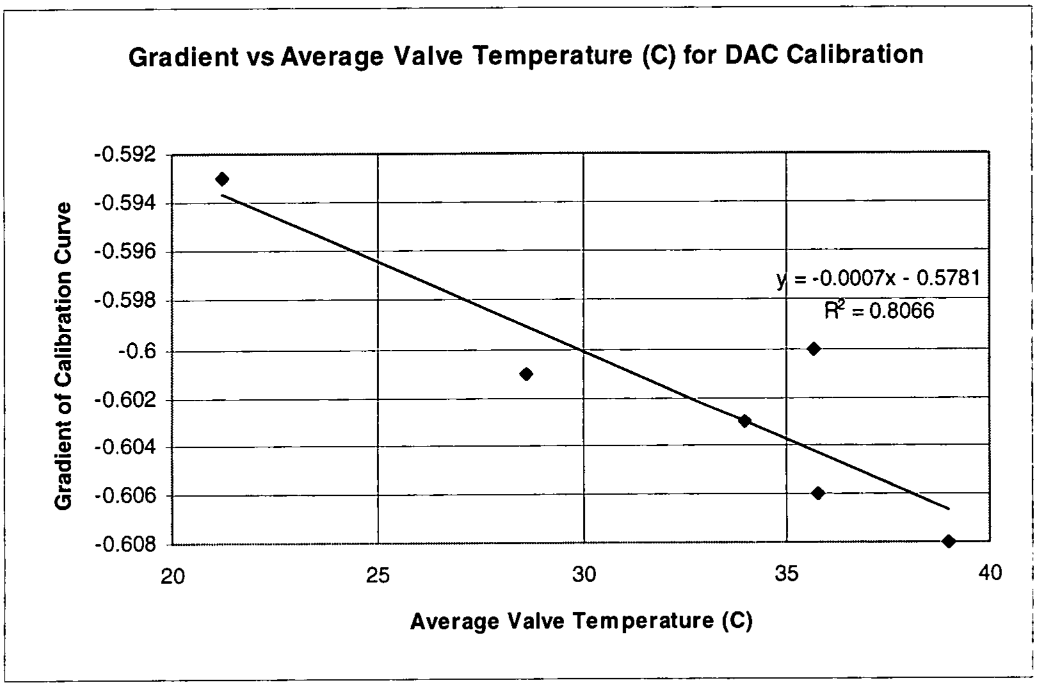

Figure A.5 Relationship between the gradient of the DAC calibration curve and servo-valve temperature

Appendix B - Losses in roller bearings

The frictional losses due to the roller bearings in the original pin on plate apparatus design were estimated by comparing a calibration of the piezoelectric force transducer through the bearings with a direct calibration of the transducer. The results obtained are shown in Figures B.1 and B.2 respectively and show that as much as 54.3% of the applied force was lost in the roller bearings.

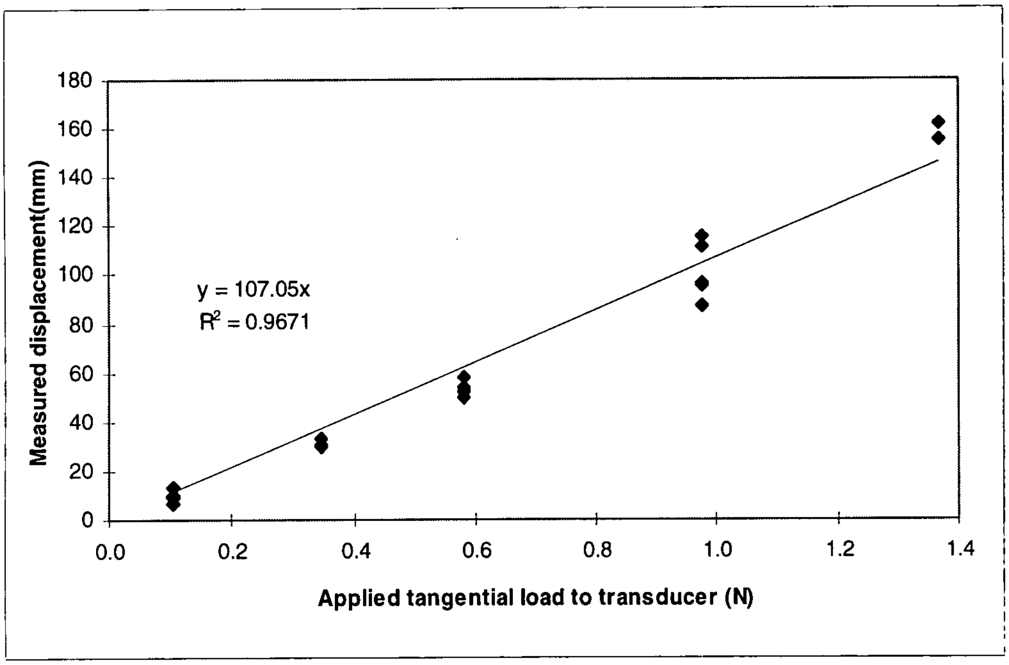

Figure B.1 Calibration of friction transducer through roller bearings

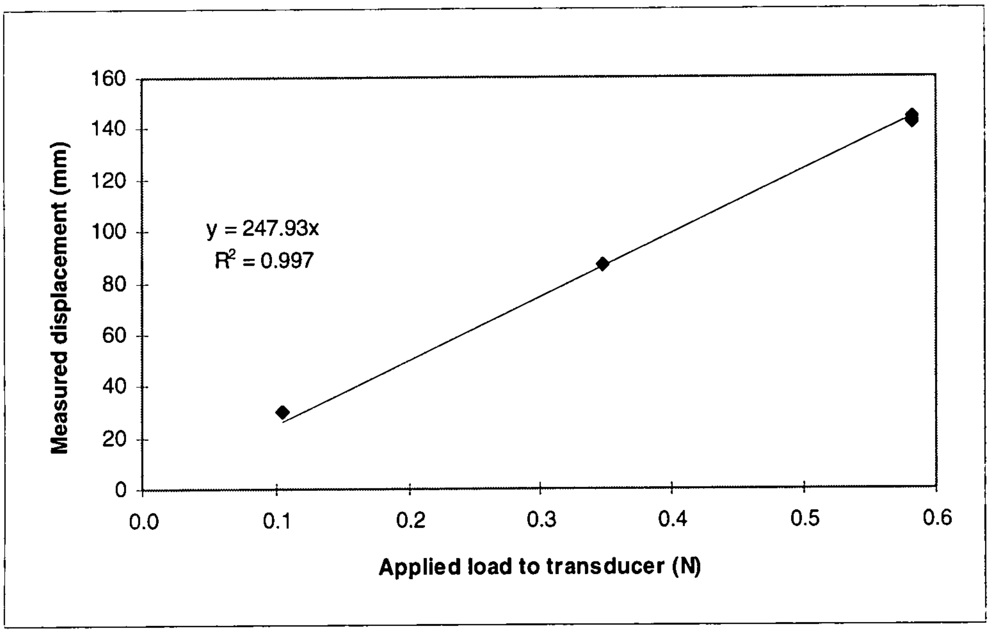

Figure B.2 Direct calibration of friction transducer

Appendix C - Air bearing design calculations

From Grassam and Powell [1964].

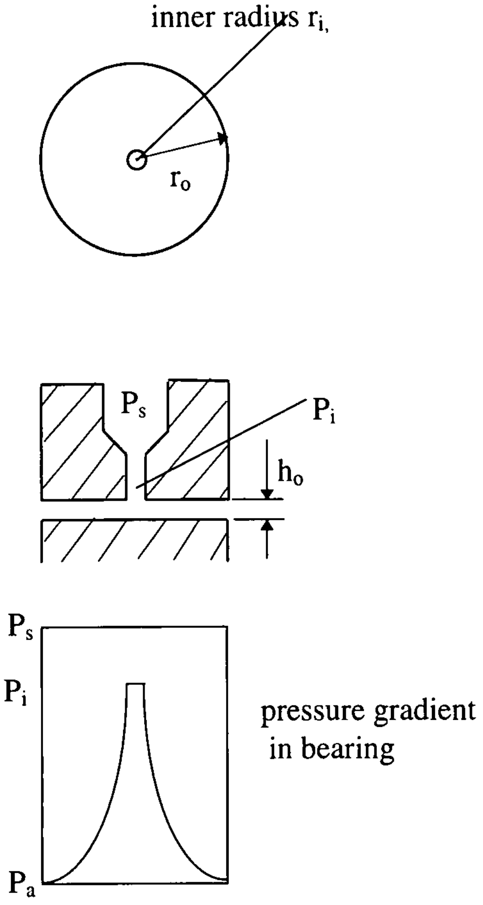

Figure C.1 A single jet hydrostatic bearing

r_o is the outer radius of the bearing or the radius of the bearing pad and r_i is the inner radius of the bearing or the radius of the orifice. To simplify the analysis, the rectangular multi-jet of the pin-on-plate apparatus were modelled as a series of discrete circular pad single jet bearings as shown in Figure C.1. This was felt to be an adequate model as it represented an conservative estimate. The analysis was exactly the same for the top bottom and side bearing pads but as the top bearing was the most critical, this was used as the base for the chosen dimensions.

P_a is atmospheric pressure, P_i the pressure at the inlet (orifice) and P_s the supply pressure to the bearing.

For each individual circular pad single jet, the following theory applies.

The bearing pressure factor, k, is given by

$$k = \frac{P_i - P_a}{P_s - P_a} \qquad \text{Eqn. C.1}$$

k is also equal to

$$k = \frac{2}{1 + \left(1 + \frac{4}{G^2}\right)^{0.5}} \qquad \text{Eqn. C.2}$$

where G is the bearing slot factor.

For incompressible flow, maximum stiffness occurs when k = 0.69 and G = 1.25.

For optimum stiffness, the load capacity of the bearing, W, is given by

$$W = k.P_s.\frac{\pi\left(r_o^{\,2} - r_i^{\,2}\right)}{2\ln\left(\frac{r_o}{r_i}\right)} \qquad \text{Eqn. C.3}$$

The optimum load coefficient, C_L, is given by

$$C_L = \frac{W}{\pi.r_o^{\,2}\left(P_s - P_a\right)} \qquad \text{Eqn. C.4}$$

It has a maximum value of 0.69 when the radius ratio, r_o/r_i is 1, but decreases exponentially towards 0.18 as r_o/r_i increases.

h_o is the bearing clearance which should be 25 μm for maximum stiffness but could only be guaranteed as 50 μm due to restrictions in manufacturing.

The bearing stiffness, λ, is given by

$$\lambda = \frac{W}{h_o} \qquad \text{Eqn. C.5}$$

The volume flow rate, Q, can be calculated as

$$Q = \frac{\pi(kP_s - P_a)h_o^{\,3}}{6\eta \ln\left(\frac{r_o}{r_i}\right)} \qquad \text{Eqn. C.6}$$

where viscosity η of air is taken as 1.8325 x 10^{-6} Pa.

Taking a conservative estimate of P_s as 4 bar (actual system pressure was 6 bar), Table C.1 shows the calculations. The table shows the actual design of the bearings, the slightly modified bearing which was actually fitted and the maximum capacity of the finished bearing. Each air bearing (top, bottom and side) consisted of a pair of pads each with multiple orifices. The total load capacity of the assembly is also given.

R_o	R_i	R_o/R_i	P_s	C_L	h_o	W	Total W	Q	λ	
(m)	(m)		(Pa)		(m)	(N)	(N)	(m3/sec)	(N/m)	
9.0E-3	2.1E-4	43.9	3.0E+5	0.093	5.0E-5	4.7	121.1	1.0E-3	9.3E+4	as fitted
9.0E-3	2.5E-4	36.0	2.5E+5	0.098	5.0E-5	3.7	95.9	7.2E-4	7.4E+4	design
9.0E-3	2.1E-4	43.9	5.5E+5	0.092	5.0E-5	10.5	272.6	2.6E-3	2.1E+5	max load

Table C.1 Air bearing design calculations

The final design incorporated bearing pads 18mm deep, i.e. circular pads with r_o of 9 mm. The orifice diameter for each jet was 0.41 mm, i.e. r_i of 0.205 mm. Each top and bottom pad had 13 orifices and each side pad 3. For the bottom bearings the load capacity required at each orifice was equal to 7.8N (the weight of the carriage) divided by 26 (the total number of orifices) and was equal to 0.3 N. For the top bearings, the capacity required was dependent on the applied pneumatic cylinder load. The bearings were over-designed for the original design load of 50 N (load capacity of each orifice 1.62 N) and P_s of only 3 bar gave a total load capacity of 121.13 N. The maximum load capacity of the finished system achievable for P_s of 5.5 bar was 272.56 N.

Appendix D - Losses in air bearings

The losses in the air bearings were calculated in the same way as for the roller bearings. The piezoelectric force transducer was calibrated through the air bearings over the range of sensitivities of measurement and then compared to a direct calibration for the same sensitivity. The calibration coefficients obtained and the calculated percentages of force lost in the air bearings are given in table D.1 and Figures D.1 to D.6 show the calibration curves.

	coefficient a where y=ax		
Sensitivity	**Bearings**	**Direct**	**% loss**
x 2 mV	0.0046	0.0043	6.5
x 5 mV	0.0117	0.0106	9.4
x 10 mV	0.0228	0.0213	6.6
x 20 mV	0.0448	0.0425	5.1
x 50 mV	0.1141	0.1061	7.0
x 100 mV	0.2265	0.2130	6.0

Table D.1 Calculated calibration coefficients and losses in the air bearings

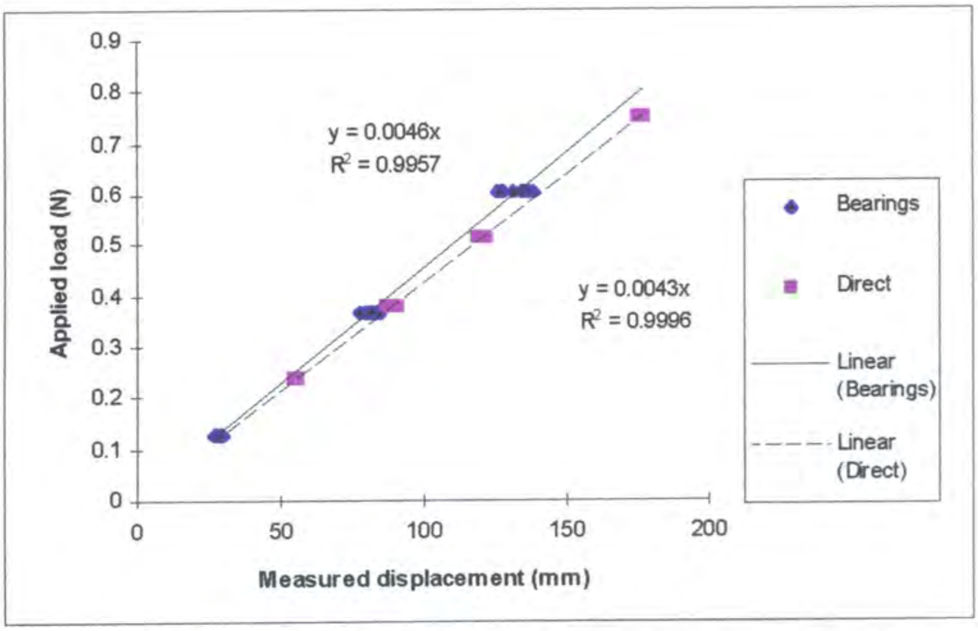

Figure D.1 Comparison of calibrations at x 2 mV (high sensitivity)

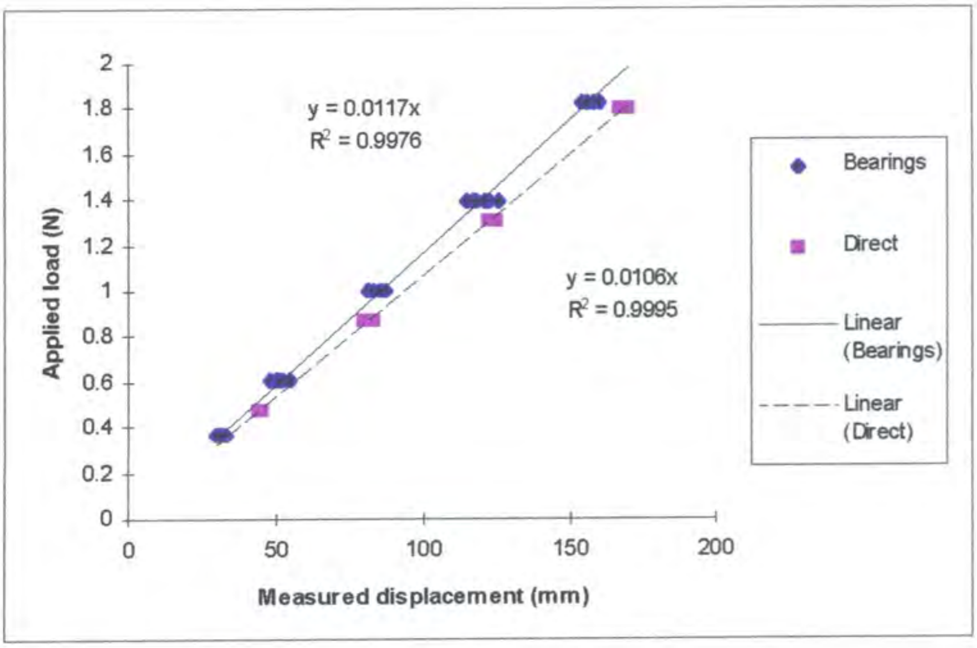

Figure D.2 Comparison of calibrations at x 5 mV

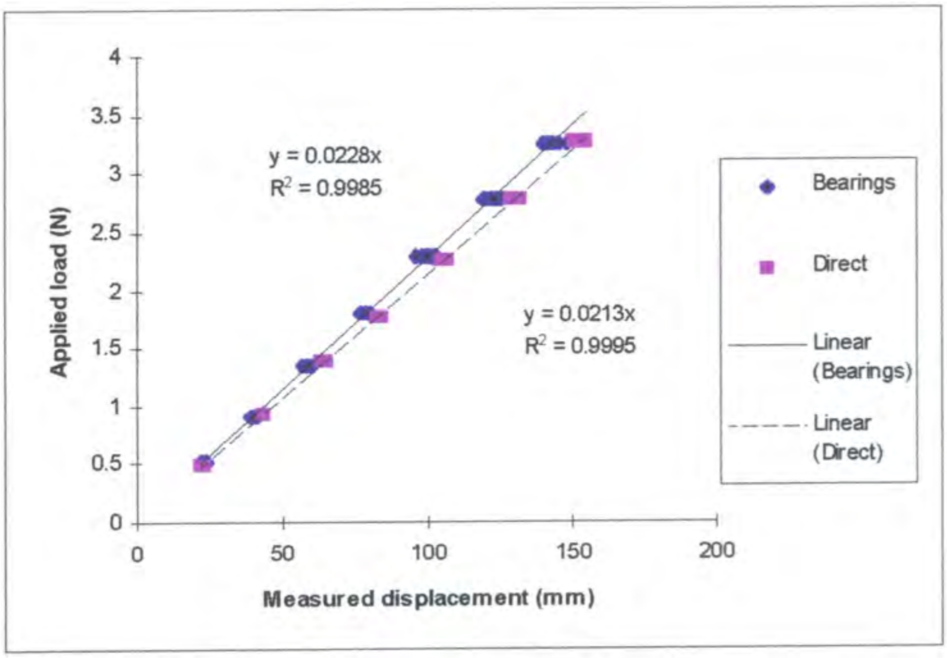

Figure D.3 Comparison of calibrations at x 10 mV

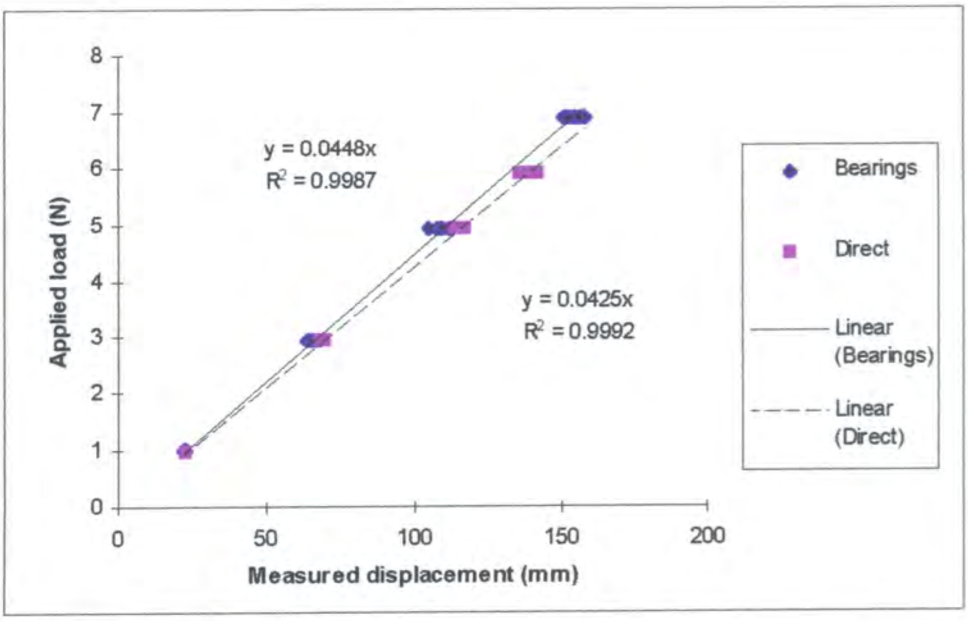

Figure D.4 Comparison of calibrations at x 20 mV

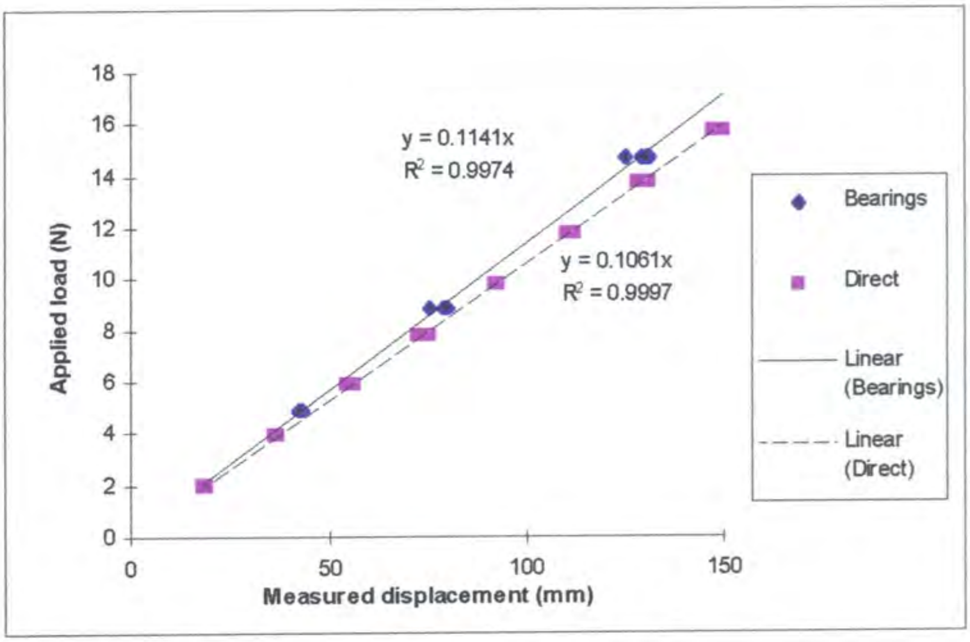

Figure D.5 Comparison of calibrations at x 50 mV

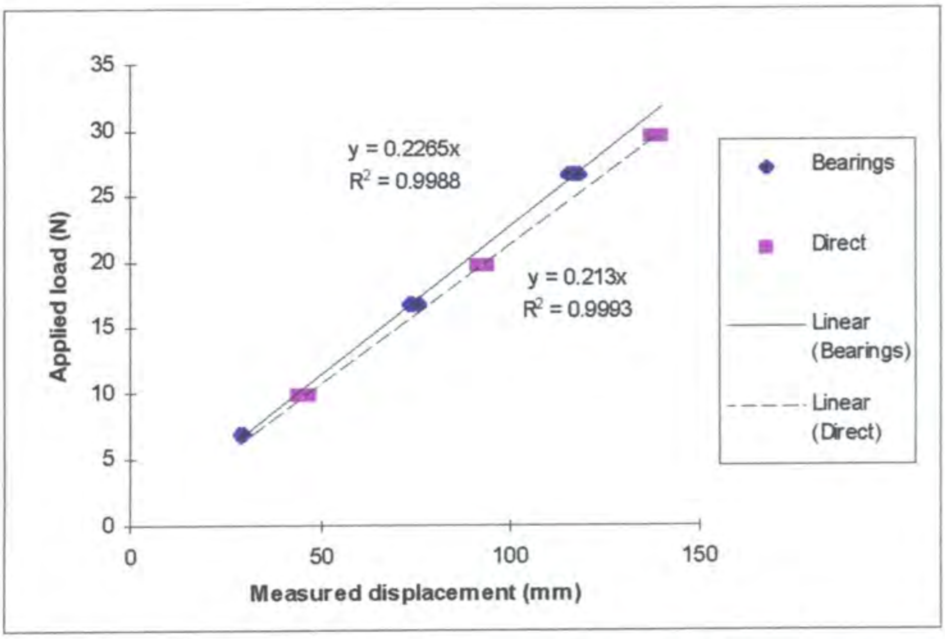

Figure D.6 Comparison of calibrations at x 100 mV (lowest sensitivity)

Appendix E - Calibration of pin on plate apparatus load cell

As described in Chapter 4, the load cell on the pin on plate apparatus was calibrated in two stages. First it was calibrated using dead weights to obtain a relationship between the measured displacement of the chart recorder. Secondly, the pneumatic loading system was attached and the measured displacment of the chart recorder was calibrated against the applied pressure to the cylinder. Figures E.1 and E.2 show the dead weight calibrations at sensitivites of 0.5 mV and 1.0 mV and Figures E.3 and E.4 show the pressure calibrations for the 10mm and 25 mm bore cylinders at the same two sensitivities.

The pressure calibration was of the form $y = ax + b$ where ax was the displacement caused by the cylinder and b was the constant displacement due to the weight of the pin holder and pin (situated beneath the load cell). By comparing the two sets of calibrations, a relationship between force and applied pressure can be obtained for each cylinder. These relationships were:

10mm bore: Force (N) = 7.99 x (pressure in bar) + 2.7 N
25mm bore: Force (N) = 50.14 x (pressure in bar) + 2.7 N

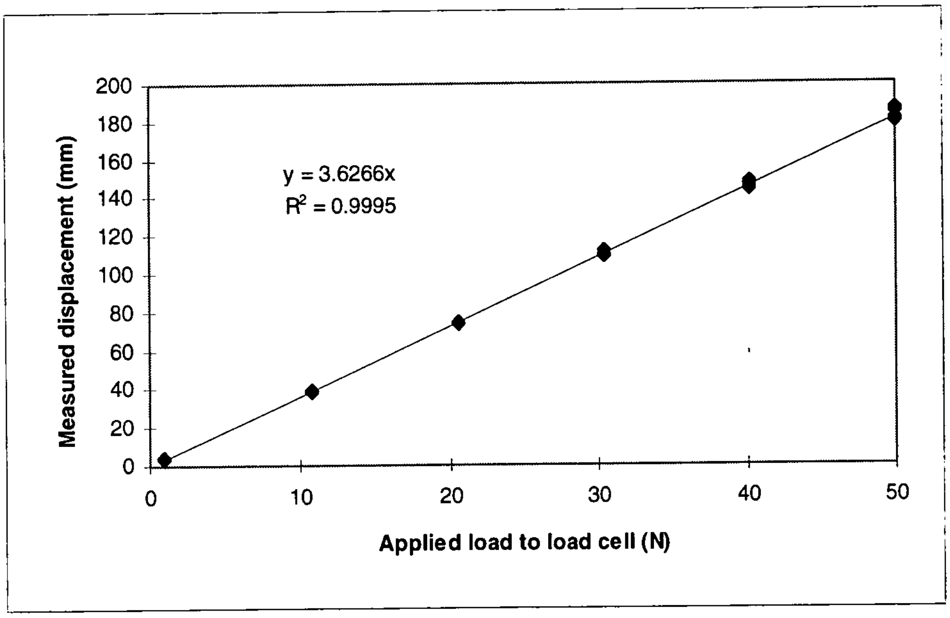

Figure E.1 Calibration of load cell against load at x 0.5 mV sensitivity

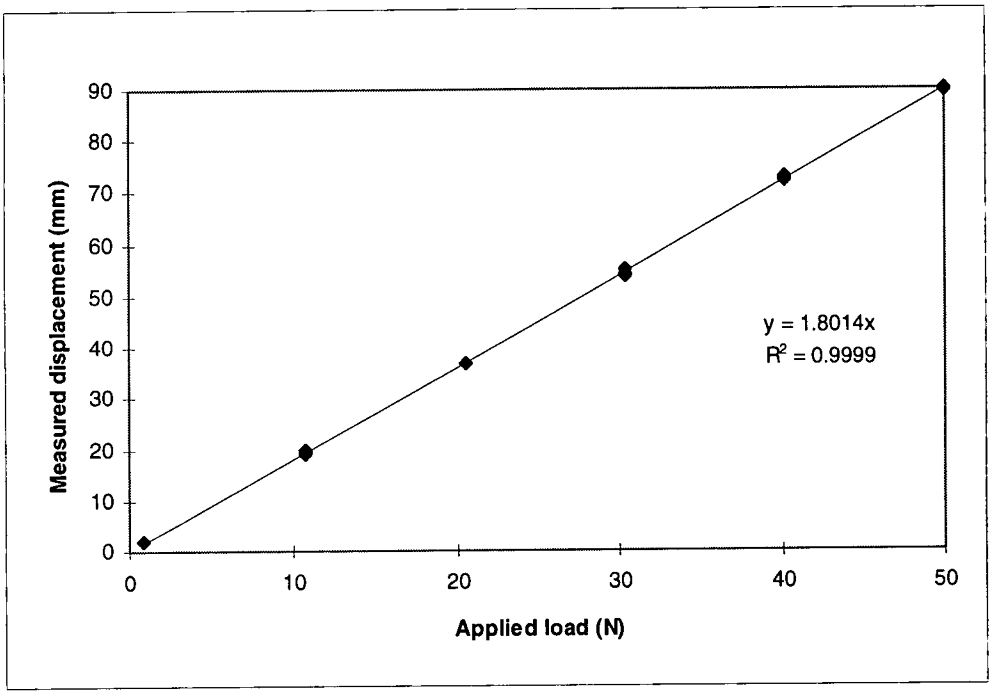

Figure E.2 Calibration of load cell against load at x 1.0 mV sensitivity

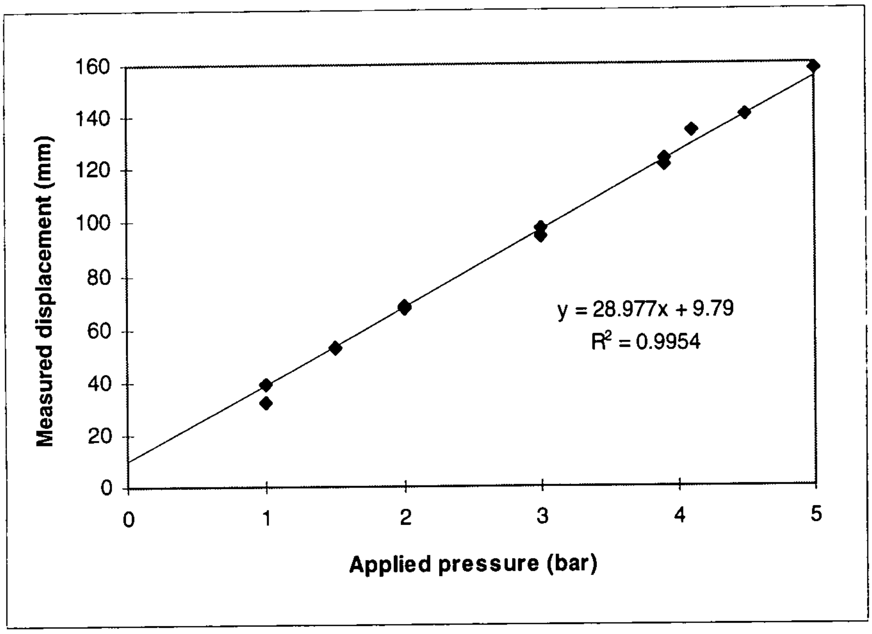

Figure E.3 Calibration of load cell against pressure for 10mm ϕ cylinder (x0.5mV)

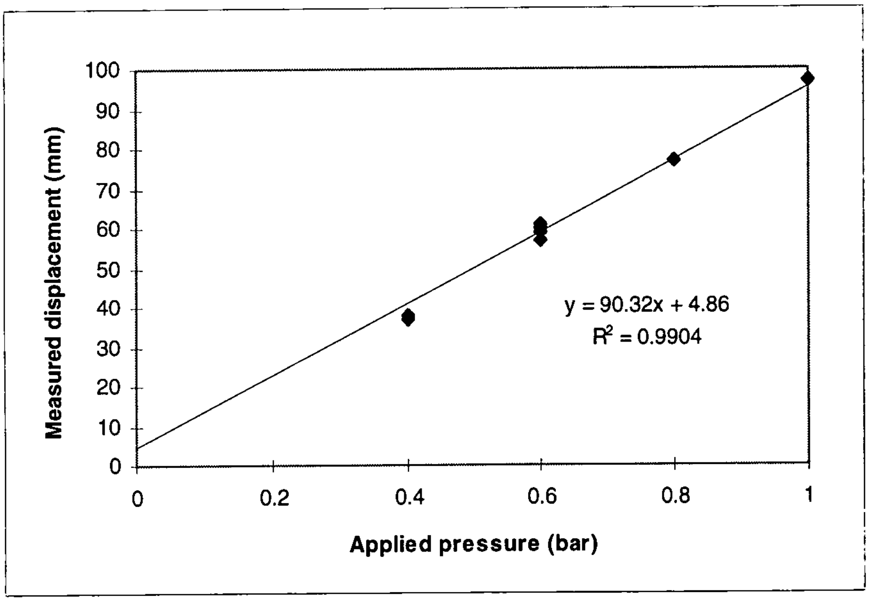

Figure E.4 Calibration of load cell against pressure for 25mm ϕ cylinder (x1.0mV)

Appendix F - Surface roughness measurements

The New View 100 optical interferometric profilometer was used to make the following measurements of the surface roughness of the bearing components used. All samples were measured under a x10 magnification unless marked * where the magnification was x40.

Sample	RMS (nm)		PV (nm)		Ra (nm)		Rsk	
	Mean	Range	Mean	Range	Mean	Range	Mean	Range
BB98*	710.7	153.4	14472	4576	522.1	135.7	0.07	0.95
CC21A	145.7	108.2	4840	8392	111.2	95.1	0.28	3.90
CC25A	148.8	104.8	3327	3221	109.1	77.0	1.11	5.55
CC27A	115.7	157.0	3952	6534	81.2	88.3	0.38	2.40
M1	157.9	648.8	6470	34170	90.8	239.1	-5.17	2.48
M2	120.2	235.7	5311	15743	75.8	160.1	-2.67	8.50
M3	246.5	1104.7	7698	19159	159.3	631.3	-2.46	2.69
M4	192.7	1179.9	3900	21165	127.8	746.6	-0.01	5.63
M5	142.3	576.2	4994	14662	94.5	382.3	0.98	14.7
M6	171.8	1034.1	4124	19515	107.2	585.3	3.49	4.33
C1	259.4	415.4	13923	16470	157.8	291.0	-3.68	11.00
C3	196.2	366.0	8732	17111	127.9	218.6	-1.72	9.40
C4	87.7	38.8	8458	15812	59.7	38.4	-0.11	3.63
PE4	1255.9	566.4	22753	6573	849.0	487.4	-1.13	1.53
Protek*	1046.6	661.1	11628	9278	835.9	551.4	-0.14	0.87

Table F.1 Surface roughness measurements of soft counterfaces

Sample	RMS nm)		PV (nm)		Ra (nm)		Rad.Curvature (mm)	
	Mean	**Range**	**Mean**	**Range**	**Mean**	**Range**	**Mean**	**Range**
28mm head	47.8	48.9	1775	8096	33.3	34.2	14.40	3.28
30mm head	69.9	132.9	1410	1492	33.9	66.5	15.40	0.36
32 mm head	178.8	362.4	5920	30137	128.5	265.5	16.46	2.82
100mm pin	55.4	44.9	954	1343	41.9	34.8	119.79	29.1
200mm pin A	66.6	126.4	1101	1794	42.1	86.8	221.6	38.2
200mm pin B	52.3	37.4	980	461	39.3	31.7	232.7	20.5
Pop cyl N	71.1	43.1	1667	2555	44.2	19.5	8.70	0.73
Pop cyl SF	48.0	29.3	999	2440	28.7	29.0	10.19	0.88
Sim cyl N	102.9	43.3	2372	2292	59.8	20.0	50.80	1.71
Sim cyl SF	62.1	99.0	1058	952	36.0	78.3	63.4	1.28

Table F.2 Surface roughness measurements of hard counterfaces

(Cyl = cylinder, Sim = simulator, Pop = pin-on-plate apparatus, N = normal finish, SF = super finish)

Appendix G - Simulator friction factor traces

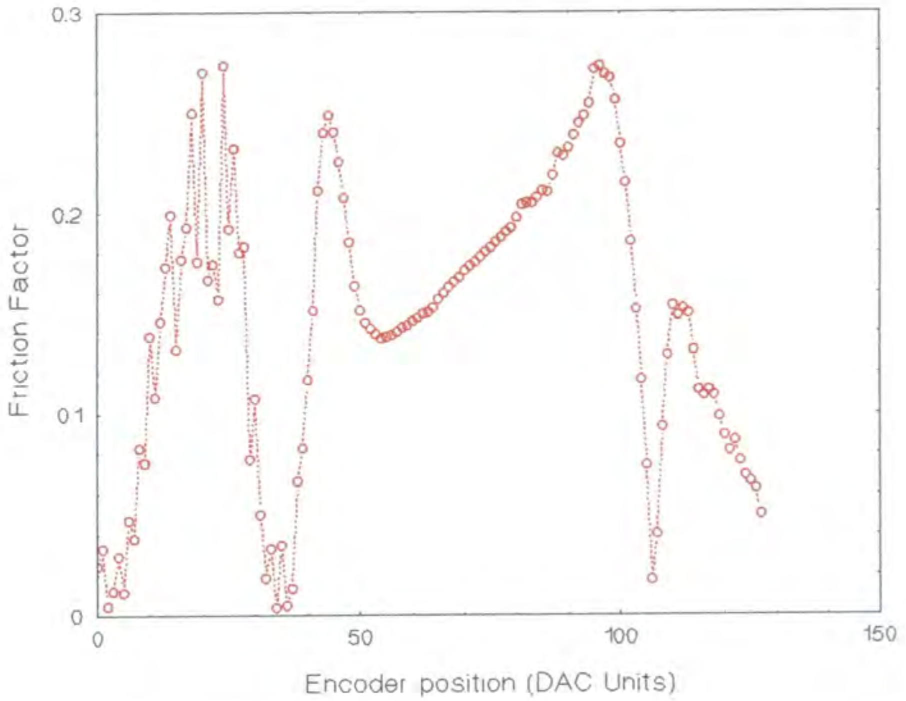

Figure G.1 Typical friction factor trace for simulator (0.000818 Pa s)

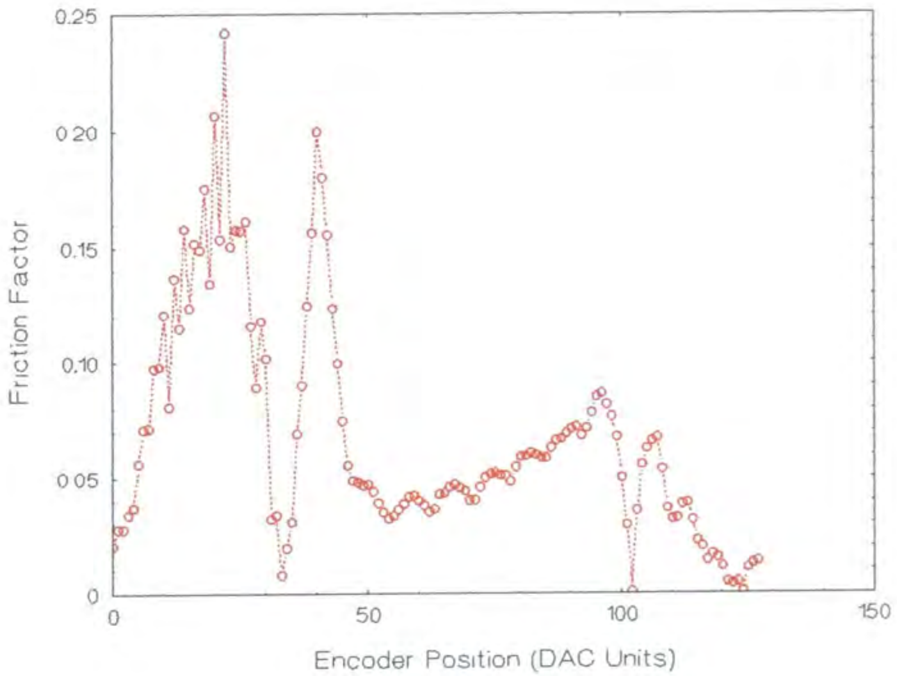

Figure G.2 Typical friction factor trace for simulator (0.00934 Pa s)

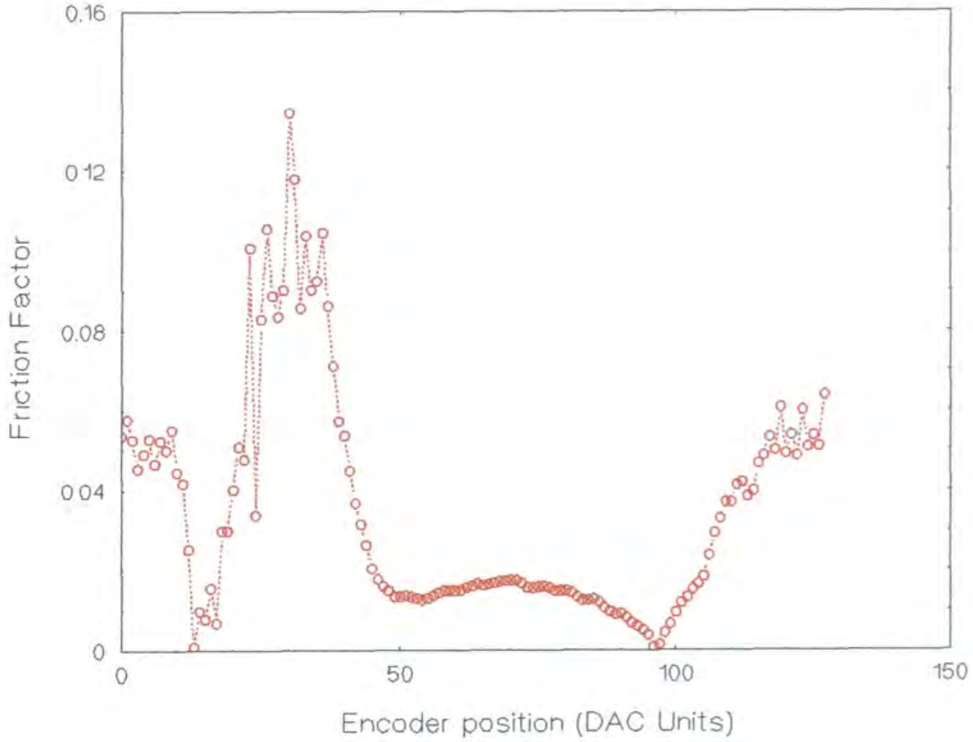

Figure G.3 Typical friction factor trace for simulator (29.25 Pa s)

UNIV DUNELM